Fatigue Risks in the Connections of Sign Support Structures

Christopher M. Foley, PhD, PE
Joseph A. Diekfuss, PhD
Baolin Wan, PhD

Marquette University
Department of Civil, Construction & Environmental Engineering

WisDOT ID no. 0092-09-07
February 2013

RESEARCH & LIBRARY UNIT

WISCONSIN HIGHWAY RESEARCH PROGRAM

WISCONSIN DOT
PUTTING RESEARCH TO WORK

Technical Report Documentation Page

1. Report No. WHRP 0092-09-07	2. Government Accession No No	3. Recipient's Catalog No
4. Title and Subtitle Fatigue Risks in the Connections of Sign Support Structures		5. Report Date May 31, 2013 6. Performing Organization Code Wisconsin Highway Research Program
7. Authors Christopher M. Foley, PhD, PE Joseph A. Diekfuss, PhD Baolin Wan, PhD		8. Performing Organization Report No.
9. Performing Organization Name and Address Department of Civil, Construction & Environmental Engineering; Marquette University, Milwaukee, WI		10. Work Unit No. (TRAIS) 11. Contract or Grant No. WisDOT SPR# 0092-09-07
12. Sponsoring Agency Name and Address Wisconsin Department of Transportation Division of Business Services Research Coordination Section 4802 Sheboygan Ave. Rm. 104 Madison, WI 53707		13. Type of Report and Period Covered Final Report, 2009-2013 14. Sponsoring Agency Code
15. Supplementary Notes		

16. Abstract

This research effort develops a reliability-based approach for prescribing inspection intervals for mast-arm sign support structures corresponding to user-specified levels of fatigue-induced fracture risk. The resulting level of risk for a particular structure is dependent upon its geographical location, the type of connection it contains, the orientation of its mast-arm relative to north and the number of years it has been in service. The results of this research effort indicate that implementation of state-of-the-art reliability-based assessment procedures can contribute very valuable procedures for assigning inspection protocols (*i.e.* inspection intervals) that are based upon probabilities of finding fatigue-induced cracking in these structures. The engineering community can use the results of this research effort to design inspection intervals based upon risk and thereby better align inspection needs with limited fiscal and human resources.

17. Key Words Fatigue-Induced Fracture, Wind-Speed Variability, Reliability-Based Fatigue Evaluation, Statistical Analysis, Fatigue Testing, Finite Element Analysis, Mast-Arm Connections	18. Distribution Statement No restriction. This document is available to the public through the National Technical Information Service 5285 Port Royal Road Springfield VA 22161

18. Security Classif.(of this report) Unclassified	19. Security Classif. (of this page) Unclassified	20. No. of Pages 194	21. Price

Form DOT F 1700.7 (8-72) Reproduction of completed page authorized

NOTICE:

This research was funded through the Wisconsin Highway Research Program by the Wisconsin Department of Transportation and the Federal Highway Administration under Project #0092-09-07. The contents of this report reflect the views of the authors who are responsible for the facts and accuracy of the data presented herein. The contents do not necessarily reflect the official views of the Wisconsin Department of Transportation or the Federal Highway Administration at the time of publication.

This document is disseminated under the sponsorship of the Department of Transportation in the interest of information exchange. The United States Government assumes no liability for its contents or use thereof. This report does not constitute a standard, specification, or regulation.

The United States Government does not endorse products or manufacturers. Trade and manufacturers' names appear in this report only because they are considered essential to the object of this document.

Table of Contents

ACKNOWLEDGMENTS

The authors would like to acknowledge the support and help from the following individuals at the Wisconsin Department of Transportation: Travis McDaniel, Bruce Karow, Joel Alsum, Kent Bahler, and Thomas Heydel. The authors would also like to acknowledge individuals that worked on the first phase of this research effort: Matthew Hellenthal, Jordan Komp, Joseph Schmidt, Andrew Smith, and Mathew Weglarz.

EXECUTIVE SUMMARY

Over the past few decades, there have been issues of poor fatigue performance (the main failure mechanism) of the welded, tube-to-transverse plate connections within sign support structures. Review of the literature has indicated that a considerable amount of research has been devoted to identifying the structural response characteristics of these signs. Others have spent time trying to identify how these connections may be repaired, retrofitted or simply better designed to sustain longer fatigue lives. However, little attention has been given to using a systematic reliability-based approach to assess the risk of fatigue-induced fracture in these structures.

Using a reliability-based approach to solve structural engineering problems requires a fundamental knowledge of the uncertainty associated with three variables: resistance, demand and modeling error. The present research effort has focused on systematically quantifying this uncertainty. The procedure utilizes statistical parameters determined from probability frequency distributions generated for each of the three variables. Resistance is defined by the fatigue life of the connection, demand is defined by the wind loading (buffeting-type only) and modeling error is evaluated using high-fidelity finite element analysis (FEA) with comparison to measured data from a field monitoring system.

This procedure required the collection of a significant amount of experimental fatigue testing data as well as measured wind speed and direction data. The experimental fatigue testing data was obtained from the literature and utilizing the Marquette University Engineering Materials and Structural Testing Laboratory (EMSTL). The wind speed and direction data was obtained both from existing national databases and from real-time health monitoring of a typical sign structure located in Milwaukee, WI. Resulting expected stress-range magnitudes from finite element models of the monitored sign support structure, subjected to loading from wind speed (converted to pressure) simulations, were compared with measured strain from the real-time monitoring system to determine the modeling error associated with the use of this procedure.

This research effort develops a reliability-based approach for prescribing inspection intervals corresponding to user-specified levels of fatigue-induced fracture risk. The resulting level of risk for a particular structure is dependent upon its geographical location, the type of connection it contains, the orientation of its mast-arm and the number of years it has been in service. The results of this research effort indicate that implementation of state-of-the-art reliability-based assessment procedures can contribute very valuable procedures for assigning inspection protocols (*i.e.* inspection intervals) that are based upon probabilities of finding fatigue-induced cracking in these structures. The engineering community can use the results of this research effort to design inspection intervals based upon risk and thereby better align inspection needs with limited fiscal and human resources.

Chapter 1 – Introduction

1.1 Introduction

Wisconsin has encountered problems with the connections contained in, and the in-service performance of, several cantilevered mast-arm sign support structures. In one case, a structure was taken down because of excessive mast-arm deflections. After detailed inspection, it was discovered that recently installed bolts were loose, which may have led to premature fatigue failure. In a second case, a routine inspection discovered a welded tube to plate connection that exhibited cracking over 50% of its perimeter since the last scheduled inspection. A third case occurred during completion of the present research effort. Sign support structures S-61-0001 and S-61-0002 in Osseo, Wisconsin were decommissioned in the fall of 2011 after cracking was found at the weld toe in the mast-arm to plate connection.

The latest edition of the AASHTO design specifications (AASHTO 2009) include provisions for fatigue design. However, many structures presently in service were designed before fatigue provisions were part of the design specifications. Furthermore, the fatigue design procedures that are now included in these specifications do not address the variability in fatigue life for structures in service, nor do these provisions allow an engineer to quantify the risk of fatigue induced fracture for structures that have been in service. As a result, Wisconsin undertook a research effort designed to assess the risk of fatigue-induced fracture in its existing sign support structures that were designed before these latest AASHTO specification revisions and to develop procedures that can be used to assign inspection protocols for mast-arm sign support structures.

The objectives of the research effort were to implement state-of-the-art fatigue reliability analysis and current knowledge regarding fatigue lives of connections in a systematic assessment of fatigue-induced fracture risk in mast-arm sign support structures within Wisconsin, and assign inspection cycle frequencies for these structures and their components. There are very clear benefits to the proposed research effort. First and foremost, there is an unknown probability of future failures in mast-arm-to-pole connections typical of sign support structures in Wisconsin. This research will result in guidelines for inspection cycles, retrofit measures, or other changes in inspection or maintenance policy to assure the safety of the traveling public. Application of the results of the effort will reduce inconvenience to the motoring public through establishing rational inspection intervals for these structures. Furthermore, these relatively innocuous structures are sources of relatively severe failure consequences and regular short-interval inspection cycles to mitigate this

risk have economic impact and the results of the present research effort will foster better use of public funds for ancillary structure inspection.

1.2 Osseo Sign Failures

Two sign support structures, S-61-0001 and S-61-0002, in Osseo, Wisconsin were found to have circumferential cracks at the weld toes of the tube-to-plate connections of their mast-arms in the fall of 2011. An aerial view of the location within Osseo is shown in Figure 1.1. The two signs were located on the northbound and southbound exit ramps from U.S. Interstate Highway 94 to U.S. Highway 10. These sign supports were found to be cracked in October 2011 and were immediately decommissioned. A forensic analysis of the sign supports was conducted as part of the present research effort to set the stage for evaluating the validity and usefulness of the reliability analysis procedures developed. It is important to demonstrate that this failure was driven by fatigue and therefore, an overview of the forensic study is included in this section of the report. Further details can be found elsewhere (Diekfuss 2013). It is interesting to note that these sign support structures went into service in 2003 and were designed in a time frame where provisions for considering fatigue were included in design specifications (AASHTO 2001). However, the research conducted indicates that these provisions are likely not adequate to result in satisfactory fatigue performance predictions without modification.

The forensic analysis conducted on the Osseo sign supports included chemical composition analysis of mast-arm circular hollow shapes (tubes), the socketed plate, and the weld. The chemical composition analysis indicated that the materials complied with ASTM A36 and API 5Lx42 materials, which were specified on the design drawings (Diekfuss 2013). Carbon equivalency numbers for the mast-arm tube and socketed plate indicated that the plates and tubes were expected to have good weldability indicating that any cracks found in the specimens retrieved were not likely caused by material with poor welding characteristics (Diekfuss 2013). Hardness testing (Rockwell B and Brinell) was conducted to estimate tensile strengths of the constituent materials for the sign support components. The results of this hardness testing indicated that the mast-arm tube and socketed plate material met specified tensile strength magnitudes indicated on the design drawings (Diekfuss 2013).

A macroscopic evaluation of the specimens retrieved from Osseo was conducted beginning with applying the dye penetrant method to outline the extent of cracking in the specimens. Figures 1.2 and 1.3 illustrate the results of this analysis and the extent of the cracks in the mast-arms. The dye penetrant evaluation clearly defined the extent of the cracking in S-61-0001. However, cracks in S-61-0002 were not clearly delineated using the dye penetrant process. Magnetic particle testing was employed to evaluate S-61-0002 in the field and the method was used to determine that cracks at the 11 o’clock and 1 o’clock positions on the mast-arm

circumference were present (Diekfuss 2013). The dye penetrant test results were used to guide sectioning of the mast-arm to socketed plate connections.

The specimens were sectioned to expose fracture surfaces. Detailed examination of the fracture surface exposed in S-61-0001 clearly exhibited ratchet marks and beach marks characteristic of fatigue crack propagation. Images of the fracture surface for this sign support structure are shown in Figures 1.4 and 1.5. The specimen from sign S-61-0002 did not have clear evidence of fracture seen in the dye penetrant analysis. Sectioned specimens from the 11 o'clock position were then polished in an attempt to expose the cracks seen in the magnetic particle testing employed in the field. Careful sectioning and polishing resulted in the crack being identified in the sections taken. A photograph of the sectioned specimen is given in Figure 1.6. The image clearly shows a crack initiating at the toe of the weld and propagating through the heat affected zone (HAZ) into the base material of the tube. The quality of the fillet weld was also evaluated using the polished and etched specimens. Figure 1.7 illustrates characteristic weld dimensions from sign S-61-0002. The weld dimensions met design specifications (Diekfuss 2013). The etched specimens did exhibit mild undercutting at the weld toe in the base material. There was a lack of galvanized coating on the surface of this undercut area which led the research team to believe that these undercuts may have been a result of grinding after decommissioning the sign support structure (Diekfuss 2013). There was no evidence of cracks at the toes of the welds where the undercutting was present and this supports the conclusion drawn.

A microscopic evaluation of the crack surfaces was also carried out using Scanning Electron Microscopy (SEM) and Light Optical Microscopy (LOM). The SEM images clearly indicated multiple ratchet marks at a variety of scales indicating fatigue crack propagation (Diekfuss 2013). These ratchet marks initiated on the outer surface of the mast-arm tube and propagated inward. There was presence of oxidation on the crack surfaces evident in the SEM images indicating that the crack front was exposed during the sign support structure's service life. Figure 1.8 illustrates the weld cross-section and the crack initiation site at the weld toe. The crack appeared to propagate in a transgranular manner directly into the base material of the tube (Diekfuss 2013). Figure 1.9 includes magnified LOM images of the base material in the mast-arm tube, socketed plate, and outside fillet weld. The images illustrate grain structures typical of low-carbon structural steels with no gross inclusions or defects. The grain structure shown in Figure 1.9(c) is indicative of higher-strength material typical of welds. An attempt to quantify crack growth rates using SEM was made. The presence of significant oxidation on the crack surface precluded definition of crack growth rates that could be used to generate estimates for fatigue life remaining after crack initiation (Diekfuss 2013).

The forensic investigation of signs S-61-0001 and S-61-0002 completed as part of the study indicated that the generation of cracks in the sign supports was a result of multi-axial bending fatigue. Multiple ratchet marks and beach marks characteristic of fatigue crack propagation and a lack of visible plastic deformation on

the fracture surface of S-61-0001 support this conclusion. SEM images showed the presence of striations typical of fatigue crack propagation and oxidation of the fracture surfaces giving evidence of fatigue crack propagation with time.

Therefore, it is clear that the Osseo sign supports suffered from premature failure resulting from fatigue-induced cracking. It is likely that application of infinite-life fatigue design procedures (AASHTO 2001) would not have precluded this poor fatigue performance. Therefore, it is imperative that the Osseo sign support structure configuration be used in the present study as a detail configuration susceptible to premature fatigue-induced fracture. The Osseo sign support structure performance can also serve as a qualitative benchmark for evaluating the reliability-based analysis procedure for establishing inspection protocols for mast-arm sign support structures.

1.3 Quantifying Fatigue-Induced Fracture Risk

When one discusses risk and recommendations of inspection cycles for structural systems, there is a natural migration toward uncertainty. With regard to sign, signal and luminaire supports, there are a large number of parameters used to define performance that contain uncertainty including: the basic fatigue-life data; the predictive methodologies used to describe fatigue crack growth under random stresses; weld fabrication issues (*e.g.* undercut severity varies tremendously); wind speeds and direction defining the loading; expressions used to migrate wind speed to pressures for structural analysis; equations used to conduct detailed stress analysis at the joints in these structures (*e.g.* stress concentration factors, stress intensity factors); ability of inspection tools (*e.g.* visual inspection, dye penetrant, magnetic particle) to detect cracks; and environmental conditions (*e.g.* corrosion, reduced material toughness). Therefore, if one were to definitively quantify risk, these uncertainties must be modeled. Fully probabilistic (reliability-based) procedures for predicting the fatigue lives of offshore structures have been proposed (Kirkemo 1988; Wirsching 1988), but they rely on highly detailed probabilistic models for the uncertainties previously described that aren’t complete for the structures considered as part of the proposed research effort.

The proposed research effort will be somewhat forced into several simplifying assumptions to make the effort tractable (Foley et al. 2004), but will also consider implementation of the probabilistic approach used extensively in the offshore industry (Wirsching 1984). As a result, risk of fatigue-related fracture can be quantified and inspection cycles can be established. A brief review of a procedure for risk assessment is prudent as it sets the foundation for the manner in which the research effort will be carried out.

The process begins with the commonly used fundamental expression relating the magnitude of a stress-range cycle (stress-ranges) to the number of times that stress-range cycle can be applied before crack initiation in a metal. This expression can be written as,

$$N \cdot \left(S_R\right)^m = A \tag{1.1}$$

where the following are defined;

N = fatigue life of the detail, which corresponds to the number of stress-range cycles accumulated at failure (initial crack formation);

S_R = constant stress-range cycle magnitude applied;

A = fatigue detail constant;

m = exponent describing the slope of the S_R-N curve for the specific detail category.

Stress-range cycles are rarely applied at constant magnitude in real structural systems and models for accumulated damage resulting from variable-amplitude stress-ranges are needed. The accumulation of damage for variable magnitude stress-range cycles can be written as,

$$D = \sum_{i=1}^{n} \frac{n_i}{N_i} = \sum_{i=1}^{n} \frac{n_i \left(S_{R,i}\right)^m}{A} = \frac{N_T}{A} \cdot \frac{n_1 \left(S_{R,1}\right)^m + n_2 \left(S_{R,2}\right)^m + \cdots + n_n \left(S_{R,n}\right)^m}{N_T} = \frac{N_T}{A} \cdot \sum_{i=1}^{n} \frac{n_i}{N_T} \left(S_{R,i}\right)^m \tag{1.2}$$

where the following additional terms are defined as:

n_i = the number of constant-amplitude stress-range cycles applied at magnitude i;

N_i = the fatigue life of the detail at stress-range magnitude i;

N_T = the total number of applied stress-range cycles of any magnitude.

Fatigue damage resulting from a stress-range applied over a defined number of cycles in a time period is widely characterized using an accumulation model (Miner 1945);

$$D = \frac{N_T}{A} \cdot S_{RE}^m \tag{1.3}$$

where S_{RE}^m is the expected stress-range that occurs during the time period, T.

Uncertainty in modeling is assumed to manifest itself in the stress-range defined for the damage analysis through an adjustment (Wirsching 1984) leading to the definition of an actual stress-range;

$$S_{R,act} = B \cdot S_R \tag{1.4}$$

The random variable, B, is defined as: $B = B_M \cdot B_N \cdot B_H$. The components then describe uncertainty in: fabrication and assembly, B_M; nominal member loads, B_N; and estimation of stress concentration (hot spot) factors, B_H.

The time to fatigue-induced cracking can now be introduced. The frequency of stress cycles occurring over a time period, T, can be written as (Wirsching 1984);

$$f_o = \frac{N_T}{T}$$

The damage can now be modified to include the passage of time and modeling uncertainty (Wirsching 1984),

$$D = \frac{N_T}{A} \cdot \left[B^m S_{RE}^m \right] = \frac{T \cdot B^m}{A} \left[f_o S_{RE}^m \right] = \frac{T \cdot B^m}{A} \cdot \Omega \tag{1.5}$$

The stress parameter, Ω, allows the expected number of stress cycles to be defined using a deterministic method, a spectral (probabilistic) method, or a Weibull modeling approach (Wirsching 1984).

If damage resulting from blocks of constant amplitude stress cycles is assumed (*i.e.* the deterministic method is employed), the fatigue damage during a time period can be determined using the following stress parameter (Wirsching 1984),

$$\Omega = f_0 \cdot \sum_i \zeta_i \cdot S_{R,i}^m \tag{1.6}$$

where: f_o is now defined as the average frequency of stress-ranges; $S_{R,i}$ is a constant amplitude stress-range; and ζ_i is the fraction of total stress-ranges for which $S_{R,i}$ acts. Wirsching (1984) describes a probabilistic method within the context of spectral (frequency domain) analysis. In this case, the cumulative fatigue damage in an offshore platform is written using the following stress parameter (Wirsching 1984);

$$\Omega = \lambda(m)\left(2\sqrt{2}\right)\Gamma\left(1+\frac{m}{2}\right) \cdot \sum_i \gamma_i f_i \sigma_i^m \tag{1.7}$$

where: $\Gamma(\cdot)$ is the gamma function; $\lambda(m)$ is a rainflow counting correction factor (Wirsching 1984); γ_i is the fraction of time for the *i*th sea state; f_i is the frequency of wave loading for the *i*th sea state; and σ_i is the root mean square of the stress process for the *i*th sea state.

Ginal (2003) and Foley et al. (2004) used a slightly different formulation of equation (1.7) and based their fatigue damage estimates upon probabilistic estimates of wind speed, direction, simulation of turbulent wind time-histories with 5-second averaging times, and rainflow counting of fatigue stress cycles. Using this procedure, equation (1.7) was re-cast into the following form (Foley et al. 2004; Ginal 2003);

$$\Omega = n_{5-\text{sec}/\,year} \sum_j \sum_i P\left[\bar{V}_{5-\text{sec}} = v_j\right] \cdot P\left[D = d \mid \bar{V}_{5-\text{sec}} = v_j\right] \cdot \left(S_i^m\right)_{v_j} \tag{1.8}$$

where: $n_{5-\text{sec}/\,year}$ is the number of 5-second intervals in the given time period (one year in this former effort); $P\left[\bar{V}_{5-\text{sec}} = v_j\right]$ is the probability that the 5-second averaged wind speed will be the user-defined magnitude, v_j; and $P\left[D = d \mid \bar{V}_{5-\text{sec}} = v_j\right]$ is the probability that the wind speed is in a user-defined direction, d, (taken as direction perpendicular to sign face) given the 5-second averaging time is equal to the user-defined magnitude; and $\left(S_i\right)_{v_j}$ is the *i*th stress cycle magnitude for a given 5-second wind speed, v_j.

Diekfuss (2013) modified this approach slightly to consider mast-arm sign support structures and the method proposed by Diekfuss (2013) is the approach taken in the present study. Damage accumulation is written using equation (1.5) with a slightly modified stress parameter (Diekfuss 2013),

$$\Omega = n_{1-hr/year} \sum_i \sum_j \left[P\left(U = u_i \cap D = d_j\right) \cdot n_{cycles/hr,i} \cdot \left(S_{RE}^m\right)_i \cdot \cos\theta_j \right] \tag{1.9}$$

where: $n_{1-hr/year}$ is the number of 1-hour intervals in a year (8,760); $P\left(U = u_i \cap D = d_j\right)$ is the probability that a 1-hour averaged wind speed of user defined magnitude will be intersected with a 1-hour averaged wind direction of user defined direction; $n_{cycles/hr}$ is the number of stress-range cycles that occurs in a one hour time interval resulting from application of a wind pressure simulation corresponding to a defined 1-hour averaged wind speed; S_{RE}^m is the expected stress-range cycle magnitude that occurs in a 1-hour simulation history; and θ is the angle between the axis of the mast-arm and the centroidal axis of the cardinal wind direction being considered.

It has been recommended that failure be defined as $D \geq \Delta$ where Δ is a threshold value describing accumulated damage at failure. With this definition, equation (1.5) can be re-written to define the time to fatigue-induced cracking or failure (Wirsching 1984),

$$D = \frac{T \cdot B^m}{A} \cdot \Omega = \Delta \quad \Rightarrow \quad T_c = \frac{A \cdot \Delta}{B^m \cdot \Omega} \tag{1.10}$$

where T_c is the critical time to fatigue-induced cracking. The ability to define fracture risk comes from casting equation (1.10) into a reliability basis. This is often done through formulation of a performance function and establishing models for random variables characterizing uncertainty and defining success or failure within the context of this performance function.

A performance function for reliability-based fatigue analysis can now be formulated such that not meeting a targeted performance indicates a fatigue-induced crack has initiated. The performance function for the present research effort is based upon equation (1.10) and is written as,

$$Y = \frac{T_c}{T} = \frac{\Delta \cdot A}{B^m \cdot \Omega \cdot T} \tag{1.11}$$

where: T is now a targeted or desired service life (time, years); and all other variables have been defined earlier. Failure is defined when $Y \leq 1.0$, which indicates that the targeted fatigue life has not been met.

The probability of not meeting a targeted service life can be formulated by casting appropriate parameters in equation (1.11) as random variables. The stress parameter, Ω, targeted service life, T, and fatigue detail category exponent, m, are deterministic quantities. The remaining parameters are assumed to be lognormal

random variables. It should be noted that the stress parameter used in the present study is defined in equation (1.9).

It is often convenient to assume that the random variables contained in equation (1.11) are lognormal (Wirsching 1984). If this assumption is made, the natural logarithm of the performance function can be written as (Swokowski 1979),

$$\ln Y = \ln A + \ln \Delta - m \ln B - \ln \Omega - \ln T \tag{1.12}$$

Equation (1.12) indicates that the lognormal random variable Y is a combination of three lognormal random variables, A, Δ, B and the logarithm of two deterministic quantities, Ω, T. The mean of the natural logarithm of the performance function can be written as (Nowak and Collins 2000),

$$\mu_{\ln Y} = \mu_{\ln A} + \mu_{\ln \Delta} - m\mu_{\ln B} - \ln \Omega - \ln T \tag{1.13}$$

Expanding using equation (1.13) using lognormal random variable mathematics (Nowak and Collins 2000),

$$\begin{aligned} \mu_{\ln Y} = &\left(\ln \mu_A - \frac{1}{2} \ln\left(1 + CV_A^2\right) \right) + \left(\ln \mu_\Delta - \frac{1}{2} \ln\left(1 + CV_\Delta^2\right) \right) \\ &- m\left(\ln \mu_B - \frac{1}{2} \ln\left(1 + CV_B^2\right) \right) - \ln \Omega - \ln T \end{aligned} \tag{1.14}$$

Simplifying gives,

$$\mu_{\ln Y} = \ln\left(\frac{\mu_A \mu_\Delta}{\mu_B^m} \right) - \frac{1}{2} \ln\left[\frac{\left(1 + CV_A^2\right)\left(1 + CV_\Delta^2\right)}{\left(1 + CV_B^2\right)^m} \right] - \ln \Omega - \ln T \tag{1.15}$$

The standard deviation of the natural logarithm of the performance function is therefore (Nowak and Collins 2000),

$$\sigma_{\ln Y} = \sqrt{\ln\left[\left(1 + CV_A^2\right)\left(1 + CV_\Delta^2\right)\left(1 + CV_B^2\right) \right]} \tag{1.16}$$

The probability of the performance function being less than one (*i.e.* a crack initiating) can be written as (Nowak and Collins 2000),

$$p_F = P\left[Y \le 0\right] = \Phi\left[-\frac{\mu_{\ln Y}}{\sigma_{\ln Y}} \right] = \Phi\left[-\beta\right] \tag{1.17}$$

where the reliability index is given by,

$$\beta = \frac{\mu_{\ln Y}}{\sigma_{\ln Y}} \tag{1.18}$$

Equations (1.15) through (1.18) allow probabilities of not meeting targeted service lives to be defined. However, application of these equations in this process is not without challenge. There are three lognormal random variables that need to be defined and a stress parameter characterizing loading demand that needs to be defined. The targeted service life is a user-defined quantity in this process. The objectives of this research

study are to define parameters (mean and coefficient of variation) of lognormal random variable models for fatigue life uncertainty, A, modeling uncertainty, B, uncertainty in damage accumulation, Δ, and loading demand suitable for defining the stress parameter, Ω, so that equations (1.15) through (1.18) can be used to quantify the risk of fatigue-induced fracture in mast-arm sign support structures.

1.4 Process for Defining Inspection Protocols

The previous discussion outlines a systematic methodology for including uncertainty in service-life predictions and therefore, establishes a formal methodology for assessing risk of fatigue-related fracture in cantilevered mast-arm signal and sign support structures. Once the random variable models are defined and targeted service lives are defined, the engineer can explore probabilities of finding fatigue-induced cracking in mast-arm sign support structures and tailor inspection intervals in a more rational manner to these expected service lives.

As an example of the process, let's consider a hypothetical example of a mast-arm sign support structure that is going into service in Milwaukee, Wisconsin. The methodology formulated in this research effort will allow probabilities of finding fatigue-induced cracking in this structure after 5-year, 10-year, 15-year and any other service life. If the probability of finding fatigue-induced cracking after 5 years is 5%, after 10 years is 40%, and after 15 years is 90%; the engineer can establish the first inspection at 10 years and then inspect in four-year intervals after that. The current process is to inspect at regular 4-year intervals. Thus, the inspection cycle scenario described would save two inspections during its service life.

The methodology formulated also allows targeted probabilities of fatigue-induced cracking to be defined with subsequent service lives meeting this threshold. Thus, if a 95% confidence level (*i.e.* 5% chance of finding a fatigue-induced crack) is set as a target, then one can establish the first inspection at a service life corresponding to a 5% probability of failure. Depending upon the location within the state and the mast-arm detail configuration, this might be 30+ years. As a result, sign structures that enter service in good condition may never need to be inspected. Furthermore, there are other sign structures that may indeed need to be inspected more frequently than the current four-year interval to meet this confidence level on service.

1.5 Report Objectives and Outline

The objectives of this research report are to formulate, apply and discuss a reliability-based formulation of a procedure for quantifying the risk of fatigue-induced fracture in mast-arm sign support structures and to generate inspection protocols for these structural systems using this procedure. This procedure is also used to identify mast-arm support structural system configurations that are likely to result in enhanced susceptibility to premature fatigue-induced cracking. It is also used to identify regions within the state of Wisconsin that may be more susceptible to having structures with fatigue problems.

The second chapter of the report (Wind Demand Uncertainty) outlines the formalized development of the information needed to determine the stress parameter using equation (1.9). Data tables defining the probability of 1-hour averaged wind speed intersected with cardinal direction, $P\left(U = u_i \cap D = d_j\right)$, is the primary objective of this chapter. These data tables in conjunction with the expected stress-range cycle magnitude and the number of cycles at this magnitude for a one-hour simulated wind record, $n_{cycles,hr,i} \cdot \left(S_{RE}^m\right)_i$, and the wind direction relative to the mast arm axis, θ_j, are addressed in this chapter.

The third chapter of the research report (Fatigue Life Uncertainty) outlines the development of random variable parameters necessary for defining uncertainty related to fatigue life. A comprehensive synthesis of fatigue testing data, including tests completed as part of the present research effort is included. Random variable fatigue life modeling parameters, μ_A, CV_A, and a best-fit fatigue life exponent, m, are formulated in this chapter.

The fourth chapter of the report (Modeling Error Uncertainty) is devoted to formulation of the modeling error uncertainty random variable given by μ_B and CV_B. This random variable model is formulated using data from a field monitoring station located in Milwaukee, Wisconsin and comparison of acquired data with low-fidelity finite element modeling.

It should be noted that the random variable model for fatigue damage accumulation has not been addressed in the present research effort. Revision to the widely accepted Palmgren-Miner damage accumulation rule was simply outside the scope of the present research effort. The present research report utilizes a lognormal random variable for accumulated fatigue damage with parameters given by $\mu_\Delta = 1.00$ and $CV_\Delta = 0.30$ used and recommended by previous researchers (Wirsching 1983; Wirsching 1984; Wirsching 1988).

The fifth chapter of the research report (Reliability-Based Assessment and Inspection Protocols) is devoted to applying equations (1.15) through (1.18) to establish fatigue-induced fracture risk for common mast-arm sign support structure configurations found in Wisconsin. An evaluation of structural configurations more susceptible to premature fracture is made and inspection protocols based upon fatigue-induced fracture risk are formulated.

1.6 References

AASHTO (2001). *Standard Specifications for Structural Supports for Highway Signs, Luminaires and Traffic Signals, 4th Edition*, American Association of State Highway and Transportation Officials, Washington, D.C.

AASHTO (2009). *Standard Specifications for Structural Supports for Highway Signs, Luminaires and Traffic Signals, 5th Edition with 2010 Interim Revisions*, American Association of State Highway and Transportation Officials, Washington, D.C.

Diekfuss, J. A. (2013). "Reliability-Based Fatigue Assessment of Mast-Arm Sign Support Structures."PhD Thesis, Marquette University, Milwaukee, WI.

Foley, C. M., Ginal, S. J., Peronto, J. L., and Fournelle, R. A. (2004). "Structural Analysis of Sign Bridge Structures and Luminaire Supports." Wisconsin Highway Research Program, Madison, WI.

Ginal, S. J. (2003). "Fatigue Performance of Full-Span Sign Support Structures Considering Truck-Induced Gust and Natural Wind Pressures."MS Thesis, Marquette University, Milwaukee, WI.

Kirkemo, F. (1988). "Applications of Probabilistic Fracture Mechanics to Offshore Structures." *Applied Mechanics Reviews*, 41(2), 61-84.

Miner, M. A. (1945). "Cumulative Damage in Fatigue." *Transaction of the ASME, Journal of Applied Mechanics*, 67, A159-A164.

Nowak, A. S., and Collins, K. R. (2000). *Reliability of Structures*, McGraw-Hill, New York, NY.

Swokowski, E. W. (1979). *Calculus with Analytic Geometry*, Prindle, Weber & Schmidt, Boston, MA.

Wirsching, P. H. (1983). "Probability-Based Fatigue Design Criteria for Offshore Structures." American Petroleum Institute, Dallas, TX.

Wirsching, P. H. (1984). "Fatigue Reliability for Offshore Structures." *Journal of Structural Engineering*, 110(10), 2340-2356.

Wirsching, P. H. (1988). "Probability-Based Fatigue Design for Marine Structures." *Marine Structures*, 11(1), 23-45.

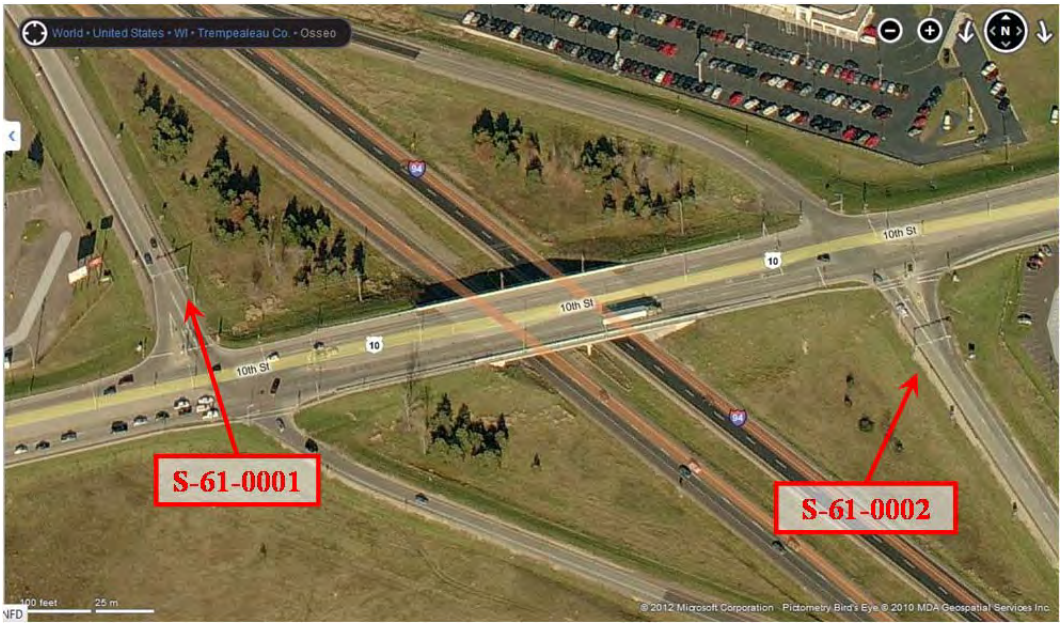

Figure 1.1 Aerial View of the Location of Sign Supports S-61-0001 and S-61-0002 in Osseo, Wisconsin (mast-arm sign supports can be seen in aerial photo).

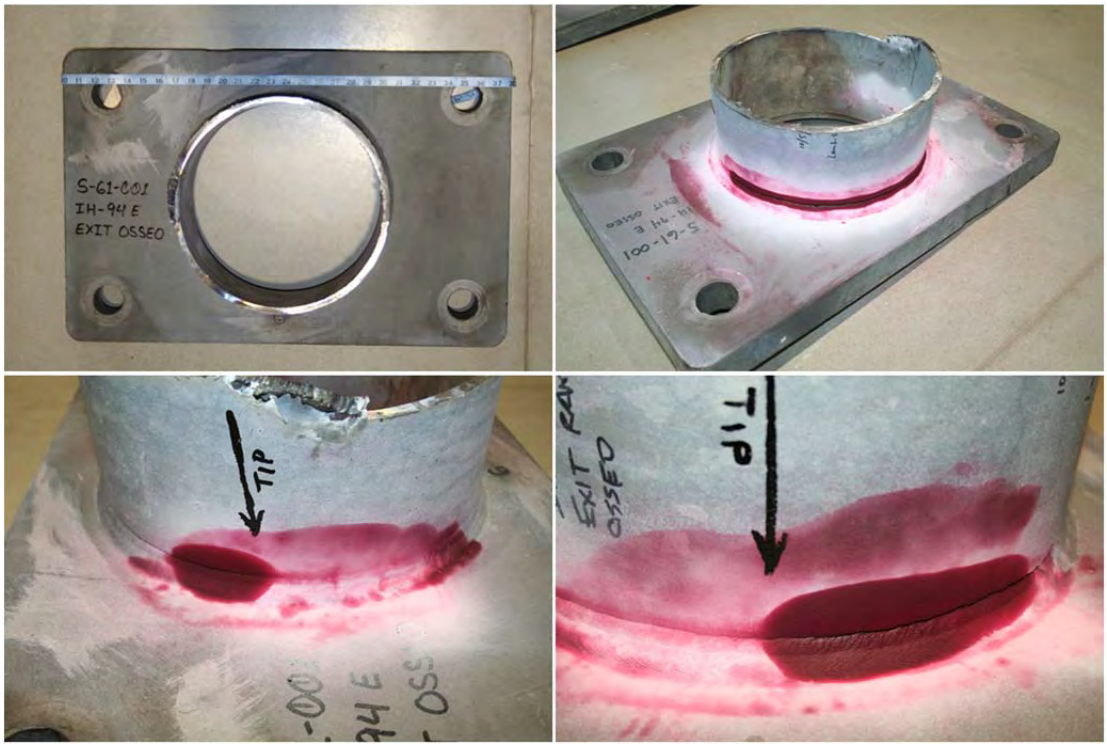

Figure 1.2 Dye Penetrant Analysis Results for S-61-001 from Osseo, Wisconsin (Diekfuss 2013).

Figure 1.3 Dye Penetrant Analysis Results for S-61-002 from Osseo, Wisconsin (Diekfuss 2013).

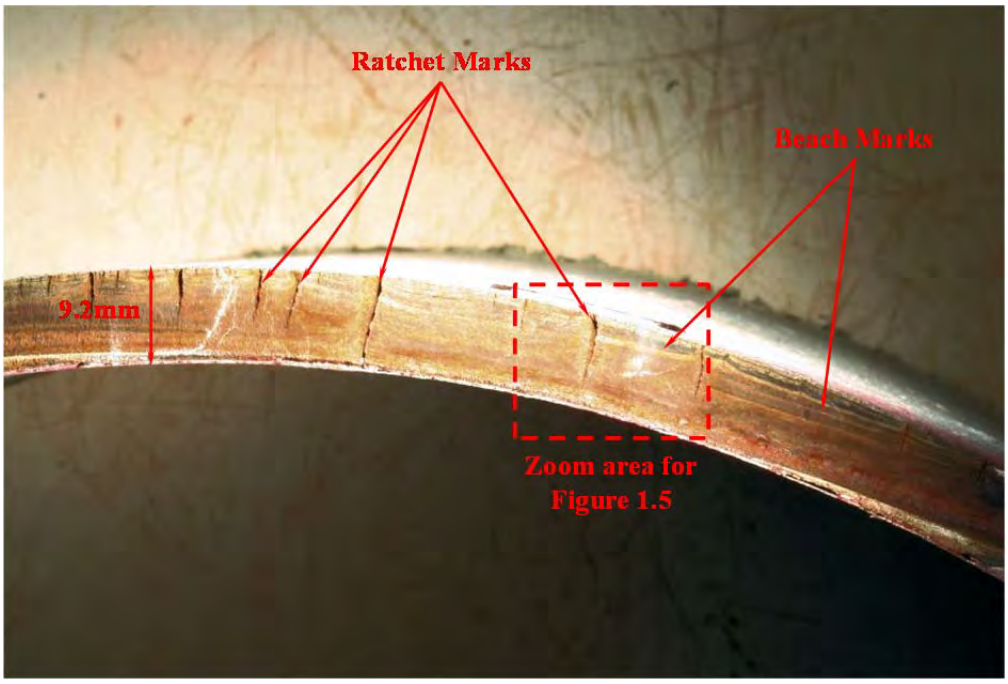

Figure 1.4 Photograph of Fracture Surface from S-61-0001 (location at the 10 o'clock position) (Diekfuss 2013).

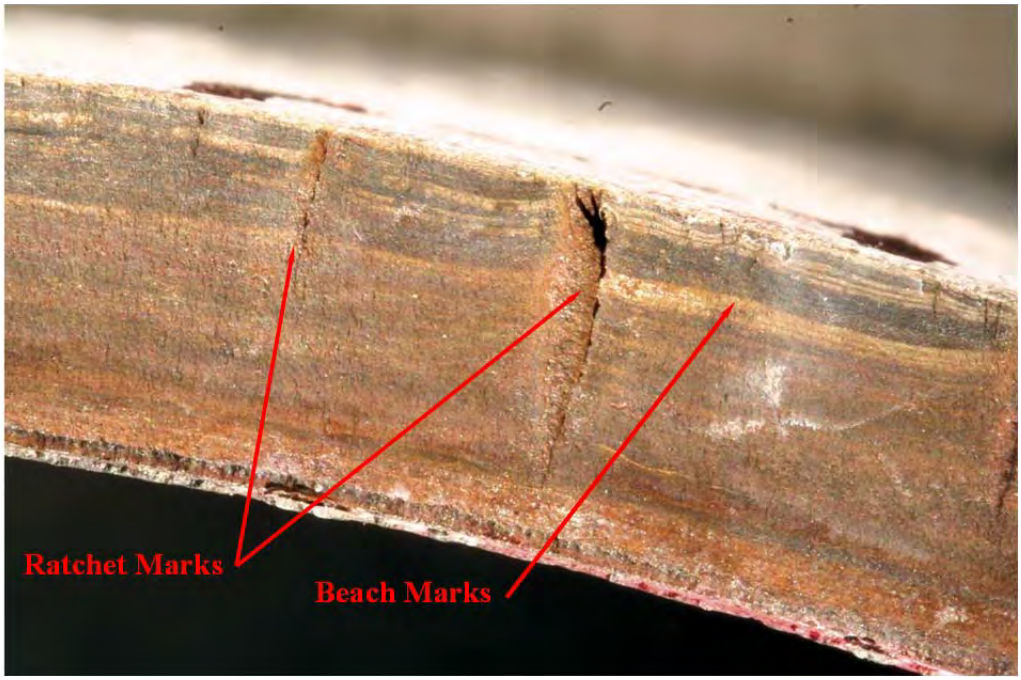

Figure 1.5 Photograph of Fracture Surface for Sign S-61-0001 (Diekfuss 2013).

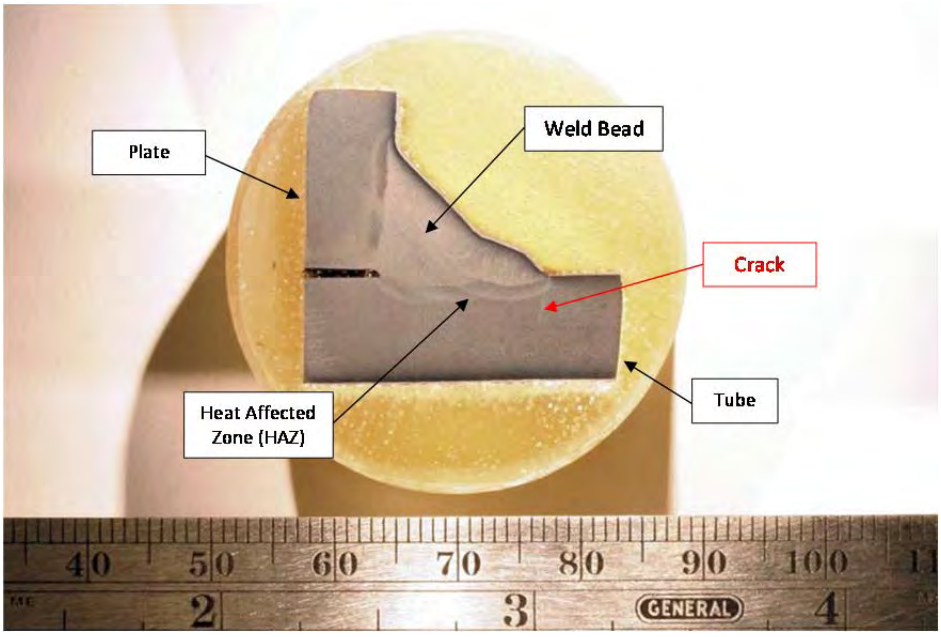

Figure 1.6 Polished and Etched Specimen from the 11 O'Clock Position in Sign Support S-61-0002 (Diekfuss 2013).

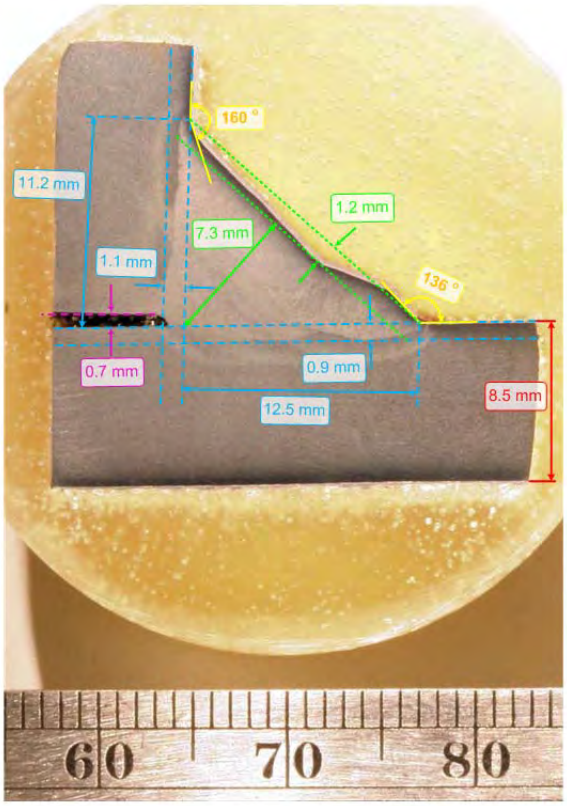

Figure 1.7 Photograph of Etched Specimen from Sign S-61-0002 at the 11 O'Clock Position (Diekfuss 2013).

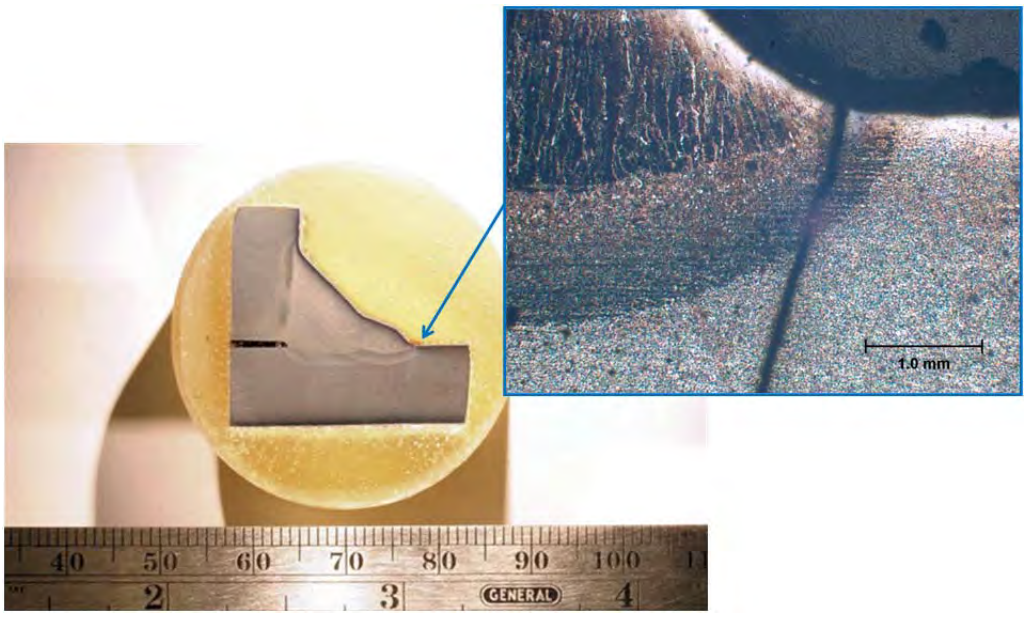

Figure 1.8 Light Optical Microscope Image of Crack Initiation Point from Section 3 of S-61-0002 at the Eleven O'clock Position (Diekfuss 2013).

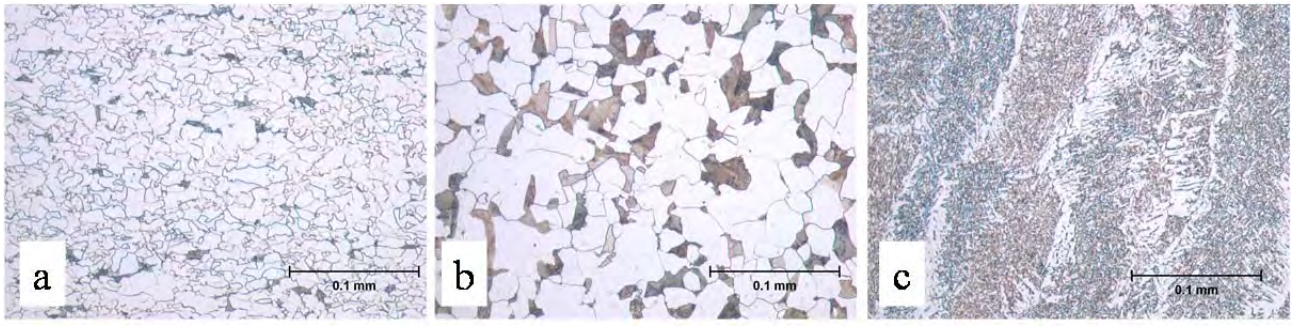

Figure 1.9 Light Optical Microscope Metallographic Images from Sign Support S-61-0002 at the Eleven O'clock Position: (a) Mast Arm Tube; (b) Socketed Plate; and (c) Weld Bead (Diekfuss 2013).

Chapter 2 – Wind Demand Uncertainty

2.1 Introduction

Quantifying the uncertainty in wind loading demand is integral to assessing fatigue-induced fracture risk in mast-arm sign support structures and establishing inspection protocols for them. In order to accomplish this, one must understand and quantify daily wind speeds and directions in the location where a sign support structure is in service. This is often in conflict with established methods for carrying out design of these structures as maximum expected wind speeds during the service life (sometimes 50 years) of a sign support structure is needed.

The majority of past research conducted for modeling wind has been in the area of extreme winds (Ellingwood and Tekie 1999; Peterka 1992; Peterka and Shahid 1998; Simiu et al. 1980; Simiu et al. 2003). Engineering models for extreme winds have been based upon fifty-year recurrence interval speeds using averaging times corresponding to fastest mile winds or 3-second gusts (ASCE 1998). Much of the fatigue-related research pertaining to sign and signal support structures has focused on quantifying structural response characteristics with regard to the aero-elastic phenomena of galloping and vortex shedding (Foley et al. 2004; Ginal 2003; Kaczinski et al. 1998; McDonald et al. 1995; South 1994). Statistical models of wind speeds (irrespective of direction) have been developed to gain understanding of what a sign structure might experience at a given location (Li et al. 2005); and probabilistic models of 5-second averaged wind speeds and directions for use in evaluating fatigue response of full-span sign and high-mast luminaire support structures have been developed (Foley et al. 2004; Ginal 2003). The effect of truck-induced wind gusts has also been investigated (Edwards and Bingham 1984; Foley et al. 2004; Ginal 2003; Hosch and Fouad 2009; Ocel et al. 2006).

The objective of this chapter is to provide a statistical modeling process for wind suitable for input into the reliability-based model for fatigue performance outlined in the introductory chapter of the report. The wind demand will be quantified through a semi-deterministic quantity identified previously as the stress parameter, Ω . For convenience, the equation for the stress parameter is restated as,

$$\Omega = n_{1-hr/yr} \cdot \sum_i \sum_j \left[P\left(U = u_i \cap D = d_j\right) \cdot n_{cycles/hr,i} \cdot (S_{RE}^m)_i \cdot \cos\theta_j \right] \tag{2.1}$$

where: $n_{1-hr/yr}$ is the number of 1-hour intervals in a single year; $n_{cycles/hr,i}$ is the number of stress-range cycles at the expected magnitude for a given one-hour averaged wind speed; $\left(S_{RE}^m\right)_i$ is the expected stress cycle

magnitude that occurs for a given one-hour averaged wind speed; $P\left(U = u_i \cap D = d_j\right)$ is the combined probability (*i.e.* probability of intersection) of a wind speed and direction; and θ_j is the angle made between the wind direction considered and the mast-arm longitudinal axis.

The objective of the present chapter is to formulate combined probabilities (probability of intersection) of wind speed and wind direction, $P\left(U = u_i \cap D = d_j\right)$, contained in equation (2.1) for any location within the state of Wisconsin where a sign support structure is in service. The discussion progresses from a synthesis of wind speed and direction data from seven National Climatic Data Center (NCDC) Automated Surface Observation System (ASOS) sites and a field monitoring station (FMS) in Wisconsin to discussion of a procedure for using NCDC-ASOS site data to interpolate combined probabilities of wind speed and directions at locations that are not NCDC-ASOS sites. Therefore, the procedure described in this chapter is suitable for determining probability models for wind loading demand throughout the state of Wisconsin that can be used as the basis of the risk-based process for establishing inspection protocols.

2.2 Wind Speed Data Sources

Sign and signal support structures tend to be located more frequently in areas of higher population density. Wind speed and direction data from the southern half of Wisconsin was collected as part of the present study. Wind speed and direction data was also collected at a field monitoring station designed, constructed, and deployed as part of the present research effort. There is a fairly wide dispersion of data collection sites within the State. It was felt that the data collected would yield significant understanding of wind speed and direction variability throughout the areas of the State where there is a significant number of sign and signal support structures. The dispersion of the data collection sites would also facilitate the interpolation of wind statistical information to locations in the State where data collection is not regularized or standardized.

National Climatic Data Center Automated Surface Observation System Sites

The National Climatic Data Center (NCDC) within the U.S. Department of Commerce maintains a weather data inventory as part of the National Oceanographic and Atmospheric Administration (NOAA) Satellite and Information Service. There are many U.S. controlled weather observation stations throughout the country continually collecting weather-related data. Many of these weather collection sites are called Automated Surface Observation System (ASOS) sites. The NCDC-ASOS sites are referenced by city and state as well as a Weather-Bureau-Army-Navy (WBAN) number. The city, WBAN number, and number of years of data collected for the seven cities considered in this research effort are given in Table 2.1 and their locations within the state of Wisconsin are shown in Figure 2.1.

Academic and government institutions can access the data at no cost through the following web-site: http://www.ncdc.noaa.gov/oa/climate/stationlocator.html. The user must specify the WBAN number and the time frame for which data is desired and spreadsheets containing an array of hourly climatic data are sent to the user via email. The user may sift through and utilize any data of interest such as dew point, relative humidity, atmospheric pressure, visibility, wind speed, wind direction, etc. Wind speed and corresponding direction were manually extracted from the dataset and placed into blank Excel spreadsheets formatted for later access by MATLAB.

Field Monitoring Station

A Field Monitoring Station (FMS) was designed, constructed, and deployed as part of the present research effort (Smith 2010). The sign chosen for monitoring in the present study was WisDOT S-40-703 and it is a cantilevered mono-tube mast-arm structure. This structure represents the typical mast-arm-pole support structure configuration found in Wisconsin. The sign is located in Milwaukee, Wisconsin just south of the intersection of Walnut Street and Fond du Lac Avenue. This is an urban area that is relatively free of wind-stream obstructions in the immediate vicinity, yet is still in the midst of buildings, overpasses and a varying topographical gradient. This location was ideal due to its proximity to the Marquette University campus. An aerial view of the sign and FMS location is provided in Figure 2.2.

The field monitoring system (FMS) provided two functions. First, it collected bi-axial bending strain data using eight Vishay Micromeasurements 350-ohm weldable strain gages mounted to the sign at four diametrically opposite locations (top, bottom and both sides). Second, it collected wind speed and corresponding direction using a Gill Windsonic 2D sonic anemometer mounted to an aluminum weather station tower. The overall anemometer height is approximately 33 feet (10 meters) above the ground with respect to the base elevation of S-40-703. Also mounted on the weather station tower was a solar panel for battery charging, an enclosure for a marine battery and solar power regulator, and an enclosure for data acquisition software and hardware. A National Instruments (NI) CompactRIO data acquisition hardware chassis and National Instruments 9237 full-bridge conditioning card, operated through LabVIEW, made up the data acquisition system (Smith 2010).

The FMS was deployed in October 2009 and was operational between March 12, 2010 and November 24, 2010. However, wind data is only available between March 12, 2010 and September 5, 2010 due to a loss of anemometer functionality for unknown reasons on September 6, 2010. The Gill anemometer used as part of the FMS was capable of a sampling rate of 4 Hz. The manufacturer rates the accuracy of velocity at +/- 2% and the accuracy of direction at +/- 3 degrees. Given the present research focus, it should be noted that the readings of the anemometer used in this study were validated using wind tunnel experimentation (Smith 2010). A single 24-hour period results in the FMS producing data files containing wind and strain

information with sizes of approximately 45 Mb. Consequently, weekly visits to the FMS were necessary to collect data and free-up memory on the NI system in order to avoid overwriting of data. A more detailed discussion of the chosen sign, FMS components as well as data validation techniques of the data acquisition hardware and software deployed can be found elsewhere (Smith 2010).

2.3 Wind Data Syntheses

There is a tremendous amount of wind speed and wind direction data that was synthesized as part of the present research effort. Data from two sources was digested. The first was the NCDC-ASOS sites. This data was used to formulate probabilities suitable for the reliability-analysis procedure developed. This included formulation and evaluation of an interpolation procedure for wind speed and wind direction combined probability models. The second data source was the FMS site deployed during the research effort. This data was used to evaluate topological effects at locations where sign structures are likely installed when compared to those locations where the data was collected (*e.g.* NCDC-ASOS sites). The FMS site data was also used to evaluate the interpolation procedure developed. This section outlines the wind data synthesis conducted as part of the present research effort. The present sections provide an overview of the synthesis process for wind modeling and further details can be found elsewhere (Diekfuss 2013).

NCDC-ASOS Wind Data Synthesis

The NCDC wind data collected was manipulated into a form suitable for subsequent statistical analysis. A two-minute averaged wind speed is one of many recorded parameters provided by NCDC-ASOS weather stations. This two-minute averaged wind speed is updated once every five seconds and reported to the database once per hour (ASOS 1998). This means that once, every hour, a two-minute averaged wind speed (and its corresponding direction) is extracted from the station and documented as the two-minute wind data for that hour. The value is representative of only the two minutes of time that contributed to the reported average. No additional information is given by the database of record between the hourly readings. Therefore, in order to obtain a pseudo-contiguous record of wind speed and corresponding direction over an extended period of time, extrapolation of this two-minute averaged wind speed, over its respective hour, is necessary.

It is prudent to provide discussion with regard to how the extrapolation procedure was conducted. With the mindset of performing a subsequent reliability study involving the fatigue evaluation of these structures and with the goal of obtaining accumulated damage caused by fatigue, it was felt that one-hour averaged wind speeds would be more appropriate than two-minute averaged wind speeds. Also, a single two-minute averaged wind speed was going to be used to represent an entire hour and this required that the averaging time be adjusted to an hourly average. In this way, a pseudo-contiguous dataset of hourly wind speeds could be generated. The concession made, however, is that a two-minute averaged wind speed is converted and used to represent one hour of time. The available data necessitated this concession. However, the quality of this

data when compared to contiguous data obtained from the FMS site indicates that this concession does not sacrifice accuracy and usefulness of the wind modeling procedure proposed.

It is widely known that averaging time has a direct impact on the magnitude of averaged wind speed. In general, as averaging time increases, the resulting averaged wind speed decreases (Simiu and Scanlon 1996). The extent to which various averaging times affect the magnitude of the resulting averaged wind speed can be quantified through the use of the Durst Curve shown in Figure 2.3. This curve allows a wind speed magnitude of one averaging time to be adjusted (converted) to the corresponding magnitude for a different averaging time. The curve provides ratios of specified averaged wind speed magnitude to its equivalent one-hour averaged wind speed magnitude.

For example, consider a two-minute averaged wind speed having a magnitude of 10 mph. The averaging time for this wind speed corresponds to a value of t in Figure 2.3 equal to two minutes or 120 seconds ($U_{120} = 10$). Converting this wind speed magnitude averaging time to that of one-hour (3,600 seconds) is performed as follows;

$$\frac{U_{120}}{U_{3,600}} = 1.175 \quad \text{(taken from Figure 2.3)}$$

$$U_{3,600} = \frac{U_{120}}{1.175} = \frac{10}{1.175} = 8.51 \ \ mph$$

Adjusting the averaging time from two minutes to one hour clearly reduces the magnitude of the averaged wind speed. All two-minute averaged wind speeds taken from the NCDC-ASOS site records were converted to one-hour averaged magnitude wind speeds as the first step in the NCDC-ASOS wind data synthesis.

There were a number of cases where the wind speed magnitude reported in the NCDC-ASOS database was very small such that a wind direction could not be defined in the weather data. In these cases, a placeholder in the data report was found (*e.g.* ***) in the database in lieu of a numerical value. All entries containing this placeholder for the wind direction, as well as its corresponding wind speed, were set equal to zero in the present synthesis. There were other instances where the wind speed was very small, but a wind direction was specified. Wind directions corresponding to very small wind speeds were considered unreliable. All wind speeds of 2.5 mph or less and their accompanying directions were set equal to zero in the present synthesis. The lower limit of 2.5 mph was chosen because it is the value of the lower limit on the 5 mph bin of values described later in this section. It was important to preserve these “zero entries” so that an accurate total number of wind speed data entries could be used when determining probabilities of occurrence for wind speed and direction. Approximately 17% of all data entries obtained from the NCDC database were manually set equal to zero and preserved for later synthesis (*i.e.* 161,769 “zero entries” out of 959,399 total wind data entries contained in the synthesis).

A schematic example illustrating the adjustment of NCDC-ASOS wind speed data from two-minute averaging to one-hour averaging time up to this point in the discussion is provided in Figure 2.4. This figure illustrates that the single value of two-minute averaged wind speed recorded every hour is converted (essentially reduced) to a one-hour averaged wind speed. This one-hour averaged wind speed is assumed to exist for the entire sixty-minute period for which the original two-minute averaged wind speed was recorded.

MATLAB programs created and used in previous research efforts (Foley et al. 2004; Foley et al. 2008; Smith 2010) were modified and utilized as the basis for the present synthesis procedures. It should be noted that all MATLAB programs used for the synthesis of the NCDC-ASOS wind data conducted in the present study are available (Diekfuss 2013).

Wind speed and wind direction was first collected from the raw NCDC dataset. The wind speed data was then identified as being from a non-applicable direction (if appropriate). The non-applicable (na) direction was used to signify a wind speed with very small or zero magnitude. The wind speed magnitudes were then aggregated into 5 mph bins. Each bin included wind speeds 2.5 mph above and below the bin designation (*e.g.* the 5 mph bin included wind speeds with magnitudes 2.5 mph through 7.5 mph). Two binning methods for direction were applied. The first method bins wind directions into one of the eight cardinal directions (N, NE, E, SE, S, SW, W and NW) or the “na” direction. The second method bins wind directions into a ten degree resolution providing higher resolution taxonomy of wind directions.

FMS Site Wind Data Synthesis

The FMS site data acquisition system had a 4 Hz data acquisition rate. Therefore, the compactRIO DAQ system collected ten strain values (five strain values pertaining to bending about the horizontal axis and five strain values pertaining to bending about the vertical axis), one wind speed value and one corresponding wind direction value four times every second that the FMS was in operation. This was an important component of the present research effort. The simultaneous collection of mast-arm bending strain, and wind information causing that bending strain, provides an ability to verify finite element models and formulate modeling error uncertainty models as discussed later in this report. In order to do this, however, the FMS wind data needed to be synthesized into one-hour averages. The process by which data synthesis was conducted for the FMS is now described.

The 4 Hz raw data set from the FMS was decimated into one-hour averages by selecting consecutive strings of 14,400 contiguous values at a time (1 hr x 60 min/hr x 60 sec/min x 4 samples/sec = 14,400 samples) and computing their average. This process results in contiguous one-hour averaged wind speeds and strain magnitudes for the entire time the FMS was in operation.

The wind direction was synthesized in a slightly more complicated manner than the wind speed and strain. This resulted from the circular nature of wind direction reported in the data acquisition system. An explanation of this synthesis can be provided within the context of an example. Consider the following eight wind directions (in degrees from true north) reported via the data acquisition system:

357 | 358 | 359 | 360 | 0 | 1 | 2 | 3

These readings from the data acquisition system all represent a direction that is essentially true north. However, the average of the numbers would give 180 degrees (representing true south). Each wind direction was considered a unit vector broken down into *x*- and *y*-components using direction cosines. After breaking the wind directions into their components, averages of the components were calculated. Finally, the average *x*-component and average *y*-component for the one hour period was identified. These components were then used to define the one-hour averaged wind direction.

Unlike the NCDC-ASOS wind data, the FMS data set had no occurrences where a resulting one-hour averaged wind speed did not have an accompanying direction value. Moreover, there were no occurrences where a one-hour average of "0" was found for either wind speed or wind direction. However, there were a relatively small number of instances (453 entries out of a total of 4,069 entries – approximately 11% of total) where the anemometer provided a value of "999.99" for both wind speed and direction at a particular point in time. A wind speed of approximately 1,000 mph and a wind direction of approximately 1,000 degrees did not make sense. Therefore, the research team decided to manually set these values equal to zero before the data synthesis was carried out. It was felt that clearly inaccurate readings would generate error in the data set.

After the entire averaging process was completed, one last step was taken to ensure the datasets obtained from both the FMS and the NCDC-ASOS sites were of equivalent form. This last step was necessary because the FMS measured wind direction in a one-degree resolution while the NCDC-ASOS sites recorded wind direction in a ten-degree resolution. Therefore, prior to synthesizing the averaged FMS data into direction specific bins, all wind directions were rounded to the nearest ten-degree increment. As an example, wind directions from 5 degrees through 14 degrees were defined as being from the 10 degree direction.

The synthesis procedures conducted for the dataset obtained at the FMS site is schematically summarized in Figure 2.5. The figure illustrates the near-contiguous wind speed data stream and the dots represent the magnitude of the one-hour averages. A comparison between Figures 2.4 and 2.5 illustrates the difference between the formats of the data as they were collected, and the procedures utilized for their respective wind speed syntheses. The field monitoring system provided wind speed and wind direction data samples at 4 Hz. This allowed 14,400 readings to be averaged each hour and thus, generates a more representative string of one-hour averaged wind speeds than the ASOS site data. The FMS data synthesis conducted as described led to wind data that was suitable for final synthesis in the same manner as the NCDC-ASOS data. Further details

regarding the data synthesis including the algorithms and programs used can be found elsewhere (Diekfuss 2013).

Statistical Analysis

The synthesized data for each NCDC-ASOS site and the FMS site were used to assemble individual probabilities of one-hour averaged wind speed and one-hour averaged wind direction events. From this point forward, one-hour averaged wind speed and one-hour averaged wind direction will be referred to as wind speed and wind direction, respectively. The mean wind speed, *U*, and mean wind direction, *D*, are both initially assumed to be continuous random variables with the following sample spaces;

Wind Speed: $\{0\ mph \le U \le \infty\ mph\}$

Wind Direction: $\{0\ \text{deg.} \le D \le 360\ \text{deg.}\}$

However, by virtue of the synthesis procedures carried out previously, wind speed and wind direction are discrete random variables. The data synthesis procedures employed result in individual probabilities for wind speed, individual probabilities for wind direction, conditional probabilities for wind speed *given* wind direction and combined (*i.e.* intersecting) probabilities of wind speed *and* wind direction.

The individual probabilities for wind speed are computed using the synthesized wind speed data and the following,

$$P(U = u_i) = \frac{N_{u_i}}{N_{speed}} \qquad u_i \in \{5,10,15,\ldots,70,75,80\} \tag{2.2}$$

where: N_{u_i} is the number of one-hour averaged wind speed u_i occurrences; N_{speed} is the total number of one-hour averaged wind speeds; u_i is a one-hour wind speed (mph) in 5-mph increments. The individual probabilities for wind direction are computed using the synthesized wind direction data and the following,

$$P(D = d_j) = \frac{N_{d_j}}{N_{direct}} \qquad d_j \in \{0,10,20,30\ldots,340,350,360\} \tag{2.3}$$

if the 10-degree resolution binning procedure is used. If the eight cardinal directions are used in the binning procedure, the probabilities are computed using,

$$P(D = d_j) = \frac{N_{d_j}}{N_{direct}} \qquad d_j \in \{N, NE, E, SE, S, SW, W, NW\} \tag{2.4}$$

The total number of wind speed directions, N_{direct}, depends upon the binning procedure used and N_{d_j} is the number of occurrences for one-hour averaged wind direction d_j.

The resulting individual probabilities of one-hour averaged wind speed and one-hour averaged wind direction using the two binning procedures for the seven Wisconsin cities and the Field Monitoring Station

are provided in Tables 2.2 through 2.9. The data indicates that measured one-hour averaged wind speeds are below 50 mph in all cities with the exception of one reading of 55 mph at the Green Bay ASOS site. All NCDC-ASOS wind data that had 0-degree directions and those with wind speeds less than 2.5 mph were assigned as "N/A" in the cardinal direction tables. As a result, "0-degree" wind directions in the 10-degree binning data tables and the "N/A" data in the cardinal direction data tables were discarded in the probability analysis.

Histograms for wind speed and wind-rose histograms for wind direction for all NCDC-ASOS sites and the FMS site are provided in Figures 2.6 and 2.7. The one-hour averaged wind speed probability mass functions (histograms) appear to have very common shapes throughout all locations indicating similar distribution of one-hour averaged wind speeds. There is some difference at the FMS site where wind speeds with one-hour averaged speeds are clustered with apparently less variability about the 5-mph magnitude wind speed. The data from the 10-degree direction binning procedure displayed in the wind-rose histograms illustrates that there is some preferred direction winds in La Crosse, Madison, Green Bay, and Oshkosh. A more uniform distribution of wind direction exists in Milwaukee, Eau Claire, and Wisconsin Rapids. The cardinal direction binning procedure appears to maintain the probabilities of these preferred directions.

The random variables of wind speed and direction (in Wisconsin) have been shown to be statistically dependent upon one another (Ginal 2003). Therefore, probability theory dictates that the probability of their intersection (*i.e.* their combined probability) must be determined using,

$$P\left(U = u_i \cap D = d_j\right) = P\left(D = d_j\right) \cdot P\left(U = u_i \middle| D = d_j\right) \tag{2.5}$$

The conditional probability (*i.e.* probability of a one-hour averaged wind speed *given* a one-hour averaged direction) is computed using,

$$P\left(U = u_i \middle| D = d_j\right) = \frac{N'_{u_i}}{N_{d_j}} \tag{2.6}$$

where N'_{u_i} is the total number of one-hour average wind speeds with magnitude u_i that have one-hour averaged direction d_j and N_{d_j} is the total number of occurrences of one-hour averaged wind direction d_j.

The conditional probabilities for wind speed given direction used in the application of equation (2.1) are provided in Tables 2.10 through 2.17 for the NCDC-ASOS and FMS sites. Cardinal directions are used in the preparation of the tables and wind speeds from 0 mph to 80 mph are considered. It should be noted that there were zero occurrences of one-hour averaged wind speeds greater than 55 mph. Also, the probability of one-hour averaged wind speeds greater than 35 mph are very, very small at all locations considered and for all cardinal directions.

Figure 2.8 provides probability mass functions (*i.e.* histograms) of one-hour averaged wind speeds given one of each of the eight cardinal directions at all NCDC-ASOS sites and the Milwaukee FMS site. The wind speed probability distributions given each of the cardinal directions are relatively consistent across all locations considered in the study. This suggests that it may be possible to use a single lognormal random variable model for one-hour averaged wind speeds from each cardinal direction and for all cities in Wisconsin. In other words, once a direction is defined, it will have a corresponding random variable model for one-hour averaged wind speed. This model, given the direction, can then be used for any city within the State.

The combined probabilities computed using equation (2.5) are found in Tables 2.18 through 2.25 for the seven ASOS sites and the Milwaukee FMS site. Each of the eight cardinal directions is represented. Probability mass functions (histograms) for these sites are found in Figure 2.9. The data in Tables 2.18 through 2.24 serve as the basis for the probability models for wind speed and direction at locations throughout Wisconsin.

Dataset Length and Topography Effects

The field monitoring station data provided the research team with the opportunity to evaluate the impact of the length of the data record used in evaluating wind speeds and directions and also the effects of topography at locations where sign support structures are likely to be in service when compared to locations where wind speed data is likely to come from (*i.e.* the NCDC-ASOS sites).

Three datasets were isolated for a detailed comparison. Two datasets from the Mitchell International Airport NCDC-ASOS site were considered. The first was composed of hourly weather data records for all years indicated in Table 2.1 and is signified by Milwaukee (1998-2011). The second includes data for the time period in which the FMS was in service and is signified by Milwaukee (2010). The last of the three datasets was that obtained from the field monitoring station identified by FMS. The probability mass functions for the natural wind speed data are shown in Figure 2.10 and the wind rose histograms for the natural wind direction data are shown in Figure 2.11.

The histograms in Figure 2.10 indicate a very similar distribution of wind speeds. The mean wind speed and standard deviation for the Milwaukee (1998-2011) data and the data in the 6-month sampling window Milwaukee (2010) are very similar to one another. This indicates that in just six months, a reasonable estimate for wind speed and direction variability can be approximated. However, it is recommended to use longer sampling periods to improve the model and provide the most accurate distributions of wind speed. The magnitude of the most frequently occurring wind speed at the field monitoring site is slightly less than the

magnitude of the most frequently occurring wind speed at the NCDC-ASOS site. There is also a slightly smaller standard deviation in the sample data for the field monitored site.

The wind rose histograms shown in Figure 2.11 illustrate that while the Milwaukee (2010) data tends to have larger peaks at some 10-degree orientations, the fundamental shape of the wind rose remains consistent. It is expected that if more data were collected at the FMS site, the wind roses with 10-degree resolutions would approach a similar configuration. When the eight cardinal directions are utilized, the wind roses take on slightly different shapes. The peaks and valleys seen in the 10-degree resolution wind roses are softened in favor of a more egalitarian distribution of wind directions among the eight possibilities.

It is widely known that topography has an effect on wind speed and direction. Design provisions (ASCE 2005) require that topographical conditions be considered. Exposure categories with unique surface roughness characteristics have been defined to differentiate between flat, open terrain as seen at airports (Surface Roughness C) and that of terrain with many, closely spaced obstructions as seen in urban and suburban areas (Surface Roughness B). Site topologies for all sites considered in the present study are provided in Figure 2.12. The two sites considered in the present discussion are located at the top of Figure 2.12. The variation in topography among the FMS and ASOS sites is significant (as expected).

The differences in what is seen between the wind speed probability mass functions shown in Figure 2.10 and 2.11 can be evaluated by looking at them in conjunction with Figure 2.12. The apparently open grassy area in the middle of a city (Figure 2.2) has significantly different topography when compared to NCDC-ASOS sites that are often located at airports. Figure 2.12 clearly indicates that the FMS site does not have the same surrounding topology as the NCDC-ASOS site at Mitchell International Airport (or any of the NCDC-ASOS sites) and therefore, differences are expected in the wind speed magnitude and direction. It is clear that locations where sign structures are typically in service (*e.g.* FMS site) will likely experience lower wind speed magnitudes and slightly altered directions when compared to locations where wind speed data is typically collected (*e.g.* NCDC-ASOS sites).

The preceding discussion clearly demonstrates that sample size has a small effect on wind speed distribution and a small effect on distribution of wind directions. It appears that site topography has a greater impact on wind speed distribution and wind speed direction, but it is not significant. Wind speed distributions at a local site where a sign structure is in service will likely have a lower mean wind speed than the location where the wind speed data will be obtained (*i.e.* the ASOS site). Furthermore, wind directions will not differ significantly from the location where the sign is in service when compared to the location where data is obtained.

The comparison between these three sample datasets was continued by looking at both conditional and combined probabilities in the form of probability mass functions. Figures 2.13 and 2.14 illustrate the variation among each of the designated cardinal directions for conditional and combined probabilities, respectively. Overall, the shapes of the probability mass functions for each type of probability and for each designated direction look very similar between the three sample datasets. Means and standard deviations in the datasets were provided in Figure 2.10. The distribution of wind speed given cardinal direction is consistent among all data sets. There is an expected variation in most frequently occurring wind speeds expected as a result of the topography difference.

All statistical analysis regarding wind speed and direction variability has been conducted and the results have been synthesized into the form of combined probabilities for wind speed and wind direction. It is essential to note that the information provided thus far is specific to the discrete locations where either NCDC-ASOS stations or the FMS measured the wind data. With the exception of the FMS, all of the sites where wind data was obtained are at some distance away from surrounding sign support structures. If the goal is to determine what the wind demand uncertainty is at some location where a sign support structure exists, then a major question arises. Which table of combined probabilities should be used when the sign structure location of interest is remote from the locations of measured data? Should the combined probabilities from the closest NCDC-ASOS site be used, or perhaps, should the combined probabilities from multiple surrounding NCDC-ASOS sites be used? The following section and discussion will answer these questions.

2.4 Virtual Weather Station Probabilistic Model

This section seeks to present a methodology for creating tables of combined probabilities of wind speed and wind direction at locations away from NCDC-ASOS sites where data regarding wind speed and wind direction will be monitored and assembled. Previous research in the pavement arena has led to the development of an interpolation method used for determining climatic parameters at desired locations where such parameters are not measured. A version of this procedure has been presented in a paper by (Diekfuss and Foley 2012). Since the presentation of this paper, modifications have been made to the model and will be addressed in the subsequent sections.

The Enhanced Integrated Climatic Model (EICM) contained within the Mechanistic-Empirical Pavement Design Guide (MEPDG) provides users the ability to generate a virtual weather station (VWS) using selected data from automated weather stations (AWS) in surrounding areas (*i.e.* ASOS stations). The interpolation method establishes weights for the climatic parameters of a particular AWS based upon the distance it is away from the VWS being generated (Li et al. 2010),

$$U_m = \frac{\sum_{k=1}^{n}\left(\frac{U_{mk}}{R_k}\right)}{\sum_{k=1}^{n}\left(\frac{1}{R_k}\right)} \tag{2.7}$$

where: U_m is the calculated virtual weather data element (*e.g.* mean wind speed, wind speed standard deviation) for day *m*; *n* is the number of weather stations for VWS interpolation; U_{mk} is the value of a data element on day *m* for weather station *k*; and R_k is the distance of weather station *k* from the virtual weather station. It was recommended that certain weather stations be omitted if they had surrounding topography that was much different than that expected at the VWS being generated, even if they are closer in proximity to the VWS than others (Li et al. 2010). Because the contributing combined probabilities of wind speed and wind direction are limited to the locations where wind data is collected (*i.e.* NCDC-ASOS sites) and since the sites where data is collected clearly does not have similar site topography/topology, this recommendation is ignored in the subsequent interpolation computations.

The results of the synthesis of wind data up to this point has yielded combined probabilities of wind speed and wind direction at several discrete locations around the state of Wisconsin. In order to make the interpolation procedure given in equation (2.7) applicable in the present research effort, it needed to be modified to reflect the interpolation of combined probabilities rather than climatic parameters. Therefore, the combined probabilities of wind speed and wind direction at any remote location within Wisconsin can be determined using,

$$P(U = u_i \cap D = d_j)_m = \frac{\sum_{k=1}^{n}\left(\frac{P(U = u_i \cap D = d_j)_k}{R_k}\right)}{\sum_{k=1}^{n}\left(\frac{1}{R_k}\right)} \tag{2.8}$$

where: $P(U = u_i \cap D = d_j)_m$ is a table of interpolated combined probabilities of wind speed and direction for remote location *m*; *n* is the number of weather stations used in the VWS interpolation; $P(U = u_i \cap D = d_j)_k$ is the table of combined probabilities from NCDC-ASOS site *k*; and R_k is the distance of NCDC-ASOS site *k* from remote location *m*.

Prior to implementing the MEPDG interpolation method, a systematic method to determine the vector distances between the ASOS sites and potential VWS sites needed to be defined. The distances utilized in this procedure were determined using the latitude and longitude coordinates from each ASOS site. In order to provide the most accurate measure of distance between the potential VWS and each of the NCDC-ASOS sites used for interpolation, consideration was given to the fact that the earth is spherical (approximately) in nature. Therefore, curvature must be accounted for in the distance measurement. The following section will describe

the procedure used to determine the vector distances between the NCDC-ASOS sites and a potential VWS site within the context of an example.

Consider an example VWS site located northeast of the Wisconsin Rapids NCDC-ASOS site. Figure 2.15 shows a map of Wisconsin that provides the latitude and longitude coordinates for each ASOS site, as well as the resulting vector distance for each ASOS site from the example VWS site. The concept of the VWS is shown on the figure as well. Equation (2.8) implies a procedure whereby a user can define the number and relative distance for the ASOS stations used in the interpolation of wind speed combined probability data. In other words, the user can define the ASOS sites and their vector distances to be used in the interpolation.

The distance between any two points on the earth's surface is not a straight line, but rather a great-circle distance (Type 2012). Therefore, the spherical law of cosines is employed to account for the curvature of the earth,

$$R_k = R_E \cdot \cos^{-1}\left(\sin\left(Lat_{VWS}\right)\cdot\sin\left(Lat_{ASOSk}\right)+\cos\left(Lat_{VWS}\right)\cdot\cos\left(Lat_{ASOSk}\right)\cdot\cos\left(Lon_{ASOSk}-Lon_{VWS}\right)\right) \qquad (2.9)$$

where: R_E is the earth's radius (approximated as 3,693 miles); Lat_{VWS} and Lon_{VWS} are the latitude and longitude coordinates (in radians) for the VWS site, respectively; and Lat_{ASOSk} and Lon_{ASOSk} are the latitude and longitude coordinates (in radians) for NCDC-ASOS site *k*, respectively. This procedure has two very important assumptions:

1.) The earth is assumed to be a perfect sphere when in fact it is slightly ellipsoidal;
2.) The end points, between which distance is determined, are assumed to be at an equal distance from the center of the spherical earth (*i.e*. there is no account for change in elevation between two points).

The VWS interpolation procedure was assessed using combined probability tables of wind speed and wind direction (Tables 2.18 through 2.24) and the interpolation model of equation (2.8). The ability for the interpolation model to reproduce ASOS site probability distributions was evaluated using two interpolation cases:

Case 1 Application of the VWS procedure utilizing the combined probability table from the single closest ASOS site to that where wind speed distributions are needed.

Case 2 Application of the VWS procedure utilizing the combined probability tables from all ASOS sites surrounding the location to that where wind speed distributions are needed.

Case 1 can be thought of as using the combined probabilities of the closest NCDC-ASOS site regardless of the actual distance between the remote location and the location where the data was measured. Case 2 can be thought of as using all ASOS wind speed data available in the interpolation.

Figures 2.16 through 2.22 provide combined probability distributions for each ASOS site using the two interpolation cases. Figure 2.15 contains radial distances among all ASOS sites. When one considers

application of interpolation Case 1, the Milwaukee ASOS site data is interpolated using the Madison ASOS data (radial distance from MKE to MSN is 73.95 miles). When one considers application of interpolation Case 2, data from all 6 other ASOS sites (excluding Milwaukee) is used. Each of the interpolation cases works reasonably well at reproducing ASOS site data and differences among the combined wind speed probability distributions is acceptable. It should be noted that the interpolation process included in the generation of these figures includes ASOS sites where the topography is relatively consistent with one another (*i.e.* all are airport sites). Some cardinal directions include more significant differences in the wind speed probability distributions at some ASOS sites in the lower one-hour averaged wind speed magnitudes (*e.g.* Eau Claire – southeast; Green Bay – west), but overall the procedure works very well.

The interpolation procedure is intended to be able to generate combined probability distributions for a site remotely located away from those where data is acquired (*e.g.* an ASOS site). Thus, both interpolation cases were applied to the FMS site in Milwaukee using the NCDC-ASOS site data. The FMS site recorded wind speed data for six months and this data allows the interpolation procedure to be evaluated for a site where data has been acquired, but is not an ASOS site. It should be emphasized that the FMS site has significantly different topography when compared to the sites from which the interpolated data originates (ASOS sites).

Figure 2.23 contains probability mass functions for the two interpolation cases applied to the field monitoring station. Interpolation Case 1 uses the Milwaukee ASOS site as it is the closest to the field monitoring station. Interpolation Case 2 uses all ASOS sites considered in this study. The probability mass functions (*i.e.* histograms) in Figure 2.23 illustrate that the interpolated combined probabilities tend to provide greater wind speed density at higher wind speed magnitudes than was measured at the FMS site. From a fatigue life characterization point of view, this should not be a problem because providing greater probability density at higher wind speed magnitudes than will actually occur can be thought of as a conservative estimate for wind speed demand. Thus, the VWS procedure proposed is suitable for generating the foundational wind speed probability models at a site where a sign structure is located. Figures 2.10 through 2.14 indicate that local topology effects should be considered, but the interpolation process yields conservative results for the uses proposed in this study.

2.5 Conclusions and Recommendations

A process through which wind speed and direction data was collected, synthesized and statistically analyzed has been described. Individual, conditional, and combined probabilities of one-hour averaged wind speed and one-hour averaged wind direction have been computed for discrete locations throughout the state of Wisconsin and at a field monitoring station designed, constructed and deployed as part of the present research effort. An interpolation procedure which allows for the computation of combined probabilities at any location throughout the state of Wisconsin has been presented.

A comparison between NCDC-ASOS site data for Milwaukee, Wisconsin and the data acquired at the FMS site indicates that local topography has a significant impact on mean one-hour average wind speed and one-hour wind speed standard deviation and a minor effect on wind direction. A lower mean and standard deviation in the wind speed appears to occur when the sign support structure site is in urban and suburban terrain compared to flat, open terrain like that found at airport ASOS sites. Therefore, use of ASOS sites will result in higher mean wind speeds and likely greater wind loading demand (from a fatigue point of view) than what will likely occur at a typical sign structure site.

An interpolation procedure for wind speed probability distributions for each of eight cardinal directions was evaluated using NCDC-ASOS site data and the FMS site data. This evaluation indicated that when interpolating combined probability distributions computed from wind speed and direction statistics gathered from NCDC-ASOS sites, the combined probability distributions in each of the eight cardinal directions appear to be conservative. Greater density of higher wind speed magnitudes result when the interpolation procedure is implemented. The wind speed variability is also likely to be slightly larger than the variability that can be expected at the sign structure location. It should be noted that these results are based upon comparisons to data collected from a single FMS site, one that is located in an urban environment.

The synthesis of wind speed data conducted indicates that because sign support structures typically exist at locations that are remote from where wind data is measured (*i.e.* NCDC-ASOS sites), there is a need to develop a rational methodology for including topographical effects. It is recommended that additional field monitoring systems be deployed throughout the state at locations resembling similar site conditions as those typically found near sign support structures in areas that are less densely populated than those found at major cities (*e.g.* Milwaukee). This would allow further evaluation, confirmation and modification of the interpolation procedure proposed in this chapter so that combined probabilities of wind speed and wind direction can be accurately computed throughout the State. This would allow much greater understanding of the impact of topography and would facilitate modifications to the interpolation procedure that allow topography to be better incorporated in the procedure.

2.6 References

ASCE (1998). *Minimum Design Loads for Buildings and Other Structures (ASCE 7-98)*, American Society of Civil Engineers, Reston, VA.

ASCE (2005). *Minimum Design Loads for Buildings and Other Structures (ASCE 7-05)*, American Society of Civil Engineers, Reston, VA.

ASOS (1998). "Automated Surface Observing System User's Guide."

Diekfuss, J. A. (2013). "Reliability-Based Fatigue Assessment of Mast-Arm Sign Support Structures."PhD Thesis, Marquette University, Milwaukee, WI.

Diekfuss, J. A., and Foley, C. M. "Probabilistic Wind Model for Reliability-Based Fatigue Evaluation of Sign Support Structures." *Proc., 3rd International Structural Specialty Conference*, Canadian Society of Civil Engineers, (CD-ROM).

Edwards, J. A., and Bingham, W. L. (1984). "Deflection Criteria for Wind Induced Vibrations in Cantilever Highway Sign Structures." Center for Transportation Engineering Studies, North Carolina State University, Rayleigh, NC, 124.

Ellingwood, B. R., and Tekie, P. B. (1999). "Wind Load Statistics for Probability-Based Structural Design." *Journal of Structural Engineering*, 125(4), 453-463.

Foley, C. M., Ginal, S. J., Peronto, J. L., and Fournelle, R. A. (2004). "Structural Analysis of Sign Bridge Structures and Luminaire Supports." Wisconsin Highway Research Program, Madison, WI.

Foley, C. M., Wan, B., Weglarz, M., Hellenthal, M., Komp, J., Smith, A., and Schmidt, J. P. (2008). "Fatigue Risks in the Connections of Sign Support Structures - Phase 1." Wisconsin Highway Research Program, Wisconsin Department of Transportation.

Ginal, S. J. (2003). "Fatigue Performance of Full-Span Sign Support Structures Considering Truck-Induced Gust and Natural Wind Pressures."MS Thesis, Marquette University, Milwaukee, WI.

Hosch, I., and Fouad, F. "Fatigue Design of Sign Support Structures for Natural Wind Loads." *Proc., Proceedings of the 88th Transportation Research Board*.

Kaczinski, M. R., Dexter, R. J., and Van Dien, J. P. (1998). "Fatigue Resistance Design of Cantilevered Signal, Sign and Light Supports." ATLSS Engineering Research Center, Bethlehem, PA.

Li, Q., Wang, K. C. P., and Hall, K. D. (2010). "Verification of Virtual Climatic Data in MEPDG Using the LTPP Database." *International Journal of Pavement Research and Technology*, 3(1), 10-15.

Li, X., Whalen, T. M., and Bowman, M. D. (2005). "Fatigue Strength and Evaluation of Double-Mast Arm Cantilevered Sign Structures." *Transportation Research Record, Journal of the Transportation Research Board, No. 1928 - Design of Structures 2005*, 64-72.

McDonald, J. R., Mehta, K. C., Oler, W., and Pulipaka, N. (1995). "Wind Load Effects on Signs, Luminaires and Traffic Signal Structures." Wind Engineering Research Center - Texas Tech University, Lubbock, TX.

Ocel, J. M., Dexter, R. J., and Hajjar, J. F. (2006). "Fatigue-Resistant Design for Overhead Signs, Mast-Arm Signal Poles, and Lighting Standards." Minnesota Department of Transportation, St. Paul, MN, 190 pages.

Peterka, J. A. (1992). "Improved Extreme Wind Prediction for the United States." *Journal of Wind Engineering and Industrial Aerodynamics*, 533-541.

Peterka, J. A., and Shahid, S. (1998). "Design Gust Wind Speeds in the United States." *Journal of Structural Engineering*, 124(2), 207-214.

Simiu, E., Changery, M. J., and Filliben, J. J. (1980). "Extreme Wind Speeds at 129 Airport Stations." *Journal of the Structural Division*, 106, 801-817.

Simiu, E., and Scanlon, R. H. (1996). *Wind Effects on Structures: Fundamentals and Applications to Design - 3rd Edition*, John Wiley & Sons, Inc., New York, NY.

Simiu, E., Wilcox, R., Sadek, F., and Filliben, J. J. (2003). "Wind Speeds in ASCE 7 Standard Peak-Gust Map: Assessment." *Journal of Structural Engineering*, 129(4), 427-439.

Smith, A. D. (2010). "Real-Time Health Monitoring System for Mast-Arm Sign Support Structures."MS Thesis, Marquette University, Milwaukee, WI.

South, J. (1994). "Fatigue Analysis of Overhead Sign and Signal Structures." Illinois Department of Transportation, Springfield, IL.

Type, M. (2012). "Movable Type Scripts." <http://www.movable-type.co.uk/scripts/latlong.html>. (May 24, 2012).

Table 2.1 Cities used for NCDC wind speed and direction data collection.

City	WBAN #	Location	Years	Data Collection Years
Green Bay	14898	Austin Straubel International Airport	14	Jan. 1998 – Dec. 2011
La Crosse	14920	La Crosse Municipal Airport	14	Jan. 1998 – Dec. 2011
Eau Claire	14991	Eau Claire Regional Airport	14	Jan. 1998 – Dec. 2011
Madison	14837	Dane County Regional Airport	14	Jan. 1998 – Dec. 2011
Milwaukee	14839	Mitchell International Airport	14	Jan. 1998 – Dec. 2011
Oshkosh	94855	Oshkosh Wittman Airport	14	Jan. 1998 – Dec. 2011
Wisconsin Rapids	04826	Wisconsin Rapids Alexander Field	14	Jan. 1998 – Dec. 2011

Table 2.2 Probabilities for Milwaukee NCDC-ASOS site.

Individual Probabilities for Wind Speed – P ($U = u_i$)

One-Hour Averaged Wind Speed (mph)	Frequency of Occurrence	Probability of Occurrence	Probability of Occurrence (%)
0	14723	0.1006	10.06
5	53430	0.3651	36.51
10	52186	0.3566	35.66
15	20726	0.1416	14.16
20	4826	0.0330	3.30
25	385	0.0026	0.26
30	50	0.0003	0.03
35	15	0.0001	0.01
40	0	0.0000	0.00
45	1	0.0000	0.00
50	0	0.0000	0.00
55	0	0.0000	0.00
60	0	0.0000	0.00
65	0	0.0000	0.00
70	0	0.0000	0.00
75	0	0.0000	0.00
80	0	0.0000	0.00
SUM	**146342**	**1.0000**	**100.00**

Individual Probabilities for Wind Direction – P ($D = d_j$) (by cardinal direction)

One-Hour Averaged Wind Direction	Frequency of Occurrence	Probability of Occurrence	Probability of Occurrence (%)
N/A	14723	0.1006	10.06
North	14808	0.1012	10.12
Northeast	13809	0.0944	9.44
East	10154	0.0694	6.94
Southeast	12725	0.0870	8.70
South	16348	0.1117	11.17
Southwest	21366	0.1460	14.60
West	22799	0.1558	15.58
Northwest	19610	0.1340	13.40
SUM	**146342**	**1.0000**	**100.00**

Individual Probabilities for Wind Direction – P ($D = d_j$) (by 10-degree increment)

One-Hour Averaged Wind Direction	Frequency of Occurrence	Probability of Occurrence	Probability of Occurrence (%)
0	14723	0.1006	10.06
10	3159	0.0216	2.16
20	4677	0.0320	3.20
30	4485	0.0306	3.06
40	3571	0.0244	2.44
50	2906	0.0199	1.99
60	2847	0.0195	1.95
70	2079	0.0142	1.42
80	1882	0.0129	1.29
90	1912	0.0131	1.31
100	1926	0.0132	1.32
110	2355	0.0161	1.61
120	3011	0.0206	2.06
130	3483	0.0238	2.38
140	3338	0.0228	2.28
150	2893	0.0198	1.98
160	2707	0.0185	1.85
170	3115	0.0213	2.13
180	2797	0.0191	1.91
190	3223	0.0220	2.20
200	4506	0.0308	3.08
210	4877	0.0333	3.33
220	6038	0.0413	4.13
230	5284	0.0361	3.61
240	5167	0.0353	3.53
250	4713	0.0322	3.22
260	4230	0.0289	2.89
270	4539	0.0310	3.10
280	4438	0.0303	3.03
290	4879	0.0333	3.33
300	6587	0.0450	4.50
310	5478	0.0374	3.74
320	4142	0.0283	2.83
330	3403	0.0233	2.33
340	2778	0.0190	1.90
350	2147	0.0147	1.47
360	2047	0.0140	1.40
SUM	**146342**	**1.0000**	**100.00**

Table 2.3 Probabilities for Eau Claire NCDC-ASOS site.

Individual Probabilities for Wind Speed – P ($U = u_i$)

One-Hour Averaged Wind Speed (mph)	Frequency of Occurrence	Probability of Occurrence	Probability of Occurrence (%)
0	25724	0.2008	20.08
5	53762	0.4198	41.98
10	37737	0.2946	29.46
15	9252	0.0722	7.22
20	1491	0.0116	1.16
25	103	0.0008	0.08
30	11	0.0001	0.01
35	0	0.0000	0.00
40	1	0.0000	0.00
45	0	0.0000	0.00
50	0	0.0000	0.00
55	0	0.0000	0.00
60	0	0.0000	0.00
65	0	0.0000	0.00
70	0	0.0000	0.00
75	0	0.0000	0.00
80	0	0.0000	0.00
SUM	**128081**	**1.0000**	**100.00**

Individual Probabilities for Wind Direction – P ($D = d_j$) (by cardinal direction)

One-Hour Averaged Wind Direction	Frequency of Occurrence	Probability of Occurrence	Probability of Occurrence (%)
N/A	25724	0.2008	20.08
North	11534	0.0901	9.01
Northeast	9954	0.0777	7.77
East	9747	0.0761	7.61
Southeast	11110	0.0867	8.67
South	17938	0.1401	14.01
Southwest	13260	0.1035	10.35
West	17473	0.1364	13.64
Northwest	11341	0.0885	8.85
SUM	**128081**	**1.0000**	**100.00**

Individual Probabilities for Wind Direction – P ($D = d_j$) (by 10-degree increment)

One-Hour Averaged Wind Direction	Frequency of Occurrence	Probability of Occurrence	Probability of Occurrence (%)
0	25724	0.2008	20.08
10	2257	0.0176	1.76
20	1988	0.0155	1.55
30	2196	0.0171	1.71
40	2442	0.0191	1.91
50	2709	0.0212	2.12
60	2607	0.0204	2.04
70	1969	0.0154	1.54
80	1849	0.0144	1.44
90	1790	0.0140	1.40
100	1989	0.0155	1.55
110	2150	0.0168	1.68
120	2488	0.0194	1.94
130	2509	0.0196	1.96
140	2838	0.0222	2.22
150	3275	0.0256	2.56
160	3541	0.0276	2.76
170	4064	0.0317	3.17
180	3814	0.0298	2.98
190	3481	0.0272	2.72
200	3038	0.0237	2.37
210	3056	0.0239	2.39
220	3195	0.0249	2.49
230	3494	0.0273	2.73
240	3515	0.0274	2.74
250	3607	0.0282	2.82
260	3729	0.0291	2.91
270	3557	0.0278	2.78
280	3598	0.0281	2.81
290	2982	0.0233	2.33
300	2818	0.0220	2.20
310	2808	0.0219	2.19
320	2940	0.0230	2.30
330	2775	0.0217	2.17
340	2456	0.0192	1.92
350	2443	0.0191	1.91
360	2390	0.0187	1.87
SUM	**128081**	**1.0000**	**100.00**

Table 2.4 Probabilities for Green Bay NCDC-ASOS site.

Individual Probabilities for Wind Speed – P ($U = u_i$)

One-Hour Averaged Wind Speed (mph)	Frequency of Occurrence	Probability of Occurrence	Probability of Occurrence (%)
0	22651	0.1433	14.33
5	65772	0.4161	41.61
10	48427	0.3063	30.63
15	16565	0.1048	10.48
20	4099	0.0259	2.59
25	512	0.0032	0.32
30	53	0.0003	0.03
35	5	0.0000	0.00
40	1	0.0000	0.00
45	0	0.0000	0.00
50	0	0.0000	0.00
55	1	0.0000	0.00
60	0	0.0000	0.00
65	0	0.0000	0.00
70	0	0.0000	0.00
75	0	0.0000	0.00
80	0	0.0000	0.00
SUM	**158086**	**1.0000**	**100.00**

Individual Probabilities for Wind Direction – P ($D = d_j$) (by cardinal direction)

One-Hour Averaged Wind Direction	Frequency of Occurrence	Probability of Occurrence	Probability of Occurrence (%)
N/A	22651	0.1433	14.33
North	16548	0.1047	10.47
Northeast	17223	0.1089	10.89
East	8682	0.0549	5.49
Southeast	8577	0.0543	5.43
South	24206	0.1531	15.31
Southwest	19854	0.1256	12.56
West	25477	0.1612	16.12
Northwest	14868	0.0941	9.41
SUM	**158086**	**1.0000**	**100.00**

Individual Probabilities for Wind Direction – P ($D = d_j$) (by 10-degree increment)

One-Hour Averaged Wind Direction	Frequency of Occurrence	Probability of Occurrence	Probability of Occurrence (%)
0	22651	0.1433	14.33
10	3714	0.0235	2.35
20	3022	0.0191	1.91
30	3156	0.0200	2.00
40	5267	0.0333	3.33
50	5309	0.0336	3.36
60	3491	0.0221	2.21
70	2183	0.0138	1.38
80	1836	0.0116	1.16
90	1671	0.0106	1.06
100	1517	0.0096	0.96
110	1475	0.0093	0.93
120	1615	0.0102	1.02
130	1752	0.0111	1.11
140	2359	0.0149	1.49
150	2851	0.0180	1.80
160	2712	0.0172	1.72
170	3597	0.0228	2.28
180	5210	0.0330	3.30
190	5792	0.0366	3.66
200	6895	0.0436	4.36
210	6807	0.0431	4.31
220	5029	0.0318	3.18
230	3919	0.0248	2.48
240	4099	0.0259	2.59
250	3889	0.0246	2.46
260	4499	0.0285	2.85
270	5653	0.0358	3.58
280	6111	0.0387	3.87
290	5325	0.0337	3.37
300	4434	0.0280	2.80
310	3748	0.0237	2.37
320	3505	0.0222	2.22
330	3181	0.0201	2.01
340	3035	0.0192	1.92
350	3142	0.0199	1.99
360	3635	0.0230	2.30
SUM	**158086**	**1.0000**	**100.00**

Table 2.5 Probabilities for La Crosse NCDC-ASOS site.

Individual Probabilities for Wind Speed – P ($U = u_i$)

One-Hour Averaged Wind Speed (mph)	Frequency of Occurrence	Probability of Occurrence	Probability of Occurrence (%)
0	19461	0.1516	15.16
5	56344	0.4388	43.88
10	38763	0.3019	30.19
15	11556	0.0900	9.00
20	2098	0.0163	1.63
25	171	0.0013	0.13
30	15	0.0001	0.01
35	2	0.0000	0.00
40	0	0.0000	0.00
45	1	0.0000	0.00
50	0	0.0000	0.00
55	0	0.0000	0.00
60	0	0.0000	0.00
65	0	0.0000	0.00
70	0	0.0000	0.00
75	0	0.0000	0.00
80	0	0.0000	0.00
SUM	**128411**	**1.0000**	**100.00**

Individual Probabilities for Wind Direction – P ($D = d_j$) (by cardinal direction)

One-Hour Averaged Wind Direction	Frequency of Occurrence	Probability of Occurrence	Probability of Occurrence (%)
N/A	19461	0.1516	15.16
North	16693	0.1300	13.00
Northeast	3411	0.0266	2.66
East	9673	0.0753	7.53
Southeast	17085	0.1330	13.30
South	28078	0.2187	21.87
Southwest	6205	0.0483	4.83
West	9639	0.0751	7.51
Northwest	18166	0.1415	14.15
SUM	**128411**	**1.0000**	**100.00**

Individual Probabilities for Wind Direction – P ($D = d_j$) (by 10-degree increment)

One-Hour Averaged Wind Direction	Frequency of Occurrence	Probability of Occurrence	Probability of Occurrence (%)
0	19461	0.1516	15.16
10	1947	0.0152	1.52
20	1331	0.0104	1.04
30	1051	0.0082	0.82
40	764	0.0059	0.59
50	788	0.0061	0.61
60	808	0.0063	0.63
70	1059	0.0082	0.82
80	1382	0.0108	1.08
90	1840	0.0143	1.43
100	2152	0.0168	1.68
110	3240	0.0252	2.52
120	4678	0.0364	3.64
130	4647	0.0362	3.62
140	3935	0.0306	3.06
150	3825	0.0298	2.98
160	4861	0.0379	3.79
170	6668	0.0519	5.19
180	7429	0.0579	5.79
190	5584	0.0435	4.35
200	3536	0.0275	2.75
210	2251	0.0175	1.75
220	1639	0.0128	1.28
230	1329	0.0103	1.03
240	986	0.0077	0.77
250	964	0.0075	0.75
260	1122	0.0087	0.87
270	1796	0.0140	1.40
280	2494	0.0194	1.94
290	3263	0.0254	2.54
300	3645	0.0284	2.84
310	4164	0.0324	3.24
320	4970	0.0387	3.87
330	5387	0.0420	4.20
340	5403	0.0421	4.21
350	4451	0.0347	3.47
360	3561	0.0277	2.77
SUM	**128411**	**1.0000**	**100.00**

Table 2.6 Probabilities for Madison NCDC-ASOS site.

Individual Probabilities for Wind Speed – P ($U = u_i$)

One-Hour Averaged Wind Speed (mph)	Frequency of Occurrence	Probability of Occurrence	Probability of Occurrence (%)
0	36602	0.2489	24.89
5	58531	0.3980	39.80
10	40398	0.2747	27.47
15	9870	0.0671	6.71
20	1567	0.0107	1.07
25	86	0.0006	0.06
30	6	0.0000	0.00
35	1	0.0000	0.00
40	1	0.0000	0.00
45	0	0.0000	0.00
50	0	0.0000	0.00
55	0	0.0000	0.00
60	0	0.0000	0.00
65	0	0.0000	0.00
70	0	0.0000	0.00
75	0	0.0000	0.00
80	0	0.0000	0.00
SUM	**147062**	**1.0000**	**100.00**

Individual Probabilities for Wind Direction – P ($D = d_j$) (by cardinal direction)

One-Hour Averaged Wind Direction	Frequency of Occurrence	Probability of Occurrence	Probability of Occurrence (%)
N/A	36602	0.2489	24.89
North	14844	0.1009	10.09
Northeast	9886	0.0672	6.72
East	10243	0.0697	6.97
Southeast	8486	0.0577	5.77
South	25492	0.1733	17.33
Southwest	12522	0.0851	8.51
West	12410	0.0844	8.44
Northwest	16577	0.1127	11.27
SUM	**147062**	**1.0000**	**100.00**

Individual Probabilities for Wind Direction – P ($D = d_j$) (by 10-degree increment)

One-Hour Averaged Wind Direction	Frequency of Occurrence	Probability of Occurrence	Probability of Occurrence (%)
0	36602	0.2489	24.89
10	2675	0.0182	1.82
20	2331	0.0159	1.59
30	2666	0.0181	1.81
40	2701	0.0184	1.84
50	2285	0.0155	1.55
60	2234	0.0152	1.52
70	2308	0.0157	1.57
80	2153	0.0146	1.46
90	1656	0.0113	1.13
100	1892	0.0129	1.29
110	2234	0.0152	1.52
120	2116	0.0144	1.44
130	2161	0.0147	1.47
140	1998	0.0136	1.36
150	2211	0.0150	1.50
160	3676	0.0250	2.50
170	5154	0.0350	3.50
180	6622	0.0450	4.50
190	6088	0.0414	4.14
200	3952	0.0269	2.69
210	3397	0.0231	2.31
220	4034	0.0274	2.74
230	3172	0.0216	2.16
240	1919	0.0130	1.30
250	1171	0.0080	0.80
260	1539	0.0105	1.05
270	2246	0.0153	1.53
280	3258	0.0222	2.22
290	4196	0.0285	2.85
300	3934	0.0268	2.68
310	4426	0.0301	3.01
320	4311	0.0293	2.93
330	3906	0.0266	2.66
340	3790	0.0258	2.58
350	3122	0.0212	2.12
360	2926	0.0199	1.99
Sum	**147062**	**1.0000**	**100.00**

Table 2.7 Probabilities for Oshkosh NCDC-ASOS site.

Individual Probabilities for Wind Speed – P ($U = u_i$)

One-Hour Averaged Wind Speed (mph)	Frequency of Occurrence	Probability of Occurrence	Probability of Occurrence (%)
0	17218	0.1362	13.62
5	54725	0.4328	43.28
10	38859	0.3074	30.74
15	12770	0.1010	10.10
20	2611	0.0207	2.07
25	225	0.0018	0.18
30	19	0.0002	0.02
35	3	0.0000	0.00
40	0	0.0000	0.00
45	1	0.0000	0.00
50	0	0.0000	0.00
55	0	0.0000	0.00
60	0	0.0000	0.00
65	0	0.0000	0.00
70	0	0.0000	0.00
75	0	0.0000	0.00
80	0	0.0000	0.00
SUM	**126431**	**1.0000**	**100.00**

Individual Probabilities for Wind Direction – P ($D = d_j$) (by cardinal direction)

One-Hour Averaged Wind Direction	Frequency of Occurrence	Probability of Occurrence	Probability of Occurrence (%)
N/A	17218	0.1362	13.62
North	10303	0.0815	8.15
Northeast	11266	0.0891	8.91
East	10659	0.0843	8.43
Southeast	7267	0.0575	5.75
South	20012	0.1583	15.83
Southwest	16205	0.1282	12.82
West	20306	0.1606	16.06
Northwest	13195	0.1044	10.44
SUM	**126431**	**1.0000**	**100.00**

Individual Probabilities for Wind Direction – P ($D = d_j$) (by 10-degree increment)

One-Hour Averaged Wind Direction	Frequency of Occurrence	Probability of Occurrence	Probability of Occurrence (%)
0	17218	0.1362	13.62
10	1661	0.0131	1.31
20	1615	0.0128	1.28
30	2224	0.0176	1.76
40	3149	0.0249	2.49
50	2976	0.0235	2.35
60	2917	0.0231	2.31
70	2438	0.0193	1.93
80	2218	0.0175	1.75
90	2131	0.0169	1.69
100	2093	0.0166	1.66
110	1779	0.0141	1.41
120	1678	0.0133	1.33
130	1772	0.0140	1.40
140	1931	0.0153	1.53
150	1886	0.0149	1.49
160	2020	0.0160	1.60
170	2529	0.0200	2.00
180	3740	0.0296	2.96
190	5297	0.0419	4.19
200	6426	0.0508	5.08
210	6356	0.0503	5.03
220	4875	0.0386	3.86
230	2870	0.0227	2.27
240	2104	0.0166	1.66
250	2672	0.0211	2.11
260	3346	0.0265	2.65
270	3751	0.0297	2.97
280	4730	0.0374	3.74
290	5807	0.0459	4.59
300	4482	0.0355	3.55
310	3368	0.0266	2.66
320	2786	0.0220	2.20
330	2559	0.0202	2.02
340	2454	0.0194	1.94
350	2473	0.0196	1.96
360	2100	0.0166	1.66
SUM	**126431**	**1.0000**	**100.00**

Table 2.8 Probabilities for Wisconsin Rapids NCDC-ASOS site.

Individual Probabilities for Wind Speed – P ($U = u_i$)

One-Hour Averaged Wind Speed (mph)	Frequency of Occurrence	Probability of Occurrence	Probability of Occurrence (%)
0	25390	0.2031	20.31
5	56321	0.4506	45.06
10	33839	0.2707	27.07
15	8192	0.0655	6.55
20	1175	0.0094	0.94
25	65	0.0005	0.05
30	4	0.0000	0.00
35	0	0.0000	0.00
40	0	0.0000	0.00
45	0	0.0000	0.00
50	0	0.0000	0.00
55	0	0.0000	0.00
60	0	0.0000	0.00
65	0	0.0000	0.00
70	0	0.0000	0.00
75	0	0.0000	0.00
80	0	0.0000	0.00
SUM	**124986**	**1.0000**	**100.00**

Individual Probabilities for Wind Direction – P ($D = d_j$) (by cardinal direction)

One-Hour Averaged Wind Direction	Frequency of Occurrence	Probability of Occurrence	Probability of Occurrence (%)
N/A	25390	0.2031	20.31
North	10938	0.0875	8.75
Northeast	6899	0.0552	5.52
East	13727	0.1098	10.98
Southeast	8851	0.0708	7.08
South	16892	0.1352	13.52
Southwest	11305	0.0905	9.05
West	17269	0.1382	13.82
Northwest	13715	0.1097	10.97
SUM	**124986**	**1.0000**	**100.00**

Individual Probabilities for Wind Direction – P ($D = d_j$) (by 10-degree increment)

One-Hour Averaged Wind Direction	Frequency of Occurrence	Probability of Occurrence	Probability of Occurrence (%)
0	25390	0.2031	20.31
10	1704	0.0136	1.36
20	1903	0.0152	1.52
30	1677	0.0134	1.34
40	1544	0.0124	1.24
50	1628	0.0130	1.30
60	2050	0.0164	1.64
70	2507	0.0201	2.01
80	2869	0.0230	2.30
90	3176	0.0254	2.54
100	2736	0.0219	2.19
110	2439	0.0195	1.95
120	2455	0.0196	1.96
130	2312	0.0185	1.85
140	2073	0.0166	1.66
150	2011	0.0161	1.61
160	2190	0.0175	1.75
170	2768	0.0221	2.21
180	3415	0.0273	2.73
190	4104	0.0328	3.28
200	4415	0.0353	3.53
210	3136	0.0251	2.51
220	2932	0.0235	2.35
230	2660	0.0213	2.13
240	2577	0.0206	2.06
250	2724	0.0218	2.18
260	3120	0.0250	2.50
270	3376	0.0270	2.70
280	3865	0.0309	3.09
290	4184	0.0335	3.35
300	4030	0.0322	3.22
310	3572	0.0286	2.86
320	3257	0.0261	2.61
330	2856	0.0229	2.29
340	2568	0.0205	2.05
350	2511	0.0201	2.01
360	2252	0.0180	1.80
SUM	**124986**	**1.0000**	**100.00**

Table 2.9 Probabilities for FMS site.

Individual Probabilities for Wind Speed – P ($U = u_i$)

One-Hour Averaged Wind Speed (mph)	Frequency of Occurrence	Probability of Occurrence	Probability of Occurrence (%)
0	453	0.1113	11.13
5	2583	0.6348	63.48
10	894	0.2197	21.97
15	129	0.0317	3.17
20	10	0.0025	0.25
25	0	0.0000	0.00
30	0	0.0000	0.00
35	0	0.0000	0.00
40	0	0.0000	0.00
45	0	0.0000	0.00
50	0	0.0000	0.00
55	0	0.0000	0.00
60	0	0.0000	0.00
65	0	0.0000	0.00
70	0	0.0000	0.00
75	0	0.0000	0.00
80	0	0.0000	0.00
SUM	**4069**	**1.0000**	**100.00**

Individual Probabilities for Wind Direction – P ($D = d_j$) (by cardinal direction)

One-Hour Averaged Wind Direction	Frequency of Occurrence	Probability of Occurrence	Probability of Occurrence (%)
N/A	453	0.1113	11.13
North	348	0.0855	8.55
Northeast	430	0.1057	10.57
East	562	0.1381	13.81
Southeast	452	0.1111	11.11
South	274	0.0673	6.73
Southwest	495	0.1217	12.17
West	672	0.1652	16.52
Northwest	383	0.0941	9.41
SUM	**4069**	**1.0000**	**100.00**

Individual Probabilities for Wind Direction – P ($D = d_j$) (by 10-degree increment)

One-Hour Averaged Wind Direction	Frequency of Occurrence	Probability of Occurrence	Probability of Occurrence (%)
0	453	0.1113	11.13
10	4	0.0010	0.10
20	306	0.0752	7.52
30	162	0.0398	3.98
40	98	0.0241	2.41
50	84	0.0206	2.06
60	86	0.0211	2.11
70	53	0.0130	1.30
80	73	0.0179	1.79
90	103	0.0253	2.53
100	173	0.0425	4.25
110	160	0.0393	3.93
120	150	0.0369	3.69
130	136	0.0334	3.34
140	84	0.0206	2.06
150	82	0.0202	2.02
160	126	0.0310	3.10
170	9	0.0022	0.22
180	0	0.0000	0.00
190	6	0.0015	0.15
200	133	0.0327	3.27
210	146	0.0359	3.59
220	132	0.0324	3.24
230	111	0.0273	2.73
240	106	0.0261	2.61
250	130	0.0319	3.19
260	103	0.0253	2.53
270	125	0.0307	3.07
280	145	0.0356	3.56
290	169	0.0415	4.15
300	154	0.0378	3.78
310	95	0.0233	2.33
320	78	0.0192	1.92
330	56	0.0138	1.38
340	38	0.0093	0.93
350	0	0.0000	0.00
360	0	0.0000	0.00
SUM	**4069**	**1.0000**	**100.00**

Table 2.10 Conditional probabilities for the Milwaukee NCDC-ASOS site – $P\left(U = u_i \mid D = d_j\right)$.

		One-Hour Averaged Wind Direction - Frequency of Occurrence									
		N/A	North	Northeast	East	Southeast	South	Southwest	West	Northwest	
One-Hour Averaged Wind Speed (mph)	0	14723	0	0	0	0	0	0	0	0	
	5	0	4622	4882	4621	4831	8773	7583	9690	8428	
	10	0	6282	5998	3531	5598	5742	8605	8746	7684	
	15	0	3019	2368	1486	1926	1544	4002	3457	2924	
	20	0	806	520	467	352	271	1053	809	548	
	25	0	77	34	38	18	15	84	94	25	
	30	0	2	6	3	0	3	32	3	1	
	35	0	0	1	8	0	0	6	0	0	
	40	0	0	0	0	0	0	0	0	0	
	45	0	0	0	0	0	0	1	0	0	
	50	0	0	0	0	0	0	0	0	0	
	55	0	0	0	0	0	0	0	0	0	
	60	0	0	0	0	0	0	0	0	0	
	65	0	0	0	0	0	0	0	0	0	
	70	0	0	0	0	0	0	0	0	0	
	75	0	0	0	0	0	0	0	0	0	
	80	0	0	0	0	0	0	0	0	0	**SUM**
	SUM	14723	14808	13809	10154	12725	16348	21366	22799	19610	**146342**

		One-Hour Averaged Wind Direction - Probability of Occurrence								
		N/A	North	Northeast	East	Southeast	South	Southwest	West	Northwest
One-Hour Averaged Wind Speed (mph)	0	1.0000	0.0000	0.0000	0.0000	0.0000	0.0000	0.0000	0.0000	0.0000
	5	0.0000	0.3121	0.3535	0.4551	0.3796	0.5366	0.3549	0.4250	0.4298
	10	0.0000	0.4242	0.4344	0.3477	0.4399	0.3512	0.4027	0.3836	0.3918
	15	0.0000	0.2039	0.1715	0.1463	0.1514	0.0944	0.1873	0.1516	0.1491
	20	0.0000	0.0544	0.0377	0.0460	0.0277	0.0166	0.0493	0.0355	0.0279
	25	0.0000	0.0052	0.0025	0.0037	0.0014	0.0009	0.0039	0.0041	0.0013
	30	0.0000	0.0001	0.0004	0.0003	0.0000	0.0002	0.0015	0.0001	0.0001
	35	0.0000	0.0000	0.0001	0.0008	0.0000	0.0000	0.0003	0.0000	0.0000
	40	0.0000	0.0000	0.0000	0.0000	0.0000	0.0000	0.0000	0.0000	0.0000
	45	0.0000	0.0000	0.0000	0.0000	0.0000	0.0000	0.0000	0.0000	0.0000
	50	0.0000	0.0000	0.0000	0.0000	0.0000	0.0000	0.0000	0.0000	0.0000
	55	0.0000	0.0000	0.0000	0.0000	0.0000	0.0000	0.0000	0.0000	0.0000
	60	0.0000	0.0000	0.0000	0.0000	0.0000	0.0000	0.0000	0.0000	0.0000
	65	0.0000	0.0000	0.0000	0.0000	0.0000	0.0000	0.0000	0.0000	0.0000
	70	0.0000	0.0000	0.0000	0.0000	0.0000	0.0000	0.0000	0.0000	0.0000
	75	0.0000	0.0000	0.0000	0.0000	0.0000	0.0000	0.0000	0.0000	0.0000
	80	0.0000	0.0000	0.0000	0.0000	0.0000	0.0000	0.0000	0.0000	0.0000
	SUM	1.0000	1.0000	1.0000	1.0000	1.0000	1.0000	1.0000	1.0000	1.0000

Table 2.11 Conditional Probabilities for the Eau Claire NCDC-ASOS site – $P\left(U = u_i \mid D = d_j\right)$.

		One-Hour Averaged Wind Direction - Frequency of Occurrence									
		N/A	North	Northeast	East	Southeast	South	Southwest	West	Northwest	
One-Hour Averaged Wind Speed (mph)	0	25724	0	0	0	0	0	0	0	0	
	5	0	7250	6385	4735	5538	8401	8296	8037	5120	
	10	0	3730	2978	3803	4479	7341	3893	6684	4829	
	15	0	515	522	1026	963	1924	881	2209	1212	
	20	0	38	65	179	128	253	167	497	164	
	25	0	1	4	3	1	15	22	42	15	
	30	0	0	0	1	1	4	1	4	0	
	35	0	0	0	0	0	0	0	0	0	
	40	0	0	0	0	0	0	0	0	1	
	45	0	0	0	0	0	0	0	0	0	
	50	0	0	0	0	0	0	0	0	0	
	55	0	0	0	0	0	0	0	0	0	
	60	0	0	0	0	0	0	0	0	0	
	65	0	0	0	0	0	0	0	0	0	
	70	0	0	0	0	0	0	0	0	0	
	75	0	0	0	0	0	0	0	0	0	
	80	0	0	0	0	0	0	0	0	0	**SUM**
	SUM	25724	11534	9954	9747	11110	17938	13260	17473	11341	**128081**

		One-Hour Averaged Wind Direction - Probability of Occurrence								
		N/A	North	Northeast	East	Southeast	South	Southwest	West	Northwest
One-Hour Averaged Wind Speed (mph)	0	1.0000	0.0000	0.0000	0.0000	0.0000	0.0000	0.0000	0.0000	0.0000
	5	0.0000	0.6286	0.6415	0.4858	0.4985	0.4683	0.6256	0.4600	0.4515
	10	0.0000	0.3234	0.2992	0.3902	0.4032	0.4092	0.2936	0.3825	0.4258
	15	0.0000	0.0447	0.0524	0.1053	0.0867	0.1073	0.0664	0.1264	0.1069
	20	0.0000	0.0033	0.0065	0.0184	0.0115	0.0141	0.0126	0.0284	0.0145
	25	0.0000	0.0001	0.0004	0.0003	0.0001	0.0008	0.0017	0.0024	0.0013
	30	0.0000	0.0000	0.0000	0.0001	0.0001	0.0002	0.0001	0.0002	0.0000
	35	0.0000	0.0000	0.0000	0.0000	0.0000	0.0000	0.0000	0.0000	0.0000
	40	0.0000	0.0000	0.0000	0.0000	0.0000	0.0000	0.0000	0.0000	0.0001
	45	0.0000	0.0000	0.0000	0.0000	0.0000	0.0000	0.0000	0.0000	0.0000
	50	0.0000	0.0000	0.0000	0.0000	0.0000	0.0000	0.0000	0.0000	0.0000
	55	0.0000	0.0000	0.0000	0.0000	0.0000	0.0000	0.0000	0.0000	0.0000
	60	0.0000	0.0000	0.0000	0.0000	0.0000	0.0000	0.0000	0.0000	0.0000
	65	0.0000	0.0000	0.0000	0.0000	0.0000	0.0000	0.0000	0.0000	0.0000
	70	0.0000	0.0000	0.0000	0.0000	0.0000	0.0000	0.0000	0.0000	0.0000
	75	0.0000	0.0000	0.0000	0.0000	0.0000	0.0000	0.0000	0.0000	0.0000
	80	0.0000	0.0000	0.0000	0.0000	0.0000	0.0000	0.0000	0.0000	0.0000
	SUM	1.0000	1.0000	1.0000	1.0000	1.0000	1.0000	1.0000	1.0000	1.0000

Table 2.12 Conditional probabilities for the Green Bay NCDC-ASOS site – $P\left(U = u_i \mid D = d_j\right)$.

		One-Hour Averaged Wind Direction - Frequency of Occurrence									
		N/A	North	Northeast	East	Southeast	South	Southwest	West	Northwest	
One-Hour Averaged Wind Speed (mph)	0	22651	0	0	0	0	0	0	0	0	
	5	0	7857	5859	5116	4234	14270	11017	10596	6823	
	10	0	5980	6666	2906	3127	7654	6972	9599	5523	
	15	0	2155	3290	608	1009	1967	1544	3992	2000	
	20	0	479	1221	47	183	300	282	1120	467	
	25	0	65	174	5	23	11	33	150	51	
	30	0	12	13	0	1	3	5	18	1	
	35	0	0	0	0	0	0	1	1	3	
	40	0	0	0	0	0	0	0	1	0	
	45	0	0	0	0	0	0	0	0	0	
	50	0	0	0	0	0	0	0	0	0	
	55	0	0	0	0	0	1	0	0	0	
	60	0	0	0	0	0	0	0	0	0	
	65	0	0	0	0	0	0	0	0	0	
	70	0	0	0	0	0	0	0	0	0	
	75	0	0	0	0	0	0	0	0	0	
	80	0	0	0	0	0	0	0	0	0	**SUM**
	SUM	22651	16548	17223	8682	8577	24206	19854	25477	14868	**158086**

		One-Hour Averaged Wind Direction - Probability of Occurrence								
		N/A	North	Northeast	East	Southeast	South	Southwest	West	Northwest
One-Hour Averaged Wind Speed (mph)	0	1.0000	0.0000	0.0000	0.0000	0.0000	0.0000	0.0000	0.0000	0.0000
	5	0.0000	0.4748	0.3402	0.5893	0.4936	0.5895	0.5549	0.4159	0.4589
	10	0.0000	0.3614	0.3870	0.3347	0.3646	0.3162	0.3512	0.3768	0.3715
	15	0.0000	0.1302	0.1910	0.0700	0.1176	0.0813	0.0778	0.1567	0.1345
	20	0.0000	0.0289	0.0709	0.0054	0.0213	0.0124	0.0142	0.0440	0.0314
	25	0.0000	0.0039	0.0101	0.0006	0.0027	0.0005	0.0017	0.0059	0.0034
	30	0.0000	0.0007	0.0008	0.0000	0.0001	0.0001	0.0003	0.0007	0.0001
	35	0.0000	0.0000	0.0000	0.0000	0.0000	0.0000	0.0001	0.0000	0.0002
	40	0.0000	0.0000	0.0000	0.0000	0.0000	0.0000	0.0000	0.0000	0.0000
	45	0.0000	0.0000	0.0000	0.0000	0.0000	0.0000	0.0000	0.0000	0.0000
	50	0.0000	0.0000	0.0000	0.0000	0.0000	0.0000	0.0000	0.0000	0.0000
	55	0.0000	0.0000	0.0000	0.0000	0.0000	0.0000	0.0000	0.0000	0.0000
	60	0.0000	0.0000	0.0000	0.0000	0.0000	0.0000	0.0000	0.0000	0.0000
	65	0.0000	0.0000	0.0000	0.0000	0.0000	0.0000	0.0000	0.0000	0.0000
	70	0.0000	0.0000	0.0000	0.0000	0.0000	0.0000	0.0000	0.0000	0.0000
	75	0.0000	0.0000	0.0000	0.0000	0.0000	0.0000	0.0000	0.0000	0.0000
	80	0.0000	0.0000	0.0000	0.0000	0.0000	0.0000	0.0000	0.0000	0.0000
	SUM	1.0000	1.0000	1.0000	1.0000	1.0000	1.0000	1.0000	1.0000	1.0000

Table 2.13 Conditional probabilities for the La Crosse NCDC-ASOS site – $P\left(U = u_i \mid D = d_j\right)$.

One-Hour Averaged Wind Speed (mph)	One-Hour Averaged Wind Direction - Frequency of Occurrence									
	N/A	North	Northeast	East	Southeast	South	Southwest	West	Northwest	
0	19461	0	0	0	0	0	0	0	0	
5	0	9415	2158	6635	13040	11955	2980	3784	6377	
10	0	5511	1120	2612	3457	12358	2256	3886	7563	
15	0	1504	128	376	547	3371	757	1496	3377	
20	0	253	5	45	39	378	183	422	773	
25	0	10	0	4	2	15	25	46	69	
30	0	0	0	0	0	1	2	5	7	
35	0	0	0	0	0	0	2	0	0	
40	0	0	0	0	0	0	0	0	0	
45	0	0	0	1	0	0	0	0	0	
50	0	0	0	0	0	0	0	0	0	
55	0	0	0	0	0	0	0	0	0	
60	0	0	0	0	0	0	0	0	0	
65	0	0	0	0	0	0	0	0	0	
70	0	0	0	0	0	0	0	0	0	
75	0	0	0	0	0	0	0	0	0	
80	0	0	0	0	0	0	0	0	0	**SUM**
SUM	19461	16693	3411	9673	17085	28078	6205	9639	18166	**128411**

One-Hour Averaged Wind Speed (mph)	One-Hour Averaged Wind Direction - Probability of Occurrence								
	N/A	North	Northeast	East	Southeast	South	Southwest	West	Northwest
0	1.0000	0.0000	0.0000	0.0000	0.0000	0.0000	0.0000	0.0000	0.0000
5	0.0000	0.5640	0.6327	0.6859	0.7632	0.4258	0.4803	0.3926	0.3510
10	0.0000	0.3301	0.3283	0.2700	0.2023	0.4401	0.3636	0.4032	0.4163
15	0.0000	0.0901	0.0375	0.0389	0.0320	0.1201	0.1220	0.1552	0.1859
20	0.0000	0.0152	0.0015	0.0047	0.0023	0.0135	0.0295	0.0438	0.0426
25	0.0000	0.0006	0.0000	0.0004	0.0001	0.0005	0.0040	0.0048	0.0038
30	0.0000	0.0000	0.0000	0.0000	0.0000	0.0000	0.0003	0.0005	0.0004
35	0.0000	0.0000	0.0000	0.0000	0.0000	0.0000	0.0003	0.0000	0.0000
40	0.0000	0.0000	0.0000	0.0000	0.0000	0.0000	0.0000	0.0000	0.0000
45	0.0000	0.0000	0.0000	0.0001	0.0000	0.0000	0.0000	0.0000	0.0000
50	0.0000	0.0000	0.0000	0.0000	0.0000	0.0000	0.0000	0.0000	0.0000
55	0.0000	0.0000	0.0000	0.0000	0.0000	0.0000	0.0000	0.0000	0.0000
60	0.0000	0.0000	0.0000	0.0000	0.0000	0.0000	0.0000	0.0000	0.0000
65	0.0000	0.0000	0.0000	0.0000	0.0000	0.0000	0.0000	0.0000	0.0000
70	0.0000	0.0000	0.0000	0.0000	0.0000	0.0000	0.0000	0.0000	0.0000
75	0.0000	0.0000	0.0000	0.0000	0.0000	0.0000	0.0000	0.0000	0.0000
80	0.0000	0.0000	0.0000	0.0000	0.0000	0.0000	0.0000	0.0000	0.0000
SUM	1.0000	1.0000	1.0000	1.0000	1.0000	1.0000	1.0000	1.0000	1.0000

Table 2.14 Conditional probabilities for the Madison NCDC-ASOS site – $P\left(U = u_i \mid D = d_j\right)$.

		One-Hour Averaged Wind Direction - Frequency of Occurrence									
		N/A	North	Northeast	East	Southeast	South	Southwest	West	Northwest	
One-Hour Averaged Wind Speed (mph)	0	36602	0	0	0	0	0	0	0	0	
	5	0	8036	4302	5006	4267	11712	7907	7821	9480	
	10	0	4983	3812	3730	3295	10660	4204	3911	5803	
	15	0	1485	1466	1209	799	2726	356	623	1206	
	20	0	311	284	282	119	379	51	54	87	
	25	0	24	21	15	6	15	4	1	0	
	30	0	3	1	1	0	0	0	0	1	
	35	0	1	0	0	0	0	0	0	0	
	40	0	1	0	0	0	0	0	0	0	
	45	0	0	0	0	0	0	0	0	0	
	50	0	0	0	0	0	0	0	0	0	
	55	0	0	0	0	0	0	0	0	0	
	60	0	0	0	0	0	0	0	0	0	
	65	0	0	0	0	0	0	0	0	0	
	70	0	0	0	0	0	0	0	0	0	
	75	0	0	0	0	0	0	0	0	0	
	80	0	0	0	0	0	0	0	0	0	**SUM**
	SUM	36602	14844	9886	10243	8486	25492	12522	12410	16577	**147062**

		One-Hour Averaged Wind Direction - Probability of Occurrence								
		N/A	North	Northeast	East	Southeast	South	Southwest	West	Northwest
One-Hour Averaged Wind Speed (mph)	0	1.0000	0.0000	0.0000	0.0000	0.0000	0.0000	0.0000	0.0000	0.0000
	5	0.0000	0.5414	0.4352	0.4887	0.5028	0.4594	0.6314	0.6302	0.5719
	10	0.0000	0.3357	0.3856	0.3642	0.3883	0.4182	0.3357	0.3151	0.3501
	15	0.0000	0.1000	0.1483	0.1180	0.0942	0.1069	0.0284	0.0502	0.0728
	20	0.0000	0.0210	0.0287	0.0275	0.0140	0.0149	0.0041	0.0044	0.0052
	25	0.0000	0.0016	0.0021	0.0015	0.0007	0.0006	0.0003	0.0001	0.0000
	30	0.0000	0.0002	0.0001	0.0001	0.0000	0.0000	0.0000	0.0000	0.0001
	35	0.0000	0.0001	0.0000	0.0000	0.0000	0.0000	0.0000	0.0000	0.0000
	40	0.0000	0.0001	0.0000	0.0000	0.0000	0.0000	0.0000	0.0000	0.0000
	45	0.0000	0.0000	0.0000	0.0000	0.0000	0.0000	0.0000	0.0000	0.0000
	50	0.0000	0.0000	0.0000	0.0000	0.0000	0.0000	0.0000	0.0000	0.0000
	55	0.0000	0.0000	0.0000	0.0000	0.0000	0.0000	0.0000	0.0000	0.0000
	60	0.0000	0.0000	0.0000	0.0000	0.0000	0.0000	0.0000	0.0000	0.0000
	65	0.0000	0.0000	0.0000	0.0000	0.0000	0.0000	0.0000	0.0000	0.0000
	70	0.0000	0.0000	0.0000	0.0000	0.0000	0.0000	0.0000	0.0000	0.0000
	75	0.0000	0.0000	0.0000	0.0000	0.0000	0.0000	0.0000	0.0000	0.0000
	80	0.0000	0.0000	0.0000	0.0000	0.0000	0.0000	0.0000	0.0000	0.0000
	SUM	1.0000	1.0000	1.0000	1.0000	1.0000	1.0000	1.0000	1.0000	1.0000

Table 2.15 Conditional probabilities for the Oshkosh NCDC-ASOS site – $P\left(U = u_i \mid D = d_j\right)$.

One-Hour Averaged Wind Speed (mph)	One-Hour Averaged Wind Direction - Frequency of Occurrence									
	N/A	North	Northeast	East	Southeast	South	Southwest	West	Northwest	
0	17218	0	0	0	0	0	0	0	0	
5	0	4279	4063	5853	4008	10416	8339	12434	5333	
10	0	4048	4767	3865	2510	6689	5727	6001	5252	
15	0	1545	1901	832	656	2382	1815	1540	2099	
20	0	373	500	109	92	480	292	296	469	
25	0	51	35	0	1	43	22	33	40	
30	0	7	0	0	0	2	7	2	1	
35	0	0	0	0	0	0	2	0	1	
40	0	0	0	0	0	0	0	0	0	
45	0	0	0	0	0	0	1	0	0	
50	0	0	0	0	0	0	0	0	0	
55	0	0	0	0	0	0	0	0	0	
60	0	0	0	0	0	0	0	0	0	
65	0	0	0	0	0	0	0	0	0	
70	0	0	0	0	0	0	0	0	0	
75	0	0	0	0	0	0	0	0	0	
80	0	0	0	0	0	0	0	0	0	**SUM**
SUM	17218	10303	11266	10659	7267	20012	16205	20306	13195	**126431**

One-Hour Averaged Wind Speed (mph)	One-Hour Averaged Wind Direction - Probability of Occurrence								
	N/A	North	Northeast	East	Southeast	South	Southwest	West	Northwest
0	1.0000	0.0000	0.0000	0.0000	0.0000	0.0000	0.0000	0.0000	0.0000
5	0.0000	0.4153	0.3606	0.5491	0.5515	0.5205	0.5146	0.6123	0.4042
10	0.0000	0.3929	0.4231	0.3626	0.3454	0.3342	0.3534	0.2955	0.3980
15	0.0000	0.1500	0.1687	0.0781	0.0903	0.1190	0.1120	0.0758	0.1591
20	0.0000	0.0362	0.0444	0.0102	0.0127	0.0240	0.0180	0.0146	0.0355
25	0.0000	0.0050	0.0031	0.0000	0.0001	0.0021	0.0014	0.0016	0.0030
30	0.0000	0.0007	0.0000	0.0000	0.0000	0.0001	0.0004	0.0001	0.0001
35	0.0000	0.0000	0.0000	0.0000	0.0000	0.0000	0.0001	0.0000	0.0001
40	0.0000	0.0000	0.0000	0.0000	0.0000	0.0000	0.0000	0.0000	0.0000
45	0.0000	0.0000	0.0000	0.0000	0.0000	0.0000	0.0001	0.0000	0.0000
50	0.0000	0.0000	0.0000	0.0000	0.0000	0.0000	0.0000	0.0000	0.0000
55	0.0000	0.0000	0.0000	0.0000	0.0000	0.0000	0.0000	0.0000	0.0000
60	0.0000	0.0000	0.0000	0.0000	0.0000	0.0000	0.0000	0.0000	0.0000
65	0.0000	0.0000	0.0000	0.0000	0.0000	0.0000	0.0000	0.0000	0.0000
70	0.0000	0.0000	0.0000	0.0000	0.0000	0.0000	0.0000	0.0000	0.0000
75	0.0000	0.0000	0.0000	0.0000	0.0000	0.0000	0.0000	0.0000	0.0000
80	0.0000	0.0000	0.0000	0.0000	0.0000	0.0000	0.0000	0.0000	0.0000
SUM	1.0000	1.0000	1.0000	1.0000	1.0000	1.0000	1.0000	1.0000	1.0000

Table 2.16 Conditional probabilities for the Wisconsin Rapids NCDC-ASOS site – $P\left(U = u_i \mid D = d_j\right)$.

		One-Hour Averaged Wind Direction - Frequency of Occurrence									
		N/A	**North**	**Northeast**	**East**	**Southeast**	**South**	**Southwest**	**West**	**Northwest**	
One-Hour Averaged Wind Speed (mph)	0	25390	0	0	0	0	0	0	0	0	
	5	0	6234	4210	7459	6595	10548	6358	8899	6018	
	10	0	3709	2254	4834	2068	5311	3990	6203	5470	
	15	0	873	402	1250	182	935	807	1862	1881	
	20	0	117	31	179	6	86	132	290	334	
	25	0	5	2	5	0	9	17	15	12	
	30	0	0	0	0	0	3	1	0	0	
	35	0	0	0	0	0	0	0	0	0	
	40	0	0	0	0	0	0	0	0	0	
	45	0	0	0	0	0	0	0	0	0	
	50	0	0	0	0	0	0	0	0	0	
	55	0	0	0	0	0	0	0	0	0	
	60	0	0	0	0	0	0	0	0	0	
	65	0	0	0	0	0	0	0	0	0	
	70	0	0	0	0	0	0	0	0	0	
	75	0	0	0	0	0	0	0	0	0	
	80	0	0	0	0	0	0	0	0	0	**SUM**
	SUM	25390	10938	6899	13727	8851	16892	11305	17269	13715	**124986**

		One-Hour Averaged Wind Direction - Probability of Occurrence								
		N/A	**North**	**Northeast**	**East**	**Southeast**	**South**	**Southwest**	**West**	**Northwest**
One-Hour Averaged Wind Speed (mph)	0	1.0000	0.0000	0.0000	0.0000	0.0000	0.0000	0.0000	0.0000	0.0000
	5	0.0000	0.5699	0.6102	0.5434	0.7451	0.6244	0.5624	0.5153	0.4388
	10	0.0000	0.3391	0.3267	0.3522	0.2336	0.3144	0.3529	0.3592	0.3988
	15	0.0000	0.0798	0.0583	0.0911	0.0206	0.0554	0.0714	0.1078	0.1371
	20	0.0000	0.0107	0.0045	0.0130	0.0007	0.0051	0.0117	0.0168	0.0244
	25	0.0000	0.0005	0.0003	0.0004	0.0000	0.0005	0.0015	0.0009	0.0009
	30	0.0000	0.0000	0.0000	0.0000	0.0000	0.0002	0.0001	0.0000	0.0000
	35	0.0000	0.0000	0.0000	0.0000	0.0000	0.0000	0.0000	0.0000	0.0000
	40	0.0000	0.0000	0.0000	0.0000	0.0000	0.0000	0.0000	0.0000	0.0000
	45	0.0000	0.0000	0.0000	0.0000	0.0000	0.0000	0.0000	0.0000	0.0000
	50	0.0000	0.0000	0.0000	0.0000	0.0000	0.0000	0.0000	0.0000	0.0000
	55	0.0000	0.0000	0.0000	0.0000	0.0000	0.0000	0.0000	0.0000	0.0000
	60	0.0000	0.0000	0.0000	0.0000	0.0000	0.0000	0.0000	0.0000	0.0000
	65	0.0000	0.0000	0.0000	0.0000	0.0000	0.0000	0.0000	0.0000	0.0000
	70	0.0000	0.0000	0.0000	0.0000	0.0000	0.0000	0.0000	0.0000	0.0000
	75	0.0000	0.0000	0.0000	0.0000	0.0000	0.0000	0.0000	0.0000	0.0000
	80	0.0000	0.0000	0.0000	0.0000	0.0000	0.0000	0.0000	0.0000	0.0000
	SUM	1.0000	1.0000	1.0000	1.0000	1.0000	1.0000	1.0000	1.0000	1.0000

Table 2.17 Conditional probabilities for the FMS site – $P\left(U = u_i \mid D = d_j\right)$.

One-Hour Averaged Wind Speed (mph)	One-Hour Averaged Wind Direction - Frequency of Occurrence									
	N/A	North	Northeast	East	Southeast	South	Southwest	West	Northwest	
0	453	0	0	0	0	0	0	0	0	
5	0	102	284	469	286	238	431	495	278	
10	0	160	133	83	156	33	63	176	90	
15	0	79	10	10	10	3	1	1	15	
20	0	7	3	0	0	0	0	0	0	
25	0	0	0	0	0	0	0	0	0	
30	0	0	0	0	0	0	0	0	0	
35	0	0	0	0	0	0	0	0	0	
40	0	0	0	0	0	0	0	0	0	
45	0	0	0	0	0	0	0	0	0	
50	0	0	0	0	0	0	0	0	0	
55	0	0	0	0	0	0	0	0	0	
60	0	0	0	0	0	0	0	0	0	
65	0	0	0	0	0	0	0	0	0	
70	0	0	0	0	0	0	0	0	0	
75	0	0	0	0	0	0	0	0	0	
80	0	0	0	0	0	0	0	0	0	**SUM**
SUM	453	348	430	562	452	274	495	672	383	**4069**

One-Hour Averaged Wind Speed (mph)	One-Hour Averaged Wind Direction - Probability of Occurrence								
	N/A	North	Northeast	East	Southeast	South	Southwest	West	Northwest
0	1.0000	0.0000	0.0000	0.0000	0.0000	0.0000	0.0000	0.0000	0.0000
5	0.0000	0.2931	0.6605	0.8345	0.6327	0.8686	0.8707	0.7366	0.7258
10	0.0000	0.4598	0.3093	0.1477	0.3451	0.1204	0.1273	0.2619	0.2350
15	0.0000	0.2270	0.0233	0.0178	0.0221	0.0109	0.0020	0.0015	0.0392
20	0.0000	0.0201	0.0070	0.0000	0.0000	0.0000	0.0000	0.0000	0.0000
25	0.0000	0.0000	0.0000	0.0000	0.0000	0.0000	0.0000	0.0000	0.0000
30	0.0000	0.0000	0.0000	0.0000	0.0000	0.0000	0.0000	0.0000	0.0000
35	0.0000	0.0000	0.0000	0.0000	0.0000	0.0000	0.0000	0.0000	0.0000
40	0.0000	0.0000	0.0000	0.0000	0.0000	0.0000	0.0000	0.0000	0.0000
45	0.0000	0.0000	0.0000	0.0000	0.0000	0.0000	0.0000	0.0000	0.0000
50	0.0000	0.0000	0.0000	0.0000	0.0000	0.0000	0.0000	0.0000	0.0000
55	0.0000	0.0000	0.0000	0.0000	0.0000	0.0000	0.0000	0.0000	0.0000
60	0.0000	0.0000	0.0000	0.0000	0.0000	0.0000	0.0000	0.0000	0.0000
65	0.0000	0.0000	0.0000	0.0000	0.0000	0.0000	0.0000	0.0000	0.0000
70	0.0000	0.0000	0.0000	0.0000	0.0000	0.0000	0.0000	0.0000	0.0000
75	0.0000	0.0000	0.0000	0.0000	0.0000	0.0000	0.0000	0.0000	0.0000
80	0.0000	0.0000	0.0000	0.0000	0.0000	0.0000	0.0000	0.0000	0.0000
SUM	1.0000	1.0000	1.0000	1.0000	1.0000	1.0000	1.0000	1.0000	1.0000

Table 2.18 Combined probabilities for the Milwaukee NCDC-ASOS site – $P\left(U = u_i \cap D = d_j\right)$.

		One-Hour Averaged Wind Direction - Probability of Occurrence									
		N/A	North	Northeast	East	Southeast	South	Southwest	West	Northwest	SUM
One-Hour Averaged Wind Speed (mph)	0	0.10061	0.00000	0.00000	0.00000	0.00000	0.00000	0.00000	0.00000	0.00000	0.10061
	5	0.00000	0.03158	0.03336	0.03158	0.03301	0.05995	0.05182	0.06621	0.05759	0.36510
	10	0.00000	0.04293	0.04099	0.02413	0.03825	0.03924	0.05880	0.05976	0.05251	0.35660
	15	0.00000	0.02063	0.01618	0.01015	0.01316	0.01055	0.02735	0.02362	0.01998	0.14163
	20	0.00000	0.00551	0.00355	0.00319	0.00241	0.00185	0.00720	0.00553	0.00374	0.03298
	25	0.00000	0.00053	0.00023	0.00026	0.00012	0.00010	0.00057	0.00064	0.00017	0.00263
	30	0.00000	0.00001	0.00004	0.00002	0.00000	0.00002	0.00022	0.00002	0.00001	0.00034
	35	0.00000	0.00000	0.00001	0.00005	0.00000	0.00000	0.00004	0.00000	0.00000	0.00010
	40	0.00000	0.00000	0.00000	0.00000	0.00000	0.00000	0.00000	0.00000	0.00000	0.00000
	45	0.00000	0.00000	0.00000	0.00000	0.00000	0.00000	0.00001	0.00000	0.00000	0.00001
	50	0.00000	0.00000	0.00000	0.00000	0.00000	0.00000	0.00000	0.00000	0.00000	0.00000
	55	0.00000	0.00000	0.00000	0.00000	0.00000	0.00000	0.00000	0.00000	0.00000	0.00000
	60	0.00000	0.00000	0.00000	0.00000	0.00000	0.00000	0.00000	0.00000	0.00000	0.00000
	65	0.00000	0.00000	0.00000	0.00000	0.00000	0.00000	0.00000	0.00000	0.00000	0.00000
	70	0.00000	0.00000	0.00000	0.00000	0.00000	0.00000	0.00000	0.00000	0.00000	0.00000
	75	0.00000	0.00000	0.00000	0.00000	0.00000	0.00000	0.00000	0.00000	0.00000	0.00000
	80	0.00000	0.00000	0.00000	0.00000	0.00000	0.00000	0.00000	0.00000	0.00000	0.00000
	SUM	0.10061	0.10119	0.09436	0.06939	0.08695	0.11171	0.14600	0.15579	0.13400	**1.00000**

Table 2.19 Combined probabilities for the Eau Claire NCDC-ASOS site – $P\left(U = u_i \cap D = d_j\right)$.

		One-Hour Averaged Wind Direction - Probability of Occurrence									
		N/A	North	Northeast	East	Southeast	South	Southwest	West	Northwest	SUM
One-Hour Averaged Wind Speed (mph)	0	0.20084	0.00000	0.00000	0.00000	0.00000	0.00000	0.00000	0.00000	0.00000	0.20084
	5	0.00000	0.05660	0.04985	0.03697	0.04324	0.06559	0.06477	0.06275	0.03997	0.41975
	10	0.00000	0.02912	0.02325	0.02969	0.03497	0.05732	0.03039	0.05219	0.03770	0.29463
	15	0.00000	0.00402	0.00408	0.00801	0.00752	0.01502	0.00688	0.01725	0.00946	0.07224
	20	0.00000	0.00030	0.00051	0.00140	0.00100	0.00198	0.00130	0.00388	0.00128	0.01164
	25	0.00000	0.00001	0.00003	0.00002	0.00001	0.00012	0.00017	0.00033	0.00012	0.00080
	30	0.00000	0.00000	0.00000	0.00001	0.00001	0.00003	0.00001	0.00003	0.00000	0.00009
	35	0.00000	0.00000	0.00000	0.00000	0.00000	0.00000	0.00000	0.00000	0.00000	0.00000
	40	0.00000	0.00000	0.00000	0.00000	0.00000	0.00000	0.00000	0.00000	0.00001	0.00001
	45	0.00000	0.00000	0.00000	0.00000	0.00000	0.00000	0.00000	0.00000	0.00000	0.00000
	50	0.00000	0.00000	0.00000	0.00000	0.00000	0.00000	0.00000	0.00000	0.00000	0.00000
	55	0.00000	0.00000	0.00000	0.00000	0.00000	0.00000	0.00000	0.00000	0.00000	0.00000
	60	0.00000	0.00000	0.00000	0.00000	0.00000	0.00000	0.00000	0.00000	0.00000	0.00000
	65	0.00000	0.00000	0.00000	0.00000	0.00000	0.00000	0.00000	0.00000	0.00000	0.00000
	70	0.00000	0.00000	0.00000	0.00000	0.00000	0.00000	0.00000	0.00000	0.00000	0.00000
	75	0.00000	0.00000	0.00000	0.00000	0.00000	0.00000	0.00000	0.00000	0.00000	0.00000
	80	0.00000	0.00000	0.00000	0.00000	0.00000	0.00000	0.00000	0.00000	0.00000	0.00000
	SUM	0.20084	0.09005	0.07772	0.07610	0.08674	0.14005	0.10353	0.13642	0.08855	**1.00000**

Table 2.20 Combined probabilities for the Green Bay NCDC-ASOS site – $P\left(U = u_i \cap D = d_j\right)$.

		One-Hour Averaged Wind Direction - Probability of Occurrence									
		N/A	North	Northeast	East	Southeast	South	Southwest	West	Northwest	SUM
One-Hour Averaged Wind Speed (mph)	0	0.14328	0.00000	0.00000	0.00000	0.00000	0.00000	0.00000	0.00000	0.00000	0.14328
	5	0.00000	0.04970	0.03706	0.03236	0.02678	0.09027	0.06969	0.06703	0.04316	0.41605
	10	0.00000	0.03783	0.04217	0.01838	0.01978	0.04842	0.04410	0.06072	0.03494	0.30633
	15	0.00000	0.01363	0.02081	0.00385	0.00638	0.01244	0.00977	0.02525	0.01265	0.10478
	20	0.00000	0.00303	0.00772	0.00030	0.00116	0.00190	0.00178	0.00708	0.00295	0.02593
	25	0.00000	0.00041	0.00110	0.00003	0.00015	0.00007	0.00021	0.00095	0.00032	0.00324
	30	0.00000	0.00008	0.00008	0.00000	0.00001	0.00002	0.00003	0.00011	0.00001	0.00034
	35	0.00000	0.00000	0.00000	0.00000	0.00000	0.00000	0.00001	0.00001	0.00002	0.00003
	40	0.00000	0.00000	0.00000	0.00000	0.00000	0.00000	0.00000	0.00001	0.00000	0.00001
	45	0.00000	0.00000	0.00000	0.00000	0.00000	0.00000	0.00000	0.00000	0.00000	0.00000
	50	0.00000	0.00000	0.00000	0.00000	0.00000	0.00000	0.00000	0.00000	0.00000	0.00000
	55	0.00000	0.00000	0.00000	0.00000	0.00000	0.00001	0.00000	0.00000	0.00000	0.00001
	60	0.00000	0.00000	0.00000	0.00000	0.00000	0.00000	0.00000	0.00000	0.00000	0.00000
	65	0.00000	0.00000	0.00000	0.00000	0.00000	0.00000	0.00000	0.00000	0.00000	0.00000
	70	0.00000	0.00000	0.00000	0.00000	0.00000	0.00000	0.00000	0.00000	0.00000	0.00000
	75	0.00000	0.00000	0.00000	0.00000	0.00000	0.00000	0.00000	0.00000	0.00000	0.00000
	80	0.00000	0.00000	0.00000	0.00000	0.00000	0.00000	0.00000	0.00000	0.00000	0.00000
	SUM	0.14328	0.10468	0.10895	0.05492	0.05426	0.15312	0.12559	0.16116	0.09405	**1.00000**

Table 2.21 Combined probabilities for the La Crosse NCDC-ASOS site – $P\left(U = u_i \cap D = d_j\right)$.

		One-Hour Averaged Wind Direction - Probability of Occurrence									
		N/A	North	Northeast	East	Southeast	South	Southwest	West	Northwest	SUM
One-Hour Averaged Wind Speed (mph)	0	0.15155	0.00000	0.00000	0.00000	0.00000	0.00000	0.00000	0.00000	0.00000	0.15155
	5	0.00000	0.07332	0.01681	0.05167	0.10155	0.09310	0.02321	0.02947	0.04966	0.43878
	10	0.00000	0.04292	0.00872	0.02034	0.02692	0.09624	0.01757	0.03026	0.05890	0.30187
	15	0.00000	0.01171	0.00100	0.00293	0.00426	0.02625	0.00590	0.01165	0.02630	0.08999
	20	0.00000	0.00197	0.00004	0.00035	0.00030	0.00294	0.00143	0.00329	0.00602	0.01634
	25	0.00000	0.00008	0.00000	0.00003	0.00002	0.00012	0.00019	0.00036	0.00054	0.00133
	30	0.00000	0.00000	0.00000	0.00000	0.00000	0.00001	0.00002	0.00004	0.00005	0.00012
	35	0.00000	0.00000	0.00000	0.00000	0.00000	0.00000	0.00002	0.00000	0.00000	0.00002
	40	0.00000	0.00000	0.00000	0.00000	0.00000	0.00000	0.00000	0.00000	0.00000	0.00000
	45	0.00000	0.00000	0.00000	0.00001	0.00000	0.00000	0.00000	0.00000	0.00000	0.00001
	50	0.00000	0.00000	0.00000	0.00000	0.00000	0.00000	0.00000	0.00000	0.00000	0.00000
	55	0.00000	0.00000	0.00000	0.00000	0.00000	0.00000	0.00000	0.00000	0.00000	0.00000
	60	0.00000	0.00000	0.00000	0.00000	0.00000	0.00000	0.00000	0.00000	0.00000	0.00000
	65	0.00000	0.00000	0.00000	0.00000	0.00000	0.00000	0.00000	0.00000	0.00000	0.00000
	70	0.00000	0.00000	0.00000	0.00000	0.00000	0.00000	0.00000	0.00000	0.00000	0.00000
	75	0.00000	0.00000	0.00000	0.00000	0.00000	0.00000	0.00000	0.00000	0.00000	0.00000
	80	0.00000	0.00000	0.00000	0.00000	0.00000	0.00000	0.00000	0.00000	0.00000	0.00000
	SUM	0.15155	0.13000	0.02656	0.07533	0.13305	0.21866	0.04832	0.07506	0.14147	**1.00000**

Table 2.22 Combined probabilities for the Madison NCDC-ASOS site – $P\left(U = u_i \cap D = d_j\right)$.

		One-Hour Averaged Wind Direction - Probability of Occurrence									
		N/A	North	Northeast	East	Southeast	South	Southwest	West	Northwest	SUM
One-Hour Averaged Wind Speed (mph)	0	0.24889	0.00000	0.00000	0.00000	0.00000	0.00000	0.00000	0.00000	0.00000	0.24889
	5	0.00000	0.05464	0.02925	0.03404	0.02901	0.07964	0.05377	0.05318	0.06446	0.39800
	10	0.00000	0.03388	0.02592	0.02536	0.02241	0.07249	0.02859	0.02659	0.03946	0.27470
	15	0.00000	0.01010	0.00997	0.00822	0.00543	0.01854	0.00242	0.00424	0.00820	0.06711
	20	0.00000	0.00211	0.00193	0.00192	0.00081	0.00258	0.00035	0.00037	0.00059	0.01066
	25	0.00000	0.00016	0.00014	0.00010	0.00004	0.00010	0.00003	0.00001	0.00000	0.00058
	30	0.00000	0.00002	0.00001	0.00001	0.00000	0.00000	0.00000	0.00000	0.00001	0.00004
	35	0.00000	0.00001	0.00000	0.00000	0.00000	0.00000	0.00000	0.00000	0.00000	0.00001
	40	0.00000	0.00001	0.00000	0.00000	0.00000	0.00000	0.00000	0.00000	0.00000	0.00001
	45	0.00000	0.00000	0.00000	0.00000	0.00000	0.00000	0.00000	0.00000	0.00000	0.00000
	50	0.00000	0.00000	0.00000	0.00000	0.00000	0.00000	0.00000	0.00000	0.00000	0.00000
	55	0.00000	0.00000	0.00000	0.00000	0.00000	0.00000	0.00000	0.00000	0.00000	0.00000
	60	0.00000	0.00000	0.00000	0.00000	0.00000	0.00000	0.00000	0.00000	0.00000	0.00000
	65	0.00000	0.00000	0.00000	0.00000	0.00000	0.00000	0.00000	0.00000	0.00000	0.00000
	70	0.00000	0.00000	0.00000	0.00000	0.00000	0.00000	0.00000	0.00000	0.00000	0.00000
	75	0.00000	0.00000	0.00000	0.00000	0.00000	0.00000	0.00000	0.00000	0.00000	0.00000
	80	0.00000	0.00000	0.00000	0.00000	0.00000	0.00000	0.00000	0.00000	0.00000	0.00000
	SUM	0.24889	0.10094	0.06722	0.06965	0.05770	0.17334	0.08515	0.08439	0.11272	**1.00000**

Table 2.23 Combined probabilities for the Oshkosh NCDC-ASOS site – $P\left(U = u_i \cap D = d_j\right)$.

		One-Hour Averaged Wind Direction - Probability of Occurrence									
		N/A	North	Northeast	East	Southeast	South	Southwest	West	Northwest	SUM
One-Hour Averaged Wind Speed (mph)	0	0.13618	0.00000	0.00000	0.00000	0.00000	0.00000	0.00000	0.00000	0.00000	0.13618
	5	0.00000	0.03384	0.03214	0.04629	0.03170	0.08238	0.06596	0.09835	0.04218	0.43284
	10	0.00000	0.03202	0.03770	0.03057	0.01985	0.05291	0.04530	0.04746	0.04154	0.30735
	15	0.00000	0.01222	0.01504	0.00658	0.00519	0.01884	0.01436	0.01218	0.01660	0.10100
	20	0.00000	0.00295	0.00395	0.00086	0.00073	0.00380	0.00231	0.00234	0.00371	0.02065
	25	0.00000	0.00040	0.00028	0.00000	0.00001	0.00034	0.00017	0.00026	0.00032	0.00178
	30	0.00000	0.00006	0.00000	0.00000	0.00000	0.00002	0.00006	0.00002	0.00001	0.00015
	35	0.00000	0.00000	0.00000	0.00000	0.00000	0.00000	0.00002	0.00000	0.00001	0.00002
	40	0.00000	0.00000	0.00000	0.00000	0.00000	0.00000	0.00000	0.00000	0.00000	0.00000
	45	0.00000	0.00000	0.00000	0.00000	0.00000	0.00000	0.00001	0.00000	0.00000	0.00001
	50	0.00000	0.00000	0.00000	0.00000	0.00000	0.00000	0.00000	0.00000	0.00000	0.00000
	55	0.00000	0.00000	0.00000	0.00000	0.00000	0.00000	0.00000	0.00000	0.00000	0.00000
	60	0.00000	0.00000	0.00000	0.00000	0.00000	0.00000	0.00000	0.00000	0.00000	0.00000
	65	0.00000	0.00000	0.00000	0.00000	0.00000	0.00000	0.00000	0.00000	0.00000	0.00000
	70	0.00000	0.00000	0.00000	0.00000	0.00000	0.00000	0.00000	0.00000	0.00000	0.00000
	75	0.00000	0.00000	0.00000	0.00000	0.00000	0.00000	0.00000	0.00000	0.00000	0.00000
	80	0.00000	0.00000	0.00000	0.00000	0.00000	0.00000	0.00000	0.00000	0.00000	0.00000
	SUM	0.13618	0.08149	0.08911	0.08431	0.05748	0.15828	0.12817	0.16061	0.10437	**1.00000**

Table 2.24 Combined probabilities for the Wisconsin Rapids NCDC-ASOS site – $P\left(U = u_i \cap D = d_j\right)$.

		One-Hour Averaged Wind Direction - Probability of Occurrence									
		N/A	North	Northeast	East	Southeast	South	Southwest	West	Northwest	SUM
One-Hour Averaged Wind Speed (mph)	0	0.20314	0.00000	0.00000	0.00000	0.00000	0.00000	0.00000	0.00000	0.00000	0.20314
	5	0.00000	0.04988	0.03368	0.05968	0.05277	0.08439	0.05087	0.07120	0.04815	0.45062
	10	0.00000	0.02968	0.01803	0.03868	0.01655	0.04249	0.03192	0.04963	0.04376	0.27074
	15	0.00000	0.00698	0.00322	0.01000	0.00146	0.00748	0.00646	0.01490	0.01505	0.06554
	20	0.00000	0.00094	0.00025	0.00143	0.00005	0.00069	0.00106	0.00232	0.00267	0.00940
	25	0.00000	0.00004	0.00002	0.00004	0.00000	0.00007	0.00014	0.00012	0.00010	0.00052
	30	0.00000	0.00000	0.00000	0.00000	0.00000	0.00002	0.00001	0.00000	0.00000	0.00003
	35	0.00000	0.00000	0.00000	0.00000	0.00000	0.00000	0.00000	0.00000	0.00000	0.00000
	40	0.00000	0.00000	0.00000	0.00000	0.00000	0.00000	0.00000	0.00000	0.00000	0.00000
	45	0.00000	0.00000	0.00000	0.00000	0.00000	0.00000	0.00000	0.00000	0.00000	0.00000
	50	0.00000	0.00000	0.00000	0.00000	0.00000	0.00000	0.00000	0.00000	0.00000	0.00000
	55	0.00000	0.00000	0.00000	0.00000	0.00000	0.00000	0.00000	0.00000	0.00000	0.00000
	60	0.00000	0.00000	0.00000	0.00000	0.00000	0.00000	0.00000	0.00000	0.00000	0.00000
	65	0.00000	0.00000	0.00000	0.00000	0.00000	0.00000	0.00000	0.00000	0.00000	0.00000
	70	0.00000	0.00000	0.00000	0.00000	0.00000	0.00000	0.00000	0.00000	0.00000	0.00000
	75	0.00000	0.00000	0.00000	0.00000	0.00000	0.00000	0.00000	0.00000	0.00000	0.00000
	80	0.00000	0.00000	0.00000	0.00000	0.00000	0.00000	0.00000	0.00000	0.00000	0.00000
	SUM	0.20314	0.08751	0.05520	0.10983	0.07082	0.13515	0.09045	0.13817	0.10973	**1.00000**

Table 2.25 Combined probabilities for the FMS site – $P\left(U = u_i \cap D = d_j\right)$.

		One-Hour Averaged Wind Direction - Probability of Occurrence									
		N/A	North	Northeast	East	Southeast	South	Southwest	West	Northwest	SUM
One-Hour Averaged Wind Speed (mph)	0	0.11133	0.00000	0.00000	0.00000	0.00000	0.00000	0.00000	0.00000	0.00000	0.11133
	5	0.00000	0.02507	0.06980	0.11526	0.07029	0.05849	0.10592	0.12165	0.06832	0.63480
	10	0.00000	0.03932	0.03269	0.02040	0.03834	0.00811	0.01548	0.04325	0.02212	0.21971
	15	0.00000	0.01942	0.00246	0.00246	0.00246	0.00074	0.00025	0.00025	0.00369	0.03170
	20	0.00000	0.00172	0.00074	0.00000	0.00000	0.00000	0.00000	0.00000	0.00000	0.00246
	25	0.00000	0.00000	0.00000	0.00000	0.00000	0.00000	0.00000	0.00000	0.00000	0.00000
	30	0.00000	0.00000	0.00000	0.00000	0.00000	0.00000	0.00000	0.00000	0.00000	0.00000
	35	0.00000	0.00000	0.00000	0.00000	0.00000	0.00000	0.00000	0.00000	0.00000	0.00000
	40	0.00000	0.00000	0.00000	0.00000	0.00000	0.00000	0.00000	0.00000	0.00000	0.00000
	45	0.00000	0.00000	0.00000	0.00000	0.00000	0.00000	0.00000	0.00000	0.00000	0.00000
	50	0.00000	0.00000	0.00000	0.00000	0.00000	0.00000	0.00000	0.00000	0.00000	0.00000
	55	0.00000	0.00000	0.00000	0.00000	0.00000	0.00000	0.00000	0.00000	0.00000	0.00000
	60	0.00000	0.00000	0.00000	0.00000	0.00000	0.00000	0.00000	0.00000	0.00000	0.00000
	65	0.00000	0.00000	0.00000	0.00000	0.00000	0.00000	0.00000	0.00000	0.00000	0.00000
	70	0.00000	0.00000	0.00000	0.00000	0.00000	0.00000	0.00000	0.00000	0.00000	0.00000
	75	0.00000	0.00000	0.00000	0.00000	0.00000	0.00000	0.00000	0.00000	0.00000	0.00000
	80	0.00000	0.00000	0.00000	0.00000	0.00000	0.00000	0.00000	0.00000	0.00000	0.00000
	SUM	0.11133	0.08552	0.10568	0.13812	0.11108	0.06734	0.12165	0.16515	0.09413	**1.00000**

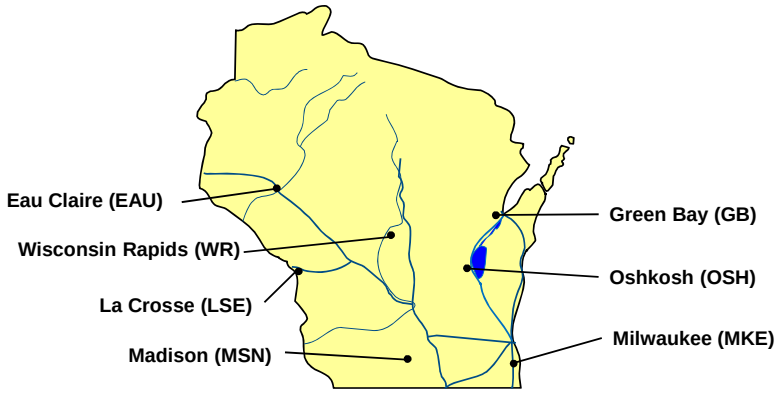

Figure 2.1 Map of Wisconsin listing the NCDC-ASOS wind data collection sites.

Figure 2.2 Location of Milwaukee sign support structure S-40-703 and the field monitoring station used to collect site/sign-specific wind data and corresponding bending strain response.

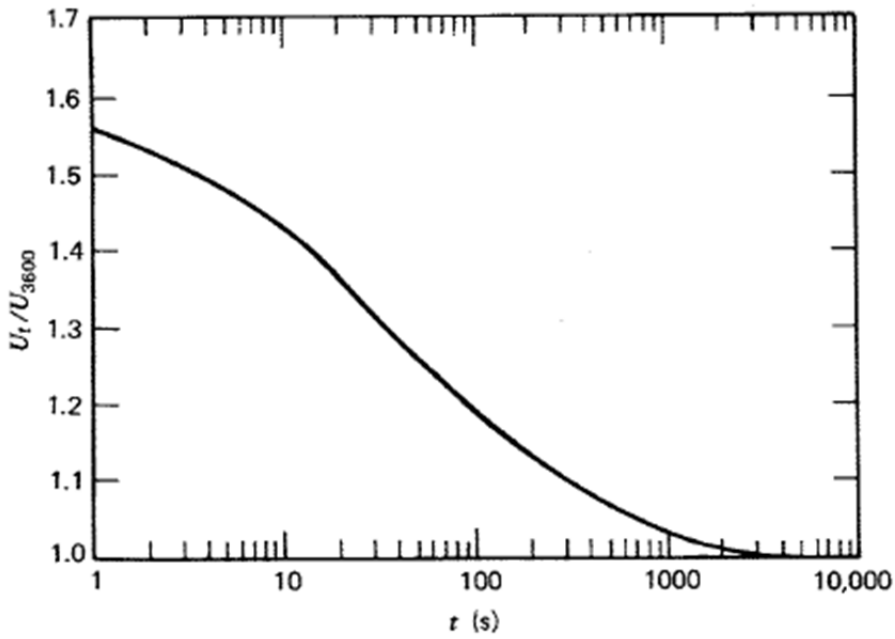

Figure 2.3 Wind speed variation with averaging time (Simiu and Scanlon 1996).

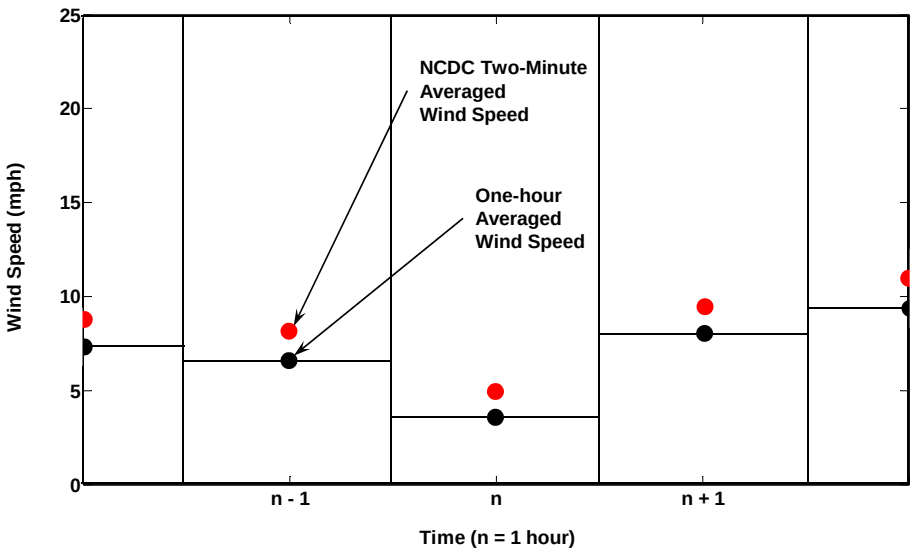

Figure 2.4 NCDC adjustment procedure utilized to obtain one-hour averaged wind speeds.

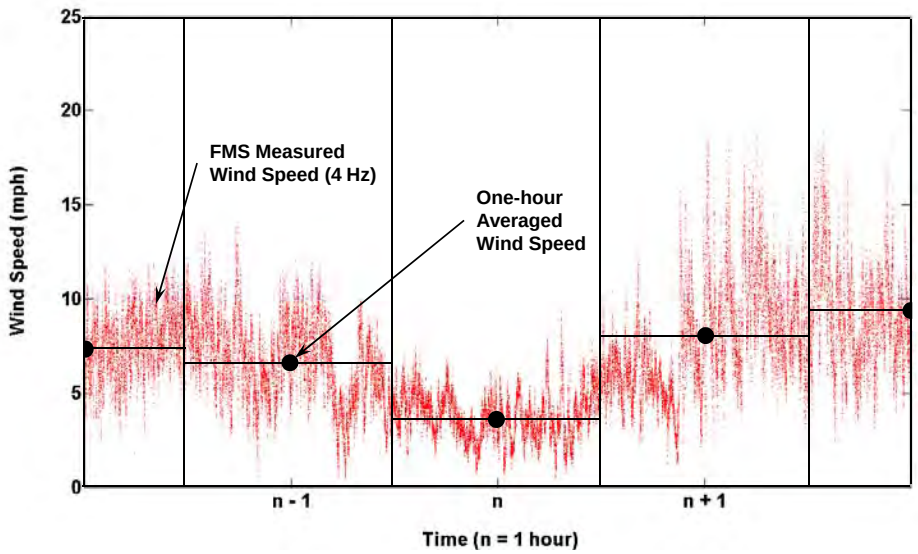

Figure 2.5 FMS averaging procedure utilized to obtain one-hour averaged wind speeds.

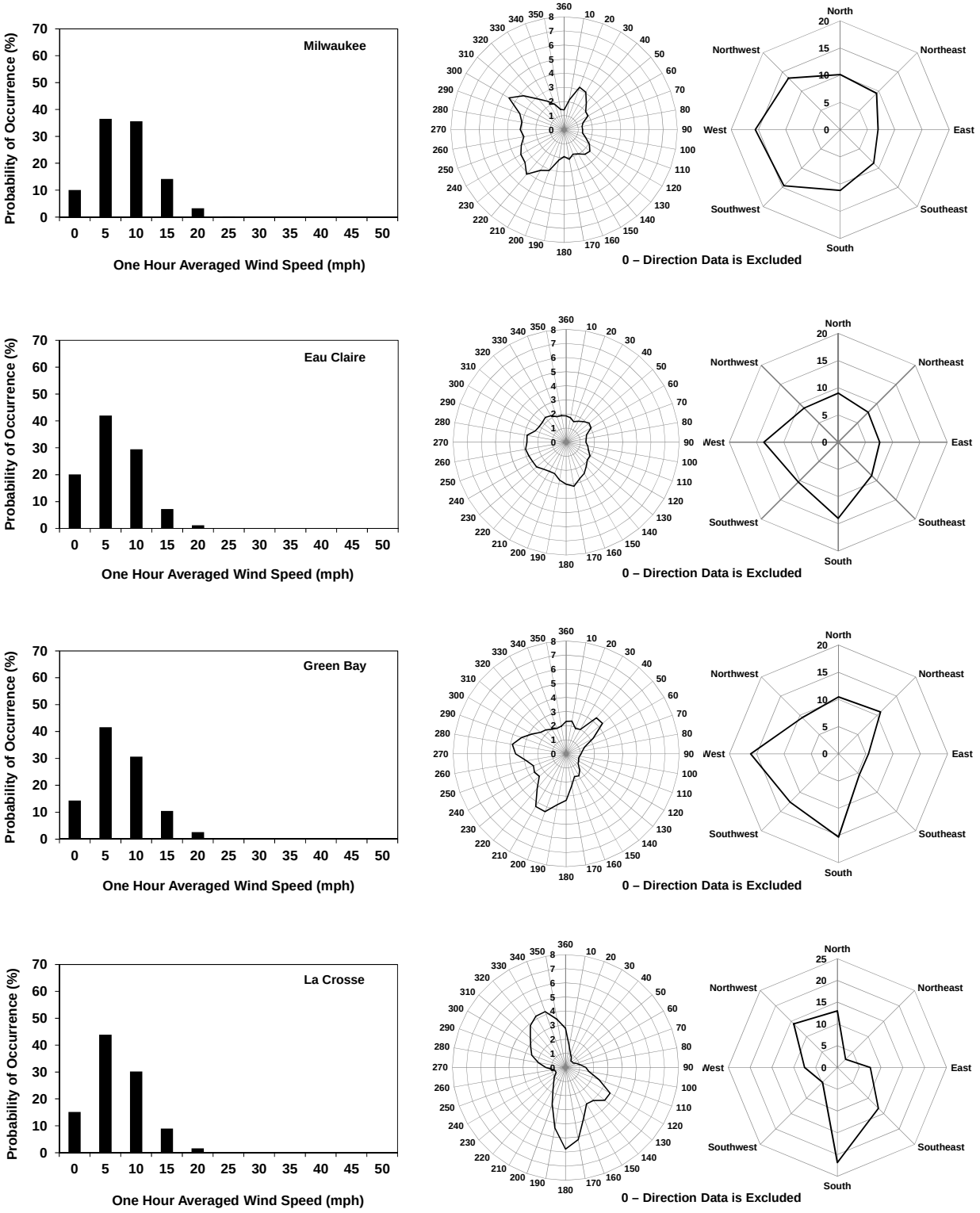

Figure 2.6 Wind Speed and Wind Direction Histograms for the Milwaukee, Eau Claire, Green Bay, and La Crosse NCDC-ASOS sites.

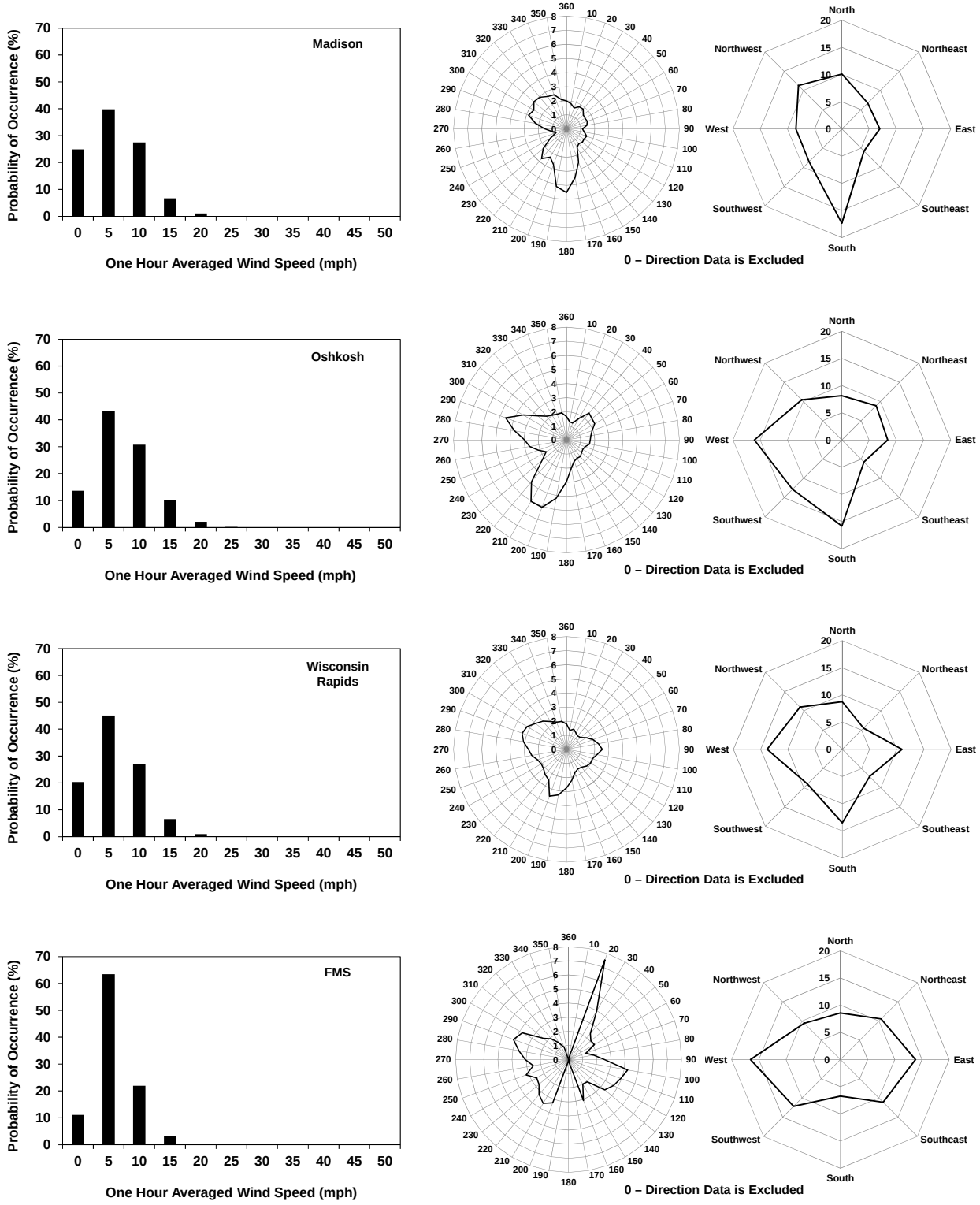

Figure 2.7 Wind Speed and Wind Direction Histograms for the Madison, Oshkosh, and Wisconsin Rapids NCDC-ASOS sites and the FMS site.

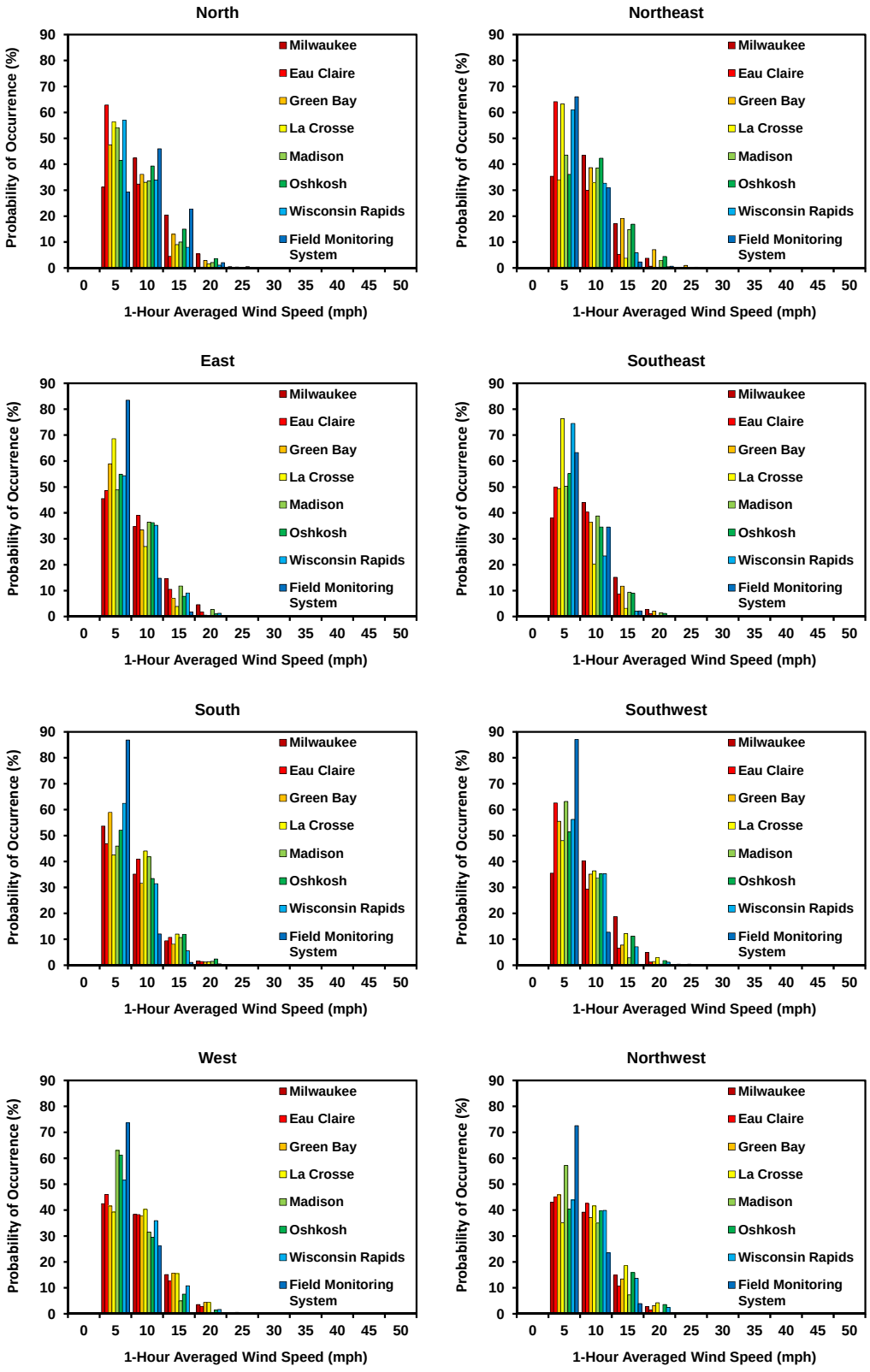

Figure 2.8 Conditional probability mass functions for Wisconsin NCDC-ASOS sites and the FMS site – $P\left(U = u_i \mid D = d_j\right)$.

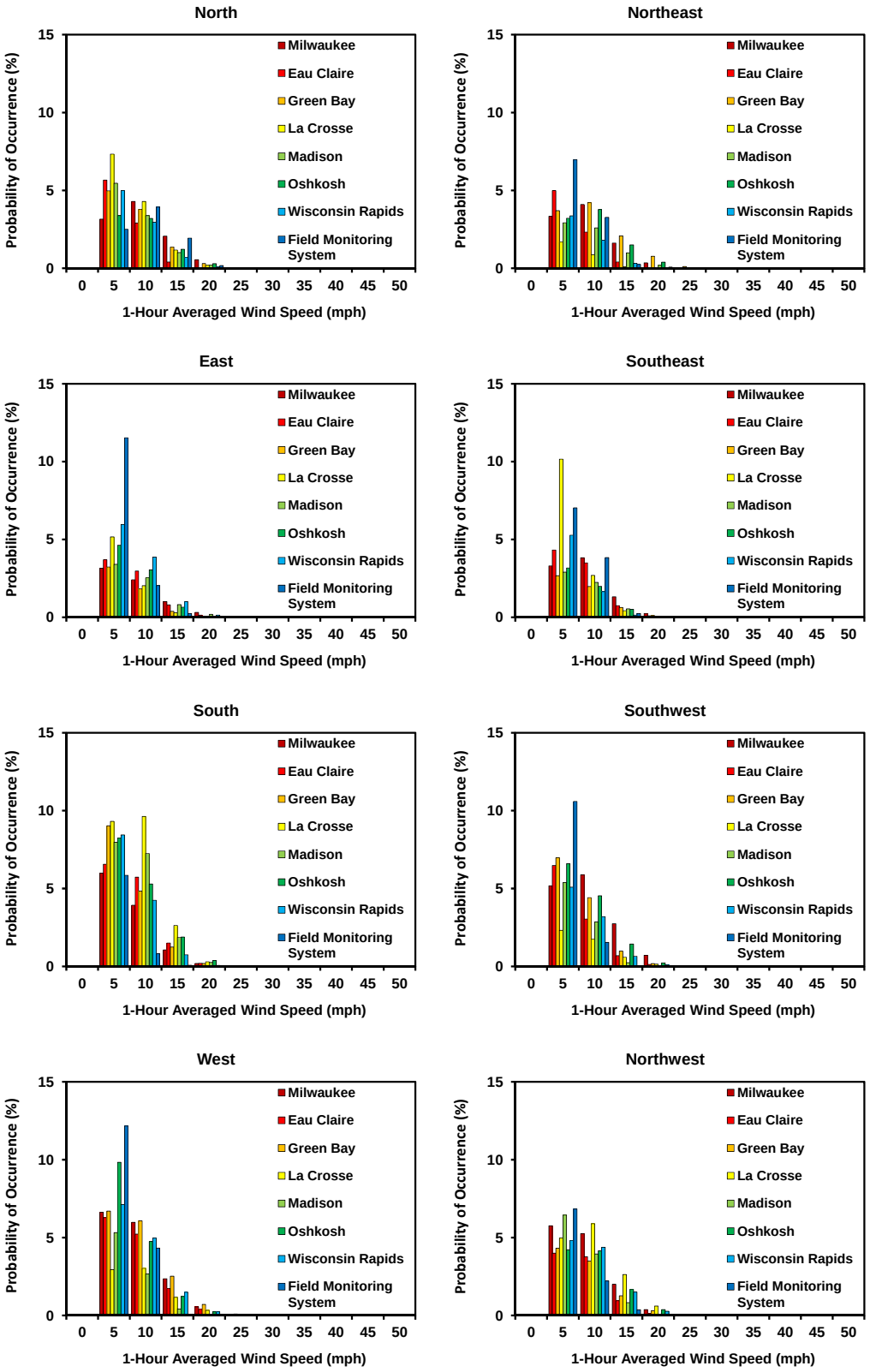

Figure 2.9 Combined probability mass functions for all NCDC-ASOS sites and the FMS site – $P\left(U = u_i \cap D = d_j\right)$.

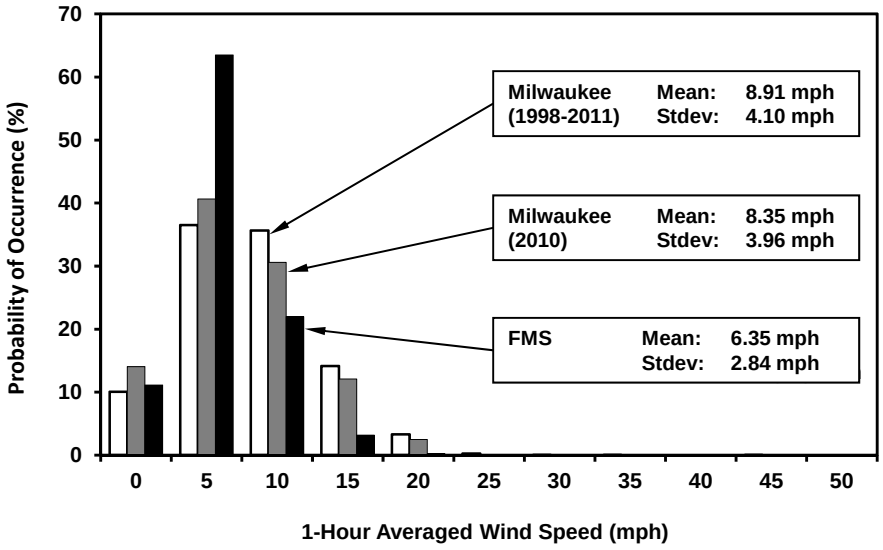

Figure 2.10 One-Hour wind speed histograms from Milwaukee NCDC-ASOS site and the FMS site – $P(U = u_i)$.

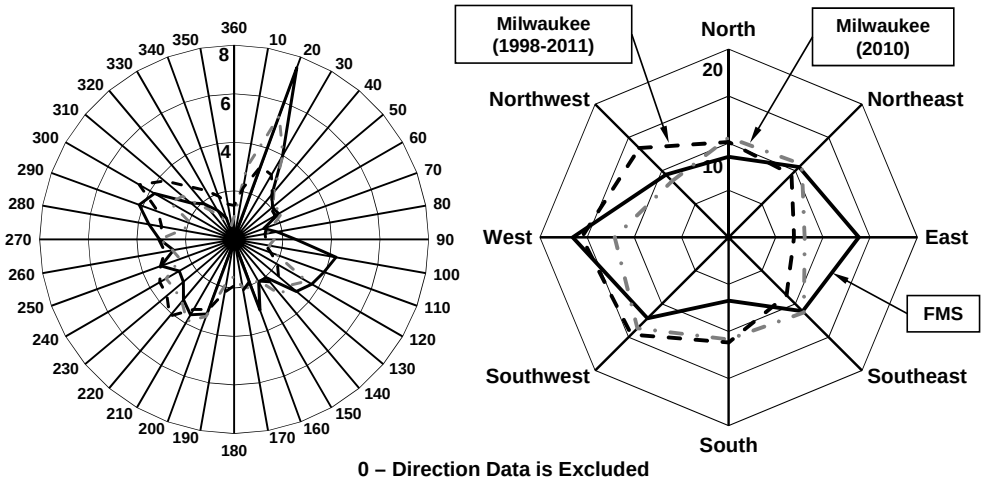

Figure 2.11 One-hour wind rose histograms from Milwaukee NCDC-ASOS site and the FMS site – $P(D = d_j)$.

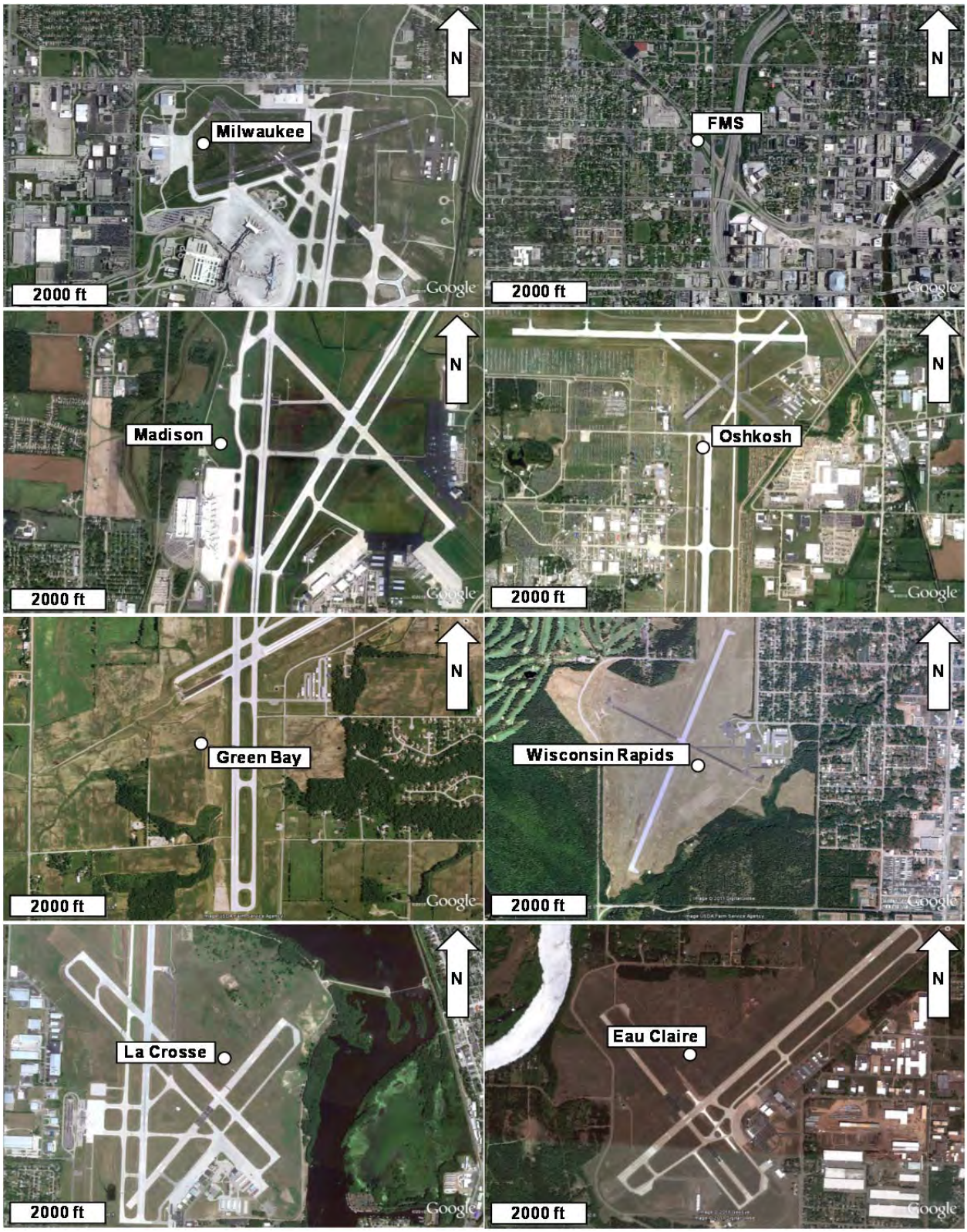

Figure 2.12 Aerial Photos of the Wisconsin NCDC-ASOS sites and the FMS site.

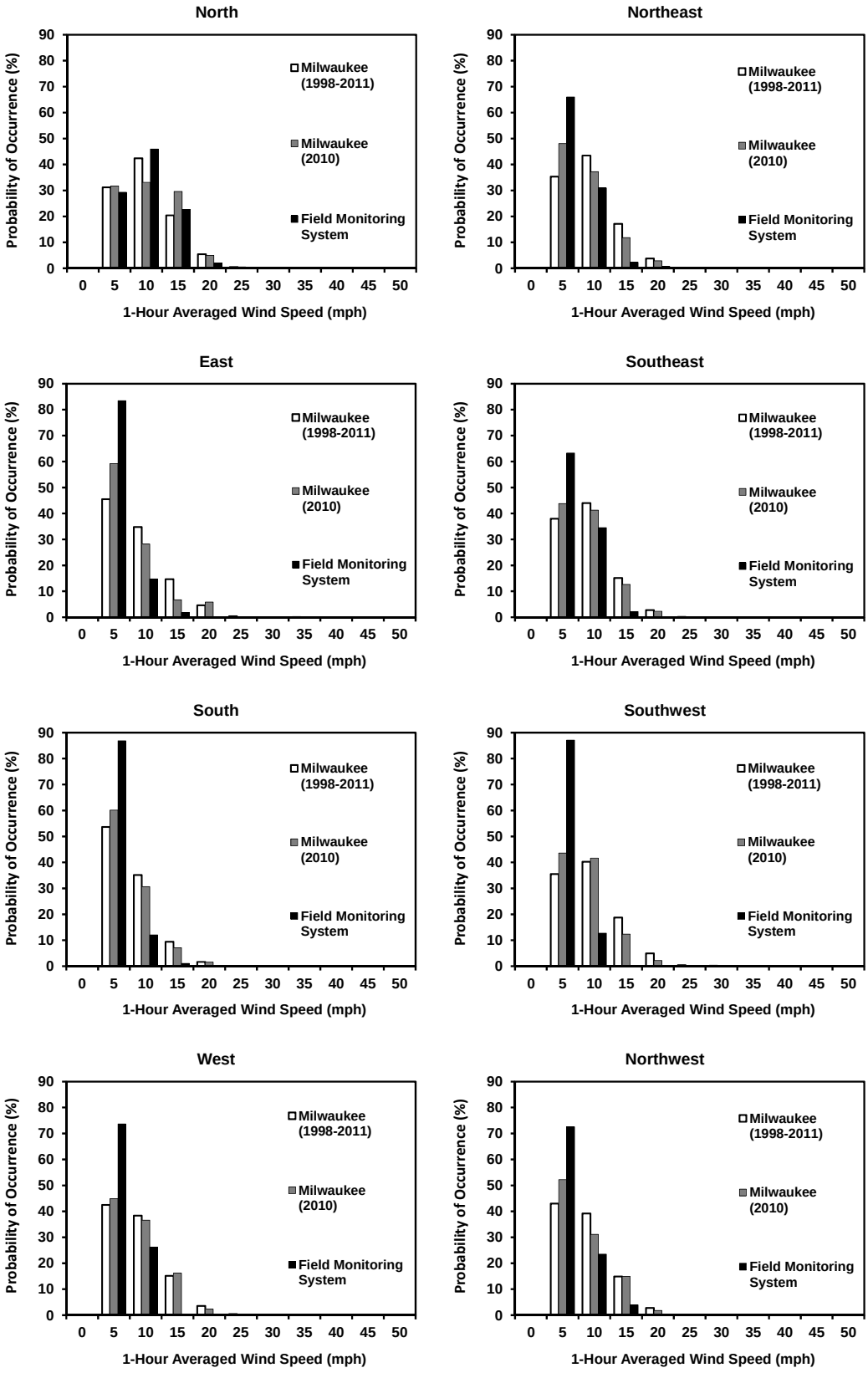

Figure 2.13 Variation between conditional probabilities of Milwaukee NCDC-ASOS site and the FMS site – $P\left(U = u_i \mid D = d_j\right)$.

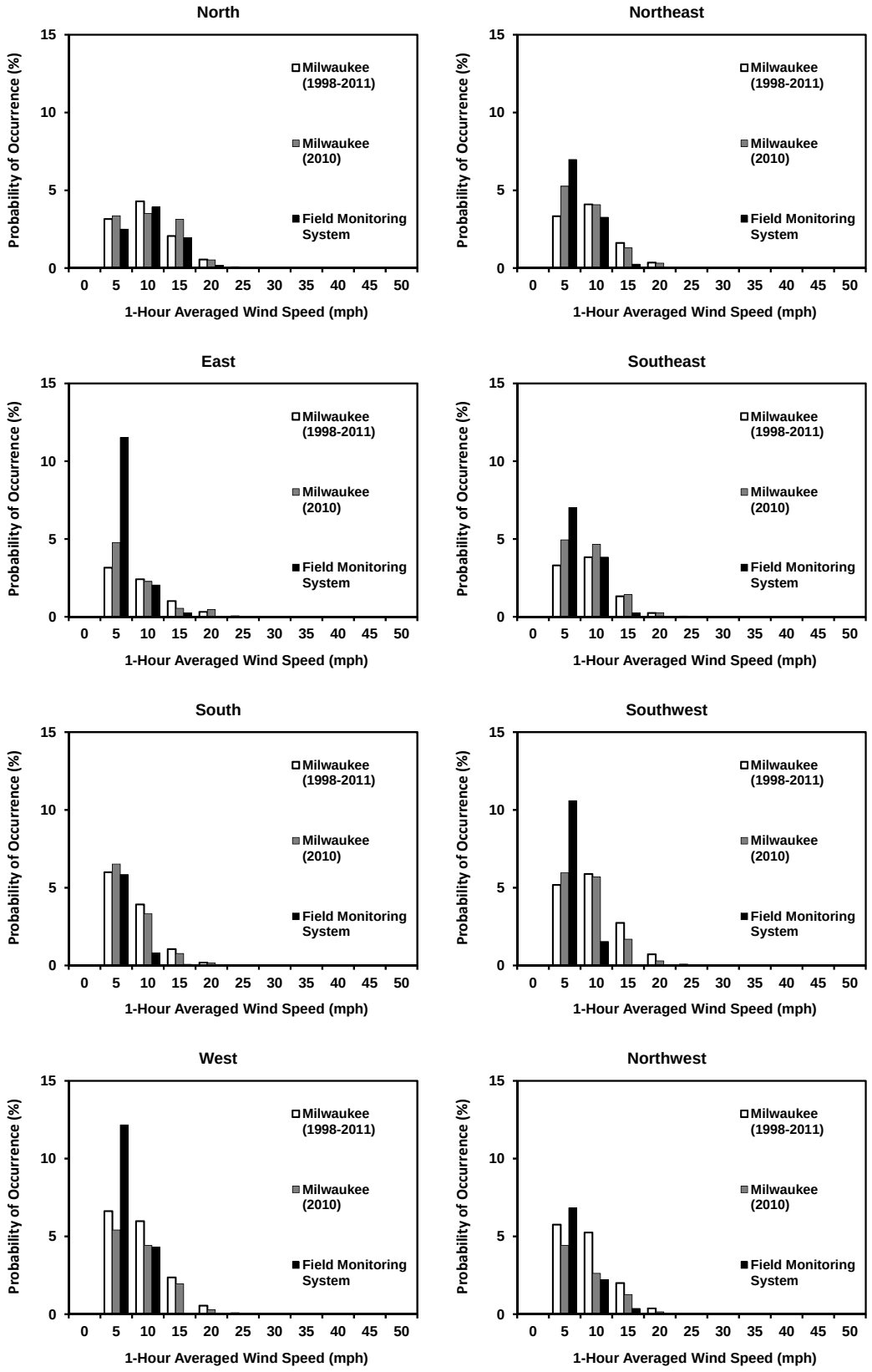

Figure 2.14 Variation between combined probabilities of Milwaukee NCDC-ASOS site and the FMS site – $P\left(U = u_i \cap D = d_j\right)$.

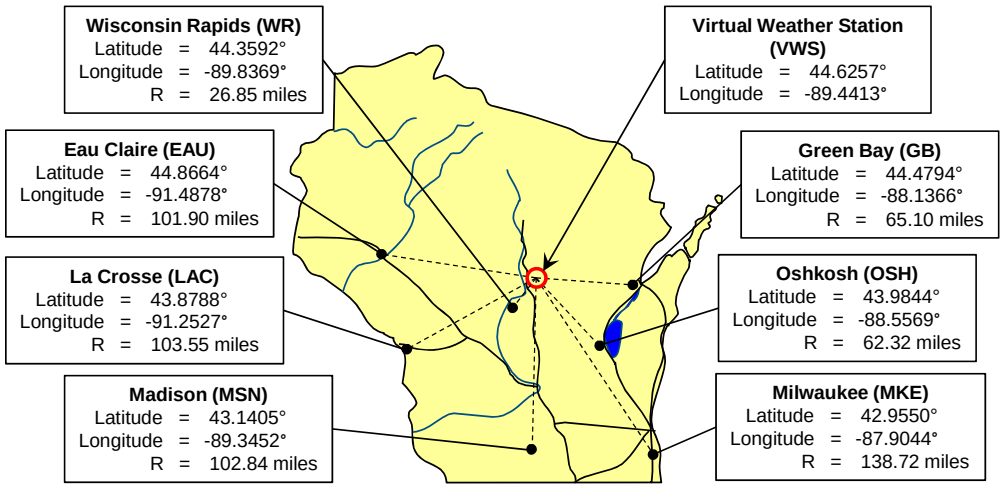

Figure 2.15 Map of Wisconsin listing the NCDC-ASOS wind data collection sites with corresponding latitudes and longitudes as well as their respective vector distance to the example VWS site.

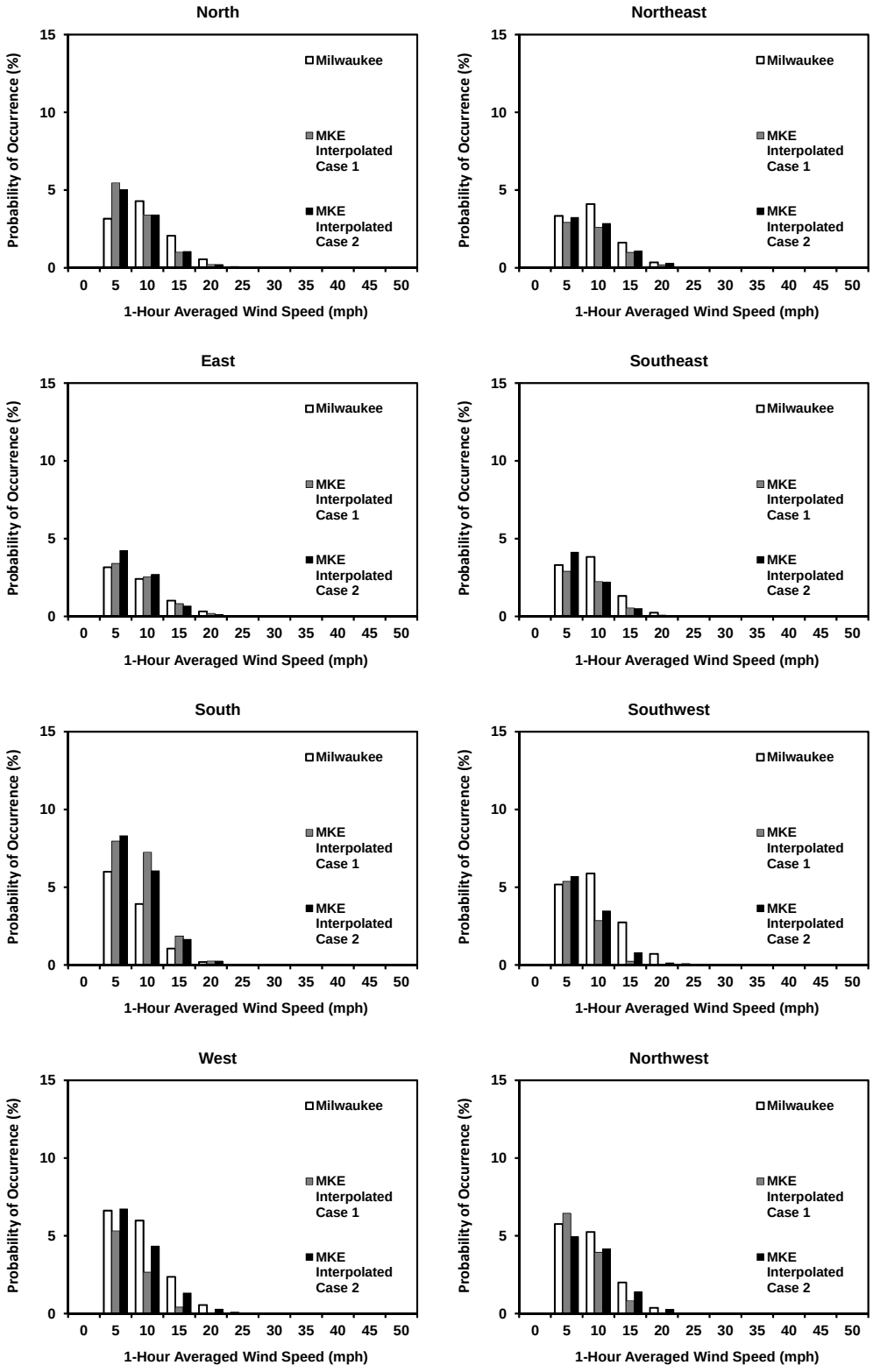

Figure 2.16 Combined probability mass function comparison for Milwaukee NCDC-ASOS data collected and interpolation cases – $P\left(U = u_i \cap D = d_j\right)$.

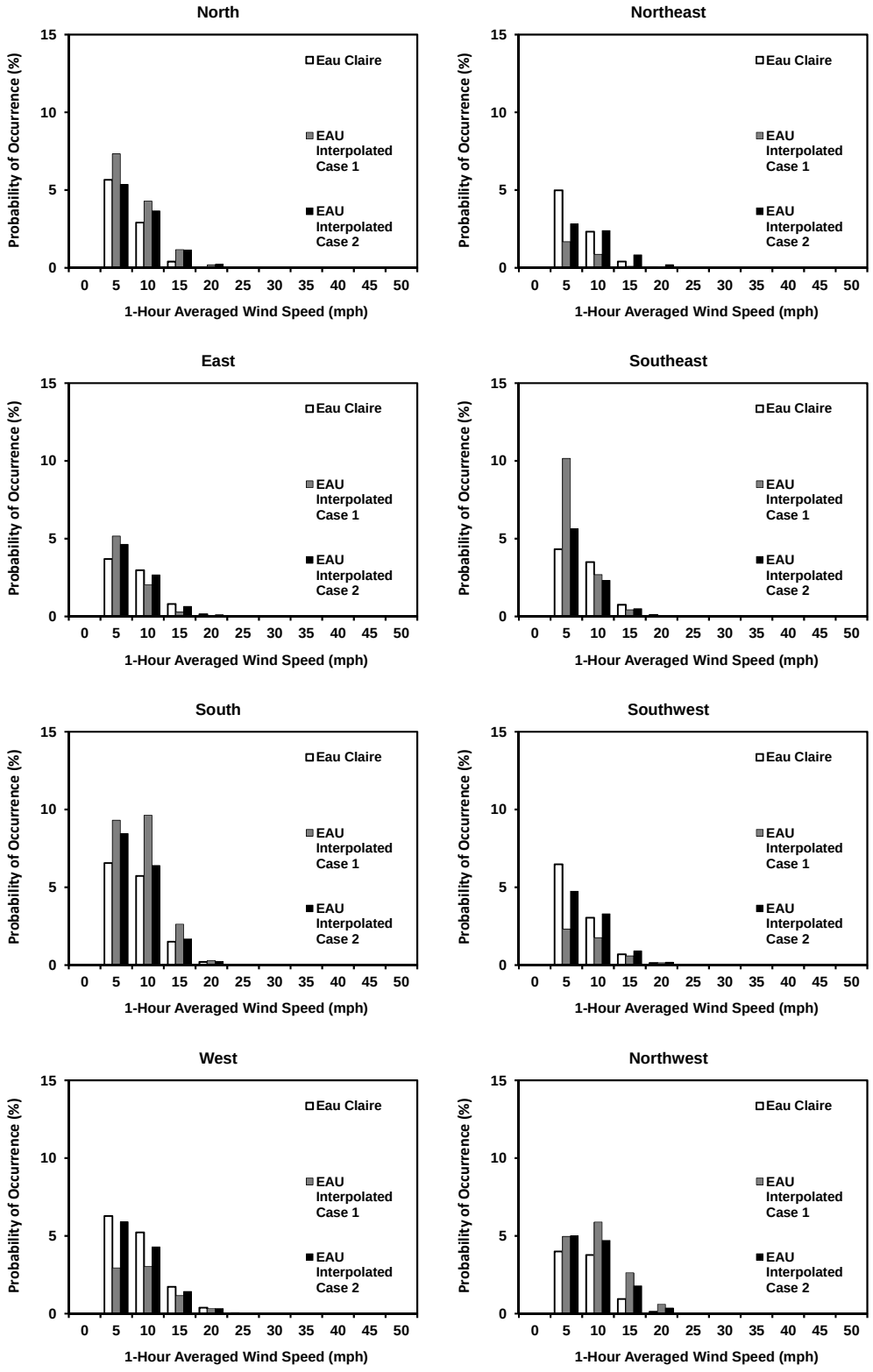

Figure 2.17 Combined probability mass function comparison for Eau Claire NCDC-ASOS data collected and interpolation cases – $P\left(U = u_i \cap D = d_j\right)$.

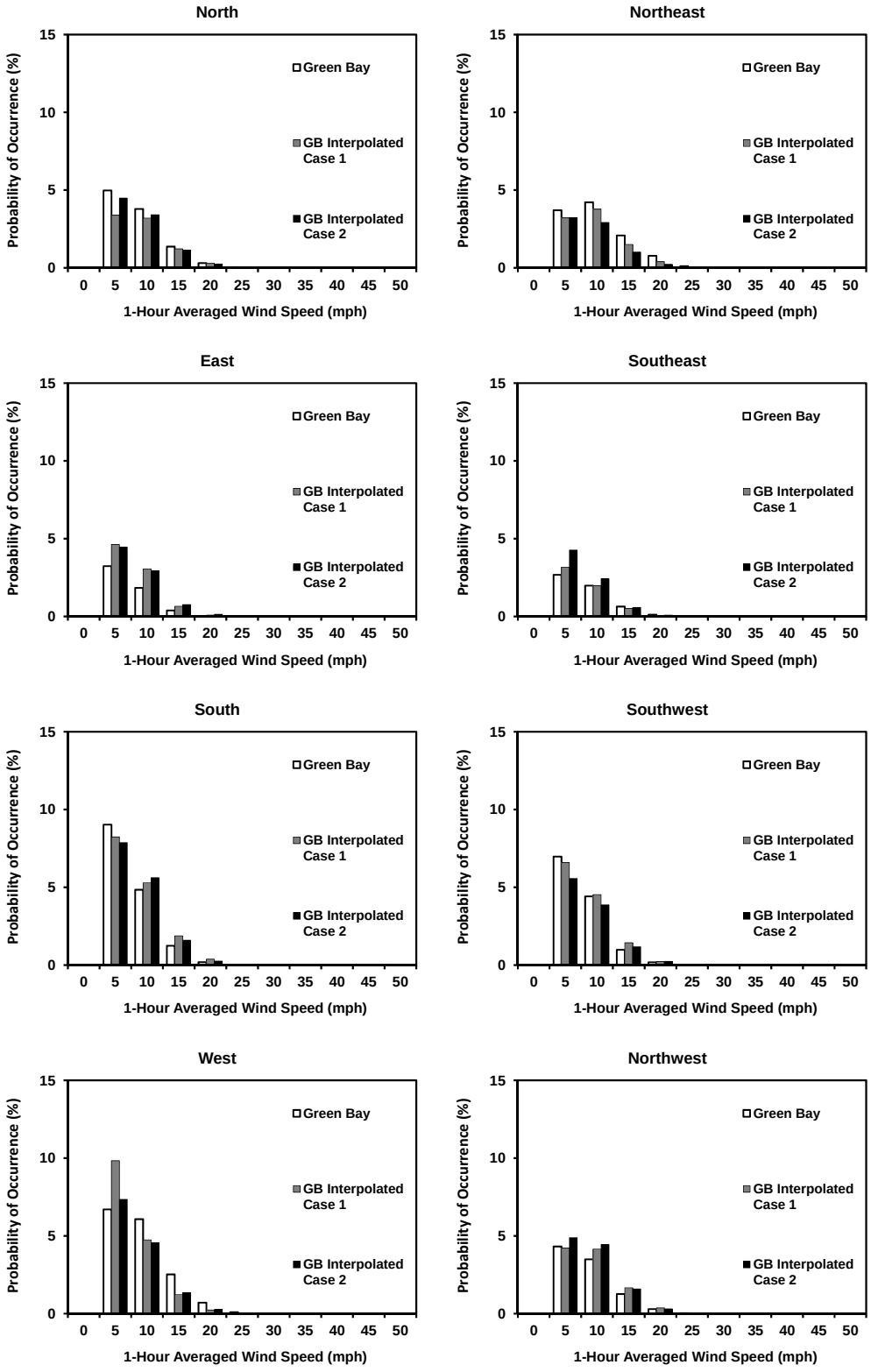

Figure 2.18 Combined probability mass function comparison for the Green Bay NCDC-ASOS data collected and interpolation cases – $P\left(U = u_i \cap D = d_j\right)$.

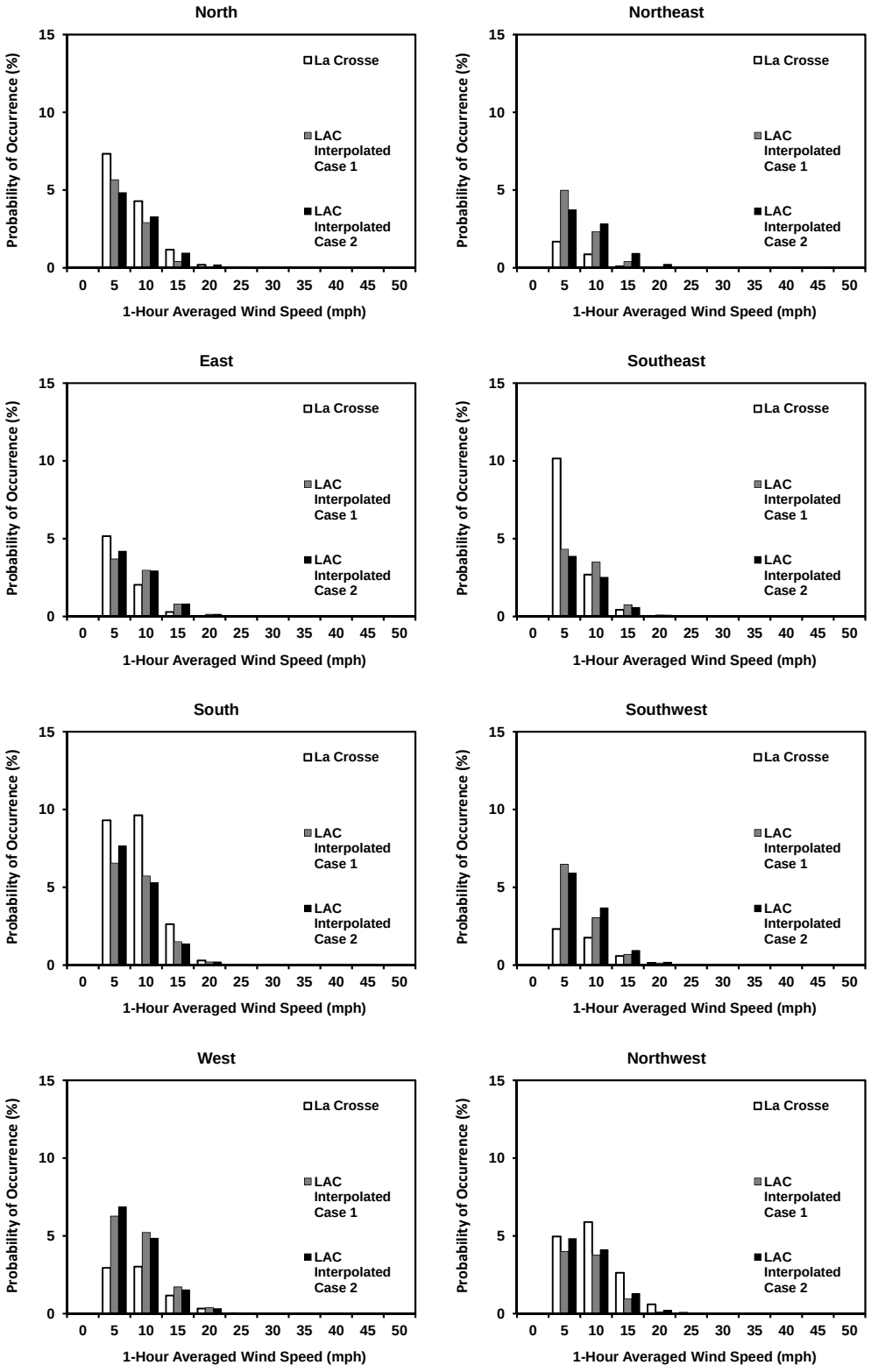

Figure 2.19 Combined probability mass function comparison for the La Crosse NCDC-ASOS data collected and interpolation cases – $P\left(U = u_i \cap D = d_j\right)$.

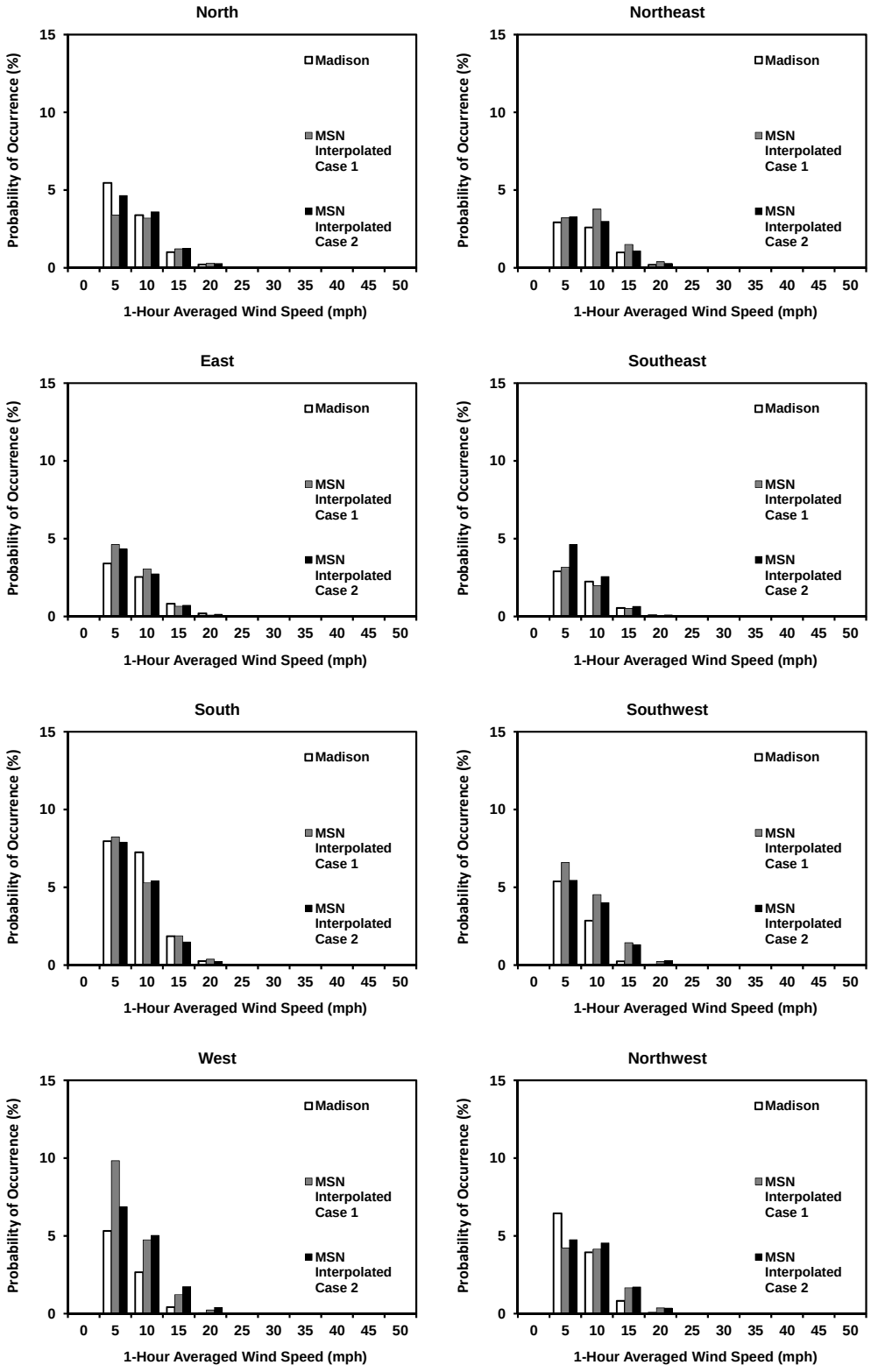

Figure 2.20 Combined probability mass function comparison for the Madison NCDC-ASOS data collected and interpolation cases – $P\left(U = u_i \cap D = d_j\right)$.

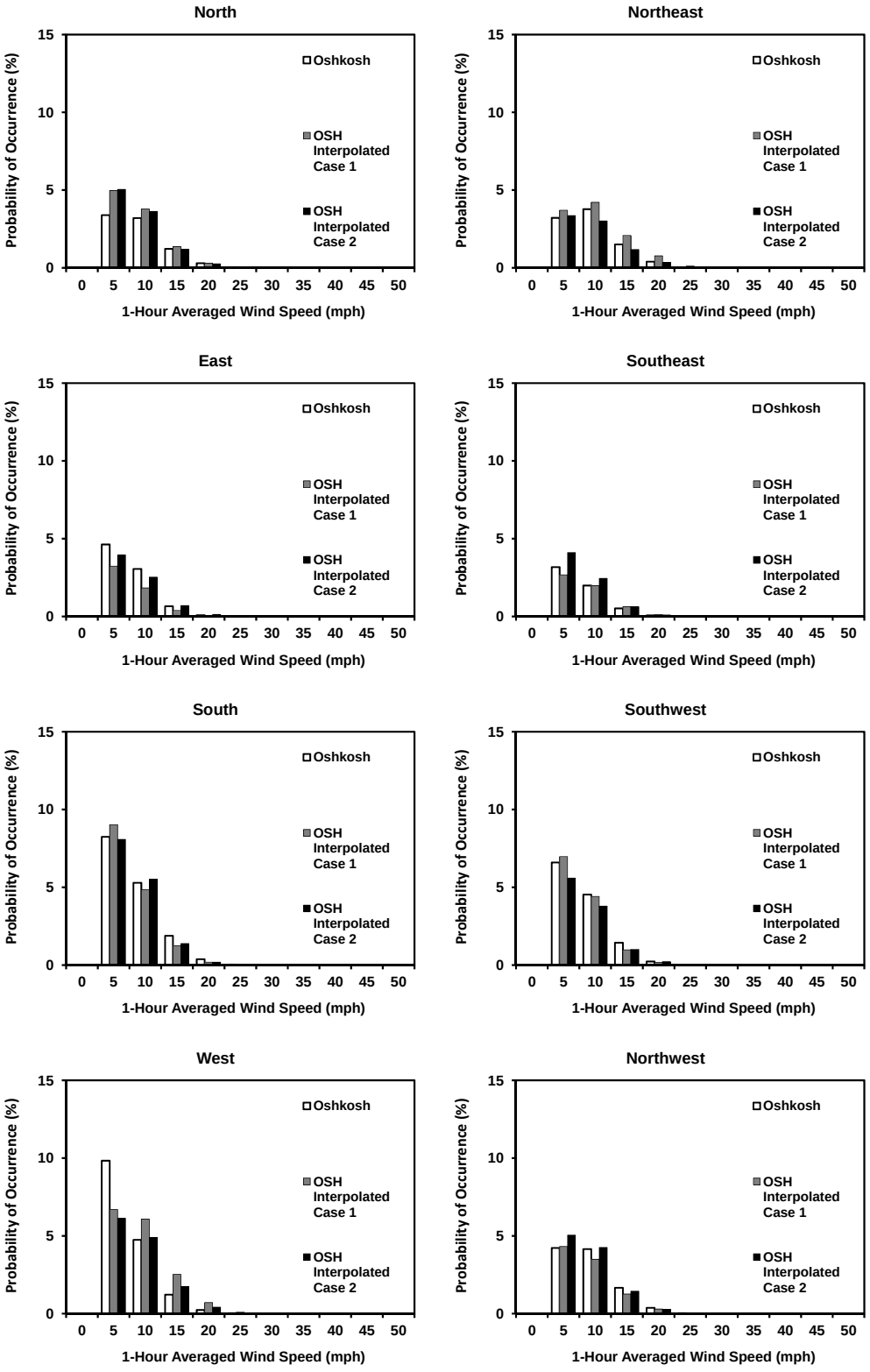

Figure 2.21 Combined probability mass function comparison for the Oshkosh NCDC-ASOS data collected and interpolation cases – $P\left(U = u_i \cap D = d_j\right)$.

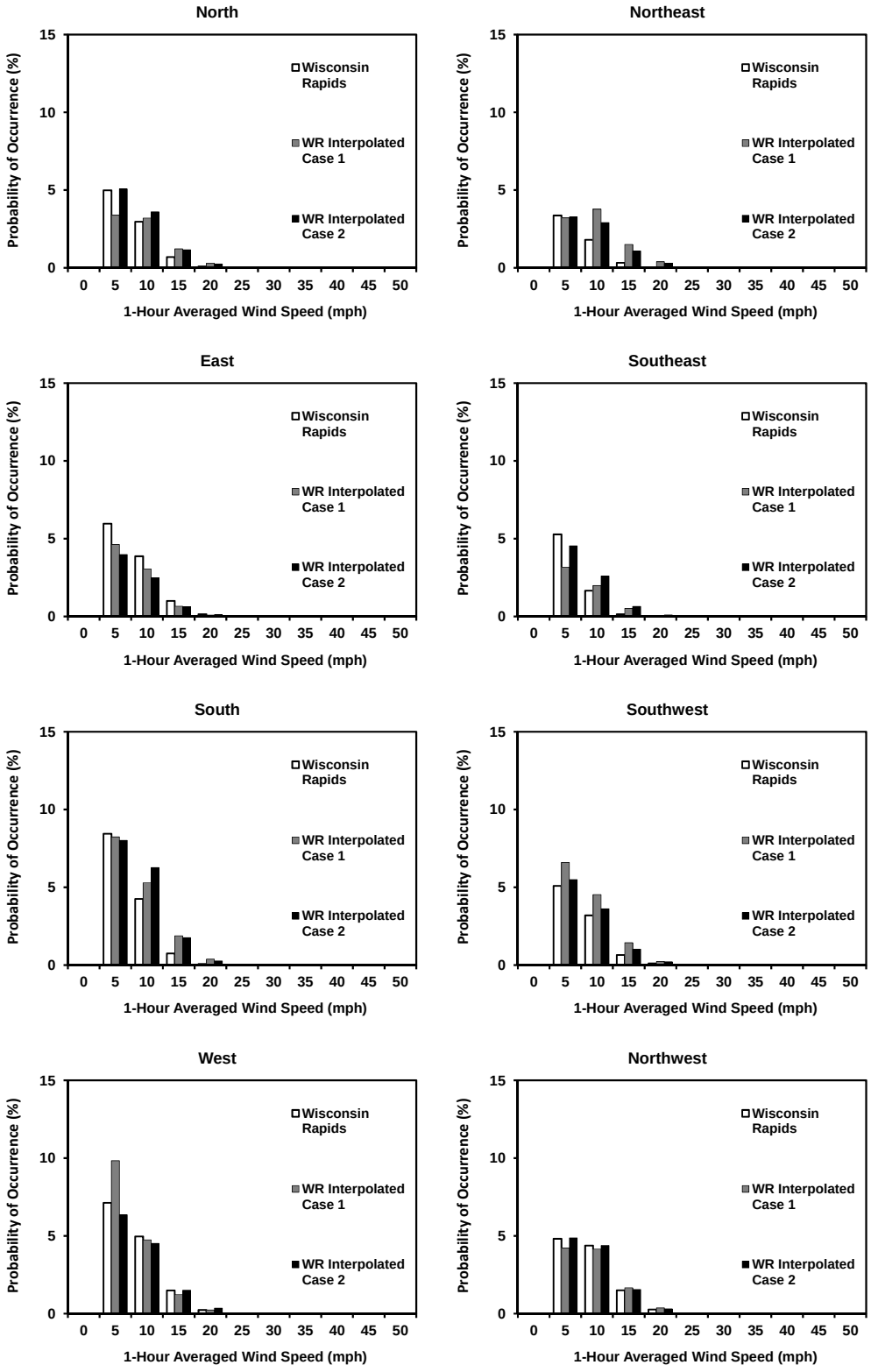

Figure 2.22 Combined probability mass function comparison for the Wisconsin Rapids NCDC-ASOS data collected and interpolation cases – $P\left(U = u_i \cap D = d_j\right)$.

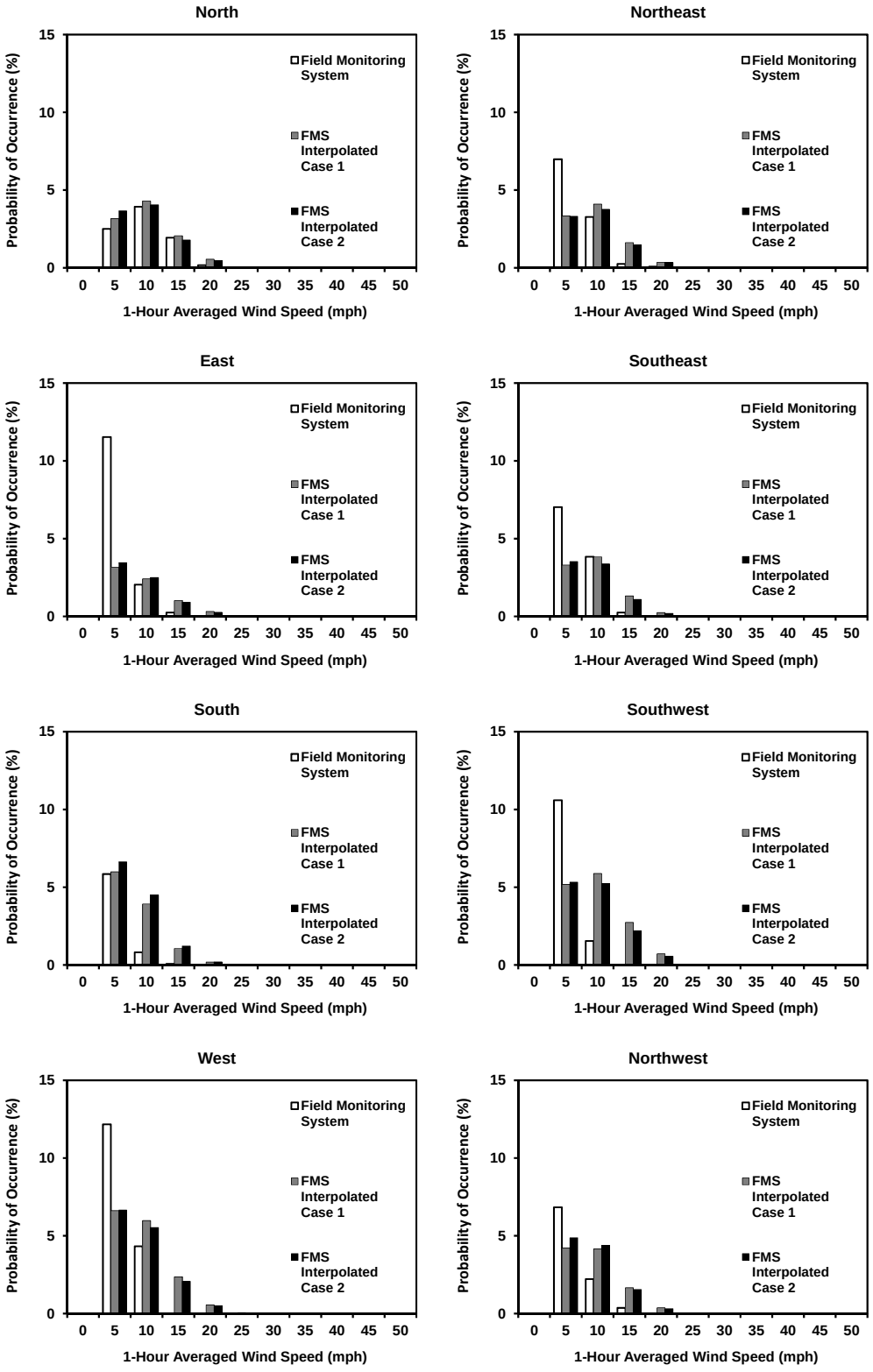

Figure 2.23 Combined probability mass function comparison for the FMS site data collected and interpolation cases – $P\left(U = u_i \cap D = d_j\right)$.

This page has been intentionally left blank.

Chapter 3 – Fatigue Life Uncertainty

3.1 Introduction

Fatigue design methodologies used in design specifications (AASHTO 2001; AASHTO 2009; AISC 2010) are predicated upon being able to quantify infinite service life for structural components susceptible to fatigue loading. They most often employ a design philosophy based upon ensuring that a specific connection detail will not see stress-range magnitudes above what is defined as the constant amplitude fatigue limit (CAFL) for a predetermined fatigue detail category. Virtually all of the connections currently used in mast-arm sign support structures are considered as Fatigue Detail Category E' corresponding to a severe fatigue condition. The variety of connections falling into this detail category is extensive and as a result, there is significant variability in service life seen by the Wisconsin Department of Transportation (*e.g.* service lives of 20+ years to service lives of less than 5 years). The connections considered in this category have a significant variety of geometric dimensions (*i.e.* tube thickness, plate thickness, bolt pattern) and the impact of this on the fatigue life requires further evaluation.

Quantifying the risk of fatigue-induced fracture in mast-arm sign supports and establishing inspection protocols for these structures requires that the variability in fatigue life of the connections in these structural systems be defined in a manner suitable for implementation in the reliability process discussed earlier in this report. The primary objective of the discussion in this chapter of the report is to define the parameters (mean and coefficient of variation) of a lognormal random variable model for fatigue life, A, so that the reliability analysis described in earlier chapters of the report can be used to quantify the risk of fatigue-induced fracture in mast-arm sign support structures. The methodology used to accomplish this goal is summarized as follows. Perform fatigue testing on connections typically used in highway mast-arm sign support structures to supplement the existing database of testing results. Synthesize the body of fatigue testing results conducted to date and develop a comprehensive database of fatigue testing results for these types of connections. Perform a complete taxonomy of these types of connections – one that synthesizes results from applicable fatigue tests into new detail categories that can be thought of as sub-details of the existing AASHTO E' Detail Category. Conduct statistical analyses on the proposed detail categories in order to quantify the fatigue life uncertainty associated with each of them. The present chapter outlines this process.

3.2 Existing Fatigue Design Philosophy

It is important to provide background with regard to the current procedure that is followed when utilizing the specifications for the design of sign and luminaire support structures (AASHTO 2009). A designer must be able to distinguish their connection configuration within the context of detail schematics. When a designer finds a connection configuration that looks like the one (or one very close to that) under consideration, he/she is referred to a table which groups examples of connection configurations into fatigue detail categories. Some connection configurations can be classified into several fatigue detail categories depending upon the loading scenario that the connection will undergo. Once the fatigue detail category is chosen, a number of cycles of loading or tension stress-ranges (until fatigue failure) may be anticipated as long as the nominal stress-range at the location of the detail is known (Fisher et al. 1998).

The procedure just described is founded upon some very important assumptions. At its most basic level, it assumes the designer has chosen a detail category, which closely represents the detail under consideration. Next, it assumes that the nominal stress-range at the location of the detail (within the structure) was correctly determined. Finally, and perhaps most critically, this procedure assumes that the stress concentration factor for the detail under consideration, at its most fatigue sensitive location, can be represented by the details used to create the fatigue detail category. This is because the procedure just described does not account for stress concentration effects directly. The effect is assumed to be embedded into the results of the fatigue tests used to generate these fatigue detail categories.

In order to quantify the variability in the number of stress cycles applied until a fatigue crack is expected to initiate, statistical analysis on groupings of fatigue test data is required. Emphasis should be placed on the word groupings. As shown in the AASHTO specification (AASHTO 2009), connections composed of different geometric configurations and details are expected to have vastly different fatigue lives (finite or infinite). Proper synthesis of fatigue testing data into appropriate categories for the reliability analysis conducted in this research effort is crucial to the adequacy and accuracy of the subsequent reliability analysis employed.

3.3 Experimental Program

The fatigue tests performed as part of this research effort were conducted in order to supplement the existing database of fatigue testing data found in the literature. Focus was given to socketed tube to transverse plate connections given their prevalence throughout the WisDOT transportation infrastructure network. A review of the literature revealed that all applicable fatigue tests for this type of connection were conducted at stress-range magnitudes that ranged from 4.9 ksi on the low end to 18.9 ksi on the high end. Earlier research work in this field indicates that there is a difference in variability for stress-range magnitudes in this range for welded connections (Little and Jebe 1975). Specifically, when stress-ranges applied to a connection are high

(*e.g.* 19 ksi), variability in the fatigue life is low and when stress-ranges applied to a connection are low (*e.g.* 5 ksi), variability in the fatigue life tends to be high (Little and Jebe 1975).

Statistical analysis performed on fatigue test results of unreinforced (un-stiffened) mast arm connections in earlier phases of the present research effort (Foley et al. 2008) indicated that additional fatigue testing be conducted at tension stress-range magnitudes of 6 ksi and 15 ksi. New statistical analysis and additional synthesis has been conducted in the final phases of this research effort and will be presented in this chapter of the report. The experimental program undertaken in the present research effort was focused on conducting fatigue tests on un-stiffened mast arm connections at stress-range magnitudes of 6 ksi and 15 ksi. The fatigue testing conducted as part of the present research effort was conducted at Marquette University and the University of Wisconsin – Milwaukee. All testing done that is pertinent to the present research effort is reviewed in this chapter and additional detail for the work completed at Marquette University is available (Diekfuss 2013).

Experimental Fixture

A test arrangement similar to that used by Koenigs et al. (2003) was used in the present research effort to perform the full scale constant amplitude fatigue tests on the round tube specimens. The arrangement consisted of bolting two specimens end-to-end utilizing what is referred to as a load box. A load may then be applied to this load box while providing end support fixturing consistent with that of a simply supported beam (*i.e.* double restraint fixture representing a pin support on one end and single restraint fixture representing a roller support on the opposite end). In this way, stresses measured by strain gages can be verified by simple statics. The fixture used in the testing done at Marquette University is shown in Figure 3.1 and Figure 3.2. The fixture used enables two specimens to be tested simultaneously at the same constant amplitude stress-range. Each specimen can be thought of as a cantilever with fixed ends located at the cross-section that is bolted to the load box and free ends located at the cross-sections bolted to the support fixtures.

It should be noted that this testing arrangement is limited to the application of tensile loads and tensile stress-ranges. The fixtures utilized are incapable of supporting compressive loads due to a lack of lateral bracing. This enables the design of the test setup to be simplified, but prevents the application of fully-reversed cyclic loading (Koenigs et al. 2003). Therefore, only the top half of each specimen was loaded in tension during each test conducted. Because only the top half of the cross-section was loaded in tension, the bottom half was assumed to remain in compression (*i.e.* not subjected to any fatigue loading) and considered as a new specimen for subsequent fatigue testing.

Test Specimens

Two types of test specimens were utilized – round and multi-sided (faceted with 16 sides). The reason for two types of specimens was because the State of Wisconsin does have round and multi-sided mast-arm connection configurations throughout the state in its inventory. The following discussion will provide a complete description of both types of test specimens.

The two round specimens used for the fatigue tests conducted in the present effort were purchased from Valmont Industries, Inc. located in Valley, Nebraska. Each specimen consisted of a 97.75-in round tube, with an outer diameter tapered from 11.0-in to 9.9-in and a wall thickness of 0.1793-in. Each end of the specimens contained a socketed connection with unequal leg fillet welds (0.44-in x 0.25-in) on the outside of the connection socket and equal leg fillet welds (0.1793-in by 0.1793-in) on the inside of the connection socket. The socketed plates were 1.75-in thick, 18.5-in square, and contained a center-to-center bolt hole spacing of 15.25 inches. No ultrasonic testing of the welds was conducted in the present research effort and visual inspection indicated no defects in the specimens. Furthermore, no material testing was conducted as it was not important for fatigue life characterization at the stress-ranges employed.

The two multi-sided specimens used for the fatigue tests conducted in the present effort were purchased from Millerbernd Manufacturing Company located in Winsted, Minnesota. Each specimen consisted of a 97.75-in multi-sided tubes (16 sides), with an outer opposite flat-to-flat distance of 11.0 inches and a wall thickness of 0.1875 inches. Each end of the specimens contained a socketed connection with unequal leg fillet welds (0.44-in. x 0.25-in.) on the outside of the connection and equal leg fillet welds (0.1875-in. x 0.1875-in.) on the inside of the connection. The socketed plates were 1.75-in. thick, 18.5 inches square and contained a center-to-center bolt hole spacing of 15.25 inches.

Fatigue Testing Protocol

The experimental fixture used in the present study was fabricated at Construction Supply & Erection, Inc. located in Germantown, Wisconsin. A photo of the overall test setup, including all fixtures, the two round specimens, the MTS control station, and the data acquisition system was shown in Figure 3.1. Images of the key individual components in the experimental fixture used in the testing are shown in Figures 3.1 and 3.2.

All of the fatigue testing conducted as part of this study was done so with the use of Vishay weldable strain gages to monitor the stress-ranges during testing. The strain gages were spot welded to the test specimens at the top most tension fiber two inches from the weld toe. The test specimens were cleaned at the locations where gages were to be mounted. The specimens were first cleaned with a wire brush and then rinsed with acetone. This procedure was conducted to ensure that the mill scale would not inhibit the accurate acquisition of strain readings and that good quality spot welds could be achieved for the gages. A photo of the strain gaged specimens, an up-close picture of a typical Vishay strain gage as well as a photo of the Vishay

spot welder used to secure the gages onto the specimen is provided in Figure 3.3. It should be noted that two strain gages were used for the first set of specimens to verify the strain gages were in good working order.

The literature on fatigue testing reviewed in the present effort has many variations in the protocols that were followed when conducting full-scale fatigue tests. A detailed review of all fatigue testing completed to date has been provided elsewhere (Diekfuss 2013) and the testing results are summarized as part of this report. Some studies simply back-calculated a required actuator loading based upon the desired stress-range magnitude and the section properties present. However, the majority of prior fatigue tests utilized strain gages to verify that the applied loading was acquiring the desired stress-range response.

As indicated earlier, stress-range magnitudes close to the limits of the existing fatigue testing results database were the targets utilized in the present fatigue testing, namely 6.0 ksi and 15.0 ksi. The procedure used to achieve the desired stress-range magnitudes will now be discussed. Figure 3.4 provides the resulting shear and moment diagrams for a given actuator loading applied to the fatigue specimens through the load box. Utilizing this diagram and geometry, the magnitude of the moment at any point along each specimen may be determined in terms of the applied actuator loading. In this procedure, four moment values were calculated: one at each strain gage location; and one at each weld-toe location.

The beam is simply-supported and the maximum moment resulting from the applied loading can be calculated using,

$$M_{MAX} = \frac{P \cdot L}{4} \tag{3.1}$$

M_{AG} and M_{AT} in Figure 3.4 are the strain gage and weld-toe moments on the side A specimen, respectively, while M_{BG} and M_{BT} are the strain gage and weld-toe moments on the side B specimen, respectively. These bending moment magnitudes can be written in terms of the maximum bending moment using the geometry of the bending moment diagram. Stress magnitudes are computed using elementary beam theory.

The method used to determine the magnitude of the applied loading for each test will now be discussed in detail. Each test began by applying load via the MTS actuator. The load was increased very slowly (quasi-static) until the pins used at both supports were “seated” to ensure a stable condition was met. The actuator loading which caused the pins to be seated (P = 2,500 lbs) was recorded and used as the minimum actuator loading in the loading cycles for all subsequent fatigue testing. After applying the 2,500-lb load, the strain readings were zeroed and additional loading was applied (quasi-statically) until an average between strain gages achieved a value, that when converted to stress using an assumed elastic modulus of 29,500 ksi, would provide the stress-range magnitude desired in the constant amplitude fatigue test (either 6.0 ksi or 15.0 ksi).

This loading was then recorded and used as a starting point in terms of target loads input into the MTS controller software.

Once the target and amplitude were input for each fatigue test, detection limits for both displacement and force were established and utilized during testing. The MTS detection limits on the application of force were used to prevent overloading of the specimens. The MTS detection limits on vertical displacement of the load application point were used as a secondary means of crack initiation detection. With all material and section properties the same, a cracked specimen is more flexible than an un-cracked specimen. Therefore, barring mechanical malfunction, any increase in displacement without changing the applied loading should indicate that a crack has initiated.

The *dynamic* response of the system was anticipated to be different than the *quasi-static* response of the system given the inertial effects that come into play when the rate at which load is applied increases. It should be expected that additional loading would be required to obtain an equivalent magnitude of strain at the gages when compared to the quasi-static loading case. Therefore, the strain readings at the beginning of each fatigue test were monitored closely to determine the extent to which loading must be increased in order to maintain the desired constant amplitude stress-range magnitude. If the strain-ranges were not at a magnitude that achieved the desired stress-range, the experiment was paused and adjustments to the loading magnitude were made. Testing then resumed and this procedure was carried out until the average value between both gages resulted in the desired stress-range magnitude for each test.

The primary technique utilized for crack detection was via dye penetrant testing. Each test was paused every 216,000 cycles (approximately) to check if a crack initiated at the weld toe. This number of cycles was chosen as it is the number of cycles that occurred in a 24-hour period. The loading frequency that provides 216,000 cycles in 24 hours is 2.5 Hz. The loading frequency was limited to 2.5 Hz to minimize the vibrations in the hoses which ran from the hydraulic service manifold (HSM) to the MTS Actuator. Preset detection limits on force and displacement were a secondary method of crack detection used in the Marquette testing. If a test stopped before the 216,000 cycle mark, the specimens were checked for cracks prior to restarting the test. Further details regarding the testing protocol are available (Diekfuss 2013).

Due to the timing of the fatigue testing conducted as part of this research, four of the eight fatigue tests completed were done at the University of Wisconsin-Milwaukee. Midway through testing, the Marquette University Engineering Materials and Structural Testing Laboratory (EMSTL) was opened at which point all remaining fatigue tests were conducted on the Marquette University campus. The results will indicate the location where each test was conducted through the use of a prefix – MU was used to indicate that the test was conducted at Marquette University and UWM was used to indicate that the test was conducted at the

University of Wisconsin-Milwaukee. A descriptor key for the fatigue test specimens used in the present research effort is provided in Figure 3.5.

Other than knowing that strain gages were used to ensure that desired stress-ranges were being achieved, very little information was provided by the sub-contractor as to the protocol that was followed during the fatigue testing conducted in the UWM laboratory. Also, the reader should note that UWM was sub-contracted to complete approximately two million cycles of stress (load) range. Given the limited number of cycles, Miner's equivalent damage rule was employed and tests were conducted with increasing stress-ranges to ensure a crack was initiated within the limited number of cycles.

Fatigue Testing Results and Discussion

Eight fatigue tests were conducted as part of the present research effort. Four of the tests were conducted at Marquette University (Diekfuss 2013) and the other four tests were conducted at UWM. The results for each test include the stress-range and number of cycles to failure for that stress-range. Failure was classified as crack initiation. Tests where cracking was not achieved are noted. Table 3.1 summarizes all of the fatigue testing results from the present study. The key to the specimens was given in Figure 3.5.

Figure 3.6 provides a graphical comparison of the fatigue test data by showing their results on a single S_R-N diagram. Also provided on this S_R-N diagram is the AASHTO E' Fatigue Detail Category in order to give reference to the current fatigue design standards. The noticeable difference in the fatigue performance of the multi-sided specimens when compared to the round specimens is apparent. Faceted specimens have significantly lower fatigue lives and also can have significantly more variability in fatigue life than round specimens. The behavior of the faceted specimen results in a fatigue life significantly below that of the E' detail category assumption. The reason for this is the significant shear lag effect over the flat facets in the hollow shape and the concentration of stress at the "corners" in the faceted shape. This spiking of stress at the corners is not new (Foley et al. 2004) and it is expected to act as a stress riser in the cross-section. Variations in stress concentrations across connection details that are all considered as E' is the motivation for the proposed alternate detail categories for assessing fatigue performance within the reliability context proposed in the present research effort. The behavior of the faceted cross-section is the first indication of this in the present research.

Photos of the test specimens in which a crack was initiated are provided in Figures 3.7 through 3.10. Each photo indicates the specimen name, approximate length of crack, crack termination points, as well as the stress-range and number of cycles to failure for that stress-range. It is important to note that all testing conducted at Marquette University in the EMSTL had crack lengths at testing conclusion for the round

specimens ranging from 6.5 inches to 7.75 inches. The specimens tested at UWM had crack lengths for the round specimens at test termination ranging from 6 to 11 inches.

3.4 Synthesis of Fatigue Testing

There has been a lot of fatigue testing on round tubular and faceted tubular shapes conducted in the last three decades. The present research effort included a detailed synthesis of world-wide fatigue testing done since 1970. The fatigue testing data generated as part of the present research effort was included into this world-wide database prior to synthesis. This section of the report outlines the synthesis of fatigue testing data conducted in the research effort. Further details for the synthesis approach are available elsewhere (Diekfuss 2013).

Fatigue Test Data Collected

Analysis of fatigue test data for connections used in sign support structures is usually conducted with a goal of determining within which existing fatigue detail category it should reside. This section will outline an approach to synthesizing fatigue test data without the confines of traditional AASHTO detail categories in place. All fatigue test data (relevant to connections considered in the present study) will be looked at holistically and synthesized with a fresh viewpoint. The following is a list of research groups upon which the fatigue test results database is founded: Archer and Gurney (1970); Fisher et al. (1981); South (1997); Deschamp (2002); Machietto (2002); Chen et al. (2003) and Alderson (1999); Koenigs et al. (2003); Ocel et al. (2006); Rios (2007); Anderson (2007); Richman (2009); Roy et al. (2011); and the experimental testing conducted as part of the present study (Diekfuss 2013).

Figure 3.11 illustrates all fatigue test data gathered in the present research effort from the literature and from the experimental testing conducted on a single S_R-N diagram to illustrate the significant variability among the experimental results. The AASHTO E' detail category S_R-N curve (solid line) is also present in the figure. An ideal scenario for design is to have all fatigue test data plotted and falling to the right of the E' detail category S_R-N curve with limited numbers of outliers if the E' detail category is to be used. The significant level of variability in fatigue life for connections typical of mast-arm sign support structures fostered a detailed examination and synthesis of all fatigue testing conducted in the past three decades. The following questions were posed when defining this process: How does one separate the existing fatigue testing results for connections contained within sign support structures? Should the test data be segregated by the physical appearance of the details? Should the test data be segregated by the stress concentration factor at the weld toes present within those details? Both of these classification methods were evaluated in the present research effort. The following sections will describe each method as well as provide the advantages and disadvantages to both methods.

The general guidelines that apply to both segregation methods will be discussed first. The goal of conducting these syntheses was to set baseline fatigue detail categories which will provide the fatigue life parameters required for the subsequent reliability analysis. Therefore, the following bulleted list contains the criteria which disqualified the results of particular fatigue tests from being considered in either of the two segregation methods:

- Any test performed on specimens that already included stress cycling was not considered, unless the same stress-range was continued or the specimen was flipped over (*e.g.* testing the reverse side or the side that was initially in compression).
- Any test that was not conducted using a single magnitude constant-amplitude stress-range (*e.g.* a Miner's equivalent stress-range) was not considered.
- Any test that did not include fatigue crack initiation was not considered (*e.g.* a test classified as run-out).
- Any test that did not include strain gaging to ensure targeted stress-range magnitudes were maintained during testing was not considered.
- Any test where the weld, weld toes, or base metal was mechanically treated (*e.g.* ultra-sonic impact, bristle blaster, etc.) was not considered.

The database of fatigue test results was first sifted using the preceding criteria. If any fatigue test met any of these criteria, the test was labeled as an *unused test* and it was not included in any of the subsequent statistical analysis. Further details of the fatigue testing syntheses conducted are available elsewhere (Diekfuss 2013).

Classification by Traditional Detail Category

This first approach to segregating the fatigue test data is similar to the existing approach presented in AASHTO (2009), which classifies connection details using similarity in appearance and weld type. All connections were first classified as unreinforced or reinforced (*e.g.* unstiffened or stiffened with welded gusset attachments). The connections were then separated based upon whether or not the tube (mast-arm or pole) was round or multi-sided (faceted). Finally, the connection was classified based upon the type of weld it contained (*e.g.* fillet weld, full-penetration weld). Thirteen potential fatigue detail configurations were identified in this manner (Diekfuss 2013). Two hundred sixty-five (265) fatigue tests were identified using the first synthesis approach. Table 3.2 lists the new fatigue detail categories generated by the first synthesis approach including the corresponding number of contributing fatigue tests for each.

Classification by Stress Concentration Factor

There are numerous variations in the geometric configurations of the welded tube-to-transverse-plate connections within sign support structures. It should be expected that the structural response and fatigue life

will differ from one to another. It is widely known that, in general, larger stress concentration factors lead to lower fatigue lives. The stress concentration factor (*SCF*) is defined as the magnitude of peak (maximum) stress within the wall of the mast-arm (near the weld toe) divided by the stress computed using the flexure formula. Several studies have performed finite element analyses with very high fidelity finite element models to gain a better understanding of what the *SCF* is for a given connection-type, where the *SCF* is a maximum on the cross-section, and the extent to which changing various properties like plate thickness, tube thickness, bolt pattern/circle, etc. have on this *SCF* and the resulting fatigue performance (Ocel 2006; Richman 2009; Roy et al. 2011).

The most recent study performed on these types of connections was by Roy et al. (2011). Aside from significantly contributing to the existing database of fatigue test data on typical highway sign-support and high-mast luminaire support connections, the results of this study developed parametric equations for determining the stress concentration factor contained within typical connections used in mast-arm sign support structures. The geometric dimensions required in order to utilize the equations for stress concentration factor computation (Roy et al. 2011) were unable to be acquired for all fatigue tests within the database assembled for this study. Therefore, the second synthesis approach was limited to 129 of the 265 possible fatigue tests.

The stress concentration factor was determined for each of the applicable connections considered and connection details were categorized based upon the magnitude of the stress concentration factor (Diekfuss 2013). Three potential fatigue detail categories based upon stress concentration factors were identified:

- E2: $2.0 \leq SCF < 3.0$
- E3: $3.0 \leq SCF < 4.0$
- E4: $SCF \geq 4.0$

Table 3.3 lists these new fatigue detail categories generated by the second synthesis approach and the number of fatigue tests available that fall within each proposed detail category. It should be noted that there are still a significant number of fatigue tests that land into these new detail categories (*e.g.* 24 to 73 tests) that can be used as the basis for determining the parameters needed to quantify the variability in fatigue life for the reliability analysis to follow.

Summary for Both Synthesis Approaches

Tables 3.4 through 3.16 provide all fatigue test results considered in the present study and Figures 3.12 through 3.23 provide keys for interpreting the labels given to each specimen. The tables and figures are separated based upon the research group that conducted the fatigue tests. Each table contains the following:

- Labeled specimens tested by each study
- Resulting fatigue detail category according to both synthesis approaches

- Stress-range magnitude each test was conducted at
- Number of stress-range cycles to failure for each test

It should be noted that only those tests that met the criteria outlined earlier have a fatigue detail category assigned to them. Some tests were able to be assigned using the first synthesis approach but not the second due to insufficient information regarding the geometric dimensions of the connection used within the test. Therefore, to keep the sample size as large as possible for both approaches, rather than labeling these tests as "Unused Test", "na" was placed in the column for the detail category assigned by the second synthesis approach.

3.5 Statistical Analysis of Fatigue Data

Wirsching (1983) summarizes a procedure whereby one may define the relationship between applied constant-amplitude stress-range and resulting cycles to failure for a large number of fatigue test results. The procedure utilizes a least squares regression analysis as the foundation to the approach and recommends use of a lognormal random variable to characterize uncertainty in fatigue life (Wirsching 1983).

The lognormal distribution is a widely used probability model in engineering applications; however, many other distribution models are also used. To determine the best possible probabilistic representation of the fatigue test data, the Kolmogorov-Smirnov (K-S) *goodness of fit* is often performed (Foley et al. 2008; Wirsching 1983). The K-S test (not performed here) is a test that compares the cumulative distribution frequency for a sample with the cumulative distribution function for a particular theoretical probability distribution. In the past, this test has been performed on fatigue test data for typical connections used in offshore structures (Wirsching 1983) and for mast-arm sign connections found in Wisconsin (Foley et al. 2008). Each of these former studies determined that a lognormal distribution provided an acceptable representation of the fatigue-life variability associated with these connections.

The lognormal distribution, like most probability distributions, requires certain parameters to define its shape which ultimately affects the resulting probabilities provided by the distribution. The required parameters in the case of the lognormal distribution are:

$$\lambda_A = \ln \mu_A - \frac{1}{2} \cdot \zeta_A^2 \tag{3.2}$$

$$\zeta_A^2 = \ln\left[1 + \left(\frac{\sigma_A}{\mu_A}\right)^2\right] = \ln\left[1 + \left(CV_A\right)^2\right] \tag{3.3}$$

where λ_A is the expected value of the lognormal random variable *A*, and ζ_A^2 is the variance of the lognormal random variable *A*. Therefore, in order to generate the lognormal distributions necessary to quantify the

variability in fatigue life of the connections under consideration, the parameters listed in equations (3.2) and (3.3) must be found for each fatigue detail category developed in the fatigue syntheses performed in the preceding section. Specifically, this includes finding the mean, μ_A, and coefficient of variation, CV_A of the lognormal random variable A.

Consider the group of n fatigue tests plotted in Figure 3.20. Each test contains a constant-amplitude stress-range magnitude, S_{Ri}, and a corresponding number of cycles to fatigue failure, N_i. A single straight line, drawn through the mean of the data and the coefficient of variation are used to characterize the variability in fatigue cycles to failure for the stress-ranges in the data set considered (Wirsching 1983). The analytical form of the typical fatigue life curve is given by:

$$N \cdot S_R^m = A \tag{3.4}$$

where: m is the slope of the straight line, and A is the value of the x-intercept. Estimates for the values of m and A can be obtained from the fatigue data being considered. Equation (3.4) can be expressed in a linear form:

$$Y = a + b \cdot X \tag{3.5}$$

where:

$$Y = \log N$$

$$X = \log S_R$$

$$a = \log A$$

$$b = -m$$

This procedure assumes that Y has a normal distribution for all X. The values for a and b are then estimated as follows (Wirsching 1983):

$$\hat{b} = \frac{\sum_{i=1}^{n}\left(X_i - \overline{X}\right)\cdot\left(Y_i - \overline{Y}\right)}{\sum_{i=1}^{n}\left(X_i - \overline{X}\right)^2} \tag{3.6}$$

$$\hat{a} = \overline{Y} - \hat{b} \times \overline{X} \tag{3.7}$$

where: $\overline{X}$ and $\overline{Y}$ are the sample means of X and Y, respectively. The estimates for $\hat{a}$ and $\hat{b}$ are random variables because Y_i is a random variable (Wirsching 1983). The least squares line is:

$$\hat{Y} = \hat{a} + \hat{b} \cdot X \tag{3.8}$$

where $\hat{Y}$ is the mean (or expected value) of Y given X.

In order to determine the coefficient of variation for A, CV_A, the standard deviation in fatigue life for the samples within this detail must first be determined. Determining the standard deviation may best be explained in graphical terms. Referencing Figure 3.24, it is clear that in addition to the least squares (mean) line, two

additional lines have been plotted, both at an equivalent slope – *m*. Each line, if continued to the *x*-axis, will provide a value for *A* that is specific to the test that created that data point. For the sample of fatigue tests considered, the least squares line provides the expected value of *A*, or μ_A, and the two additional lines provide minimum and maximum values of *A*. Continuing this process for all data within the E4 detail category provides values of *A* for each individual fatigue test. A measure of the spread of these values about μ_A is termed the variance of *A* and is determined as (Haldar and Mahadevan 2000):

$$Var(A) = \frac{1}{n-1}\sum_{i=1}^{n}(A_i - \mu_A)^2 \tag{3.9}$$

The standard deviation may then be determined as (Haldar and Mahadevan 2000):

$$\sigma_A = \sqrt{Var(A)} \tag{3.10}$$

and finally, the coefficient of variation for *A* is:

$$CV_A = \frac{\sigma_A}{\mu_A} \tag{3.11}$$

Summaries of the statistical parameters generated for the detail categories developed in *Synthesis Approach No. 1* and *Synthesis Approach No. 2* are provided in Tables 3.17 and 3.18, respectively. The least squares lines that represent their respective relationships between stress-range magnitude and cycles to failure are provided in Figures 3.25 and 3.26. It should be noted that in some cases regarding Synthesis Approach No. 1, the statistical parameters were unable to be determined due to an insufficient sample size (U6, R2 and R5), or in other cases, the data for the particular category generated unrealistic results (U4, U7, and R4).

Special Note on New Fatigue Detail Categories

It is clear that the new fatigue detail categories are empirical and based upon a limited number of fatigue tests conducted at a limited number of stress-ranges. Therefore, one should be cautious of extrapolating the use of these curves beyond the stress-range magnitudes used as the empirical foundation for the curves. For example, extrapolating the S_R-N curve of Figure 3.24 (E4 detail) would provide a stress-range magnitude of well over 100 ksi at N = 1000 cycles. A connection cycled at a stress-range of 100 ksi magnitude would certainly fail prior to 1000 cycles. A similar, but opposite argument can be made for low-end stress-ranges. At very low stress-ranges (< 1ksi), these connections are expected to sustain much longer lives than predicted by the new details. In other words, a straight line over all stress-ranges is physically unrealistic. One must be careful when extrapolating the details beyond the range of stress-ranges used during testing.

The present study established unique limits on the range of applicability for the new fatigue detail categories. The curves for each detail category were capped at the maximum stress-range contributing to that detail. The maximum applicable stress-range for each new fatigue detail category is provided in the far right columns of Tables 3.17 and 3.18. It should be noted that all stress-ranges below the listed maximum

applicable magnitudes in the present study contributed to damage accumulation. Therefore, extrapolation of the straight line behavior below the low-end stress-ranges for each new detail was necessary. This can be considered a conservative approach since each detail would perform much better than the curve indicates at very low stress-ranges (*i.e.* $S_R < 1$ksi).

3.6 Concluding Remarks

The goal of this chapter was to formulate a method for defining an expected fatigue life, with known variability, to a connection being considered such that a statistical model for fatigue life could be used in a reliability procedure for assessing the expected life of mast-arm sign support structures. Two distinctly different approaches have been presented in order to complete this task. A comparison of these two approaches will now be discussed.

Qualitatively, the results from the statistical analyses of both synthesis approaches seem reasonable. For the first synthesis approach (Table 3.17 and Figure 3.25), it appears that reinforced connections tend to perform better than unreinforced connections as illustrated by their locations being the farthest right in the figure. The second synthesis approach (Table 3.18 and Figure 3.26) seems to illustrate a very clear trend that an increase in SCF decreases fatigue performance. The E4 category used in this second synthesis approach includes significantly less variability (steeper slope in log-log space).

Two very important things to look at when assessing the summary of results provided in Tables 3.17 and 3.18 are the slope of the line defining the expected life for each detail category, m, and the expected value μ_A. For a particular detail category, as the magnitude of m increases, so does the magnitude of μ_A. This is because a larger magnitude of m corresponds to a flattening of the regression line. If the regression line is flattened, its corresponding x-intercept is shifted to the right. Consider two details, U5 and R3, both taken from Synthesis Approach No. 1 with data in Table 3.17 and Figure 3.25. The slope of the regression line for U5 is 1.80 while the slope of the regression line for R3 is 1.27. Clearly, U5 has the larger slope. However, comparing the resulting values for μ_A, U5 provides a value of $1.58 \cdot 10^7$ while R3 provides a value of $5.74 \cdot 10^7$. This effect can be seen by looking at the regression lines provided in Figure 3.25. Although the regression line defining the U5 detail category has a flatter slope (*i.e.* higher magnitude) than the R3 detail category, it provides a lower value for μ_A because of its relative horizontal location residing much further to the left on the same S-N diagram. A comparison between the U2 (lower m, higher μ_A) and R6 (higher m, lower μ_A) detail categories is another example where a slope of lower magnitude provides a larger value for μ_A. Again, this can be seen by looking at Figure 3.25 where the R6 regression line resides to the left of the U2 regression line.

The results of this chapter indicate that it is reasonable to classify connections based upon the appearance of their configuration and obtain satisfactory statistical information regarding their fatigue

performance. However, given the very clear trend illustrated by the regression lines provided by the second synthesis approach that uses the stress concentration factor. When sufficient information regarding the dimensions of the connection are known, it is recommended to classify connections based upon the stress concentration factor determined using the equations provided by Roy et al. (2011).

Tables 3.17 and 3.18 provide lognormal statistical modeling information for the fatigue life uncertainty found in typical mast-arm sign support connections (mast-arm to pole). These statistical parameters have been formulated for use in the reliability analysis procedure presented in chapter one of this report.

3.7 References

AASHTO (2001). *Standard Specifications for Structural Supports for Highway Signs, Luminaires and Traffic Signals, 4th Edition*, American Association of State Highway and Transportation Officials, Washington, D.C.

AASHTO (2009). *Standard Specifications for Structural Supports for Highway Signs, Luminaires and Traffic Signals, 5th Edition with 2010 Interim Revisions*, American Association of State Highway and Transportation Officials, Washington, D.C.

AISC (2010). *Specifications for the Design and Construction of Structural Steel Buildings*, American Insititute of Steel Construction, Chicago, IL.

Alderson, J. L. (1999). "Fatigue Study of Cantilevered Traffic Signal Mast Arms."MS Thesis, University of Missouri - Columbia.

Anderson, T. H. (2007). "Fatigue Life Investigation of Traffic Signal Mast-Arm Connection Details."MS Thesis, University of Texas - Austin.

Archer, G., and Gurney, M. (1970). "Fatigue Strength of Mild-Steel Fillet Weld Tube to Plate Joints." *Metal Construction and British Welding Journal*, 2(5), 207-210.

Chen, G., Barker, M., Dharani, L. R., and Ramsay, C. (2003). "Signal Mast Arm Fatigue Failure Investigation." Missouri Department of Transportation, Jefferson City, MO.

Deschamp, B. (2002). "Fatigue Testing of Traffic Signal Structures."M.S. Thesis, University of Wyoming, Laramie, WY.

Diekfuss, J. A. (2013). "Reliability-Based Fatigue Assessment of Mast-Arm Sign Support Structures."PhD Thesis, Marquette University, Milwaukee, WI.

Fisher, J. W., Kulak, G. L., and Smith, I. F. C. (1998). *A Fatigue Primer for Structural Engineers*, American Institute of Steel Constrution, National Steel Bridge Alliance, Chicago, IL.

Fisher, J. W., Slutter, R. G., and Miki, C. (1981). "Fatigue Behavior of Steel Light Poles." California Department of Transportation, Sacramento, CA.

Foley, C. M., Ginal, S. J., Peronto, J. L., and Fournelle, R. A. (2004). "Structural Analysis of Sign Bridge Structures and Luminaire Supports." Wisconsin Highway Research Program, Madison, WI.

Foley, C. M., Wan, B., Weglarz, M., Hellenthal, M., Komp, J., Smith, A., and Schmidt, J. P. (2008). "Fatigue Risks in the Connections of Sign Support Structures - Phase 1." Wisconsin Highway Research Program, Wisconsin Department of Transportation.

Haldar, A., and Mahadevan, S. (2000). *Probability, Reliability, and Statistical Methods in Engineering Design*, John Wiley & Sons, Inc., New York, NY.

Koenigs, M. T., Botros, T. A., Freytag, D., and Frank, K. H. (2003). "Fatigue Strength of Signal Mast Arm Connections." Center for Transportation Research at the University of Texas at Austin, Austin, TX.

Little, R. E., and Jebe, E. H. (1975). *Statistical Design of Fatigue Experiments*, Applied Science Publishers, Ltd., London, U.K.

Machietto, C. "Valmont Fatigue Testing Presentation." *Proc., AASHTO T-12 Committee, November*.

Ocel, J. M. (2006). "The Behavior of Thin Hollow Structural Section (HSS) to Plate Connections."PhD Thesis, University of Minnesota, Minneapolis, MN.

Ocel, J. M., Dexter, R. J., and Hajjar, J. F. (2006). "Fatigue-Resistant Design for Overhead Signs, Mast-Arm Signal Poles, and Lighting Standards." Minnesota Department of Transportation, St. Paul, MN, 190 pages.

Richman, N. B. (2009). "Fatigue Life Investigation of High Performance Mast Arm Base Plate Connections."MS Thesis, University of Texas - Austin.

Rios, C. A. (2007). "Fatigue Performance of Multi-Sided High-Mast Lighting Towers." M.S. MS Thesis, University of Texas at Austin, Austin, TX.

Roy, S., Park, Y. C., Sause, R., Fisher, J. W., and Kaufmann, E. J. (2011). "Cost-Effective Connection Details for Highway Sign, Luminaire, and Traffic Signal Structures." ATLSS Center, Bethlehem, PA.

South, J. (1997). "Fatigue of Tube-to-Plate Fillet Welds and Methods for Their Improvement." Illinois Department of Transportation, Springfield, IL.

Wirsching, P. H. (1983). "Probability-Based Fatigue Design Criteria for Offshore Structures." American Petroleum Institute, Dallas, TX.

Table 3.1 Fatigue Testing Results (note: mean stress = 0.5 x stress-range for all MU tests and unknown for UWM tests).

Specimen Designation	Cycles to Failure	Stress Range (ksi)
MU-CSR-R-L-A1-1	4374464	6.00
UWM-MR-R-S-A1-2 (a)	2246094	5.42
MU-CSR-R-S-A2-3	72660	15.37
MU-CSR-R-L-B1-4 (a)	4374464	6.00
UWM-MR-R-S-B1-5	2246094	4.80
MU-CSR-R-S-B2-6 (a)	6893	15.37
UWM-CSR-M-N-A1-7	139000	6.50
UWM-CSR-M-S-B1-8 (a)	139000	6.50

Notes:

(a) Testing stopped with no failure (no cracks found).

Table 3.2 Number of contributing fatigue tests to each of the new fatigue detail categories developed in Synthesis Approach No. 1.

Fatigue Detail Category	Description	No. of Contributing Fatigue Tests
U1	**Unreinforced Round Socket - Equal Leg**	23
U2	**Unreinforced Round Socket - Unequal Leg**	45
U3	**Unreinforced Round Flush Fillet Weld**	26
U4	**Unreinforced Round Full-Penetration**	2
U5	**Unreinforced Multi-Sided Socket**	38
U6	**Unreinforced Multi-Sided Flush Fillet Weld**	0
U7	**Unreinforced Multi-Sided Full-Penetration**	9
R1	**Reinforced Round Socket**	50
R2	**Reinforced Round Flush Fillet Weld**	0
R3	**Reinforced Round Full-Penetration**	45
R4	**Reinforced Multi-Sided Socket**	4
R5	**Reinforced Multi-Sided Flush Fillet Weld**	0
R6	**Reinforced Multi-Sided Full-Penetration**	23

Table 3.3 Minimum, maximum and average SCF as well as number of contributing fatigue tests for each of the new fatigue detail categories developed in Synthesis Approach No. 2.

Fatigue Detail Category	SCF_{MIN}	SCF_{MAX}	SCF_{AVG}	No. of Contributing Fatigue Tests
E2	2.24	2.93	2.57	73
E3	3.08	3.87	3.51	24
E4	4.25	4.66	4.48	31

Table 3.4 Fatigue test results and corresponding fatigue detail categories assigned by both synthesis approaches for fatigue data obtained by Archer and Gurney (1970).

Specimen Designation	Synthesis Approach No. 1 Detail Category	Synthesis Approach No. 2 Detail Category	Cycles to Failure	Stress Range (ksi)
AG-F-5/16-W-A-1	U3	na	28000	12.60
AG-F-5/16-W-B-2	U3	na	130000	10.60
AG-F-5/16-W-C-3	U3	na	230000	9.20
AG-F-5/16-W-D-4	U3	na	420000	8.00
AG-F-5/16-W-E-5	U3	na	600000	6.90
AG-F-5/16-W-F-6	U3	na	850000	5.60
AG-F-5/16-W-G-7	U3	na	2700000	4.60
AG-F-7/16-W-A-8	U3	na	550000	7.40
AG-F-7/16-W-B-9	U3	na	1400000	4.90
AG-F-7/16-W-C-10	U3	na	3300000	3.30
AG-F-5/16-RHS-A-11	U3	na	28000	11.00
AG-F-5/16-RHS-B-12	U3	na	120000	9.00
AG-F-5/16-RHS-C-13	U3	na	240000	8.00
AG-F-5/16-RHS-D-14	U3	na	430000	7.00
AG-F-5/16-RHS-E-15	U3	na	550000	6.00
AG-F-5/16-RHS-F-16	U3	na	850000	5.00
AG-F-5/16-RHS-G-17	U3	na	2700000	4.00
AG-F-7/16-RHS-A-18	U3	na	550000	9.00
AG-F-7/16-RHS-B-19	U3	na	1400000	6.00
AG-F-7/16-RHS-C-20	U3	na	3400000	4.00
AG-F-11/16-RHS-A-21	U3	na	800000	11.00
AG-F-11/16-RHS-B-22	U3	na	850000	10.00
AG-F-11/16-RHS-C-23	U3	na	1200000	8.00
AG-F-11/16-RHS-D-24	U3	na	1300000	9.00
AG-F-11/16-RHS-E-25	U3	na	1900000	7.00
AG-F-11/16-RHS-F-26	U3	na	2000000	7.00
AG-S-7/16-W-A-27	U1	na	350000	8.20
AG-S-7/16-W-B-28	U1	na	430000	7.60
AG-S-7/16-W-C-29	U1	na	800000	5.40
AG-S-7/16-W-D-30	U1	na	1100000	4.50
AG-S-9/16-W-A-31	U1	na	310000	7.00
AG-S-9/16-W-B-32	U1	na	550000	5.10
AG-S-9/16-W-C-33	U1	na	2300000	3.70
AG-S-7/16-RHS-A-34	U1	na	380000	10.00
AG-S-7/16-RHS-B-35	U1	na	430000	8.00
AG-S-7/16-RHS-C-36	U1	na	800000	6.50
AG-S-7/16-RHS-D-37	U1	na	1300000	5.50
AG-S-9/16-RHS-A-38	U1	na	310000	11.00
AG-S-9/16-RHS-B-39	U1	na	440000	7.00
AG-S-9/16-RHS-C-40	U1	na	590000	8.00
AG-S-9/16-RHS-D-41	U1	na	2400000	6.00

Table 3.5 Fatigue test results and corresponding fatigue detail categories assigned by both synthesis approaches for fatigue data obtained by Fisher et al. (1981).

Specimen Designation	Synthesis Approach No. 1 Detail Category	Synthesis Approach No. 2 Detail Category	Cycles to Failure	Stress Range (ksi)
LEH-40-A-45CA-1-1	U1	E2	36100	18.80
LEH-40-A-45CA-2-2	U1	E2	117800	12.40
LEH-40-A-45CA-3-3	U1	E2	1892400	6.40
LEH-40-A-45CA-4-4	U1	E2	174200	12.40
LEH-40-A-45CA-5-5	U1	E2	1208700	6.40
LEH-40-A-45CA-6-6	U1	E2	1472900	6.40
LEH-40-A-34CA-1-7	U2	E2	3751600	6.40
LEH-40-A-34CA-2-8	U2	E2	3573400	6.40
LEH-48-V-28CA-1-9	U2	E2	87000	18.90
LEH-48-V-28CA-2-10	U2	E2	317500	12.40
LEH-48-V-28CA-3-11 (a)	U2	E2	5244000	6.50
LEH-48-V-28CA-4-12	U2	E2	198100	12.40
LEH-48-V-28CA-5-13 (b)	U2	E2	5186500	6.50
LEH-48-V-28CA-6-14 (c)	U2	E2	8832300	6.40

Notes:

(a) Large crack reported in mast-arm, but failure reported in pole at base connection.

(b) Failure in pole at base, but failure seen in mast-arm.

(c) Small crack reported in mast-arm, but no failure in pole.

Table 3.6 Fatigue test results and corresponding fatigue detail categories assigned by both synthesis approaches for fatigue data obtained by South (1997).

Specimen Designation	Synthesis Approach No. 1 Detail Category	Synthesis Approach No. 2 Detail Category	Cycles to Failure	Stress Range (ksi)
IDOT-1-1	Unused Test	Unused Test	62565	33.70
IDOT-1-2	Unused Test	Unused Test	216372	22.50
IDOT-1-3	Unused Test	Unused Test	581212	19.70
IDOT-1-4	Unused Test	Unused Test	299657	16.90
IDOT-1-5 (a)	Unused Test	Unused Test	15000000	11.20
IDOT-1-6 (a)	Unused Test	Unused Test	10416673	8.40
IDOT-2-7	Unused Test	Unused Test	157804	33.70
IDOT-2-8	Unused Test	Unused Test	213422	22.50
IDOT-2-9	Unused Test	Unused Test	570601	19.70
IDOT-2-10	Unused Test	Unused Test	2568000	16.90
IDOT-2-11 (a)	Unused Test	Unused Test	15000000	11.20
IDOT-2-12 (a)	Unused Test	Unused Test	10416673	8.40
IDOT-3-13	Unused Test	Unused Test	35629	33.70
IDOT-3-14	Unused Test	Unused Test	291300	22.50
IDOT-3-15	Unused Test	Unused Test	199694	19.70
IDOT-3-16	Unused Test	Unused Test	1322214	16.90
IDOT-3-17 (a)	Unused Test	Unused Test	15000000	11.20
IDOT-3-18 (a)	Unused Test	Unused Test	10416673	8.40
IDOT-4-19	Unused Test	Unused Test	40819	33.70
IDOT-4-20	Unused Test	Unused Test	182166	22.50
IDOT-4-21	Unused Test	Unused Test	581206	19.70
IDOT-4-22	Unused Test	Unused Test	1181967	16.90
IDOT-4-23 (a)	Unused Test	Unused Test	15000000	11.20
IDOT-4-24	Unused Test	Unused Test	6243700	8.40

Notes:

(a) Testing stopped with no failure. Considered runout.

Table 3.7 Fatigue test results and corresponding fatigue detail categories assigned by both synthesis approaches for fatigue data obtained by Deschamp (2002).

Specimen Designation	Synthesis Approach No. 1 Detail Category	Synthesis Approach No. 2 Detail Category	Cycles to Failure	Stress Range (ksi)
WY-IS-S-1.75-4-10.00-1	Unused Test	Unused Test	500000	24.02
WY-IS-S-2.00-6-12.25-2	Unused Test	Unused Test	750000	5.51
WY-IS-FP-2.00-5-11.50-3 (a, b, f)	Unused Test	Unused Test	7000000	8.47
WY-IS-S-1.50-6-12.50-4 (b, e)	Unused Test	Unused Test	2750000	5.17
WY-V-FP-2.00-4-10.00-5 (b, c)	Unused Test	Unused Test	3712687	19.58
WY-V-FP-2.00-4-10.00-6 (b, c)	Unused Test	Unused Test	3750000	10.00
WY-V-FP-2.00-4-10.50-7 (b, c)	Unused Test	Unused Test	3250000	17.00
WY-V-FP-2.00-4-10.50-8 (b, c)	Unused Test	Unused Test	3000000	16.98
WY-V-FP-2.00-4-11.25-9 (b, d)	Unused Test	Unused Test	19500000	8.36
WY-V-FP-2.00-4-12.75-10 (b, d)	Unused Test	Unused Test	2250000	6.39

Notes:

(a) ECASR represents an Equivalent Constant Amplitude Stress Range.

(b) Indicates specimen was considered as a run-out (no cracking found when terminated)

(c) Mast-arm wall thickness rounded up to 4/16-in. (actually 0.239 inches)

(d) Mast-arm wall thickness rounded down to 4/16-in. (actually 0.267 inches)

(e) Indicates an open-box connection configuration (only one in test matrix).

(f) Multi-sided specimen.

Table 3.8 Fatigue test results and corresponding fatigue detail categories assigned by both synthesis approaches for fatigue data obtained by Machietto (2002).

Specimen Designation	Synthesis Approach No. 1 Detail Category	Synthesis Approach No. 2 Detail Category	Cycles to Failure	Stress Range (ksi)
VAL-R-45FW-A-1	R1	na	575000	13.40
VAL-R-45FW-B-2	R1	na	376740	13.40
VAL-R-15FP-A-3	R3	na	950040	13.40
VAL-R-TCFP-A-4	R3	na	657540	17.60
VAL-R-RFWS-A-5	R1	na	514085	17.60
VAL-R-RFWS-B-6	R1	na	673989	17.60
VAL-U-SFW-A-7 (a)	Unused Test	Unused Test	4808700	13.40
VAL-U-SFW-B-8	U2	na	1240200	17.60
VAL-U-SFW-C-9 (a)	Unused Test	Unused Test	5321160	17.60
VAL-U-SFW-D-10 (a)	Unused Test	Unused Test	1982743	17.60
VAL-U-FP-A-11	U4	na	498960	17.60
VAL-U-FP-B-12	U4	na	4504500	17.60

Notes:

(a) Testing stopped with no failure. Considered runout.

Table 3.9 Fatigue test results and corresponding fatigue detail categories assigned by both synthesis approaches for fatigue data obtained by Chen et al. (2003) and Alderson (1999).

Specimen Designation	Synthesis Approach No. 1 Detail Category	Synthesis Approach No. 2 Detail Category	Cycles to Failure	Stress Range (ksi)
UMO-VAL-O-1-1	U1	na	1800000	8.00
UMO-VAL-N-1-2	U2	na	2100000	8.00
UMO-VAL-N-2-3 (a)	U2	na	400000	8.00
UMO-UM-O-1-4 (b)	U1	na	500000	8.00
UMO-JEM-O-1-5 (c)	Unused Test	Unused Test	na	na

Notes:

(a) Lack of fusion noted as potential cause for low cycle count.

(b) NDT using magnetic particle testing indicated a flaw was present in weld.

(c) NDT inspection resulted in weld flaw being detected and no testing conducted.

Table 3.10 Fatigue test results and corresponding fatigue detail categories assigned by both synthesis approaches for fatigue data obtained by Koenigs et al. (2003).

Specimen Designation	Synthesis Approach No. 1 Detail Category	Synthesis Approach No. 2 Detail Category	Cycles to Failure	Stress Range (ksi)
VAL-U-N-A-1	U2	E2	249446	11.90
VAL-U-N-B-2	U2	E2	453948	11.90
VAL-U-N-C-3	U2	E2	2072592	6.29
VAL-U-N-D-4 (a)	Unused Test	Unused Test	6856881	6.20
TX-U-N-A-5	U2	E2	2199343	6.00
TX-U-N-B-6	U2	E2	2816706	6.10
TX-U-N-C-7	U2	E2	177596	11.80
TX-U-N-D-8	U2	E2	194694	12.00
VALN-U-N-A-9	U2	E2	389428	11.90
VALN-U-N-B-10	U2	E2	265540	11.80
VALN-U2-N-A-11	U2	E2	5144528	11.90
VALN-U2-N-B-12	U2	E2	1683127	11.80
VALN-W-N-A-13	R3	E3	422400	17.71
VALN-W-N-B-14	R3	E3	422400	17.56
VALN-U-P-A-15 (a)	Unused Test	Unused Test	4557126	11.60
VALN-U-P-B-16 (a)	Unused Test	Unused Test	4557126	11.50
VALN-U-P-C-17	Unused Test	Unused Test	1301077	19.95
VAL-U-P-E-18	Unused Test	Unused Test	393767	11.40
VAL-U-P-F-19	Unused Test	Unused Test	353103	11.50
VALN-U-G-A-20	U2	E2	183132	11.60
VALN-U-G-B-21	U2	E2	151679	11.50
VAL-U-GP-A-22	Unused Test	Unused Test	4545952	11.60
VAL-U-GP-B-23	Unused Test	Unused Test	224240	19.91
VALN-U-PG-A-24	Unused Test	Unused Test	277634	11.60
VALN-U-PG-B-25	Unused Test	Unused Test	313727	11.50
VALN-U-P-A-UL-26	Unused Test	Unused Test	5004729	11.60
VALN-U-P-B-UL-27	Unused Test	Unused Test	5440165	11.50
VALN-EC-N-A-28	R1	na	4245460	5.49
VALN-EC-N-B-29	R1	na	2363152	5.73

Notes:

(a) Runout.

(b) Lack of fusion defect detected post-testing.

Possible repeats within data.

Table 3.10 Continued… Fatigue test results and corresponding fatigue detail categories assigned by both synthesis approaches for fatigue data obtained by Koenigs et al. (2003).

Specimen Designation	Synthesis Approach No. 1 Detail Category	Synthesis Approach No. 2 Detail Category	Cycles to Failure	Stress Range (ksi)
VALN-IC-N-A-30	R1	na	227030	10.75
VALN-IC-N-B-31	R1	na	227030	10.68
VAL-3x3/8-P-C-32	Unused Test	Unused Test	393767	11.50
VAL-3x3/8-P-C2-33	Unused Test	Unused Test	353103	11.50
VAL-3x3/8-P-C-LMS-34	Unused Test	Unused Test	1707128	12.10
VAL-3x1/4-N-A-35	R1	E4	476269	11.10
VAL-3x1/4-N-B-36	R1	E4	696326	11.40
VAL-3x1/4-N-C-37	R1	E4	3592372	6.10
TX-3x1/4-N-A-38	R1	E4	616136	11.70
TX-3x1/4-N-B-39	R1	E4	416146	11.80
TX-3x1/4-N-C-LMS-40	R1	E4	523397	11.90
VAL-3x3/8-N-A-41	R1	E3	386253	11.70
VAL-3x3/8-N-B-42	R1	E3	410410	11.60
TX-3x3/8-N-A-43	R1	E3	473735	11.70
TX-3x3/8-N-B-44	R1	E3	657716	11.60
VAL-6x3/8-N-A-45 (b)	R1	E3	242728	11.20
VAL-6x3/8-N-B-46	R1	E3	653392	11.30
VAL-6x3/8-N-C-47	R1	E3	3592372	5.90
TX-6x3/8-N-A-48	R1	E2	783857	11.20
TX-6x3/8-N-B-49	R1	E2	783857	11.30
TX-6x3/8-N-C-50	R1	E2	7503037	5.76
VALN-6x3/8@45-N-A-51	R1	E3	238515	11.96
VALN-6x3/8@45-N-B-52	R1	E3	161843	11.98
VALN-6x3/8@45-N-C-53	R1	E3	6066817	4.30
VALN-6x3/8@45-N-D-54	R1	E3	6066817	4.30
VALN-UR-N-A-55	R1	na	1776724	7.62
VALN-UR-N-B-56	R1	na	950670	7.60
VALN-UR-N-B2-57	R1	na	339152	12.57

Notes:

(a) Runout.

(b) Lack of fusion defect detected post-testing.

Possible repeats within data.

Table 3.11 Fatigue test results and corresponding fatigue detail categories assigned by both synthesis approaches for fatigue data obtained by Ocel et al. (2006).

Specimen Designation	Synthesis Approach No. 1 Detail Category	Synthesis Approach No. 2 Detail Category	Cycles to Failure	Stress Range (ksi)
MN-P-FR1-IP-N-CSR-5-1.25-1	U5	E4	83806	8.25
MN-P-FR1-IP-N-CSR-5-1.25-2	U5	E4	981490	3.43
MN-P-FR1-IP-N-CSR-5-1.25-3	U5	E4	610124	3.80
MN-P-FR1-OP-N-CSR-5-1.25-4 (a)	Unused Test	Unused Test	5038549	4.09
MN-P-FR1-OP-N-CSR-5-1.25-5	U5	E4	170606	5.41
MN-P-FR1-OP-N-CSR-5-1.25-6 (a)	Unused Test	Unused Test	1292565	5.41
MN-P-FR1-OP-N-CSR-5-1.25-7	U5	E4	301484	5.41
MN-P-FR1-OP-N-CSR-5-1.25-8	U5	E4	2293739	5.41
MN-P-FR2-IP-N-CSR-5-1.25-9	U5	E4	591696	4.26
MN-P-FR2-IP-N-CSR-5-1.25-10	U5	E4	868266	3.65
MN-P-FR2-IP-N-CSR-5-1.25-11	U5	E4	1658906	4.10
MN-P-FR1-IP-HPR-MR-5-1.25-12	Unused Test	Unused Test	4126888	4.55
MN-P-FR2-IP-HPR-CSR-5-1.25-13	Unused Test	Unused Test	1106830	6.99
MN-P-FR2-IP-HP-MR-5-1.25-14	Unused Test	Unused Test	8501877	5.82
MN-P-FR2-IP-HP-MR-5-1.25-15	Unused Test	Unused Test	2558528	7.10
MN-P-FR2-IP-HP-MR-5-1.25-16	Unused Test	Unused Test	124147	10.00
MN-P-FR2-IP-HP-MR-5-1.25-17	Unused Test	Unused Test	5571296	6.00
MN-P-FR2-IP-HPR-MR-5-1.25-18	Unused Test	Unused Test	1131798	7.91
MN-P-FR2-IP-HP-MR-5-1.25-19	Unused Test	Unused Test	5366869	7.91
MN-P-FR2-IP-N-MR-5-2.50-1-20	Unused Test	Unused Test	4222993	11.17
MN-P-FR2-IP-N-CSR-5-2.50-2-21	U5	E4	81924	14.90
MN-P-FR2-IP-HP-CSR-5-2.50-2-22	Unused Test	Unused Test	978382	14.90
MN-P-FR2-IP-N-CSR-5-2.50-1-23	U5	E4	566119	14.90
MN-P-FR2-IP-N-CSR-5-2.50-2-24	U5	E4	101916	14.90
MN-P-FR2-IP-N-CSR-3-2.50-1-25	U5	E4	330137	15.00
MN-P-FR2-IP-N-CSR-3-2.50-2-26	U5	E4	140545	15.00
MN-P-FR2-IP-N-CSR-3-2.50-1-27	U5	E4	183638	15.00
MN-P-FR2-IP-N-CSR-3-2.50-2-28	U5	E4	86888	15.00
MN-MA-FR3-IP-N-CSR-5-1.25-1-29	Unused Test	Unused Test	6997582	8.54
MN-MA-FR3-IP-N-CSR-5-1.25-1-30	U7	E4	420785	15.37
MN-MA-FR3-IP-N-CSR-5-1.25-1-31	U7	E4	434329	15.37
MN-MA-FR3-IP-N-CSR-5-1.25-1-32	U7	E4	242060	15.37
MN-MA-FR3-IP-N-CSR-5-1.25-2-33	U7	E4	420662	15.37
MN-MA-FR3-IP-N-CSR-5-1.25-2-34	U7	E4	372056	15.37
MN-MA-FR3-IP-N-CSR-5-1.25-2-35	U7	E4	298023	15.37
MN-MA-FR3-IP-N-CSR-5-1.25-2-36	U7	E4	267922	15.37
MN-MAG-FR3-IP-N-MR-5-1.25-1-37	Unused Test	Unused Test	1642305	4.15
MN-MAG-FR3-IP-N-MR-5-1.25-1-38	Unused Test	Unused Test	1300949	11.30
MN-MAG-FR3-IP-N-CSR-5-1.25-1-39	R4	E3	171695	10.38
MN-MAG-FR3-IP-N-CSR-5-1.25-1-40	R4	E3	186036	10.33
MN-MAG-FR3-IP-N-CSR-5-1.25-2-41	R4	E3	223987	10.38
MN-MAG-FR3-IP-N-CSR-5-1.25-2-42	R4	E3	157123	10.33

Notes:

(a) Runout.

Table 3.12 Fatigue test results and corresponding fatigue detail categories assigned by both synthesis approaches for fatigue data obtained by Rios (2007).

Specimen Designation	Synthesis Approach No. 1 Detail Category	Synthesis Approach No. 2 Detail Category	Cycles to Failure	Stress Range (ksi)
UTX-24-1.5-8-S-A-1	U5	E4	13193	12.00
UTX-24-1.5-8-S-B-2	U5	E4	13193	12.00
UTX-24-2.0-8-S-A-3	U5	E3	46772	12.00
UTX-24-2.0-8-S-B-4	U5	E3	46772	12.00
UTX-24-3.0-8-S-A-5	U5	E2	147550	12.00
UTX-24-3.0-8-S-B-6	U5	E2	147550	12.00
UTX-24-1.5-12-S-A-7	U5	E3	27977	12.00
UTX-24-1.5-12-S-B-8	U5	E3	27977	12.00
UTX-24-2.0-12-S-A-9	U5	E2	143214	12.00
UTX-24-2.0-12-S-B-10	U5	E2	143214	12.00
UTX-24-2.0-8-WY-A-11	R3	na	133819	12.00
UTX-24-2.0-8-WY-B-12	R3	na	133819	12.00
UTX-24-3.0-12-TX-A-13	U7	E2	236154	12.00
UTX-24-3.0-12-TX-B-14	U7	E2	327487	12.00
UTX-24-2.0-8-SB-A-15	R1	na	785058	12.00
UTX-24-2.0-8-SB-B-16	R1	na	483314	12.00

Table 3.13 Fatigue test results and corresponding fatigue detail categories assigned by both synthesis approaches for fatigue data obtained by Anderson (2007).

Specimen Designation	Synthesis Approach No. 1 Detail Category	Synthesis Approach No. 2 Detail Category	Cycles to Failure	Stress Range (ksi)
S-1.75-10-B-1	U2	E2	142857	12.00
S-1.75-10-B-2 (b)	U2	E2	134197	12.00
S-1.75-10-A-3 (a)	Unused Test	Unused Test	515365	12.00
EC-1.75-10-A-4 (2)	R1	na	2345896	12.00
EC-1.75-10-A-5 (2) (b)	R1	na	2889260	12.00
EC-1.75-10-B-6 (2)	R1	na	5755111	12.00
EC-1.75-10-B-7 (1)	R1	na	3304490	12.00
EC-1.75-10-B-8 (1) (b)	R1	na	2382309	12.00
EC-1.75-10-A-9 (1) (a)	Unused Test	Unused Test	6206754	12.00
S-2.00-10-B-10	U2	E2	165998	12.00
S-2.00-10-A-11	U2	E2	235854	12.00
S-2.00-10-A-12 (2)	U2	E2	210793	12.00
S-2.00-10-A-13 (2) (b)	U2	E2	260700	12.00
S-2.00-10-B-14 (2)	U2	E2	622928	12.00
EC-2.00-10-A-15 (2)	R1	na	3939099	12.00
EC-2.00-10-B-16 (2)	R1	na	6927606	12.00
EC-2.00-10-A-17 (1)	R1	na	5384143	12.00
EC-2.00-10-A-18 (1) (b)	R1	na	2863521	12.00
EC-2.00-10-B-19 (1) (a)	Unused Test	Unused Test	8247664	12.00
WY-2.00-10-A-20	R3	na	4997925	12.00
WY-2.00-10-B-21	R3	na	7527441	12.00
CA-2.00-10-A-22	U2	E2	253657	12.00
CA-2.00-10-B-23	U2	E2	310352	12.00
S-3.00-10-B-24	U2	E2	792576	12.00
S-3.00-10-B-25 (b)	U2	E2	376291	12.00
S-3.00-10-A-26 (a)	Unused Test	Unused Test	1168867	12.00

Notes:

(a) Runout.

(b) Flip side of specimen with a fatigue crack present in the compression zone.

Table 3.14 Fatigue test results and corresponding fatigue detail categories assigned by both synthesis approaches for fatigue data obtained by Richman (2009).

Specimen Designation	Synthesis Approach No. 1 Detail Category	Synthesis Approach No. 2 Detail Category	Cycles to Failure	Stress Range (ksi)
WY-S-B-P-2-10-A-1	R3	na	6734487	12.00
WY-S-B-P-2-10-B-2	R3	na	5219304	12.00
WY-S-G-V-2-10-A-3 (a)	Unused Test	Unused Test	12602940	12.00
WY-S-G-V-2-10-B-4 (a)	Unused Test	Unused Test	12602940	12.00
WY-S-G-V-2-8-A-5 (a)	Unused Test	Unused Test	12464800	12.00
WY-S-G-V-2-8-B-6 (a)	Unused Test	Unused Test	12464800	12.00
WY-S-G-V-2-8-A-7	R3	na	856122	24.00
WY-S-G-V-2-8-A-8 (b)	R3	na	747510	24.00
WY-S-G-V-2-8-B-9 (a)	Unused Test	Unused Test	1603632	24.00
EC-S-G-V-2-8-A-10	R1	na	512860	18.00
EC-S-G-V-2-8-B-11	R1	na	653208	18.00
WY-S-G-V-2-12-A-12	R3	na	1053554	18.00
WY-S-G-V-2-12-B-13	R3	na	880807	18.00
EC-S-G-V-2-12-A-14 (a)	Unused Test	Unused Test	805991	18.00
EC-S-G-V-2-12-B-15	R1	na	468601	18.00
EC-S-G-V-2-12-B-16 (b)	R1	na	337390	18.00
WY-R-G-V-3-10-A-17 (a)	Unused Test	Unused Test	8037420	18.00
WY-R-G-V-3-10-B-18 (a)	Unused Test	Unused Test	8037420	18.00
WY-R-G-V-3-10-A-19	R3	na	439511	24.00
WY-R-G-V-3-10-B-20	R3	na	343175	24.00
WY-R-B-V-3-10-A-21 (a)	Unused Test	Unused Test	10055123	24.00
WY-R-B-V-3-10-B-22 (a)	Unused Test	Unused Test	10055123	24.00
WY-R-B-V-3-10-A-23	R3	na	2232742	19.07
WY-R-B-V-3-10-A-24 (b)	R3	na	490061	24.00
WY-R-B-V-3-10-B-25	R3	na	3516775	21.14
WY-R-G-A-3-10-A-26	R3	na	222649	24.00
WY-R-G-A-3-10-A-27 (b)	R3	na	212891	24.00
WY-R-G-U-3-10-A-28	R3	na	1873499	24.00
ZZ88734-A-29	Unused Test	Unused Test	677763	24.00
ZZ88734-B-30	Unused Test	Unused Test	633458	24.00
ZZ88735-A-31	Unused Test	Unused Test	286526	28.00
ZZ88735-B-32	Unused Test	Unused Test	123072	28.00
ZZ88735-B-33 (b)	Unused Test	Unused Test	129090	28.00
WY-SR-G-V-2-10-A-34 (a)	Unused Test	Unused Test	9881390	12.00
WY-SR-G-V-2-10-B-35	R3	na	3051996	12.00
EC-SR-G-V-2-10-A-36 (a)	Unused Test	Unused Test	10652284	12.00
EC-SR-G-V-2-10-B-37 (a)	Unused Test	Unused Test	10652284	12.00
WY-R-G-P-3-10-A-38	R3	na	1272665	24.00
WY-R-G-P-3-10-B-39	R3	na	1210499	24.00
EC-R-G-P-2-10-A-40	R1	na	137220	24.00
EC-R-G-P-2-10-B-41	R1	na	244763	24.00
WY-R-G-P-3-12-A-42	R3	na	292468	24.00
WY-R-G-P-3-12-B-43	R3	na	328833	24.00
EC-R-G-P-2-12-A-44	R1	na	169059	24.00
EC-R-G-P-2-12-B-45	R1	na	119289	24.00

Notes:

(a) Runout.

(b) Flip side of specimen with a fatigue crack present in the compression zone.

Table 3.15 Fatigue test results and corresponding fatigue detail categories assigned by both synthesis approaches for fatigue data obtained by Roy et al. (2011).

Specimen Designation	Synthesis Approach No. 1 Detail Category	Synthesis Approach No. 2 Detail Category	Cycles to Failure	Stress Range (ksi)
LEH-AB-R-I-SF-CSR-1	U2	E2	180000	12.00
LEH-AB-R-I-SF-CSR-2	U2	E2	370000	12.00
LEH-AB-R-I-SF-CSR-3	U2	E2	1260000	12.00
LEH-AB-R-I-SF-CSR-4	U2	E2	2300000	7.00
LEH-AB-R-I-SF-CSR-5	U2	E2	3110000	7.00
LEH-AB-R-I-SF-CSR-6	U2	E2	1400000	7.00
LEH-AB-R-I-SF-CSR-7	U2	E2	1840000	7.00
LEH-PB-R-I-SF-MR-8	Unused Test	Unused Test	4880000	4.60
LEH-PB-R-I-SF-CSR-9	U2	E2	3050000	4.00
LEH-AB-R-II-BP1-CSR-10	R3	na	1610000	11.90
LEH-AB-R-II-BP1-CSR-11	R3	na	1320000	9.90
LEH-AB-R-II-BP1-CSR-12	R3	na	1410000	9.90
LEH-AB-R-II-BP1-CSR-13	R3	na	1170000	9.90
LEH-AB-R-II-BP1-CSR-14	R3	na	1290000	9.90
LEH-AB-R-II-BP1-CSR-15	R3	na	1490000	9.90
LEH-PB-R-II-BP1-CSR-16	R3	na	1980000	6.90
LEH-AB-R-III-BP2-CSR-17	R3	na	980000	12.00
LEH-AB-R-III-BP2-CSR-18	R3	na	1860000	12.00
LEH-AB-R-III-BP2-CSR-19	R3	na	1250000	12.00
LEH-AB-R-III-BP2-MR-20	Unused Test	Unused Test	29830000	9.00
LEH-AB-R-III-BP2-CSR-21	R3	na	6960000	10.00
LEH-AB-R-III-BP2-CSR-22	R3	na	9230000	10.00
LEH-AB-R-III-BP2-MR-23	Unused Test	Unused Test	15920000	11.20
LEH-AB-R-III-BP2-CSR-24	R3	na	5840000	16.00
LEH-AB-R-III-BP2-CSR-25	R3	na	270000	16.00
LEH-AB-R-III-BP2-CSR-26	R3	na	4790000	16.00
LEH-AB-R-IVA-BP2-MR-27	Unused Test	Unused Test	26150000	8.60
LEH-AB-R-IVA-BP2-MR-28	Unused Test	Unused Test	42640000	11.20
LEH-PB-R-IVA-BP2-MR-29	Unused Test	Unused Test	44100000	6.50
LEH-PB-R-IVA-BP2-MR-30	Unused Test	Unused Test	22120000	8.50
LEH-PB-R-V-BP2-CSR-31	R3	na	270000	12.00
LEH-PB-R-V-BP2-CSR-32	R3	na	1100000	12.00
LEH-PB-R-V-BP2-CSR-33	R3	na	1460000	12.00
LEH-PB-R-VI-BP2-MR-34	Unused Test	Unused Test	17200000	11.10
LEH-PB-R-VI-BP2-MR-35	Unused Test	Unused Test	40210000	10.60
LEH-PB-R-VI-BP2-MR-36	Unused Test	Unused Test	21000000	13.80
LEH-PB-R-VI-BP2-MR-37	Unused Test	Unused Test	31020000	6.10
LEH-PB-R-VI-BP2-MR-38	Unused Test	Unused Test	28230000	5.50
LEH-PB-R-VI-BP2-MR-39	Unused Test	Unused Test	20200000	15.20
LEH-PB-R-VI-BP2-MR-40	Unused Test	Unused Test	1750000	11.70
LEH-PB-R-VI-BP2-MR-41	Unused Test	Unused Test	7770000	13.40
LEH-AB-M-VII-SF-CSR-42	U5	E2	40000	12.00
LEH-AB-M-VII-SF-CSR-43	U5	E2	40000	12.00
LEH-AB-M-VII-SF-CSR-44	U5	E2	10000	12.00

Notes:

(a) Failure at stool stiffener.

(b) Failure at tube to stiffener weld toe on the tube wall.

Table 3.15 Continued… Fatigue test results and corresponding fatigue detail categories assigned by both synthesis approaches for fatigue data obtained by Roy et al. (2011).

Specimen Designation	Synthesis Approach No. 1 Detail Category	Synthesis Approach No. 2 Detail Category	Cycles to Failure	Stress Range (ksi)
LEH-AB-M-VII-SF-CSR-45	U5	E2	1030000	4.50
LEH-AB-M-VII-SF-CSR-46	U5	E2	390000	4.50
LEH-AB-M-VII-SF-MR-47	Unused Test	Unused Test	40890000	3.60
LEH-AB-M-VII-SF-CSR-48	U5	E2	70000	2.50
LEH-PB-M-VII-SF-CSR-49	U5	E3	90000	6.60
LEH-PB-M-VII-SF-CSR-50	U5	E3	90000	6.60
LEH-PB-M-VII-SF-CSR-51	U5	E3	100000	6.60
LEH-PB-M-VII-SF-MR-52	Unused Test	Unused Test	20650000	2.60
LEH-PB-M-VII-SF-MR-53	Unused Test	Unused Test	51500000	2.40
LEH-PB-M-VII-SF-MR-54	Unused Test	Unused Test	44620000	2.20
LEH-PB-M-IX-LSS-CSR-55 (a)	R6	na	590000	12.00
LEH-PB-M-IX-LSS-CSR-56 (a)	R6	na	270000	12.00
LEH-PB-M-IX-LSS-CSR-57 (a)	R6	na	510000	12.00
LEH-PB-M-IX-LSS-CSR-58 (a)	R6	na	450000	10.00
LEH-PB-M-IX-LSS-CSR-59 (a)	R6	na	2570000	7.00
LEH-PB-M-IX-LSS-CSR-60 (a)	R6	na	2640000	4.50
LEH-PB-M-IX-LSS-CSR-61 (a)	R6	na	4000000	4.50
LEH-PB-M-IX-LSS-CSR-62 (a)	R6	na	70000	16.00
LEH-PB-M-IX-LSS-CSR-63 (a)	R6	na	130000	16.00
LEH-PB-M-IX-LSS-CSR-64 (a)	R6	na	120000	16.00
LEH-PB-M-X-SF-MR-65	Unused Test	Unused Test	31380000	6.70
LEH-PB-M-X-SF-CSR-66	U5	E2	1750000	8.00
LEH-PB-M-X-SF-CSR-67	U5	E2	680000	8.00
LEH-PB-M-XI-BP1-CSR-68	R6	na	750000	12.00
LEH-PB-M-XI-BP1-CSR-69	R6	na	1560000	12.00
LEH-PB-M-XI-BP1-CSR-70	R6	na	330000	12.00
LEH-PB-M-XI-BP1-MR-71	Unused Test	Unused Test	15350000	7.10
LEH-PB-M-XI-BP1-MR-72	Unused Test	Unused Test	15380000	7.10
LEH-PB-M-XI-BP1-MR-73	Unused Test	Unused Test	15240000	7.10
LEH-PB-M-XI-BP1-MR-74	Unused Test	Unused Test	15200000	7.10
LEH-PB-M-XI-BP1-CSR-75	R6	na	100000	14.00
LEH-PB-M-XI-BP1-CSR-76	R6	na	140000	16.00
LEH-PB-M-XI-BP1-CSR-77	R6	na	60000	16.00
LEH-PB-M-XII-LS-CSR-78 (b)	R6	E2	230000	12.00
LEH-PB-M-XII-LS-CSR-79 (b)	R6	E2	400000	12.00
LEH-PB-M-XII-LS-CSR-80 (b)	R6	E2	580000	12.00
LEH-PB-M-XII-LS-MR-81 (b)	Unused Test	Unused Test	15310000	7.10
LEH-PB-M-XII-LS-MR-82 (b)	Unused Test	Unused Test	19390000	7.70
LEH-PB-M-XII-LS-CSR-83 (b)	R6	E2	4060000	7.00
LEH-PB-M-XII-LS-MR-84 (b)	Unused Test	Unused Test	20940000	7.90
LEH-PB-M-XII-LS-CSR-85 (b)	R6	E2	50000	16.00
LEH-PB-M-XII-LS-CSR-86 (b)	R6	E2	200000	16.00
LEH-PB-M-XII-LS-CSR-87 (b)	R6	E2	50000	16.00

Notes:

(a) Failure at stool stiffener.

(b) Failure at tube to stiffener weld toe on the tube wall.

Table 3.16 Fatigue test results and corresponding fatigue detail categories assigned by both synthesis approaches for fatigue data obtained by the experimental program of this study.

Specimen Designation	Synthesis Approach No. 1 Detail Category	Synthesis Approach No. 2 Detail Category	Cycles to Failure	Stress Range (ksi)
MU-CSR-R-L-A1-1	U2	E2	4374464	6.00
UWM-MR-R-S-A1-2 (a)	Unused Test	Unused Test	2246094	5.42
MU-CSR-R-S-A2-3	U2	E2	72660	15.37
MU-CSR-R-L-B1-4 (a)	Unused Test	Unused Test	4374464	6.00
UWM-MR-R-S-B1-5	Unused Test	Unused Test	2246094	4.80
MU-CSR-R-S-B2-6 (a)	Unused Test	Unused Test	6893	15.37
UWM-CSR-M-N-A1-7	U5	E2	139000	6.50
UWM-CSR-M-S-B1-8 (a)	Unused Test	Unused Test	139000	6.50

Notes:

(a) Testing stopped with no failure (no cracks found).

Table 3.17 Statistical results for Synthesis Approach No. 1.

Fatigue Detail Category		m (1)	μ_A (2)	CV_A	$S_{R,max}$ (ksi)
U1	**Unreinforced Round Socket - Equal Leg**	2.34	7.40E+07	0.66	18.80
U2	**Unreinforced Round Socket - Unequal Leg**	3.03	1.12E+09	1.53	18.90
U3	**Unreinforced Round Flush Fillet Weld**	2.76	1.94E+08	0.87	12.60
U4	**Unreinforced Round Full-Penetration**	na	na	na	na
U5	**Unreinforced Multi-Sided Socket**	1.80	1.58E+07	1.30	15.00
U6	**Unreinforced Multi-Sided Flush Fillet Weld**	na	na	na	na
U7	**Unreinforced Multi-Sided Full-Penetration**	na	na	na	na
R1	**Reinforced Round Socket**	1.91	1.46E+08	1.17	24.00
R2	**Reinforced Round Flush Fillet Weld**	na	na	na	na
R3	**Reinforced Round Full-Penetration**	1.27	5.74E+07	0.98	24.00
R4	**Reinforced Multi-Sided Socket**	na	na	na	na
R5	**Reinforced Multi-Sided Flush Fillet Weld**	na	na	na	na
R6	**Reinforced Multi-Sided Full-Penetration**	3.16	1.03E+09	0.80	16.00

(1) *Deterministic value defining slope of fatigue life curve*

(2) *X-Intercept of fatigue life curve*

Table 3.18 Statistical results for Synthesis Approach No. 2.

Fatigue Detail Category	m (1)	μ_A (2)	CV_A	$S_{R,max}$ (ksi)
E2 ($2.0 \le SCF < 3.0$)	2.97	6.73E+08	1.49	18.90
E3 ($3.0 \le SCF < 4.0$)	2.24	9.02E+07	0.89	17.71
E4 ($SCF \ge 4.0$)	1.04	5.22E+06	0.88	15.37

(1) *Deterministic value defining slope of fatigue life curve*

(2) *X-Intercept of fatigue life curve*

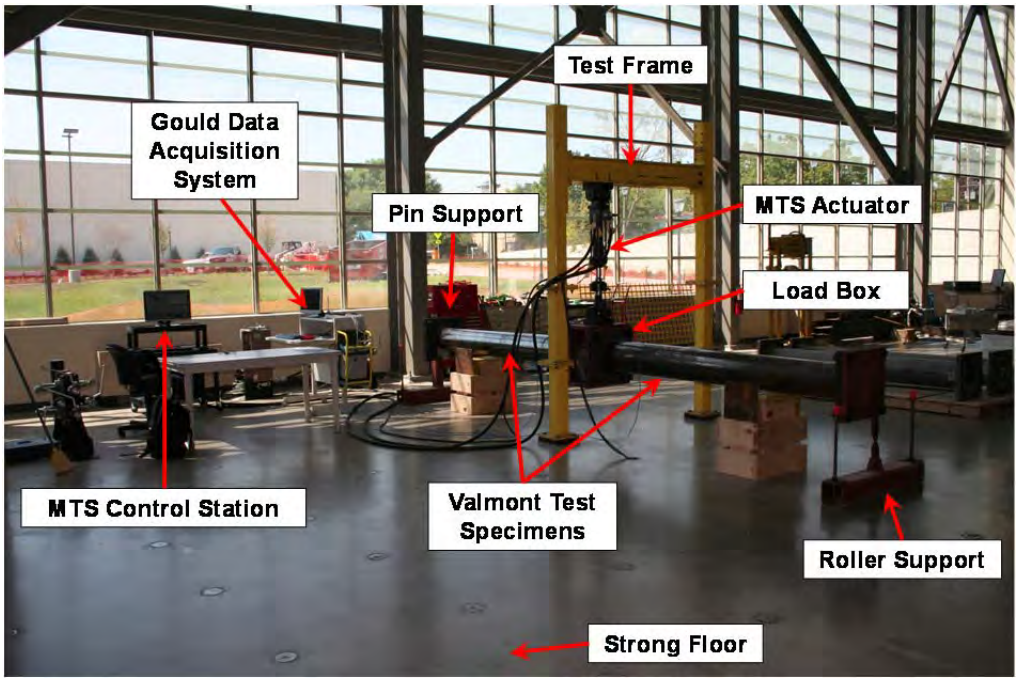

Figure 3.1 Test Setup inside Marquette University Engineering Materials and Structural Testing Laboratory (EMSTL).

Figure 3.2 Test setup in EMSTL: (a) roller support, (b) pin support, (c) Gould data acquisition system, (d) MTS control station, (e) MTS actuator and load box.

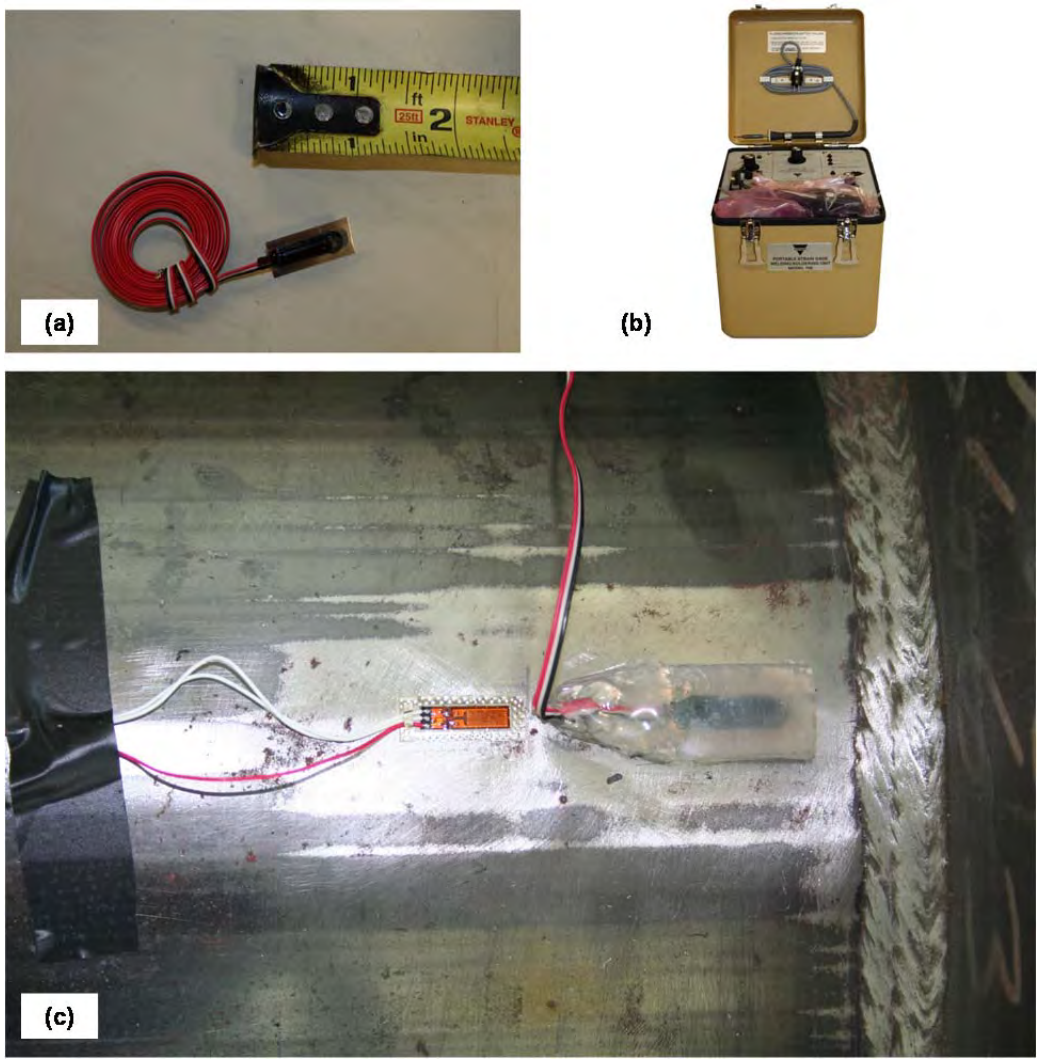

Figure 3.3 Strain Gauging: (a) Vishay strain gage, (b) Vishay spot welder, and (c) round specimen with strain gage installed.

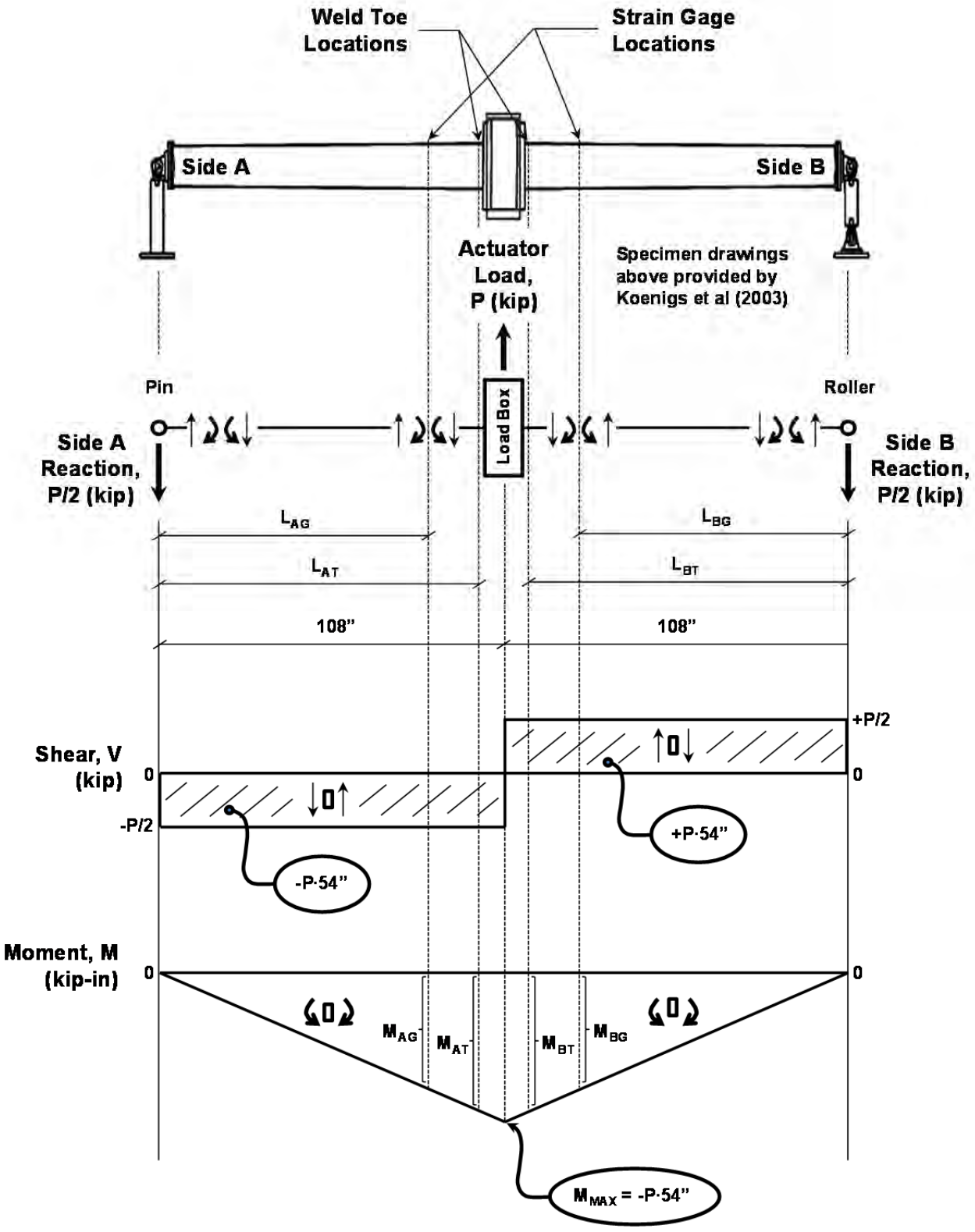

Figure 3.4 Guide for stress-range extrapolation from strain gage to weld toe.

A-B-C-D-E-F		
Testing Location		
A	MU	Marquette University
	UWM	University of Wisconsin-Milwaukee
Stress Range Methodology		
B	CSR	Constant Amplitude Stress Range
	MR	Miner's Cumulative Fatigue Damage Equivalent
Specimen Type		
C	R	Round tube
	M	Multi-sided tube
Specimen Designation - End Tested		
D	If tested at MU:	
	L	Large diameter end tested (d = 11.0 in.)
	S	Small diameter end tested (d = 9.9 in.)
	If tested at UWM:	
	N	North side of specimen tested
	S	South side of specimen tested
Specimen Designation - Top or Bottom		
E	A1	Top of specimen A
	A2	Bottom of specimen A
	B1	Top of specimen B
	B2	Bottom of specimen B
Specimen Serial Number for MU Synthesis		
F	#	

Figure 3.5 Key to testing specimens for the present study.

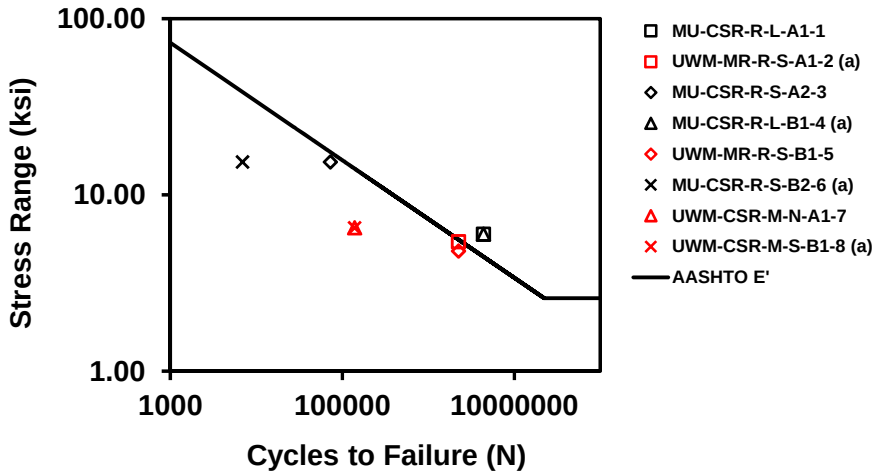

Figure 3.6 Stress-range vs. cycles to fatigue failure for tests conducted in the present study and those completed at the University of Wisconsin at Milwaukee (note: mean stress = 0.5 x stress-range for all MU tests and unknown for UWM tests).

Figure 3.7 Fatigue crack detected after 4,374,464 cycles at 6.0 ksi on MU-CSR-R-L-A1-1.

Figure 3.8 Fatigue crack detected after 72,660 cycles at 15.37 ksi on MU-CSR-R-S-A2-3.

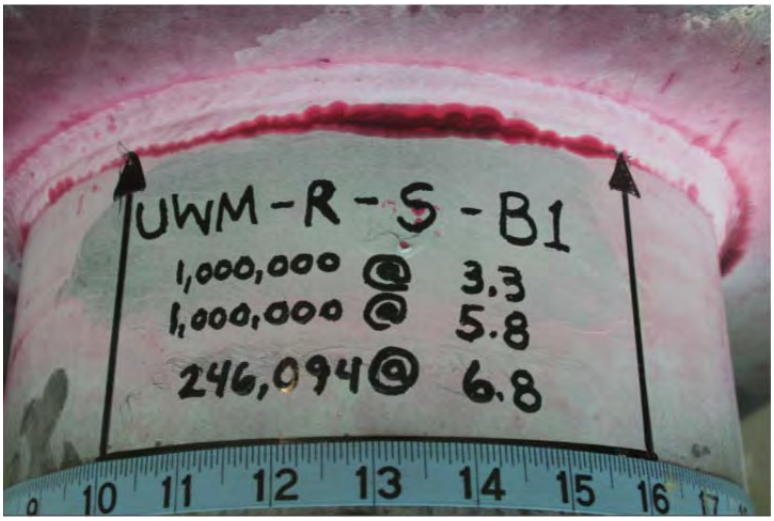

Figure 3.9 Fatigue crack detected after one million cycles at 3.3 ksi, one million cylces at 5.8 ksi and 246,094 cycles at 6.8 ksi on UWM-MR-R-S-B1-5.

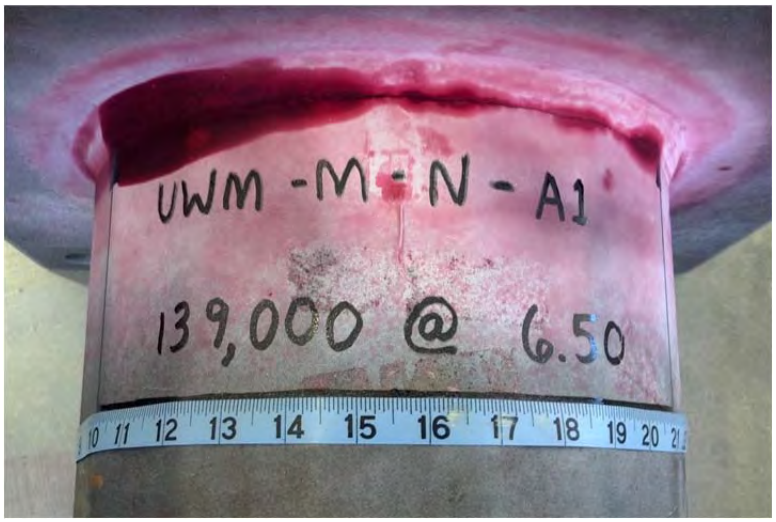

Figure 3.10 Fatigue crack detected after 139,000 cycles at 6.5 ksi on UWM-CSR-M-N-A1-7.

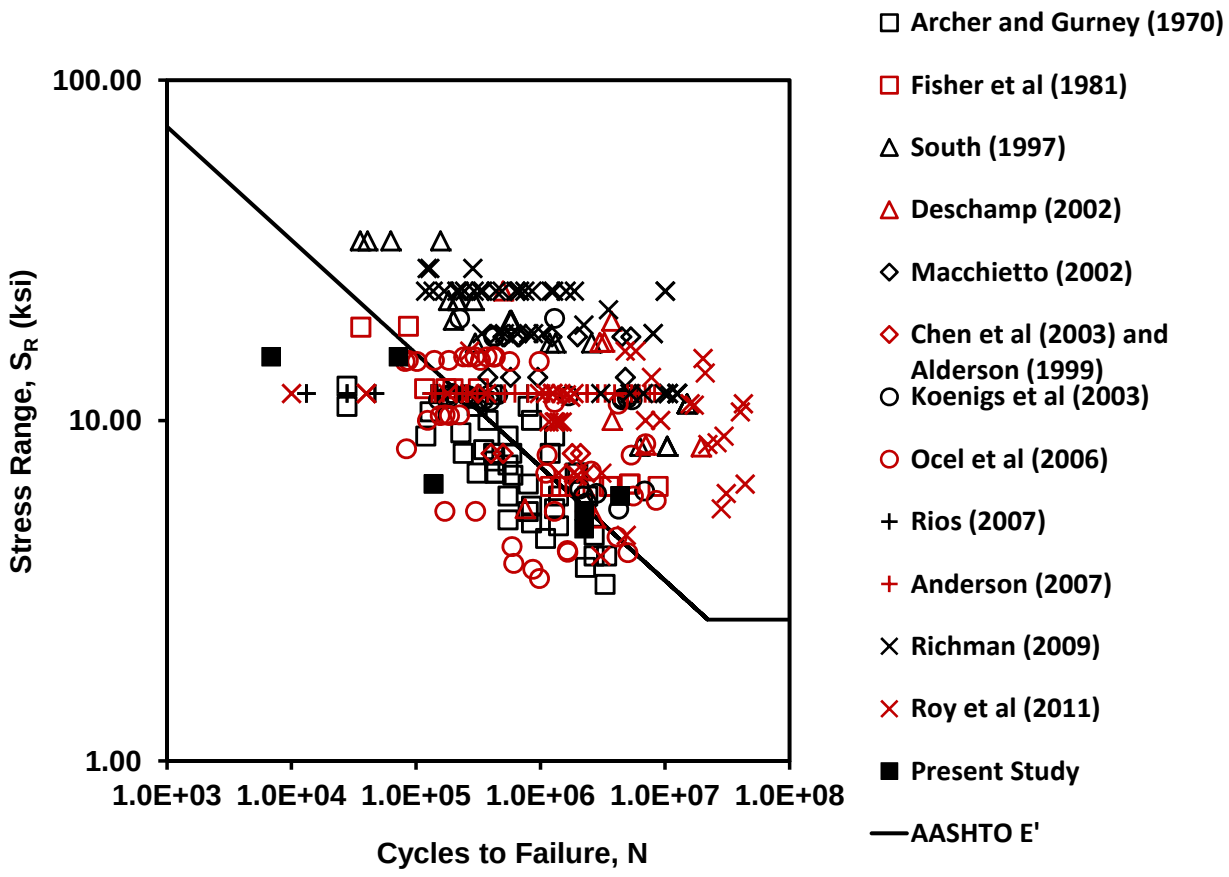

Figure 3.11 S_R-N diagram illustrating variability in fatigue test results.

AG-A-B-C-D-E		
Connection Detail Configuration		
A	S	sleeved connection similar to fillet-welded socket connection
	F	flush fillet welds
Weld Configuration and Size		
B	Weld Size	
	5/16	5/16-in. fillet weld
	7/16	7/16-in. fillet weld
	9/16	9/16-in. fillet weld
	11/16	11/16-in. fillet weld
Failure Location		
C	W	failure in fillet weld
	RHS	failure in round hollow shape wall
Specimen Designation for Series		
D		specimen designation: A, B, C, etc.
Specimen Serial Number for MU Synthesis		
E	#	

Figure 3.12 Key to specimen labels for Archer and Gurney (1970).

LEH-A-B-C-D-E		
Mast-Arm and Vertical Pole Seam Weld Location		
A	40	mast arm and vertical column seam welds located at points of tension or compression stress
	48	mast arm and vertical column seam welds located randomly
Mast-Arm and Vertical Pole Material Type		
B	A	ASTM A283 Grade D Steel, galvanized after fabrication
	V	ASTM A595 Grade A Steel, galvanized after fabrication
Fillet Weld Configuration - Contact Angle		
C	45CA	45-degree contact angle
	34CA	34-degree contact angle
	28CA	28-degree contact angle
Specimen Designation for Series		
D		specimen designation: 1, 2, 3, etc.
Specimen Serial Number for MU Synthesis		
E	#	

Figure 3.13 Key to specimen labels for Fisher et al. (1981).

WY-A-B-C-D-E-F		
Specimen Designation		
A	IS	in-service specimen
	V	virgin (manufactured) specimen
Mast-Arm Connection Configuration		
B	S	socketed with fillet weld
	FP	full-penetration weld
Mast-Arm Connection Plate Thickness		
C	#	connection plate thickness in inches
Mast-Arm Wall Thickness		
D	#	mast-arm wall thickness in sixteenths of an inch
Mast-Arm Diameter		
E	#	mast-arm diameter in inches
Specimen Serial Number for MU Synthesis		
F	#	

Figure 3.14 Key to specimen labels for Deschamp (2002).

VAL-A-B-C-D		
Reinforcement Configuration		
A	U	unreinforced specimen
	R	reinforced specimen
Connection Detail Configuration		
B	If U-type specimen	
	SFW	socketed connection, unequal-leg fillet welds (long leg on mast-arm)
	FP	full penetration welds, backing ring attached with continuous fillet welds, 1-in. tall backing ring
	If R-type specimen	
	45FW	45-degree gussets, fillet welded, 3.25-in. long
	15FP	15-degree contour gussets, full penetration welds, 6 in. long, weld ground smooth at transition
	TCFP	Tangent-contour gussets, full penetration welds, 5.83-in. long, weld ground smooth at transition
	RFWS	Radial gusset, fillet welds terminated 1/2-in. short of gusset ends, 5.44-in. long
Specimen Designation for Series		
C		specimen designation: A, B, C, etc.
Specimen Serial Number for MU Synthesis		
D	#	

Figure 3.15 Key to specimen labels for Machietto (2002).

UMO-A-B-C-D		
Fabricator		
A	VAL	Valmont
	JEM	Acronym Unknown
	UM	Union Metals
Fillet Weld Configuration		
B	O	Standard (equal-leg) fillet weld
	N	New (fatigue-resistant, unequal leg) fillet weld
Specimen Designation for Series		
C		specimen designation: 1, 2, 3, etc.
Specimen Serial Number for MU Synthesis		
D	#	

Figure 3.16 Key to specimen labels for Chen et al. (2003) and Alderson (1999).

A-B-C-D-E-F		
Mast-Arm Wall Thickness and Manufacturing Entity		
A	VAL	0.179-in. thick, Brenham, TX
	TX	0.239-in. thick, Brenham, TX
	VALN	0.179-in. thick, Valley, NE
Connection Detail Configuration		
B	U	unreinforced, fillet weld, socketed
	U2	unreinforced, fillet weld, socketed, 2-inch plate
	W	reinforced, full-penetration weld with backing ring
	EC	reinforced, external collar
	IC	reinforced, internal collar
	UR	reinforced, U-rib stiffener
	L x t_s	reinforced, triangular stiffener (L - length in inches) (t_s - thickness in inches)
	L x t_s @ 45	reinforced, triangular stiffener at 45-degree orientation
Retrofit Treatment or Specialized Coating		
C	N	no retrofit treatment or galvanizing
	P	ultra-sonic impact treatment (UIT)
	G	galvanized
	PG	UI treated then galvanized
	GP	galvanized then UI treated
Specimen Designation for Series		
D		specimen designation: A, B, C, etc.
Special Notes (no entry indicates no special testing treatment or treatment scenario)		
E	LMS	fatigue testing done at low mean stress
	UL	UIT performed in unloaded state
Specimen Serial Number for MU Synthesis		
F	#	

Figure 3.17 Key to specimen labels for Koenigs et al. (2003).

MN-A-B-C-D-E-F-G-H-I		
Specimen Designation		
A	P	Pole Base Plate Connection
	MA	Unstiffened Mast-Arm Connection - Mast-Arm with full-penetration weld
	MAG	Gusset Stiffened Mast-Arm Connection - Mast-Arm with socket connection and gusset stiffeners
Test Frame Configuration		
B	FR1	Test Frame Configuration 1
	FR2	Test Frame Configuration 2
	FR3	Test Frame Configuration 3
Loading Direction		
C	IP	In-Plane Loading
	OP	Out-of-Plane Loading
Retrofit Treatment Implemented		
D	N	None
	HP	Hammer Peening
	HPR	Hammer Peening with Simulated Dead Load and Crack Present
Stress Range Methodology		
E	CSR	Constant Amplitude Stress Range
	MR	Miner's Cumulative Fatigue Damage Equivalent
Pole or Mast-Arm Tube Wall Thickness		
F	#	Number of sixteenths of an inch (e.g. 5 - indicates 5/16 inch)
Connection Plate Thickness		
G	#	Plate thickness (e.g. 1.25 in. or 2.50 in.)
Test Direction		
H	1	Indicates first side testing
	2	Indicates second side testing
Specimen Serial Number for MU Synthesis		
I	#	

Figure 3.18 Key to specimen labels for Ocel et al. (2006).

UTX-A-B-C-D-E-F		
Pole Diameter		
A	#	pole diameter in inches
Base Plate Thickness in inches		
B	#	
Number of Bolts used in Base Plate		
C	#	
Connection Detail		
D	S	Socketed Connection
	SB	Stool Base
	TX	Texas Full Penetration Weld
	WY	Wyoming Full Penetration Weld
Specimen Designation for Series		
E		specimen designation: A, B, C, etc.
Specimen Serial Number for MU Synthesis		
F	#	

Figure 3.19 Key to specimen labels for Rios (2007).

A-B-C-D-E (#)		
Specimen Connection Detail		
A	WY	Full Penetration (Wyoming Detail)
	EC	External Collar
	S	Standard Socket
	CA	California Weld Profile Socket Connection
Base Plate Thickness in inches		
B	#	
Outside Tube Diameter in inches		
C	#	
Specimen Designation for Series		
D		specimen designation: A, B, C, etc.
Specimen Serial Number for MU Synthesis		
E	#	
Weld Quality		
(#)	(1)	Specimen suspected of having unsatisfactory welds.
	(2)	Indicates replicate of specimen suspected of unsatisfactory welds.

Figure 3.20 Key to specimen labels for Anderson (2007).

A-B-C-D-E-F-G-H		
Specimen Connection Detail		
A	WY	Full Penetration (Wyoming Detail)
	EC	External Collar
Base Plate Detail		
B	S	Square Base Plate/Square Bolt Pattern
	R	Rectangular Base Plate/Rectangular Bolt Pattern
	SR	Square Base Plate/Rectangular Bolt Pattern
Galvanizing		
C	G	Galvanized
	B	Not Galvanized (Black)
Manufacturer Identification		
D	A	Ameron
	P	Pelco
	U	Union Metal
	V	Valmont
Base Plate Thickness in inches		
E	#	
Tube Diameter in inches		
F	#	
Specimen Designation for Series		
G		specimen designation: A, B, C, etc.
Specimen Serial Number for MU Synthesis		
H	#	

Figure 3.21 Key to specimen labels for Richman (2009).

LEH-A-B-C-D-E-F		
Pole or Mast-Arm		
A	AB	Arm Base
	PB	Pole Base
Specimen Type		
B	R	Round tube
	M	Multi-sided tube
Lehigh Identification Number		
C	#	I,II,III,IV,…X,XI,XII
Conection Detail Identification		
D	BP1	Full-penetration groove-welded round tube-to-transverse plate with backing ring welded to plate and tube
	BP2	Full-penetration groove-welded round tube-to-transverse plate with backing ring welded to plate only
	FPG	Full-penetration groove-welded round tube-to-transverse plate
	SF	Socketed fillet-welded tube-to-transverse plate connections
	LS	Tube-to-transverse plate connection stiffened by welded longitudinal attachments
	LSS	Tube-to-transverse plate connection stiffened by stool type welded longitudinal attachments
Stress Range Methodology		
E	CSR	Constant Amplitude Stress Range
	MR	Miner's Cumulative Fatigue Damage Equivalent
Specimen Serial Number for MU Synthesis		
F	#	

Figure 3.22 Key to specimen labels for Roy et al. (2011).

A-B-C-D-E-F		
Testing Location		
A	MU	Marquette University
	UWM	University of Wisconsin-Milwaukee
Stress Range Methodology		
B	CSR	Constant Amplitude Stress Range
	MR	Miner's Cumulative Fatigue Damage Equivalent
Specimen Type		
C	R	Round tube
	M	Multi-sided tube
Specimen Designation - End Tested		
D	If tested at MU:	
	L	Large diameter end tested (d = 11.0 in.)
	S	Small diameter end tested (d = 9.9 in.)
	If tested at UWM:	
	N	North side of specimen tested
	S	South side of specimen tested
Specimen Designation - Top or Bottom		
E	A1	Top of specimen A
	A2	Bottom of specimen A
	B1	Top of specimen B
	B2	Bottom of specimen B
Specimen Serial Number for MU Synthesis		
F	#	

Figure 3.23 Key to specimen labels for the experimental program of this study.

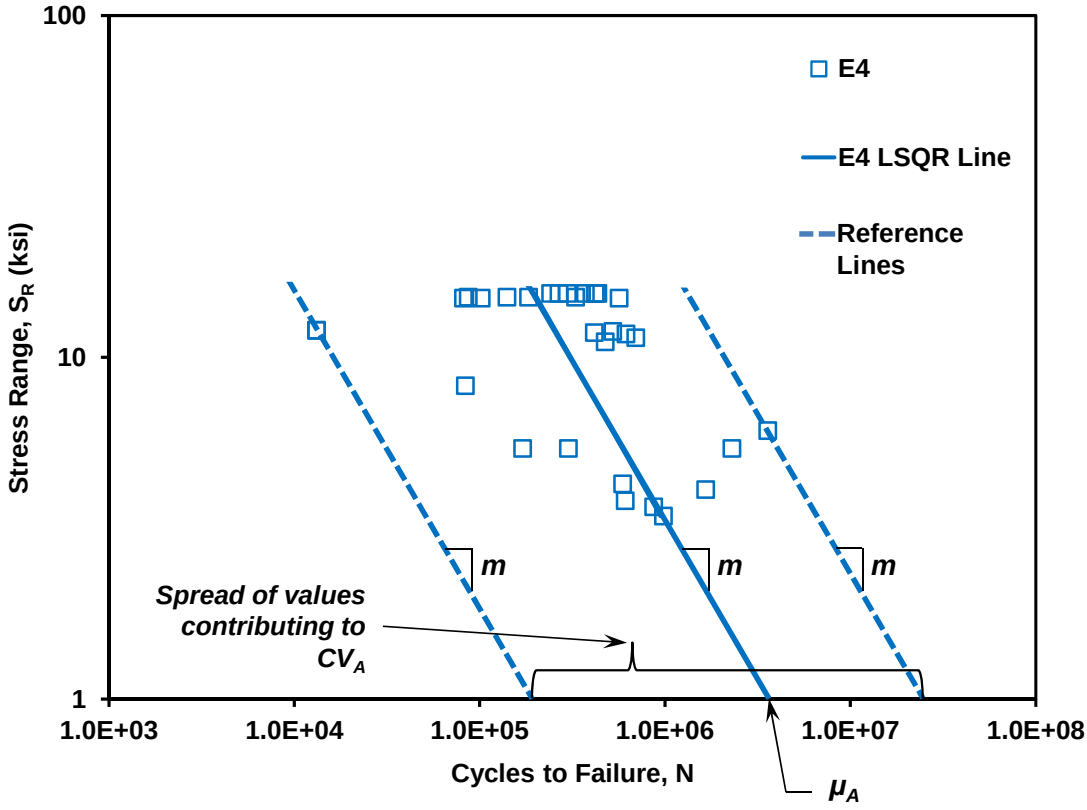

Figure 3.24 Example figure for explanation of statistical analysis (note: this figure also provides real S_R-N data and corresponding regression line for the E4 fatigue detail category).

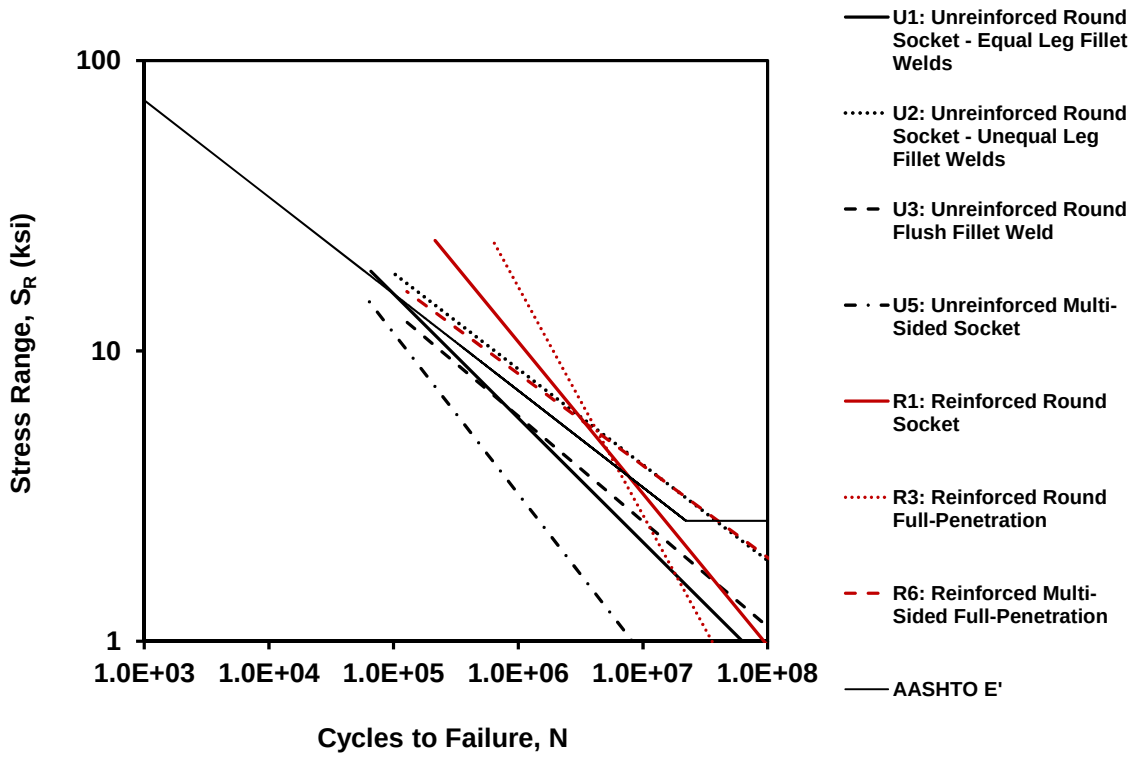

Figure 3.25 S_R-N diagram illustrating variation in least squares regression lines for each detail category generated in Synthesis Approach No. 1.

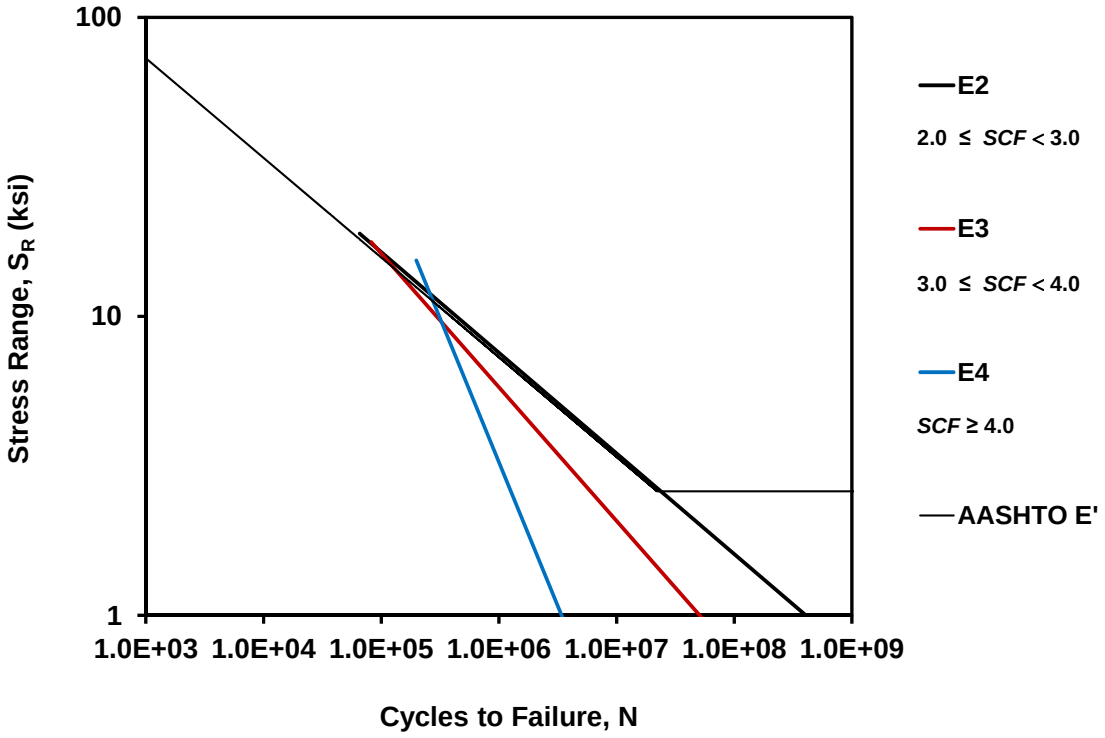

Figure 3.26 S_R-N diagram illustrating variation in least squares regression lines for each detail category generated in Synthesis Approach No. 2.

This page has been intentionally left blank.

Chapter 4 – Modeling Error Uncertainty

4.1 Introduction

The reliability-based risk-assessment procedure formulated in chapter one of this report includes uncertainty in loading demands (wind), fatigue life, modeling error, and accumulated fatigue damage. The two immediately preceding chapters focused on developing models to characterize uncertainty in wind loading and fatigue performance. Modeling error uncertainty characterization is often done using assumptions based upon engineering judgment and experience (Wirsching 1983) and a lack of correlation with measured behavior. The present research effort included design, construction and operation of a field monitoring system (Smith 2010), which allows the unique opportunity to characterize differences between predictions made via models and behaviors measured in the field. The ability to do this and to formulate models for error uncertainty is novel and a unique contribution to the body of knowledge in the area of fatigue performance.

The objectives of the present chapter in the report are to outline and discuss a process for simulating the transient nature of wind speed, formulate a procedure for simulating stress-range histories likely to be present at critical details in sign support structures, develop a systematic process for correlating predicted stress-range histories to those measured at the field monitoring station employed in this research effort, and formulate lognormal statistical modeling parameters for modeling error used in the risk-based assessment procedure. It should be noted that this chapter is a synthesized version of former work by a report co-author and much greater detail can be found elsewhere (Diekfuss 2013).

4.2 Finite Element Modeling

Finite element (FE) modeling, be it low-fidelity or high-fidelity, is the cornerstone of much of the engineering research conducted today. A low-fidelity model, for purposes of the present research effort, is a stick model without details regarding connections present within the structural system and omission of detailed modeling of cross-section shape and mass distribution. A high-fidelity finite element model is one in which detailed modeling of connection behavior (*e.g.* bolt pretension, plate interface behavior, weld geometry) is included. A high-fidelity finite element model often requires several orders of magnitude increases in computer simulation time and considerable effort is often employed to assess the level to which a finite element model must reach to create accurate and usable engineering results. The present section of the report discusses the finite element models generated for development of models for modeling error uncertainty.

Two sign support structure configurations were used in the present effort. The first mast-arm sign support was the Milwaukee sign support structure whose configuration is shown in Figure 4.1. This sign was the structure used in the field monitoring station from which wind speed data and strain data was collected. Two aluminum signs are affixed to the sign support as shown in the figure. Each sign is 4.5-ft by 6-ft in dimension and located along the mast-arm as shown in Figure 4.1. The mast-arm and pole are both tapered. The second sign support structure is the Osseo sign support that experienced a very short service life. The mast-arm and pole in this sign support structure do not taper. The mast-arm-to-pole connection is also significantly different than that seen in the Milwaukee sign support. Three very small aluminum signs (2-ft by 2.5-ft) were located along the mast-arm as shown in Figure 4.2.

High-fidelity FE models were created for both sign support structures found in Figures 4.1 and 4.2. These FE models included very detailed modeling of the mast-arm-to-pole connection region, rigid regions at appropriate distances from the connection zone, and one-dimensional (*i.e.* stick) models for the mast-arm and pole that extends away from the connection region. Static and dynamic loading behavior and modal analysis was considered. The present section of the report will outline the process that was used to arrive at the FE models employed in the development of the modeling parameters for error uncertainty.

The high-fidelity FE models for the sign support structures considered in the present research effort included detailed modeling of the connection region and stick modeling in regions away from the connection region. The connection region model for the Milwaukee sign support structure is shown in Figures 4.3 and 4.4. The connection region model for the Osseo sign support structure is shown in Figures 4.5 and 4.6. The high-fidelity FE models included detailed modeling of the weld regions (Figures 4.4 and 4.6), bolt pretension, socketed plate gap (Figures 4.4 and 4.6), and contact modeling at mast-arm plate and pole connection plate interfaces. These detailed models of the connection region were utilized to study the stress flow behavior through the connections in these structures and formulation of the stress-concentration-factor-based fatigue performance curves discussed in chapter three of this report. Further details regarding this analysis can be found elsewhere (Diekfuss 2013).

The high-fidelity models for the sign supports considered were compared to lower-fidelity models that were composed of one-dimensional elements (*i.e.* stick elements) and omitted detailed modeling of the connection region. Modal analysis was conducted for both modeling approaches and for both sign support structures. The first five mode shapes were compared in these models. Figures 4.7 through 4.10 provide graphical comparison of mode shapes for these two modeling approaches. The connection region modeling is apparent in Figures 4.7 and 4.9 for the Milwaukee and Osseo high-fidelity models, respectively.

Examination of the mode shapes for both modeling approaches indicates that there is very little (if any) difference in the first five fundamental mode shapes across all models. This is to be expected when consistent

modeling of cross-section shape and mass is employed. The frequencies and periods for all FE models generated are given in Tables 4.1 and 4.2. There is very little difference in the magnitudes of the first to vibration modes (twisting and hatchet) for all the models developed. There are, however, more significant differences in the 3rd and 4th modes of vibration. These differences result from the greater flexibility present in the model when detailed connection region geometry is considered. Accounting for gap-contact and connection plate flexibility within the connection region of the model results in a reduction in model stiffness (albeit slight). This stiffness reduction results in a reduction in the natural frequency of the mode shape and a lengthening of the natural period. This behavior is consistent across all models.

The comparison of low and high-fidelity finite element models with respect to modal analysis allowed the research team to be confident that a low-fidelity model would not significantly disrupt the model's ability to capture transient behavior resulting from loading simulations of natural wind. The error uncertainty could then be assumed to be dominated by local differences in the stress fields within the vicinity of the welds.

The detailed finite element modeling of the sign support connection regions provided very important information regarding where maximum stresses would exist in the connection region. This knowledge was then used to flavor the stress-concentration factor approach for fatigue curve characterization and it also provided valuable information related to the magnitude of the strain readings measured in the field monitoring station and how these were expected to correlate with the low-fidelity finite element models employed in the simulations for developing uncertainty models for error.

Figure 4.11 illustrates the stress concentration factor magnitude variability as one migrates away from the weld toe along the mast-arm surface in the Milwaukee sign support structure. The stress concentration factor is defined simply as the stress magnitude resulting from the high-fidelity finite element model divided by the stress magnitude predicted using the flexure formula. The figure clearly indicates a drop in stress concentration factor (below 1.0) within a distance of 1-inch from the weld toe. The stress concentration factor returns to 1.0 when a distance from the weld toe of approximately 4 inches is attained. This behavior results from ovalization of the mast arm as bending deformations are applied and has been seen in previous research work (Roy et al. 2011).

It should be noted that the strain gages mounted to the mast-arm at the field monitoring station were located at 1 inch from the weld toe. Thus, it is expected that the stress-ranges at this location should be less than that predicted using the flexure formula and a low-fidelity finite element model. This behavior is very important and influenced the development of models for error uncertainty as will be described in the following sections.

4.3 Wind Speed Simulation

The FE modeling procedure used in the present study to characterize modeling error uncertainty is founded upon "stick" modeling of the mast-arm sign support structures and simulations of transient wind histories founded upon previously established procedures (Foley et al. 2004; Ginal 2003). The development of these wind speed histories is discussed in this section of the report. Detailed discussion of wind speed simulation procedures can be found elsewhere (Diekfuss 2013; Foley et al. 2004; Ginal 2003).

The Kaimal (1972) spectrum for transient wind speed variability (*i.e.* turbulence) is used in the present effort. This spectrum can be used to model transient time-varying wind speeds of user-defined duration. The present study utilizes the Kaimal spectrum to generate one-hour wind speed histories that are then migrated to one-hour duration loading histories for application in the finite element analysis. Transient wind speed histories over a two-minute period are shown in Figure 4.12. The important item of note with reference to this figure is that the level of wind speed variability (*i.e.* turbulence) increases significantly as the mean wind speed magnitude over the two minute interval increases from 5 mph to 50 mph. The wind speed simulation procedure utilizes a normal distribution of wind speeds about the mean.

The wind speed simulations found in Figure 4.12 follow the Kaimal spectrum quite closely for frequency content up to approximately 2 Hz (see Figure 4.13). The jaggedness in the simulated results comes from the fact that a finite number of simulations are used in generating the power spectrum comparisons. As more simulations are included in the suite of simulations, the power spectra are expected to become less jagged and would approach the Kaimal model.

The variability in wind speeds about the mean wind speed for a target averaging time was evaluated for one-hour averaging times and average wind speeds of 5 mph through 50 mph. This evaluation was conducted so that expected behavior could be confirmed. Figure 4.14 illustrates the wind speed distributions about the one-hour average for wind speed magnitudes ranging from 5-50 mph. The coefficients of variation about the one-hour average wind speeds exhibit the expected increase as the one-hour average wind speed increases. In other words, as the mean wind speed for the one-hour duration increases, the variability of wind speed magnitude increases. This is shown in Figure 4.14 by the flattening of the wind speed histograms. The evaluation of the simulation procedure developed for use in this study suggests that application of the Kaimal spectrum to model wind speed frequency content is acceptable. These wind speed simulations are used to generate time-varying pressures (loading) for application in finite element analysis of the sign support structures. This process then leads to the ability to generate lognormal statistical parameters for modeling error uncertainty. This is described in the following section of the report.

4.4 Error Uncertainty Modeling

One hour averaging times for wind speeds and the Kaimal turbulence spectrum were utilized to generate one-hour simulated records of wind speed. These wind speed histories were then used to generate loading histories for application in low-fidelity finite element models for the Milwaukee sign support structure. Simulated stress histories for the Milwaukee sign support structure were then compared to measured stress histories obtained from the field monitoring station for similar one-hour averaged winds. The expected stress-ranges for simulations and measurements were then used to generate statistical information needed to develop lognormal statistical modeling parameters for error uncertainty.

Figure 4.15 illustrates the low-fidelity finite element modeling procedure with respect to loading application. The wind speed simulations were transient pressures generated using conventional wind engineering procedures (Diekfuss 2013). These pressures were then converted to linear transient loadings of uniform magnitude applied to the mast-arm. The loading at sign locations reflects the increased area resulting from the signs being supported. Gravity loading was also included in the structural analysis. It should be noted that both sign supports (Osseo and Milwaukee) are included in the figure even though only the Milwaukee sign support is considered at present.

The field monitoring station data contained one-hour average wind speed magnitudes of 5 mph, 10 mph and 15 mph. It should be noted that an averaging time of one-hour results in significantly fewer mean wind speeds that can be used in developing the model for error uncertainty. Shorter duration averaging times were investigated, but the one-hour average was felt to be the best value to conduct fatigue analysis and therefore, the limited number of wind speeds was the concession made.

Transient wind pressures based upon one-hour wind-speed simulations following the Kaimal spectrum were used to develop the transient loading for the finite element analysis. These one-hour response histories and the expected stress-range magnitude obtained using rainflow counting procedures were compared to expected stress-range magnitudes seen for the same one-hour wind speed magnitude at the field monitoring station. Figure 4.16 provides illustration of this comparison. The simulated histories are shown in blue and the measured histories are shown in red. Also provided in this figure are histograms of the expected stress-ranges with the same color-coded technique. It should be noted that the stress-ranges obtained from the field monitoring station were adjusted to account for the location of the strain gage with respect to the weld toe as discussed earlier with reference to Figure 4.11. In other words, the finite element model computes stress-ranges using the flexure formula without regard to stress concentration effects. The strain gages located at the field monitoring station were located such that there is an expected stress reduction at the gage location relative to the flexure formula prediction. Thus, the measured strains (and corresponding stresses computed using an assumed material modulus of 29,500 ksi) were adjusted to make the measured behavior consistent

with a predicted value based upon the flexure formula found in the finite element analysis. This was done to ensure that the geometric effects (*e.g.* stress concentration effects) were included exclusively in the fatigue life modeling parameters that are also based upon predictions of stress from the flexure formula.

The simulated and measured stress histories were then subjected to rainflow counting procedures to determine the mean or expected stress-range magnitude, S_{RE}, and the number of expected cycles at this magnitude (Diekfuss 2013). The measured stress-ranges were obtained through a relatively complicated process involving identification of one-hour average measured wind histories and identifying stress histories that corresponded to that one-hour averaged wind speed. In other words, the wind speed history from the field monitoring station (six months of 4 Hz data) was explored to identify one-hour windows where the wind speed was a targeted value (*e.g.* 5 mph, 10 mph, 15 mph, etc). The measured wind histories resulted in three one-hour averaged winds corresponding to 5, 10, and 15 mph being identified. There were multiple histories at each of these averaged magnitudes, but only one history at each magnitude was chosen. These wind histories then had corresponding stress histories upon which the rainflow counting was implemented. The procedure was also conducted using simulated wind speed histories of one-hour duration where the average wind speed over that hour was 5, 10, and 15 mph. These wind speed histories were then migrated to wind pressures and then wind loadings which were applied to the finite element model. The simulated one-hour in duration stress histories from the FEA were then subjected to rainflow counting procedures. Further details of this process can be found elsewhere (Diekfuss 2013).

Figure 4.16 illustrates that the shapes of the expected stress-range histograms are consistent with one another and that differences in variability about the mean is more significant than differences in the expected stress-range. A value of the modeling error bias factor is defined as,

$$B = \frac{S_{RE,s}}{S_{RE,m}} \tag{4.1}$$

where: $S_{RE,s}$ is the expected stress-range for the simulated history and $S_{RE,m}$ is the expected stress-range for the measured history. Mean values for this factor and coefficients of variation can then be computed to define the parameters needed for the lognormal statistical model for modeling error uncertainty.

Table 4.3 includes the expected stress-ranges for each one-hour averaged wind speed of both simulated and measured histories at one-hour averaged wind speeds of 5, 10, and 15 mph. The mean and coefficient of variation for this limited data set is also given in the table. The tabulated data indicates that the simulated expected stress-range will likely be larger than the expected stress-range seen in an actual structure and the mean modeling error can be characterized by $\mu_B = 1.288$. The coefficient of variation is relatively high $\left(CV_B = 0.241\right)$, but that can be expected given the complexity of what is being modeled. It is interesting to

note that former research related to offshore structural systems assumed a mean modeling error of 1.00 and a coefficient of variation equal to 0.30 (Wirsching 1984). The significant contribution of the present effort is that measured data from the field monitoring station is used to generate estimates for modeling error uncertainty. As more field data is obtained for different sign support structures, these modeling error parameters can be improved.

It should be noted that vortex shedding was not considered in the loading scenarios evaluated through the course of this research. Simplified procedures for estimating the sustained mean wind speed required to generate vortex shedding along the tapered Milwaukee mast-arm and the Osseo non-tapered mast-arms suggest that vortices will shed along portions of the mast-arm structures. However, the magnitude of the forcing functions corresponding to these vortices is very, very small and can be considered negligible for the mast-arms considered in this effort (Diekfuss 2013).

4.5 Concluding Remarks

The present chapter in the report outlines the process used to compute the parameters used to characterize the uncertainty in modeling error. High- and low-fidelity finite element modal analysis was used to evaluate sensitivity of the model in predicting modal frequencies of vibration and mode shapes. It was found that the low-fidelity finite element models were acceptable for dynamic analysis of the structural systems.

The Kaimal turbulence spectrum for wind speed was used as a target when simulating wind speed histories for one-hour time intervals. Simulated wind histories were evaluated at one-hour mean wind speed magnitudes of 5 through 50 mph. The simulated wind speed histories exhibited expected variability about the mean at all one-hour average wind speeds and therefore, the simulation procedure was deemed accurate for use with the finite element modeling.

Stress-range histories of one-hour duration generated using simulated wind speed histories (and loading) for one-hour averaged wind speeds of 5, 10, and 15 mph were subjected to rainflow counting procedures to define expected stress-ranges for these simulations. The measured stress histories from the field monitoring station deployed during the research effort were scanned to identify portions of the six-month measured history where one-hour averages of wind speed were 5, 10, and 15 mph. These one-hour wind speed histories were used to identify one-hour stress-range histories to subject to the rainflow counting procedure. The results of this rainflow counting on the measured stress histories resulted in expected stress-range magnitudes for each of these one-hour averaged measured winds. The simulated and measured expected stress-ranges were used to define a mean bias factor for the simulation and a coefficient of variation. These lognormal modeling parameters were $\mu_B = 1.288$ and $CV_B = 0.241$ and are consistent with assumptions made in the past when conducting reliability analysis of structures in the offshore industry (Wirsching 1984).

Inspection of mast-arm sign support structures can be streamlined if locations around the perimeter of the mast arm weld toe where cracks are likely to initiate could be identified. The Osseo and Milwaukee sign support structures were considered with this goal in mind. The high-fidelity and low-fidelity finite element models for these sign supports were used to identify locations around the mast-arm perimeter where fatigue-induced cracks were likely to form first. Figure 4.17 indicates that while the Milwaukee sign support structure is expected to experience larger magnitude expected stress-ranges, the location where these stress-ranges occur are significantly different when compared to the Osseo sign support structure. The maximum expected stress-ranges in the Milwaukee sign support tend to form near the 80-90 degree location relative to vertical. This location is a significant difference from the location where peak gravity load tensile stress exists for the Milwaukee sign. In the case of the Osseo sign support structure, the peak expected stress-range magnitudes migrate to locations in the 60-80 degree range from vertical and the stress-range actually reduces at 80-90 degrees from the vertical axis.

This relatively simplistic analysis indicates that the extremely wide spacing of the bolts in the mast-arm-to-pole connection found in the Osseo sign support suggests that there will be a significant tendency for the gravity (dead) load tensile stress-ranges to act in concert with the tensile stress-ranges resulting from the lateral wind loads acting on the sign support. Thus, it is expected that crack initiation is likely to occur in locations lying along a line extending from the centroidal axis of the mast arm to the top bolt in the connection (on either side of the mast arm). This is consistent with the crack locations found in the Osseo sign supports (Diekfuss 2013).

4.6 References

Diekfuss, J. A. (2013). "Reliability-Based Fatigue Assessment of Mast-Arm Sign Support Structures."PhD Thesis, Marquette University, Milwaukee, WI.

Foley, C. M., Ginal, S. J., Peronto, J. L., and Fournelle, R. A. (2004). "Structural Analysis of Sign Bridge Structures and Luminaire Supports." Wisconsin Highway Research Program, Madison, WI.

Ginal, S. J. (2003). "Fatigue Performance of Full-Span Sign Support Structures Considering Truck-Induced Gust and Natural Wind Pressures."MS Thesis, Marquette University, Milwaukee, WI.

Roy, S., Park, Y. C., Sause, R., Fisher, J. W., and Kaufmann, E. J. (2011). "Cost-Effective Connection Details for Highway Sign, Luminaire, and Traffic Signal Structures." ATLSS Center, Bethlehem, PA.

Smith, A. D. (2010). "Real-Time Health Monitoring System for Mast-Arm Sign Support Structures."MS Thesis, Marquette University, Milwaukee, WI.

Wirsching, P. H. (1983). "Probability-Based Fatigue Design Criteria for Offshore Structures." American Petroleum Institute, Dallas, TX.

Wirsching, P. H. (1984). "Fatigue Reliability for Offshore Structures." *Journal of Structural Engineering*, 110(10), 2340-2356.

Table 4.1 Variation in Natural Frequencies for Dominant Modes of Vibration for both High and Low Fidelity Milwaukee Sign Models.

Milwaukee Sign Support Structure - S-40-703

Vibration Mode	Vibration Shape	High Fidelity Model		Low Fidelity Model		Abs. Diff. (%)
		Frequency (Hz)	Period (sec.)	Frequency (Hz)	Period (sec.)	
1	1st Twist	1.597	0.626	1.608	0.622	0.68
2	1st Hatchet	1.704	0.587	1.751	0.571	2.67
3	2nd Twist	3.863	0.259	4.696	0.213	17.74
4	2nd Hatchet	4.118	0.243	5.158	0.194	20.16
5	3rd Twist	12.047	0.083	12.863	0.078	6.34

Table 4.2 Variation in Natural Frequencies for Dominant Modes of Vibration for both High and Low Fidelity Osseo Sign Models.

Osseo Sign Support Structures - S-61-0001 and S-61-0002

Vibration Mode	Vibration Shape	High Fidelity Model		Low Fidelity Model		Abs. Diff. (%)
		Frequency (Hz)	Period (sec.)	Frequency (Hz)	Period (sec.)	
1	1st Twist	1.143	0.875	1.137	0.879	0.53
2	1st Hatchet	1.220	0.819	1.224	0.817	0.27
3	2nd Hatchet	4.099	0.244	4.447	0.225	7.84
4	2nd Twist	4.563	0.219	5.287	0.189	13.70
5	3rd Hatchet	9.940	0.101	9.945	0.101	0.05

Table 4.3 Expected Stress-Range Magnitudes and Modeling Error Uncertainty Parameters.

Mean Wind Speed Magnitude, i	Simulated Expected Stress-Range (ksi)	Simulated Number of Cycles	Measured Expected Stress-Range (ksi)	Measured Number of Cycles	B-value $(S_{RE,s})_i / (S_{RE,m})_i$
	$(S_{RE,s})_i$	$n_{cycles/hr,i}$	$(S_{RE,m})_i$	$n_{cycles/hr,i}$	
5.23 mph	0.1012	4034.5	0.1050	4294.0	0.964
10.18 mph	0.4090	3982.0	0.3108	3941.0	1.316
15.97 mph	1.0228	3975.5	0.6458	3815.0	1.584

μ_B	**1.288**
σ_B	**0.311**
CV_B	**0.241**

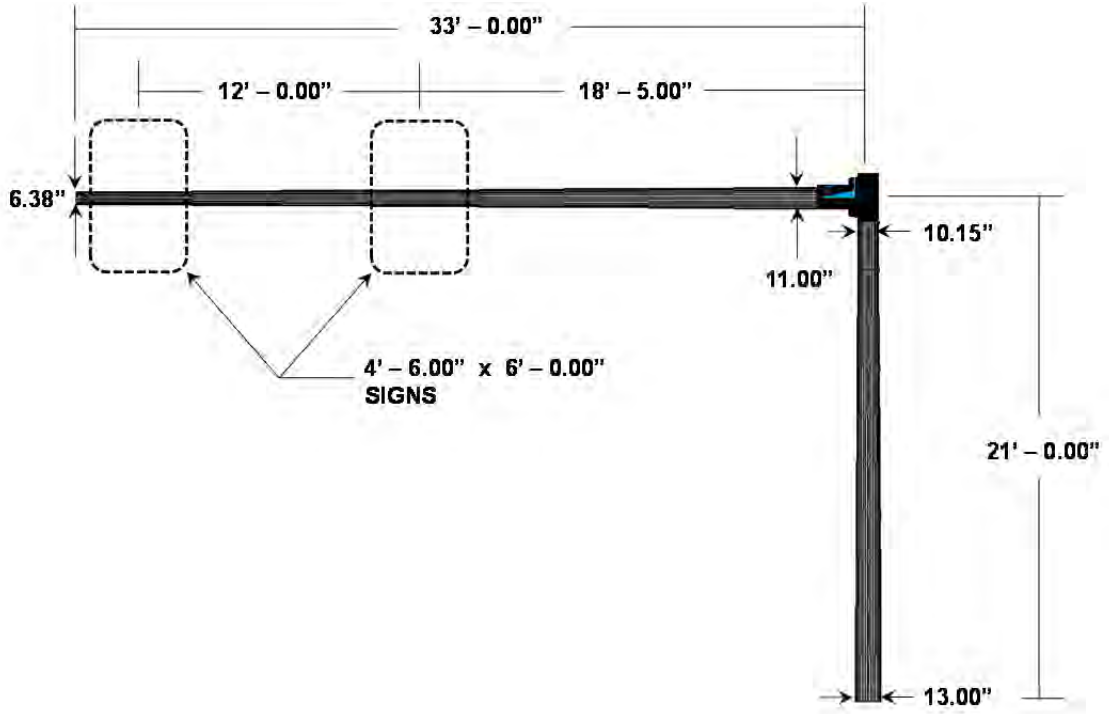

Figure 4.1 Milwaukee Sign Support Structure – illustrating tapered mast-arm and pole as well as the locations of the supported signs.

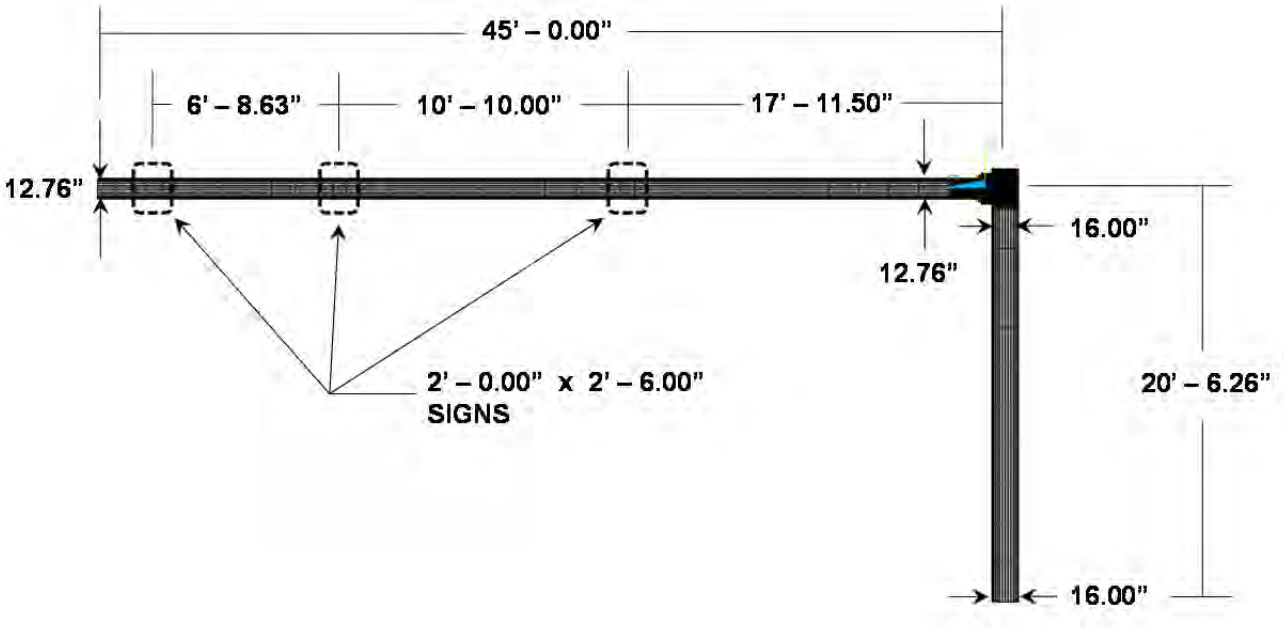

Figure 4.2 Osseo Sign Support Structure – illustrating non-tapered mast-arm and pole as well as the locations of the supported signs.

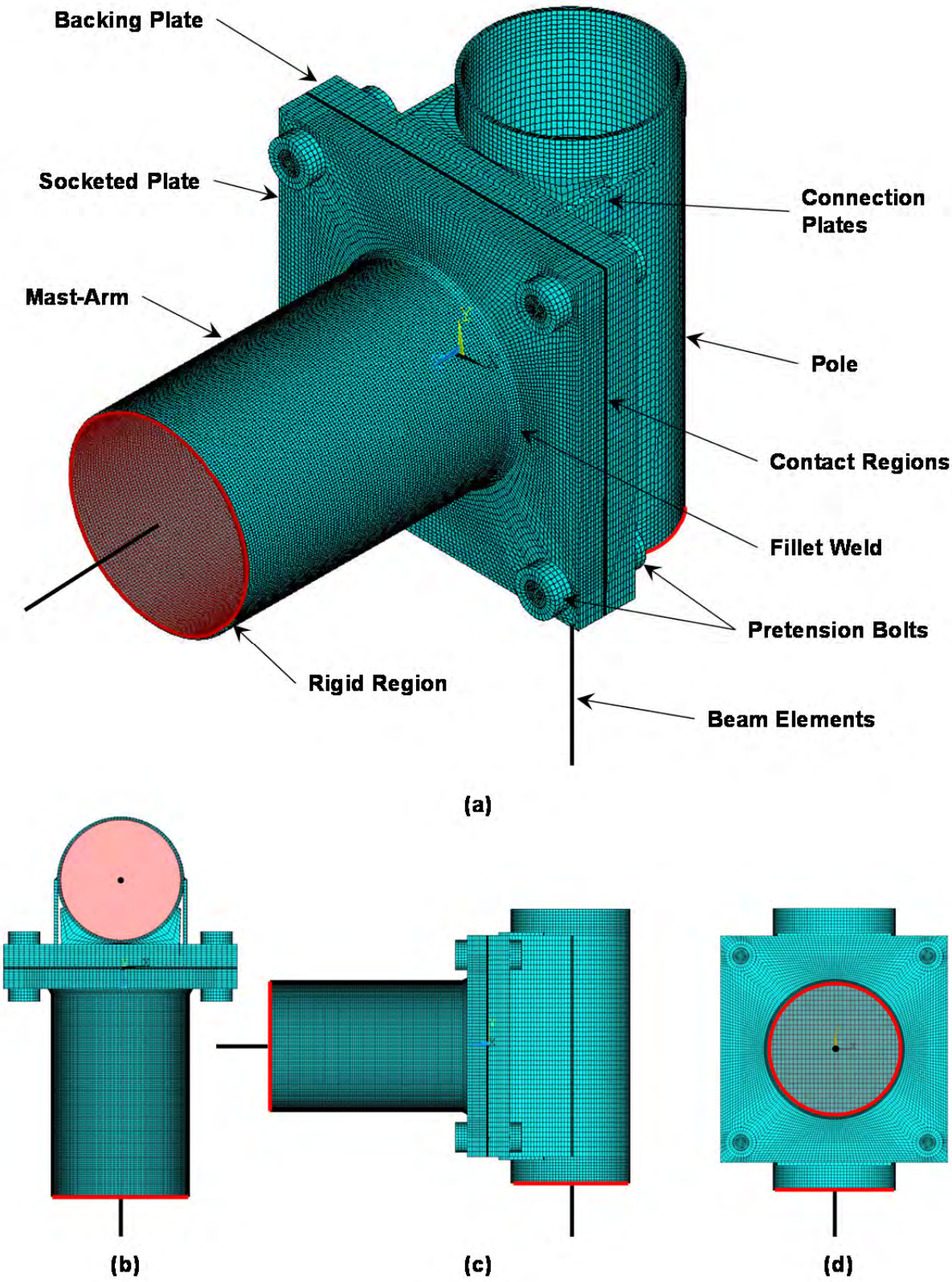

Figure 4.3 Milwaukee Sign Support Structure – detailed views of high-fidelity connection geometry and mesh: (a) labeled isometric view, (b) top view, (c) side view and (d) front view.

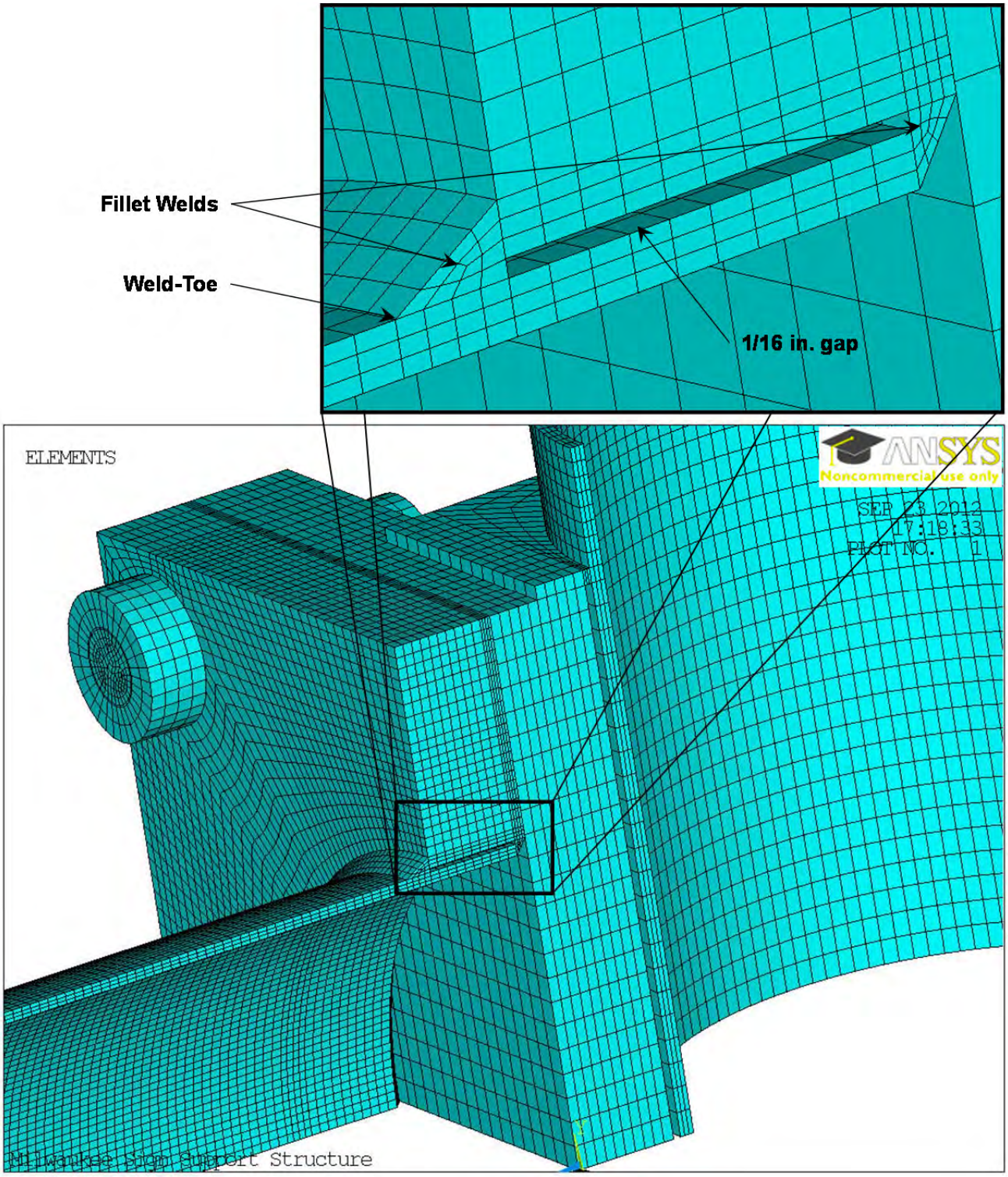

Figure 4.4 Milwaukee Sign Support Structure – up-close view of high-fidelity connection geometry and mesh illustrating fillet welds and 1/16 in. gap.

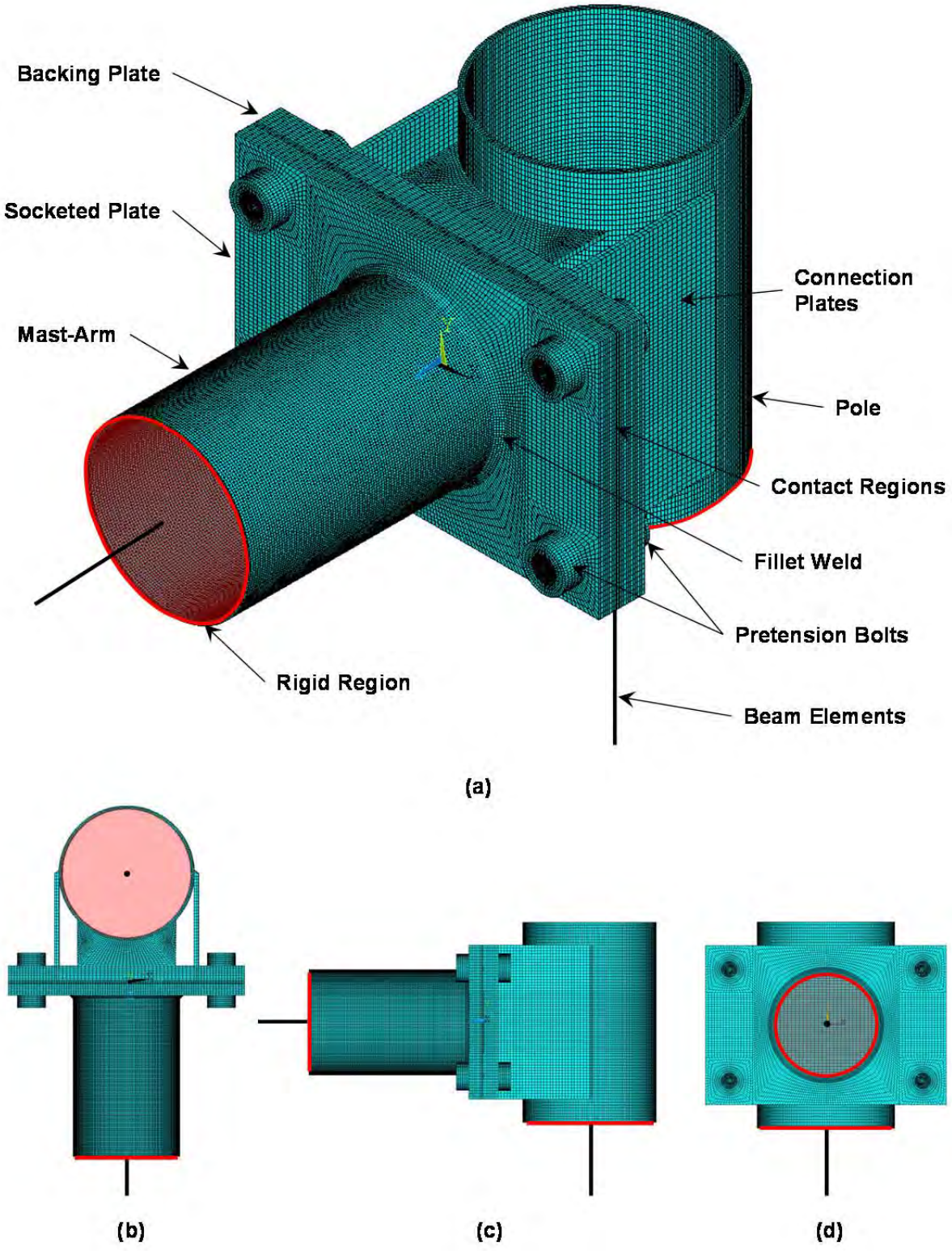

Figure 4.5 Osseo Sign Support Structure – detailed views of high-fidelity connection geometry and mesh: (a) labeled isometric view, (b) top view, (c) side view and (d) front view.

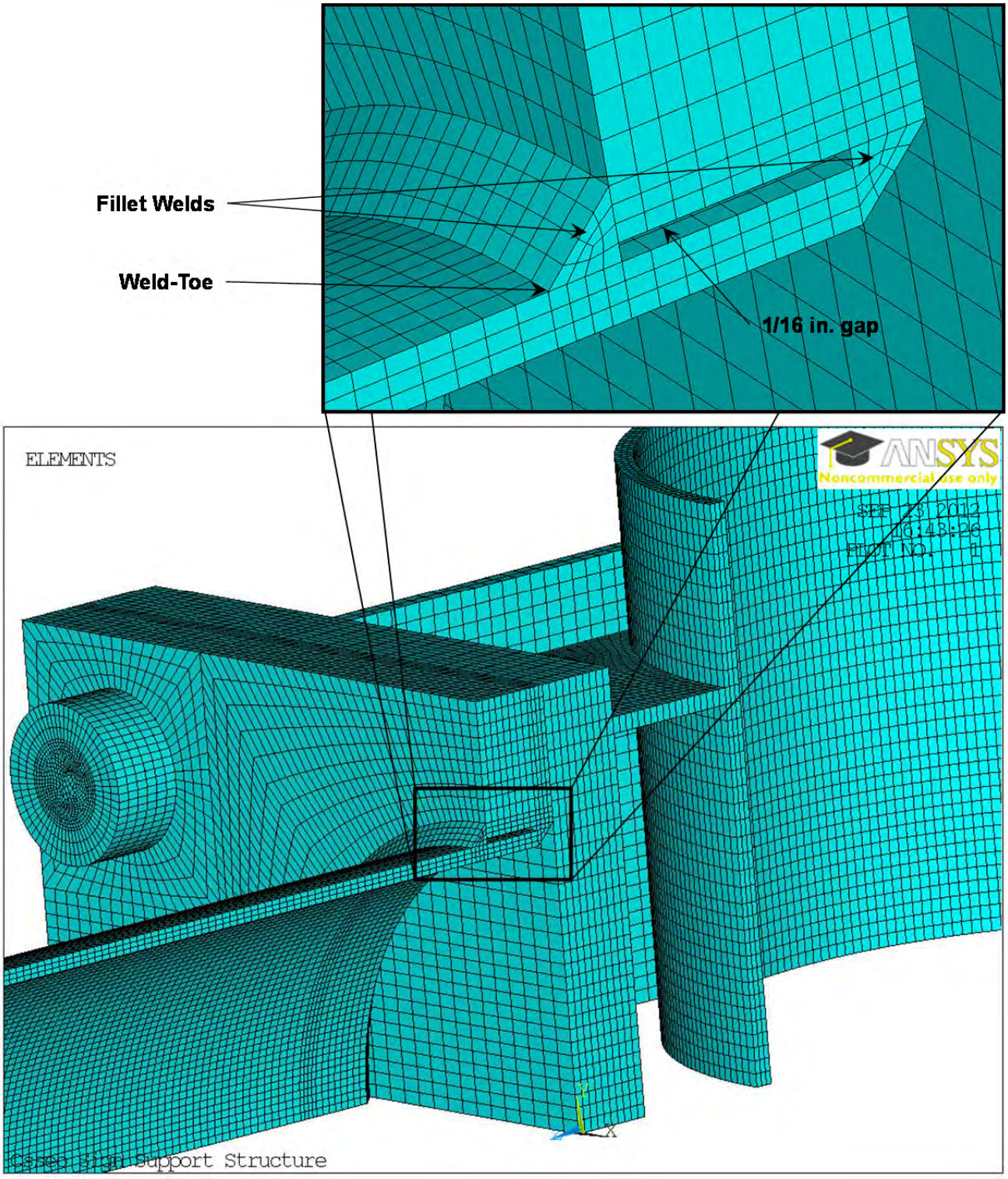

Figure 4.6 Osseo Sign Support Structure – up-close view of high-fidelity connection geometry and mesh illustrating fillet welds and 1/16 in. gap.

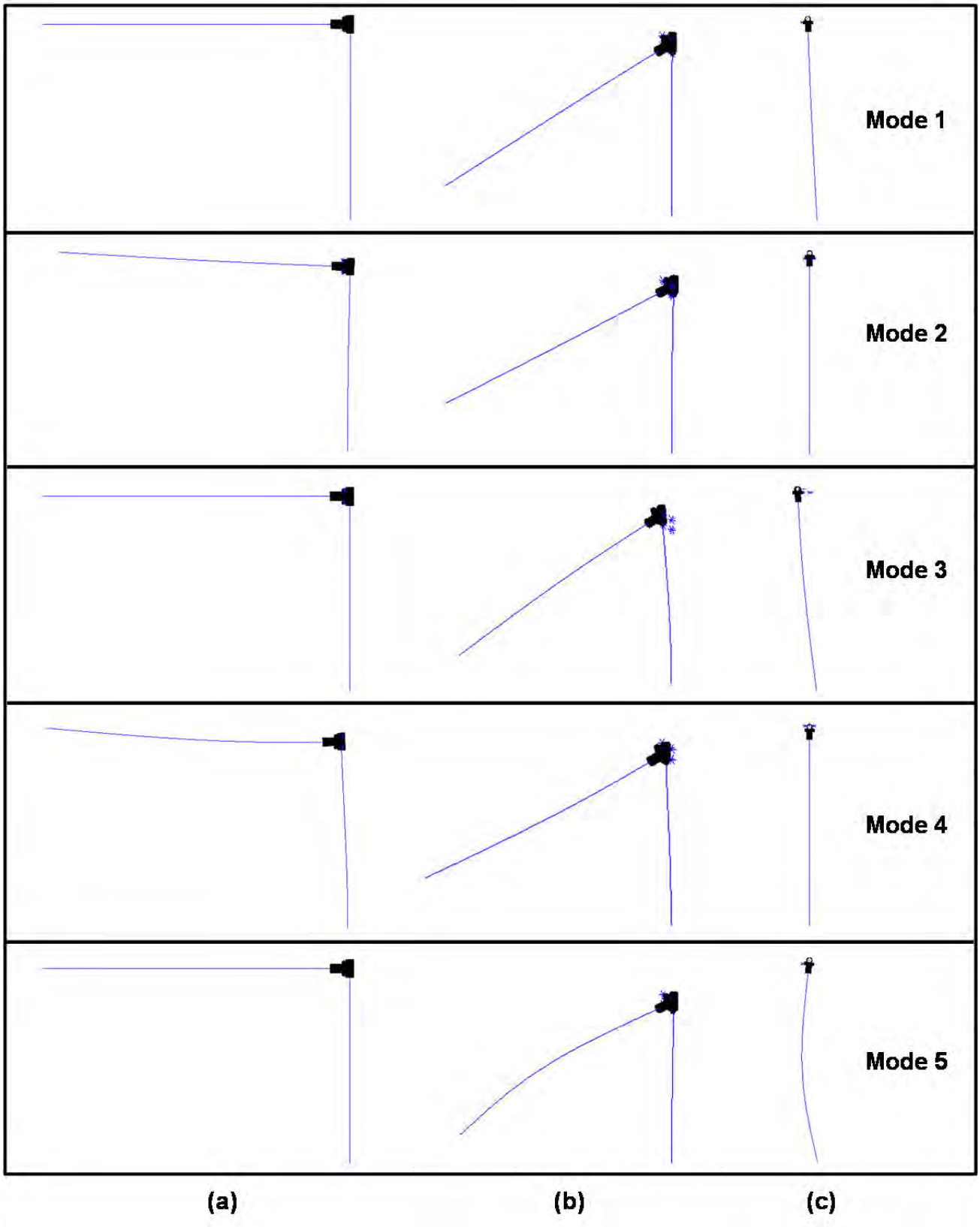

Figure 4.7 First Five Vibrational Mode Shapes of High-Fidelity FEM of Milwaukee Sign Support Structure: (a) side view; (b) isometric view; and (c) top view.

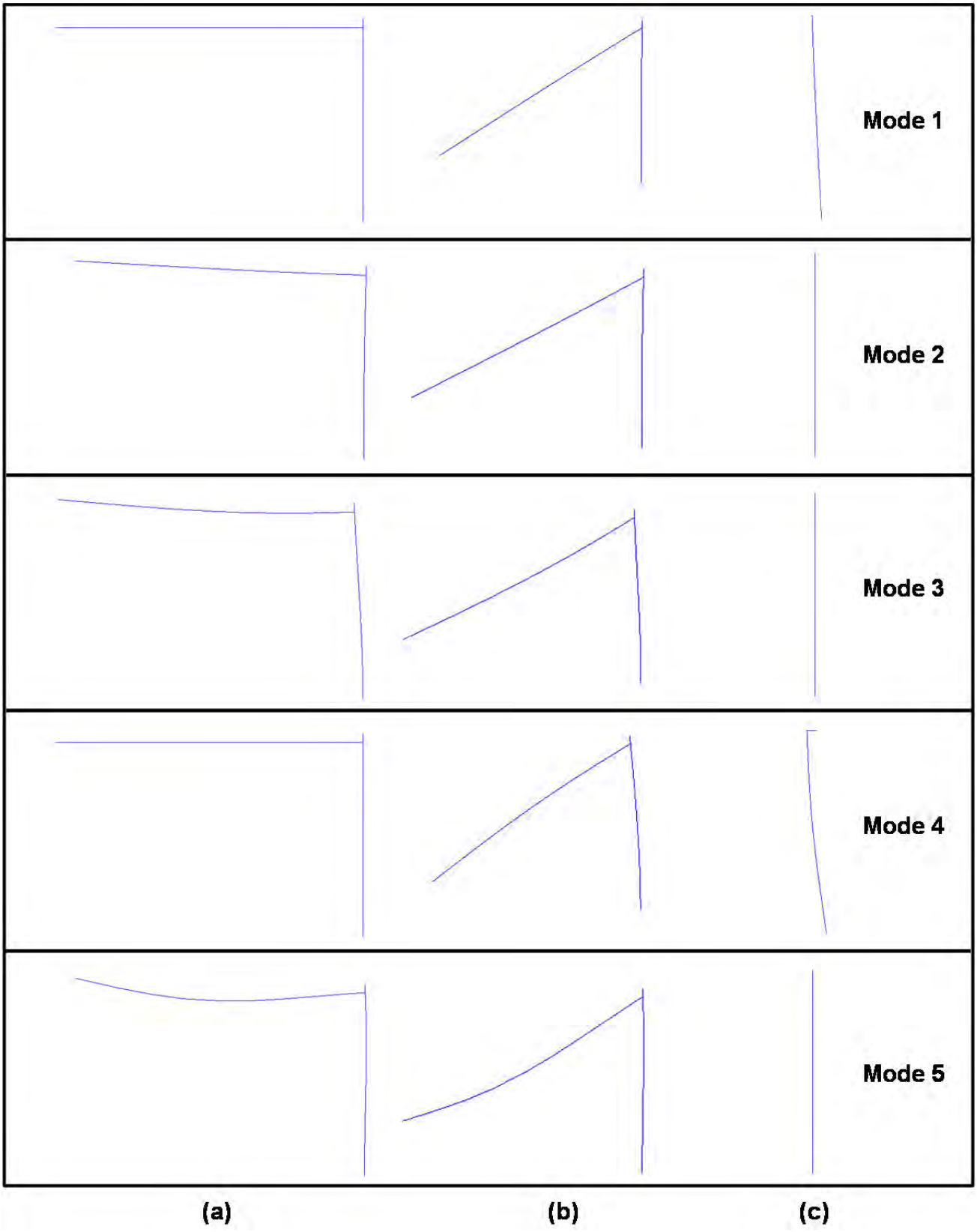

Figure 4.8 First Five Vibrational Mode Shapes of Low-Fidelity FEM of Milwaukee Sign Support Structure: (a) side view; (b) isometric view; and (c) top view.

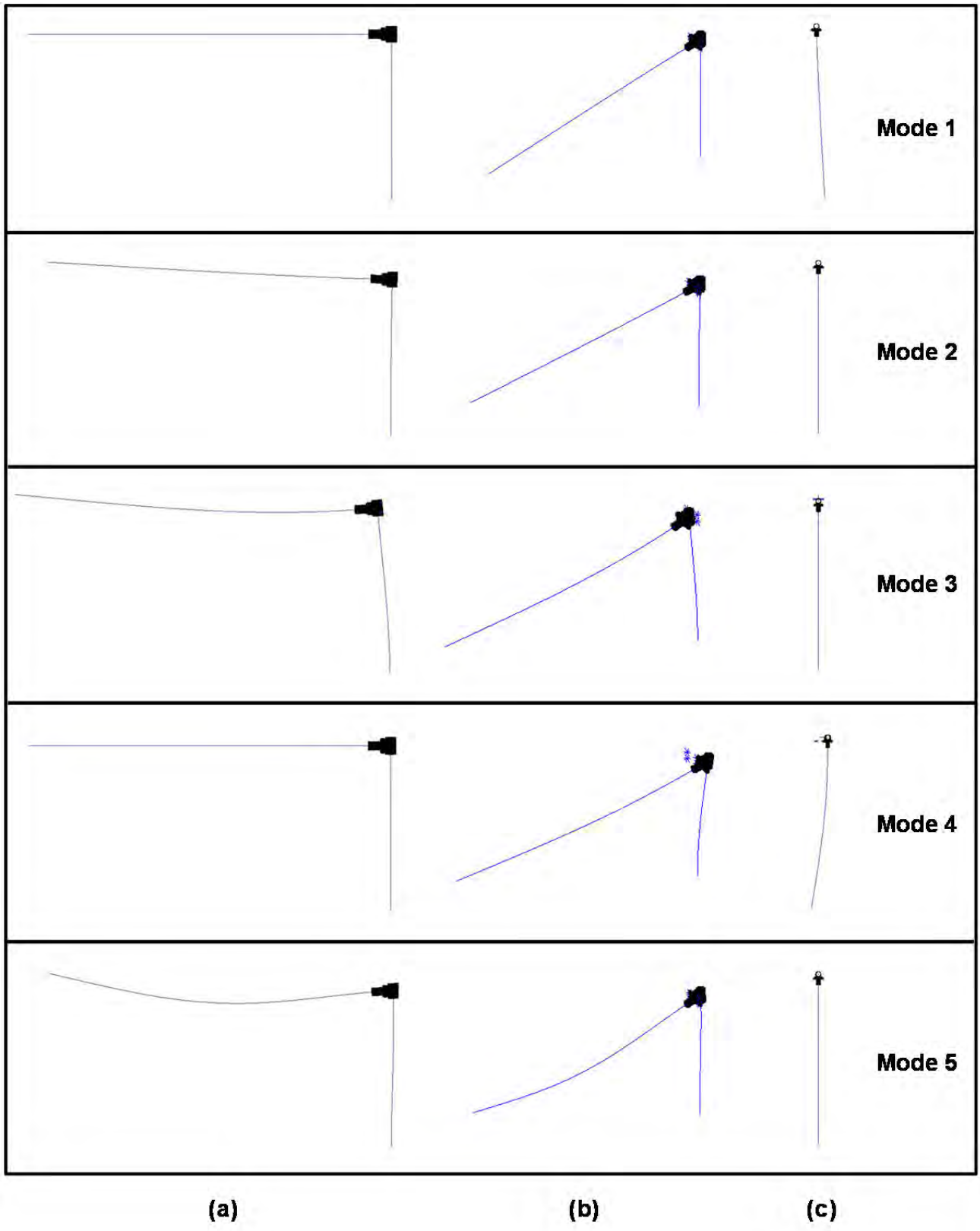

Figure 4.9 First Five Vibrational Mode Shapes of High-Fidelity FEM of Osseo Sign Support Structure: (a) side view; (b) isometric view; and (c) top view.

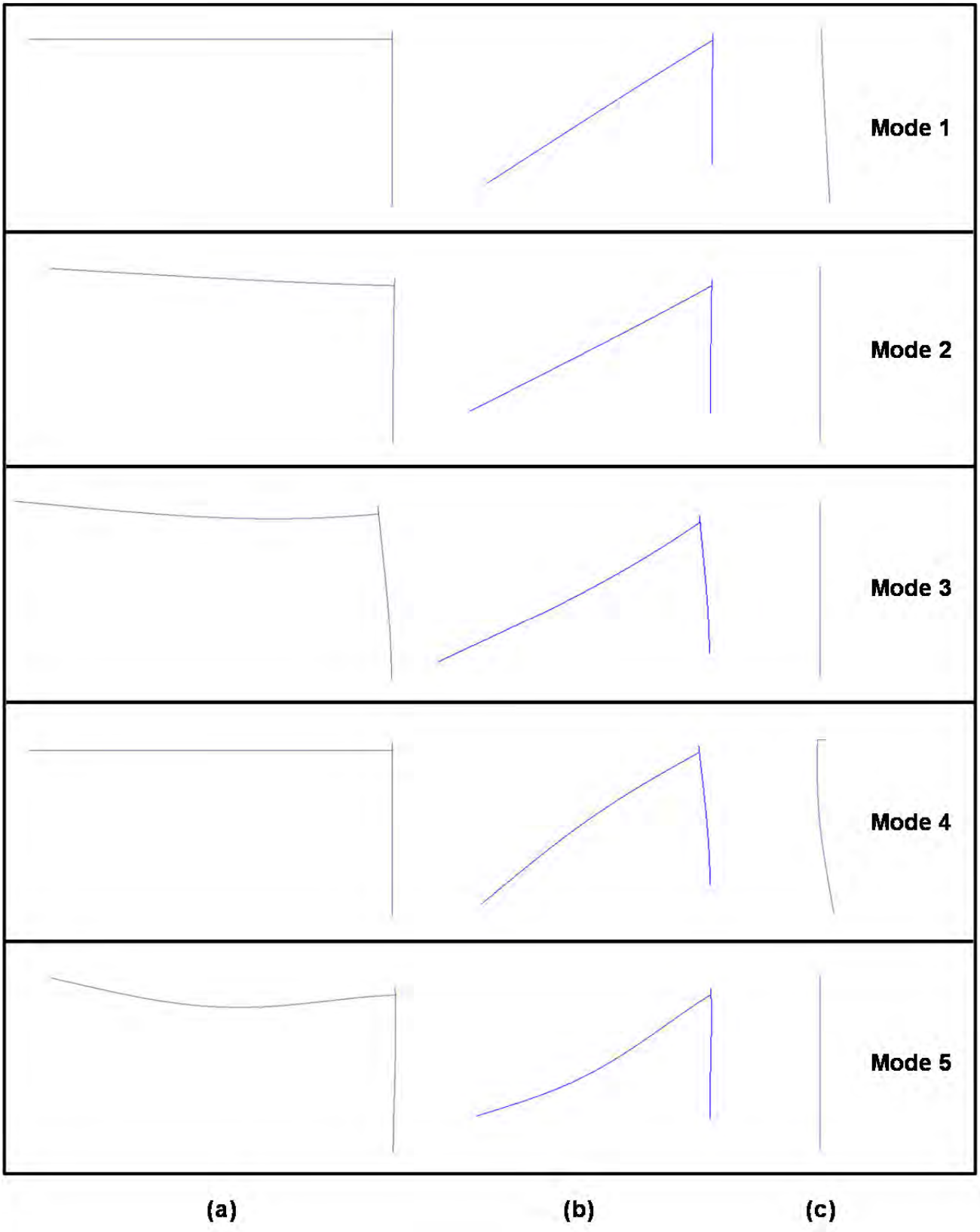

Figure 4.10 First Five Vibrational Mode Shapes of Low-Fidelity FEM of Osseo Sign Support Structure: (a) side view; (b) isometric view; and (c) top view.

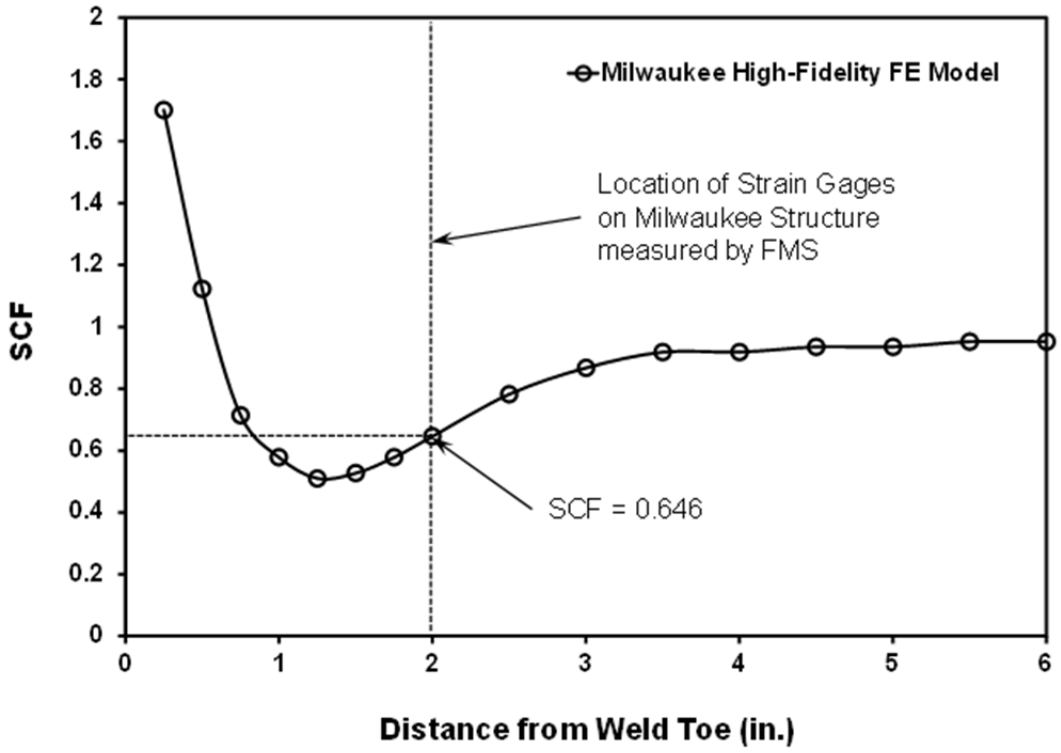

Figure 4.11 SCF at Top Fiber of Mast-Arm (Note: The distance is measured from the weld-toe toward the free end of the mast-arm).

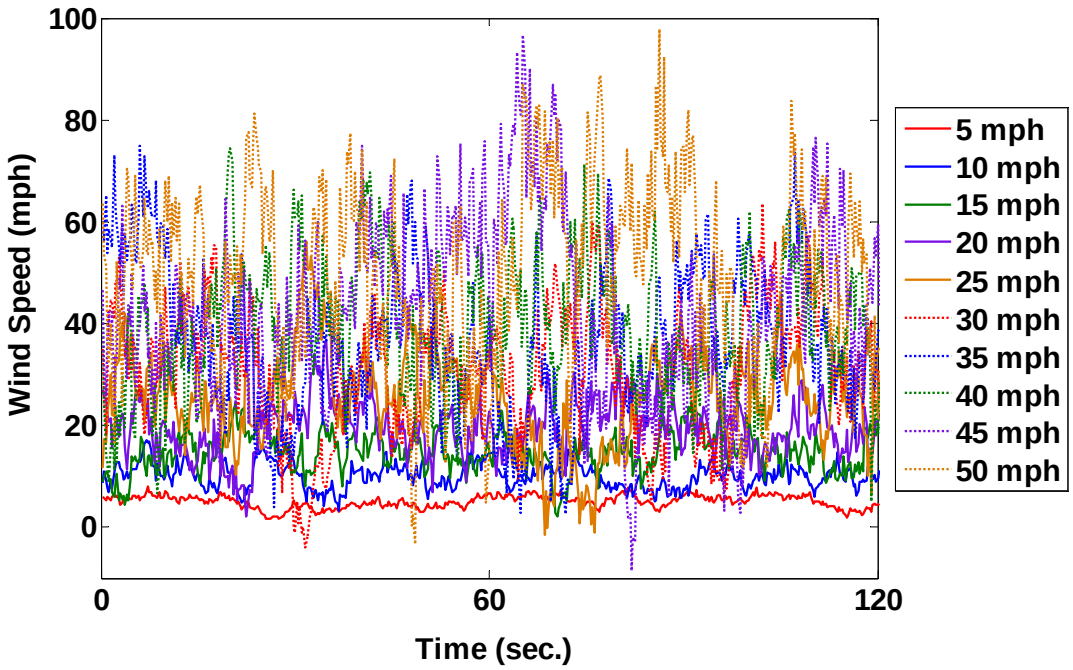

Figure 4.12 Time domain wind speed simulations generated using the 1972 Kaimal Spectrum.

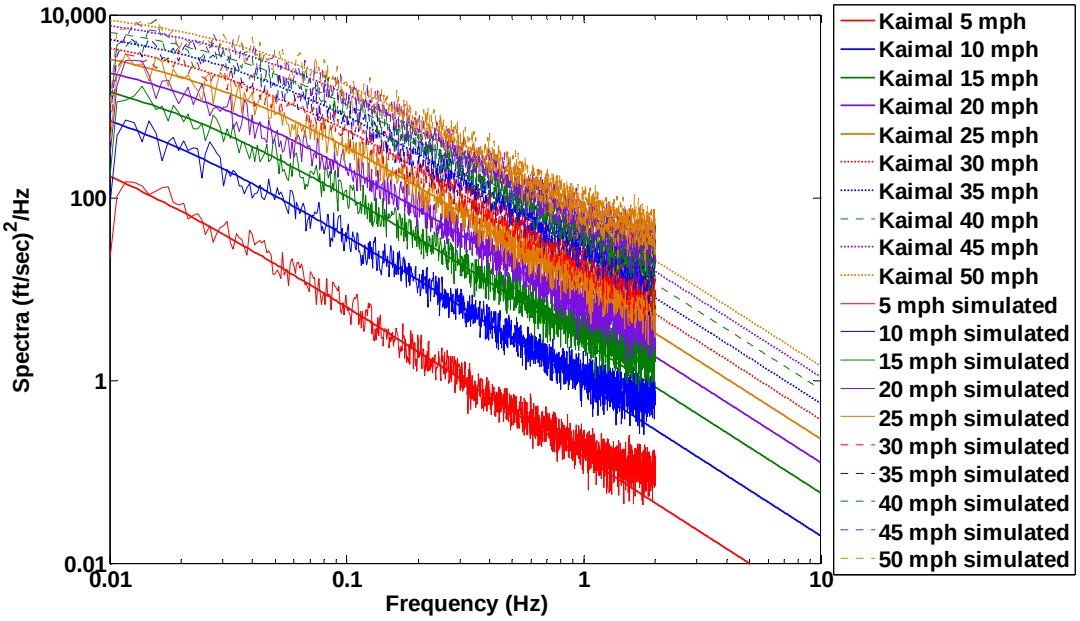

Figure 4.13 Frequency domain wind speed simulations generated using the 1972 Kaimal Spectrum.

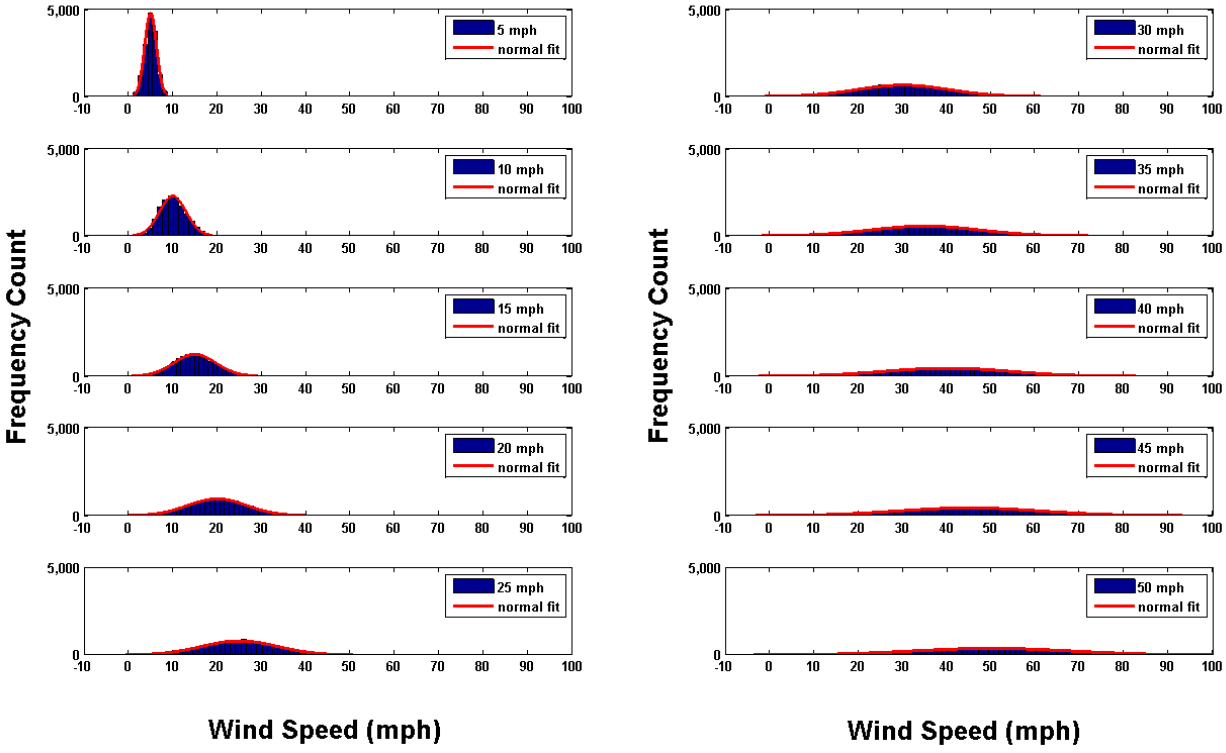

Figure 4.14 Variation in frequency count for all wind speed simulations given a one hour counting window.

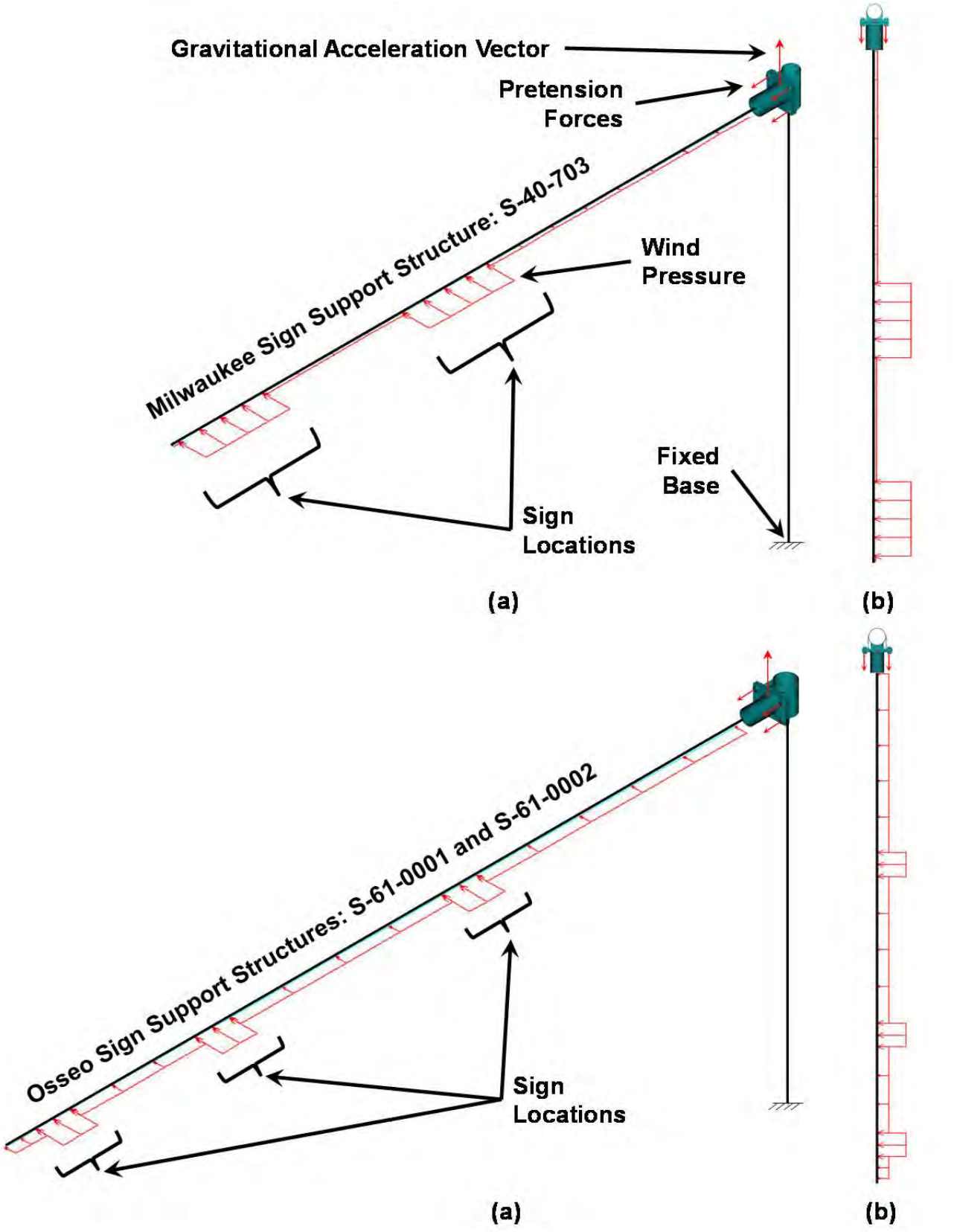

Figure 4.15 Milwaukee and Osseo gravity and wind loading schematics: (a) isometric view and (b) top view (note the increase in wind pressure magnitude at sign locations).

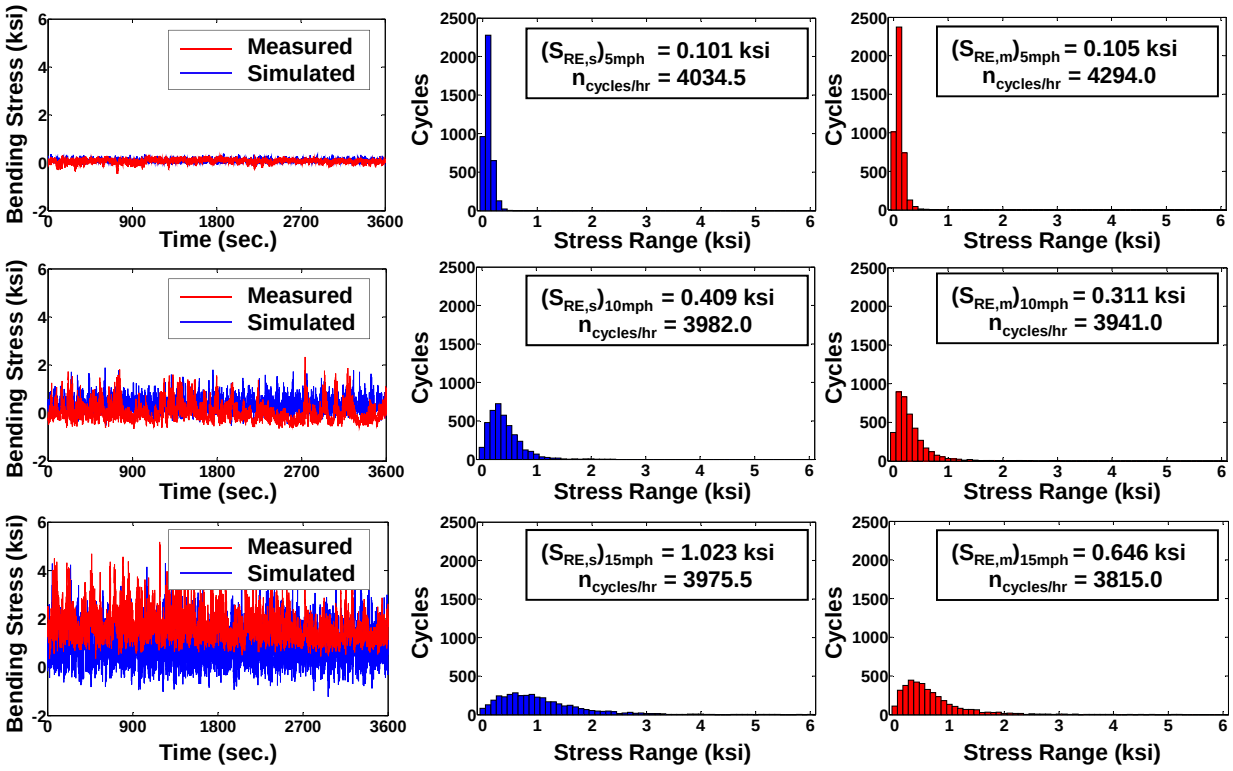

Figure 4.16 Bending Stress Time Histories and corresponding rainflow counts of stress-ranges for both simulated (blue) and measured (red) stress histories (note the resulting expected stress ranges and corresponding number of cycles for each mean wind speed history considered).

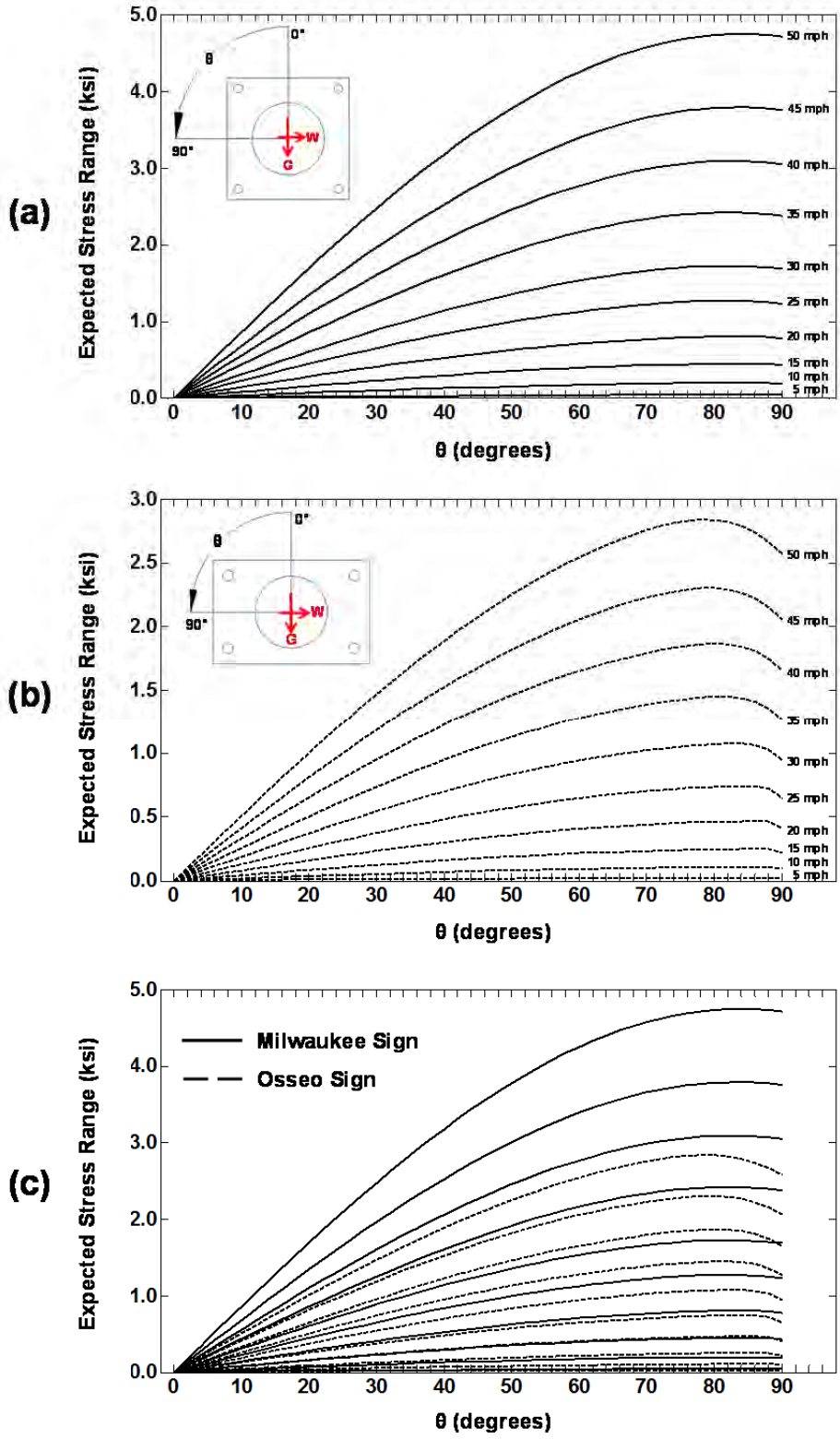

Figure 4.17 Expected stress-ranges vs. location around ¼ section resulting from each mean wind speed history considered: (a) Milwaukee Sign, (b) Osseo Sign and (c) both signs.

This page has been intentionally left blank.

Chapter 5 – Reliability-Based Risk Assessment and Inspection Protocols

5.1 Introduction

The reliability-based fatigue assessment procedure for sign support structures includes uncertainty in variables which represent loading demand (wind), resistance (fatigue life), modeling error, and accumulated fatigue damage. In order to quantify the risk of fatigue-induced fracture in these types of structures, one must first quantify the uncertainty associated with these variables. The demand was defined by a stress parameter which summed damage caused by variable-magnitude and variable-direction wind loading; the resistance was defined as the fatigue life (number of cycles to crack-initiation) of a typical welded connection; and modeling error was defined by the ratio of simulated expected stress-ranges to measured expected stress-ranges.

This chapter will begin by providing a synthesized version of the necessary results used to define reliability-based inspection protocols. The major objective is to implement the reliability-based fatigue assessment procedure in order to prescribe inspection frequencies based upon user-defined levels of risk found in typical sign supports used throughout the state of Wisconsin. The protocols will be developed for the test-group structures (*i.e.* the Milwaukee and Osseo structures) situated at various locations throughout the state of Wisconsin.

5.2 Reliability-Based Assessment Process

The foundation for the reliability based procedure employed in the present study was described in chapter one of this report. It is founded upon several expressions repeated here for clarity and an outline discussion of the procedure will be provided in this section of the report. It should be noted that a detailed description of all aspects of the procedure can be found elsewhere (Diekfuss 2013).

The assessment of probabilities of failure, also referred to as the reliability-based assessment procedure in this report, for mast-arm sign support structures begins with evaluation of the wind loading demand. Detailed derivation of the foundation for this assessment was provided in chapter two of this report. The demand in the reliability-based assessment process is based upon the stress parameter given by,

$$\Omega = n_{1-hr/year} \sum_i \sum_j \left[P\left(U = u_i \cap D = d_j\right) \cdot n_{cycles/hr,i} \cdot \left(S_{RE}^m\right)_i \cdot \cos\theta_j \right] \tag{5.1}$$

where: $n_{1-hr/year}$ is the number of 1-hour intervals in a year (8,760); $P\left(U = u_i \cap D = d_j\right)$ is the probability that a 1-hour averaged wind speed of user defined magnitude will be intersected with a 1-hour averaged wind direction of user defined direction (Tables 2.18 through 2.24); $n_{cycles/hr,i}$ is the number of stress-range cycles that occurs in a one-hour time interval resulting from application of a wind pressure simulation corresponding to a defined 1-hour averaged wind speed, *i*; $\left(S_{RE}^{m}\right)_i$ is the expected stress-range cycle magnitude that occurs in a 1-hour simulation history; and θ_j is the angle between the axis of the mast-arm and the centroidal axis of the cardinal wind direction, *j*, being considered.

It should be noted that the number of stress-range cycles and the expected stress-range cycle magnitudes are based upon rainflow counting of stress response histories for simulated wind histories with one-hour averages of 5, 10, 15, 20, 25, 30, 35, 40, 45, and 50 mph. As a result, there are values of Ω corresponding to each of these one-hour wind speed magnitudes. The stress-range histories upon which the rainflow counting is conducted are based upon finite element models of the sign support structure that are stick models outlined earlier in this report.

The parameters needed to model uncertainty in fatigue life were described in chapter three of this report. Entries in Table 3.18 include μ_A, CV_A, and m for each of three proposed detail categories synthesized in the present research. These detail categories model fatigue life uncertainty for mast-arm-to-pole connections that encompass all likely connections seen in Wisconsin mast-arm sign supports. It should be emphasized that these detail categories are different than those used in design specifications (AASHTO 2009) because it is believed that the typical detail categories found in these specifications do not capture important behavioral characteristics seen in socketed mast-arm sign support structure connections and are not able to accurately predict fatigue performance in these structures.

Uncertainty in modeling error was addressed in chapter four of this report. The lognormal modeling parameters defined to model this uncertainty were based upon comparisons of simulated stress histories computed using simulated winds and finite element models that utilized "stick" elements with measured stress histories collected from the field monitoring system designed and deployed in the present research effort. The modeling parameters synthesized from the measured and simulated response histories used in the reliability assessment are: $\mu_B = 1.288$ and $CV_B = 0.241$.

Uncertainty in models for accumulated fatigue damage is modeled using existing procedures (Wirsching 1984). The lognormal modeling parameters for uncertainty in accumulated fatigue damage used in the present procedure for defining probabilities of failure are: $\mu_\Delta = 1.00$ and $CV_\Delta = 0.30$.

The probability of a fatigue-induced crack initiating is defined using the performance function described in chapter one of this report. The probability of a fatigue-induced crack can be written as,

$$p_F = P\left[Y \le 1.0\right] = \Phi\left[-\frac{\mu_{\ln Y}}{\sigma_{\ln Y}}\right] = \Phi\left[-\beta\right] \tag{5.2}$$

where the reliability index is given by,

$$\beta = \frac{\mu_{\ln Y}}{\sigma_{\ln Y}} \tag{5.3}$$

and the mean of the lognormal random variable is computed as,

$$\mu_{\ln Y} = \ln\left(\frac{\mu_A \mu_\Delta}{\mu_B^m}\right) - \frac{1}{2}\ln\left[\frac{\left(1+CV_A^2\right)\left(1+CV_\Delta^2\right)}{\left(1+CV_B^2\right)^m}\right] - \ln\Omega - \ln T \tag{5.4}$$

and the standard deviation of the natural logarithm of the performance function is,

$$\sigma_{\ln Y} = \sqrt{\ln\left[\left(1+CV_A^2\right)\left(1+CV_\Delta^2\right)\left(1+CV_B^2\right)\right]} \tag{5.5}$$

Therefore, the reliability-assessment procedure and subsequent definitions of failure as a function of service life are computed using equations (5.1) through (5.5).

The procedure is outlined in the following. It begins by defining a location of a sign support structure and its orientation relative to North. Thus, a latitude and longitude for the mast-arm sign support is defined and the orientation of the mast-arm is defined: N-S, NE-SW, E-W, and SE-NW. The mast-arm orientation defines the angle of the mast-arm relative to the "centroidal axis" of each of the eight cardinal wind directions considered defined as θ_j in equation (5.1) .

A finite element model (composed of one-dimensional finite elements) is then subjected to one-hour averaged wind speed simulations constructed using the Kaimal spectrum as described in chapter four for defined one-hour averaged wind speeds in the following set: 5, 10, 15, 20, 25, 30, 35, 40, 45, and 50 mph. Each of these simulations results in stress histories for critical locations around the perimeter of the mast-arm cross-section. Rainflow counting procedures for each wind speed simulation are used to define expected stress-range magnitudes for that wind speed, $\left(S_{RE}^m\right)_i$, and a number of stress-range cycles for that wind speed in the one-hour averaging window, $n_{cycles/hr,i}$. Equation (5.1) is then used along with the data in Tables 2.18 through 2.24 to compute the stress parameter, Ω, for each one-hour averaged wind speed simulation.

A stress parameter for each wind speed direction generating stress-ranges in the mast-arm sign support is computed. In other words, if the sign support is oriented in the *pure* NE direction, then winds out of the E, SE, and S will cause tensile stress-ranges on one side of the mast arm and winds out of the N, NW, and W

will cause tensile stress-ranges on the opposite side of the mast arm. Both of these scenarios are crucial to defining the fatigue performance of the mast arm and therefore two stress parameters are computed using equation (5.1). The larger magnitude stress parameter is used in equation (5.4) to facilitate computation of the probability of failure (*i.e.* probability that a fatigue-induced crack initiated).

Each of the three detail categories, E2, E3, and E4 has its own unique set of lognormal modeling parameters described earlier. These then allow fatigue performance and probability of failures to be assessed for each type of detail expected in the mast-arm sign support structure. These parameters are then used in equations (5.4) and (5.5) to facilitate computation of the probability of failure for each type of detail.

Uncertainty in accumulated fatigue damage modeling using Miner's rule is included with the single lognormal modeling parameters described earlier and equations (5.4) and (5.5) to allow computation of the probability of fatigue failure.

The assessment procedure is relatively straightforward, but admittedly computationally intensive when one reflects on all the computations and data needed to execute the procedure. The process is applied in the computation of probabilities of failure for specific sign locations, specific sign orientations, three different detail types, and two different types of mast-arm sign support structure. The two types of mast-arm configuration considered are an Osseo (non-tapered, heavy wall thickness, relatively small bluff area) structural system and a Milwaukee (tapered, light wall thickness, relatively large bluff area) structural system. Therefore, the procedure developed in this study allows the expected fatigue performance of sign support structures throughout the state of Wisconsin to be evaluated and studied.

5.3 Mast-Arm Sign Support Service-Life Evaluation

The procedure outlined in section 5.2 allows the probabilities of failure (*i.e.* fatigue-induced cracks to initiate) to be defined for various types of sign support structures, in various orientations, with various detail types, in various locations throughout the state of Wisconsin. The procedure was applied to the following scenarios:

Milwaukee-Type Sign Support (tapered, light wall thickness, relatively large bluff area):

Detail Types: E2, E3, E4 (ranging from square to rectangular four-bolt patterns)
Orientations: N-S, NE-SW, E-W, SE-NW
Locations: Milwaukee, Eau Claire, La Crosse, Green Bay, Madison, Oshkosh, Wisconsin Rapids

Osseo-Type Sign Support (non-tapered, heavy wall thickness, relatively small bluff area):

Detail Types: E2, E3, E4 (ranging from square to rectangular four-bolt patterns)
Orientations: N-S, NE-SW, E-W, SE-NW
Locations: Milwaukee, Eau Claire, La Crosse, Green Bay, Madison, Oshkosh, Wisconsin Rapids

Equations (5.1) through (5.5) allow cumulative distribution functions (CDFs) describing the probabilities of fatigue-crack initiation with service life to be defined. These equations and the procedure described earlier were used to generate these CDFs for the sign support types, detail types, orientations, and cities described. Figures 5.1 through 5.7 illustrate CDFs for Milwaukee-type sign supports in the seven Wisconsin cities considered and Figures 5.8 through 5.14 illustrate the CDFs for Osseo-type sign supports in these same cities.

A very useful way to look at Figures 5.1 through 5.14 is to evaluate expected service life (number of years in service) for a single probability of finding a fatigue-induced crack. Service lives expected for a Milwaukee-type structure in Milwaukee, Wisconsin with three different detail types and four different orientations can be evaluated using Figure 5.1. A 30% probability of finding a fatigue-induced crack can be defined as a threshold for service life expectation. Figure 5.1 illustrates that an E4-type mast-arm connection detail will be expected to have a service life of approximately 1 year with very, very little variability about that one-year life resulting from connection detail behavior and mast-arm orientation. An E3 type detail is expected to have service lives in the range of 5-8 years and this depends, in larger relative extent, to the orientation of the mast-arm relative to North. The E2 detail type is expected to have service life in the range of 20-28 years depending upon orientation. A holistic view of the information in this figure suggests that one should avoid details that are in the E3 and E4 categories in Milwaukee-type mast-arms at this location within the State. The figure also indicates that mast-arms oriented in the N-S direction will have service lives that are expected to be lower than other orientations.

The effects of mast-arm sign support orientation on the expected service life for a specific detail type (*e.g.* E2) can be studied using these CDFs. As an example, consider the E2 detail type and a Milwaukee-type sign support. Figure 5.2 illustrates that E-W and NE-SW sign orientations in Eau Claire will have substantially similar fatigue life performance. Mast-arms oriented N-S and SE-NW will also have substantially similar performance and will have fatigue lives that are shorter than the mast-arms oriented in the previous two directions. Figure 5.3 illustrates the CDF for the Milwaukee-type sign support in La Crosse, WI. Figure 2.6 illustrates the wind-speed-direction histograms for La Crosse, WI. It is clear from Figure 2.6 that winds of greater speeds come from the North and South directions. Figure 5.3 illustrates that the service life for a Milwaukee sign support oriented in the NE-SW direction will have the lowest service life. Mast-arms oriented in the E-W direction will have the longest expected service lives. This is clearly consistent with the wind rose histogram in Figure 2.6. This type of discussion is more difficult to make for other cities because the wind speeds of significant magnitude are more equally distributed throughout all cardinal directions.

The impact of sign support type (*e.g.* Milwaukee versus Osseo) on the expected fatigue life can be evaluated by examining pairs of CDFs from Figures 5.1 through 5.14. Examination of Figure 5.1 and 5.8 illustrates that the Osseo-type sign support structure with E2 and E3 details will have much better

performance than the same sign located in Milwaukee, Wisconsin. This is illustrated by the flatter slopes of the CDFs for these details. It is interesting to note that E4 details exhibit relatively poor service lives irrespective of sign support type. The expected service performance of the Osseo sign in Eau Claire is also better than a Milwaukee sign type in Eau Claire as illustrated in Figures 5.2 and 5.9. This behavior is consistent for all cities within Wisconsin. The reason for this is that the Milwaukee-type sign support structure has a much higher state of stress and stress-range magnitudes resulting from wind loading. The Osseo-type sign has a much greater second moment of area and therefore, the stress-ranges are, relatively speaking, much lower. The most important take away from these figures is that the E4 detail type should be avoided in mast-arm sign support structures. Mast-arm-to-pole connections that have bolt holes in a configuration similar to that in the Osseo sign support (*i.e.* rectangular pattern, horizontal orientation, large bolt spacing relative to tube wall) should be avoided.

One characteristic of the CDFs that provides insight with regard to variability in fatigue life is the slope of the CDF. If the slope of the CDF is steep (*e.g.* the E4 detail category in Figure 5.1 and Figure 5.8), it indicates that a defined service life will have a range of probabilities of failure. These two figures indicate that a service life in the range of 1-3 years for the E4 detail category is expected to have probabilities of finding fatigue-induced cracks ranging from 50-75%. This indicates that fatigue-induced cracks are likely to appear very suddenly in the service of the sign support structure and, in general, should be avoided. The flatter slopes (*i.e.* the E2 and E3 details) indicate that the mast-arm sign support has a better defined probability of failure and greater distinction among different service lives. For the E3 details of Figure 5.8, a service life of 20 years has a probability of fatigue-induced crack initiation of 20%, a service life of 25 years has a probability of failure of approximately 30%, and a service life of 30 years has a probability of failure of 35%. This behavior suggests that this type of CDF would suggest in-service performance conducive to setting inspection intervals of longer duration than the former E4 detail category.

As longer service lives are reached in the sign support structures, the flattening of the CDF indicates that the limiting service life expectation has been reached. The nearly bilinear nature of the E4 detail CDFs irrespective of location suggests that one should not expect service lives for this type of detail longer than five years. In the case of the E2 and E3 detail categories, the service life limit is more difficult to detect because of the flattening of the CDF over longer service life intervals. This suggests that the E2 and E3 details can be expected to have longer service lives, but that inspection intervals will need to gradually shorten as longer lives are encountered.

5.4 Mast-Arm Sign Support Inspection Protocols

The cumulative distribution functions can be used to establish inspection protocols for mast-arm sign support structures for various types, various detail configurations, various locations, and various orientations.

Inspection protocols can be established in the following manner. All probabilities of failure discussed earlier are based upon *time-zero* references. In other words, the probabilities of failure are always referenced to an undamaged, un-cracked state at time-zero in the mast-arm's service life. There is no accounting for finding fatigue-induced cracks at a specific time interval and its impact on the service life thereafter. However, the procedure formulated is very valuable as it allows an un-damaged sign support installed into service at time-zero to have various probabilities of finding fatigue-induced cracks as the driving parameter defining the inspection interval.

The process begins by having the engineer define threshold probabilities for finding fatigue-induced cracks in the mast-arm. These are then threshold probabilities of failure in the current discussion and formulations. Two threshold probabilities are defined in the present study: 20% and 50%. Service lives corresponding to these thresholds can be used to set inspection intervals for mast-arm sign supports. For example, when the probability of finding a fatigue-induced crack is less than 20%, the probability of not finding a crack initiated is 80%. This can be thought of as a lower-threshold that sets the boundary for the first inspection of a mast-arm after installation. The second threshold corresponds to a 50% chance of finding a fatigue-induced crack in the sign support. This, of course, corresponds to a 50% chance of not finding a crack. The 50/50 breakpoint can then be defined as the service life interval when the traditional four-year inspection cycle can begin. The time interval in between first inspection and four-year inspections can be very wide, or can be very narrow depending upon the detail configuration found in the sign support, its orientation, its location, and its type (*i.e.* Milwaukee versus Osseo).

Tables 5.1 through 5.7 include tabulated time-zero probabilities of finding fatigue induced cracks in mast-arm sign supports with Milwaukee configurations as a function of service life, orientation, location, and detail category type. Tables 5.8 through 5.14 include these same probabilities for Osseo configurations. The 20% and 50% thresholds are used to color service life intervals as green, yellow and red. The green regions suggest that inspections not occur until the yellow regions are encountered. The yellow regions suggest that one might tighten the inspection interval somewhat, but that it might not get down to the four-year interval that the red region would suggest.

An example of how inspection intervals would be set for Milwaukee-type and Osseo-type sign supports in Milwaukee, Wisconsin can be explored using Tables 5.1 and 5.8. Table 5.1 indicates the following for a Milwaukee-type sign support, located in Milwaukee, Wisconsin with an E2-type connection detail. The tabulated data indicates that the first inspection for such a mast-arm need not occur for 13 years when the mast-arm is oriented N-S. The first inspection need not occur for 16 years, 18 years, and 14 years for NE-SW, E-W, and SE-NW orientations, respectively. As a result, one could conservatively say that 13 years can be defined as the first inspection for a Milwaukee-type mast-arm sign support put into service in Milwaukee,

Wisconsin. The inspection intervals can then be tightened slightly as the 50% probability of finding a fatigue-induced crack is approached. The 50/50 probability threshold occurs at 40 years, 49 years, greater than 50 years, and 41 years for the N-S, NE-SW, E-W and SE-NW orientations, respectively. During this 27-year period, from 13 years to 40 years, the risk of a crack initiating from fatigue grows from 20% to 50%. If 50% risk of finding a fatigue-induced crack initiating is acceptable, then inspections would not need to take place in this 27-year period. However, if only 20% risk of finding a fatigue-induced crack initiating is acceptable, then the four-year typical inspection interval should be followed. Overall, if acceptable levels of risk can be identified for these structures, inspection intervals can be tailored to those risk levels.

Table 5.1 also indicates that there is a very short yellow region for E3 type details thereby indicating that a lengthening of inspection intervals is likely not appropriate. Furthermore, the green region is very, very short for the E3 detail when compared to E2 detail configurations. The tabulated data suggests that E3 details used in Milwaukee-type sign supports should have their first inspections after five years, should then be inspected after an additional five years and then at four-year intervals after that. Therefore, the E3 detail configuration will require more inspections during the service life when compared to the E2 detail configuration. The tabulated data in Table 5.1 confirms the previous conclusion that E4 detail configurations should be avoided and will require very, very short inspection intervals.

Table 5.8 can be used in a similar manner as Table 5.1. It is interesting to note that if Osseo-type sign supports (*i.e.* non-tapered, heavy wall thickness, relatively small bluff area) are used with E2 detail types, these signs would never require inspection in Milwaukee, Wisconsin. When the detail types migrate to E3, the first inspection can be conducted at 19 years. The yellow regions indicate that inspection intervals can increase to something larger than four-year intervals after that until 43 years of service. After 43 years of service with no cracks present, the sign support should be inspected every four years. This results in a significant reduction in inspections when compared to a 50-year service-life with four-year intervals. The tabulated data also indicates that E4 type details with Osseo-type configuration should be avoided in Milwaukee, Wisconsin as fatigue-induced cracking is expected to occur at very short service lives.

The finite element analysis conducted for the Osseo-type mast-arm connection (Diekfuss 2013) suggests that the Osseo-type mast-arm-to-pole connection tends to behave as an E4 detail type. The reason for this is because the bolt-hole configuration relative to the mast-arm centroidal axis results in stress concentration factors that are consistent with that suggested for the E4 detail types (Diekfuss 2013). The tabulated data contained in Table 5.9 indicates that E4 detail types in Osseo-type sign supports located in Eau Claire, Wisconsin have greater than 50% chance of having fatigue-induced cracks after three years of service. The Osseo sign support found with fatigue-induced cracks discussed in chapter one was in service for approximately eight years and the reliability-based procedure formulated provides clear indication that this

type of sign support would suffer from very, very poor in-service performance. This helps to confirm the ability of the procedure formulated in setting inspection protocols and identifying configurations, locations, and orientations with potential for poor in-service performance.

A summary of the data in Tables 5.1 through 5.14 is given in Table 5.15. This table allows one to gain a feel for how the inspection thresholds described earlier (*i.e.* 20% chance of finding a crack and 50% chance of finding a crack) maps onto all locations throughout the state of Wisconsin for all detail types and all mast-arm configurations. The summary data confirms that E4 details should be avoided throughout the state of Wisconsin. While E3 details do not perform as well as E2 details, they can be used, but they will likely need relatively short first inspection intervals when compared to E2 detail types. The data also suggests that if an Osseo-type configuration can be implemented with E2 detail categories, 50-year service lives should be expected and inspections of these types of sign supports may never need to occur with this service life expectation. In the case of Milwaukee-type mast-arm configurations with E2 detail types, first inspection intervals range from 13-36 years depending upon location with Milwaukee, Wisconsin experiencing the shortest interval. The service life interval to four-year inspection intervals for the E2 detail type ranges from 40 years to greater than 50 years with Milwaukee, Wisconsin again requiring the shortest interval.

5.5 Concluding Remarks

A reliability-based assessment procedure was outlined in the present chapter. The process formulated was applied to compute probabilities of finding fatigue-induced cracks initiating with variation in service life. Cumulative distribution functions describing these failure probabilities were presented for two different mast-arm structure configurations (Milwaukee-type and Osseo-type), with the potential for three different detail categories (E2, E3, E4), located in seven different cities throughout Wisconsin (Milwaukee, Eau Claire, La Crosse, Green Bay, Madison, Oshkosh, Wisconsin Rapids), and four orientations relative to North (N-S, NE-SW, E-W, NW-SE). These cumulative distribution functions were then displayed in tabulated format to define service life intervals and inspection protocols for mast-arm sign supports.

The reliability-based assessment process developed and implemented in this study suggests that E4 detail types be avoided in mast-arm sign support structures. The orientation of the bolt holes relative to the centroidal axis of the mast-arm as seen in the Osseo-type mast-arm-to-pole connection results in significant stress concentration factors that approach this detail category. As a result, mast-arm-to-pole connection details that are like the Osseo sign support structure studied in this research effort should be avoided as well. Milwaukee-type connection details are preferable and approach E2 type behavior.

The reliability-based assessment conducted suggests that E2 detail types used in Osseo-type mast-arm configurations are ideal and may never need inspections during their service life. In other words, the

Milwaukee-type connection detail is preferable with larger second moments of area used in the mast-arm as seen in the Osseo sign support. The assessment also suggests that Milwaukee-type mast-arm support structures with E2 detail types can have significantly reduced inspections from the regular four-year interval currently used. It is recommended that the first inspection interval for these types of mast-arms with E2 connection types be as short as 13 years and as long as 36 years depending upon location. Sign supports located in Milwaukee should have their first inspection interval set at shorter duration than elsewhere within the State. The time to four-year inspection intervals for these sign types and details can then be after 40 years of service life in Milwaukee and longer elsewhere within the State.

5.6 References

AASHTO (2009). *Standard Specifications for Structural Supports for Highway Signs, Luminaires and Traffic Signals, 5th Edition with 2010 Interim Revisions,* American Association of State Highway and Transportation Officials, Washington, D.C.

Diekfuss, J. A. (2013). "Reliability-Based Fatigue Assessment of Mast-Arm Sign Support Structures."PhD Thesis, Marquette University, Milwaukee, WI.

Wirsching, P. H. (1984). "Fatigue Reliability for Offshore Structures." *Journal of Structural Engineering*, 110(10), 2340-2356.

Table 5.1 Variation in Time-Zero Probability of Fatigue-Crack Initiation with Service Life Interval for Milwaukee-Style Mast-Arm Sign Supports in Milwaukee, Wisconsin.

Location: Milwaukee							Latitude: 42.9550°					
							Longitude: -87.9044°					
Number of Years in Service	Orientation of Sign: N-S			Orientation of Sign: NE-SW			Orientation of Sign: E-W			Orientation of Sign: SE-NW		
	Probability of Failure			Probability of Failure			Probability of Failure			Probability of Failure		
	E2	E3	E4	E2	E3	E4	E2	E3	E4	E2	E3	E4
0	0.000	0.000	0.000	0.000	0.000	0.000	0.000	0.000	0.000	0.000	0.000	0.000
1	0.003	0.010	0.724	0.002	0.007	0.676	0.001	0.005	0.620	0.003	0.008	0.694
2	0.012	0.053	0.921	0.008	0.038	0.898	0.007	0.030	0.869	0.012	0.046	0.907
3	0.026	0.114	0.970	0.018	0.087	0.960	0.015	0.071	0.945	0.025	0.103	0.964
4	0.043	0.182	0.987	0.030	0.143	0.981	0.026	0.120	0.974	0.040	0.165	0.984
5	0.060	0.248	0.994	0.044	0.201	0.991	0.037	0.172	0.986	0.057	0.228	0.992
6	0.079	0.310	0.997	0.058	0.257	0.995	0.050	0.224	0.992	0.075	0.288	0.996
7	0.097	0.368	0.998	0.073	0.311	0.997	0.063	0.274	0.995	0.093	0.344	0.997
8	0.116	0.421	0.999	0.088	0.360	0.998	0.077	0.321	0.997	0.111	0.396	0.998
9	0.134	0.468	0.999	0.103	0.406	0.999	0.090	0.366	0.998	0.128	0.443	0.999
10	0.152	0.511	1.000	0.118	0.449	0.999	0.104	0.407	0.999	0.146	0.485	0.999
11	0.169	0.550	1.000	0.133	0.487	0.999	0.118	0.445	0.999	0.163	0.524	1.000
12	0.187	0.585	1.000	0.147	0.523	1.000	0.131	0.480	0.999	0.180	0.559	1.000
13	0.203	0.616	1.000	0.162	0.555	1.000	0.144	0.513	1.000	0.196	0.592	1.000
14	0.219	0.645	1.000	0.176	0.585	1.000	0.157	0.543	1.000	0.212	0.621	1.000
15	0.235	0.671	1.000	0.189	0.612	1.000	0.170	0.571	1.000	0.227	0.647	1.000
16	0.250	0.694	1.000	0.203	0.637	1.000	0.183	0.597	1.000	0.242	0.671	1.000
17	0.265	0.716	1.000	0.216	0.660	1.000	0.195	0.620	1.000	0.257	0.693	1.000
18	0.279	0.735	1.000	0.229	0.681	1.000	0.207	0.642	1.000	0.271	0.714	1.000
19	0.293	0.753	1.000	0.242	0.701	1.000	0.219	0.663	1.000	0.284	0.732	1.000
20	0.307	0.769	1.000	0.254	0.719	1.000	0.231	0.682	1.000	0.298	0.749	1.000
21	0.320	0.784	1.000	0.266	0.735	1.000	0.242	0.699	1.000	0.310	0.765	1.000
22	0.332	0.798	1.000	0.277	0.751	1.000	0.253	0.716	1.000	0.323	0.779	1.000
23	0.345	0.810	1.000	0.289	0.765	1.000	0.264	0.731	1.000	0.335	0.792	1.000
24	0.357	0.822	1.000	0.300	0.778	1.000	0.275	0.745	1.000	0.347	0.805	1.000
25	0.368	0.833	1.000	0.311	0.790	1.000	0.285	0.758	1.000	0.358	0.816	1.000
26	0.379	0.842	1.000	0.321	0.802	1.000	0.295	0.771	1.000	0.369	0.826	1.000
27	0.390	0.852	1.000	0.331	0.812	1.000	0.305	0.782	1.000	0.380	0.836	1.000
28	0.401	0.860	1.000	0.341	0.822	1.000	0.315	0.793	1.000	0.391	0.845	1.000
29	0.411	0.868	1.000	0.351	0.831	1.000	0.324	0.803	1.000	0.401	0.853	1.000
30	0.421	0.875	1.000	0.361	0.840	1.000	0.334	0.812	1.000	0.411	0.861	1.000
31	0.431	0.882	1.000	0.370	0.848	1.000	0.343	0.821	1.000	0.420	0.869	1.000
32	0.440	0.888	1.000	0.379	0.855	1.000	0.352	0.830	1.000	0.430	0.875	1.000
33	0.449	0.894	1.000	0.388	0.862	1.000	0.360	0.838	1.000	0.439	0.882	1.000
34	0.458	0.899	1.000	0.397	0.869	1.000	0.369	0.845	1.000	0.448	0.888	1.000
35	0.467	0.905	1.000	0.405	0.875	1.000	0.377	0.852	1.000	0.457	0.893	1.000
36	0.475	0.909	1.000	0.413	0.881	1.000	0.385	0.858	1.000	0.465	0.898	1.000
37	0.484	0.914	1.000	0.421	0.886	1.000	0.393	0.865	1.000	0.473	0.903	1.000
38	0.492	0.918	1.000	0.429	0.892	1.000	0.401	0.870	1.000	0.481	0.908	1.000
39	0.499	0.922	1.000	0.437	0.896	1.000	0.408	0.876	1.000	0.489	0.912	1.000
40	0.507	0.926	1.000	0.444	0.901	1.000	0.416	0.881	1.000	0.497	0.916	1.000
41	0.515	0.929	1.000	0.452	0.905	1.000	0.423	0.886	1.000	0.504	0.920	1.000
42	0.522	0.932	1.000	0.459	0.909	1.000	0.430	0.891	1.000	0.511	0.924	1.000
43	0.529	0.936	1.000	0.466	0.913	1.000	0.437	0.895	1.000	0.518	0.927	1.000
44	0.536	0.938	1.000	0.473	0.917	1.000	0.444	0.899	1.000	0.525	0.930	1.000
45	0.542	0.941	1.000	0.480	0.920	1.000	0.451	0.903	1.000	0.532	0.933	1.000
46	0.549	0.944	1.000	0.486	0.924	1.000	0.457	0.907	1.000	0.539	0.936	1.000
47	0.555	0.946	1.000	0.493	0.927	1.000	0.464	0.911	1.000	0.545	0.939	1.000
48	0.562	0.949	1.000	0.499	0.930	1.000	0.470	0.914	1.000	0.551	0.941	1.000
49	0.568	0.951	1.000	0.505	0.933	1.000	0.476	0.917	1.000	0.558	0.944	1.000
50	0.574	0.953	1.000	0.511	0.935	1.000	0.482	0.921	1.000	0.564	0.946	1.000

Table 5.2 Variation in Time-Zero Probability of Fatigue-Crack Initiation with Service Life Interval for Milwaukee-Style Mast-Arm Sign Supports in Eau Claire, Wisconsin.

Location: Eau Claire							Latitude: 44.8664°					
							Longitude: -91.4878°					
Number of Years in Service	Orientation of Sign: N-S			Orientation of Sign: NE-SW			Orientation of Sign: E-W			Orientation of Sign: SE-NW		
	Probability of Failure			Probability of Failure			Probability of Failure			Probability of Failure		
	E2	E3	E4	E2	E3	E4	E2	E3	E4	E2	E3	E4
0	0.000	0.000	0.000	0.000	0.000	0.000	0.000	0.000	0.000	0.000	0.000	0.000
1	0.000	0.001	0.506	0.000	0.001	0.450	0.000	0.001	0.474	0.000	0.001	0.531
2	0.002	0.010	0.797	0.001	0.006	0.755	0.001	0.006	0.773	0.002	0.010	0.814
3	0.006	0.028	0.904	0.004	0.018	0.878	0.003	0.017	0.890	0.006	0.029	0.915
4	0.010	0.053	0.950	0.007	0.035	0.934	0.005	0.033	0.941	0.010	0.054	0.956
5	0.016	0.083	0.972	0.010	0.057	0.961	0.009	0.054	0.966	0.016	0.084	0.976
6	0.023	0.115	0.983	0.015	0.082	0.976	0.013	0.078	0.979	0.022	0.117	0.985
7	0.030	0.148	0.989	0.020	0.108	0.985	0.017	0.104	0.987	0.029	0.151	0.991
8	0.037	0.182	0.993	0.025	0.136	0.990	0.022	0.131	0.991	0.036	0.185	0.994
9	0.045	0.216	0.995	0.031	0.164	0.993	0.027	0.158	0.994	0.043	0.219	0.996
10	0.053	0.249	0.997	0.037	0.192	0.995	0.032	0.185	0.996	0.051	0.252	0.997
11	0.061	0.280	0.998	0.043	0.220	0.996	0.038	0.212	0.997	0.059	0.284	0.998
12	0.069	0.311	0.998	0.050	0.247	0.997	0.043	0.239	0.998	0.067	0.314	0.999
13	0.078	0.341	0.999	0.056	0.273	0.998	0.049	0.265	0.998	0.076	0.344	0.999
14	0.086	0.369	0.999	0.063	0.299	0.999	0.055	0.291	0.999	0.084	0.372	0.999
15	0.095	0.396	0.999	0.069	0.324	0.999	0.061	0.315	0.999	0.092	0.399	0.999
16	0.103	0.421	0.999	0.076	0.348	0.999	0.067	0.339	0.999	0.101	0.425	1.000
17	0.112	0.446	1.000	0.083	0.371	0.999	0.073	0.362	0.999	0.109	0.449	1.000
18	0.120	0.469	1.000	0.090	0.393	0.999	0.079	0.384	1.000	0.117	0.473	1.000
19	0.128	0.491	1.000	0.096	0.415	1.000	0.086	0.405	1.000	0.125	0.495	1.000
20	0.137	0.512	1.000	0.103	0.435	1.000	0.092	0.426	1.000	0.133	0.516	1.000
21	0.145	0.532	1.000	0.110	0.455	1.000	0.098	0.445	1.000	0.142	0.535	1.000
22	0.153	0.550	1.000	0.117	0.474	1.000	0.104	0.464	1.000	0.150	0.554	1.000
23	0.161	0.568	1.000	0.123	0.492	1.000	0.111	0.482	1.000	0.158	0.572	1.000
24	0.169	0.585	1.000	0.130	0.509	1.000	0.117	0.500	1.000	0.165	0.589	1.000
25	0.177	0.602	1.000	0.137	0.526	1.000	0.123	0.516	1.000	0.173	0.605	1.000
26	0.185	0.617	1.000	0.143	0.542	1.000	0.129	0.532	1.000	0.181	0.621	1.000
27	0.193	0.632	1.000	0.150	0.557	1.000	0.135	0.548	1.000	0.188	0.635	1.000
28	0.200	0.646	1.000	0.156	0.572	1.000	0.141	0.562	1.000	0.196	0.649	1.000
29	0.208	0.659	1.000	0.163	0.586	1.000	0.147	0.576	1.000	0.203	0.662	1.000
30	0.215	0.671	1.000	0.169	0.599	1.000	0.153	0.590	1.000	0.211	0.675	1.000
31	0.222	0.683	1.000	0.175	0.612	1.000	0.159	0.603	1.000	0.218	0.687	1.000
32	0.230	0.695	1.000	0.182	0.625	1.000	0.165	0.615	1.000	0.225	0.698	1.000
33	0.237	0.706	1.000	0.188	0.636	1.000	0.171	0.627	1.000	0.232	0.709	1.000
34	0.244	0.716	1.000	0.194	0.648	1.000	0.177	0.639	1.000	0.239	0.719	1.000
35	0.251	0.726	1.000	0.200	0.659	1.000	0.182	0.650	1.000	0.246	0.729	1.000
36	0.257	0.736	1.000	0.206	0.669	1.000	0.188	0.660	1.000	0.252	0.739	1.000
37	0.264	0.745	1.000	0.212	0.679	1.000	0.194	0.671	1.000	0.259	0.748	1.000
38	0.271	0.753	1.000	0.218	0.689	1.000	0.199	0.680	1.000	0.266	0.756	1.000
39	0.277	0.762	1.000	0.224	0.698	1.000	0.205	0.690	1.000	0.272	0.765	1.000
40	0.284	0.770	1.000	0.230	0.707	1.000	0.210	0.699	1.000	0.279	0.773	1.000
41	0.290	0.777	1.000	0.235	0.716	1.000	0.216	0.708	1.000	0.285	0.780	1.000
42	0.296	0.785	1.000	0.241	0.724	1.000	0.221	0.716	1.000	0.291	0.787	1.000
43	0.302	0.792	1.000	0.246	0.732	1.000	0.226	0.724	1.000	0.297	0.794	1.000
44	0.309	0.798	1.000	0.252	0.740	1.000	0.231	0.732	1.000	0.303	0.801	1.000
45	0.315	0.805	1.000	0.257	0.747	1.000	0.237	0.739	1.000	0.309	0.807	1.000
46	0.320	0.811	1.000	0.263	0.754	1.000	0.242	0.747	1.000	0.315	0.813	1.000
47	0.326	0.817	1.000	0.268	0.761	1.000	0.247	0.754	1.000	0.321	0.819	1.000
48	0.332	0.822	1.000	0.273	0.768	1.000	0.252	0.760	1.000	0.326	0.825	1.000
49	0.338	0.828	1.000	0.279	0.774	1.000	0.257	0.767	1.000	0.332	0.830	1.000
50	0.343	0.833	1.000	0.284	0.780	1.000	0.262	0.773	1.000	0.338	0.835	1.000

Table 5.3 Variation in Time-Zero Probability of Fatigue-Crack Initiation with Service Life Interval for Milwaukee-Style Mast-Arm Supports in La Crosse, Wisconsin.

Location: La Crosse							Latitude: 43.8788°					
							Longitude: -91.2527°					
Number of Years in Service	Orientation of Sign: N-S			Orientation of Sign: NE-SW			Orientation of Sign: E-W			Orientation of Sign: SE-NW		
	Probability of Failure			Probability of Failure			Probability of Failure			Probability of Failure		
	E2	E3	E4	E2	E3	E4	E2	E3	E4	E2	E3	E4
0	0.000	0.000	0.000	0.000	0.000	0.000	0.000	0.000	0.000	0.000	0.000	0.000
1	0.001	0.002	0.506	0.001	0.004	0.614	0.000	0.001	0.581	0.000	0.002	0.528
2	0.005	0.018	0.797	0.006	0.027	0.865	0.002	0.011	0.846	0.003	0.012	0.812
3	0.011	0.046	0.904	0.014	0.064	0.943	0.006	0.029	0.933	0.007	0.033	0.913
4	0.019	0.082	0.950	0.023	0.110	0.973	0.011	0.055	0.967	0.012	0.062	0.955
5	0.028	0.122	0.972	0.034	0.160	0.985	0.017	0.086	0.982	0.018	0.095	0.975
6	0.038	0.164	0.983	0.046	0.209	0.992	0.023	0.119	0.990	0.026	0.131	0.985
7	0.049	0.206	0.989	0.059	0.257	0.995	0.030	0.153	0.994	0.033	0.167	0.991
8	0.060	0.247	0.993	0.072	0.303	0.997	0.038	0.188	0.996	0.042	0.203	0.994
9	0.071	0.286	0.995	0.084	0.346	0.998	0.046	0.222	0.997	0.050	0.239	0.996
10	0.083	0.324	0.997	0.097	0.387	0.999	0.054	0.255	0.998	0.059	0.274	0.997
11	0.094	0.360	0.998	0.110	0.424	0.999	0.063	0.288	0.999	0.068	0.307	0.998
12	0.106	0.393	0.998	0.123	0.460	0.999	0.071	0.319	0.999	0.077	0.339	0.999
13	0.117	0.425	0.999	0.136	0.492	1.000	0.080	0.348	0.999	0.086	0.369	0.999
14	0.128	0.455	0.999	0.149	0.522	1.000	0.088	0.377	1.000	0.095	0.398	0.999
15	0.140	0.483	0.999	0.161	0.550	1.000	0.097	0.404	1.000	0.104	0.426	0.999
16	0.151	0.509	0.999	0.173	0.576	1.000	0.105	0.430	1.000	0.113	0.452	1.000
17	0.162	0.534	1.000	0.185	0.600	1.000	0.114	0.454	1.000	0.122	0.476	1.000
18	0.172	0.557	1.000	0.197	0.623	1.000	0.123	0.477	1.000	0.131	0.500	1.000
19	0.183	0.579	1.000	0.208	0.644	1.000	0.131	0.499	1.000	0.140	0.522	1.000
20	0.193	0.599	1.000	0.220	0.663	1.000	0.139	0.520	1.000	0.149	0.542	1.000
21	0.204	0.618	1.000	0.231	0.681	1.000	0.148	0.540	1.000	0.158	0.562	1.000
22	0.214	0.636	1.000	0.242	0.698	1.000	0.156	0.559	1.000	0.166	0.581	1.000
23	0.224	0.653	1.000	0.252	0.713	1.000	0.164	0.577	1.000	0.175	0.599	1.000
24	0.233	0.669	1.000	0.263	0.728	1.000	0.172	0.594	1.000	0.183	0.615	1.000
25	0.243	0.684	1.000	0.273	0.742	1.000	0.180	0.610	1.000	0.192	0.631	1.000
26	0.252	0.698	1.000	0.283	0.755	1.000	0.188	0.625	1.000	0.200	0.646	1.000
27	0.262	0.712	1.000	0.292	0.766	1.000	0.196	0.640	1.000	0.208	0.660	1.000
28	0.271	0.724	1.000	0.302	0.778	1.000	0.204	0.653	1.000	0.216	0.674	1.000
29	0.279	0.736	1.000	0.311	0.788	1.000	0.211	0.666	1.000	0.224	0.687	1.000
30	0.288	0.747	1.000	0.320	0.798	1.000	0.219	0.679	1.000	0.231	0.699	1.000
31	0.297	0.758	1.000	0.329	0.807	1.000	0.226	0.691	1.000	0.239	0.710	1.000
32	0.305	0.768	1.000	0.338	0.816	1.000	0.233	0.702	1.000	0.246	0.721	1.000
33	0.313	0.777	1.000	0.346	0.824	1.000	0.240	0.713	1.000	0.254	0.732	1.000
34	0.321	0.786	1.000	0.355	0.832	1.000	0.247	0.723	1.000	0.261	0.742	1.000
35	0.329	0.795	1.000	0.363	0.840	1.000	0.254	0.733	1.000	0.268	0.751	1.000
36	0.337	0.803	1.000	0.371	0.846	1.000	0.261	0.743	1.000	0.275	0.760	1.000
37	0.344	0.811	1.000	0.379	0.853	1.000	0.268	0.752	1.000	0.282	0.769	1.000
38	0.352	0.818	1.000	0.386	0.859	1.000	0.275	0.760	1.000	0.289	0.777	1.000
39	0.359	0.825	1.000	0.394	0.865	1.000	0.281	0.768	1.000	0.296	0.785	1.000
40	0.366	0.831	1.000	0.401	0.871	1.000	0.288	0.776	1.000	0.302	0.793	1.000
41	0.373	0.838	1.000	0.408	0.876	1.000	0.294	0.784	1.000	0.309	0.800	1.000
42	0.380	0.844	1.000	0.415	0.881	1.000	0.300	0.791	1.000	0.315	0.807	1.000
43	0.387	0.849	1.000	0.422	0.886	1.000	0.307	0.798	1.000	0.322	0.813	1.000
44	0.393	0.855	1.000	0.429	0.890	1.000	0.313	0.804	1.000	0.328	0.819	1.000
45	0.400	0.860	1.000	0.436	0.894	1.000	0.319	0.810	1.000	0.334	0.825	1.000
46	0.406	0.865	1.000	0.442	0.898	1.000	0.325	0.816	1.000	0.340	0.831	1.000
47	0.413	0.870	1.000	0.449	0.902	1.000	0.331	0.822	1.000	0.346	0.836	1.000
48	0.419	0.874	1.000	0.455	0.906	1.000	0.336	0.828	1.000	0.352	0.842	1.000
49	0.425	0.878	1.000	0.461	0.909	1.000	0.342	0.833	1.000	0.358	0.847	1.000
50	0.431	0.883	1.000	0.467	0.913	1.000	0.348	0.838	1.000	0.364	0.852	1.000

Table 5.4 Variation in Time-Zero Probability of Fatigue-Crack Initiation with Service Life Interval for Milwaukee-Style Mast-Arm Supports in Green Bay, Wisconsin.

Location: Green Bay							Latitude: 44.4794°					
							Longitude: -88.1366°					
Number of Years in Service	Orientation of Sign: N-S			Orientation of Sign: NE-SW			Orientation of Sign: E-W			Orientation of Sign: SE-NW		
	Probability of Failure			Probability of Failure			Probability of Failure			Probability of Failure		
	E2	E3	E4	E2	E3	E4	E2	E3	E4	E2	E3	E4
0	0.000	0.000	0.000	0.000	0.000	0.000	0.000	0.000	0.000	0.000	0.000	0.000
1	0.002	0.005	0.636	0.002	0.005	0.605	0.002	0.004	0.570	0.001	0.003	0.619
2	0.008	0.032	0.878	0.008	0.029	0.860	0.008	0.028	0.839	0.006	0.023	0.868
3	0.018	0.076	0.949	0.017	0.070	0.940	0.017	0.067	0.929	0.015	0.057	0.944
4	0.031	0.127	0.976	0.029	0.119	0.971	0.028	0.114	0.964	0.025	0.099	0.973
5	0.044	0.181	0.987	0.042	0.170	0.984	0.041	0.164	0.981	0.037	0.145	0.986
6	0.059	0.234	0.993	0.055	0.221	0.991	0.055	0.214	0.989	0.049	0.191	0.992
7	0.073	0.285	0.996	0.070	0.271	0.995	0.069	0.263	0.993	0.062	0.237	0.995
8	0.089	0.333	0.997	0.084	0.318	0.997	0.083	0.309	0.996	0.075	0.281	0.997
9	0.104	0.378	0.998	0.099	0.362	0.998	0.098	0.353	0.997	0.089	0.323	0.998
10	0.119	0.420	0.999	0.113	0.403	0.999	0.112	0.394	0.998	0.102	0.363	0.999
11	0.134	0.458	0.999	0.128	0.441	0.999	0.126	0.432	0.999	0.115	0.400	0.999
12	0.148	0.493	0.999	0.142	0.476	0.999	0.141	0.467	0.999	0.129	0.434	0.999
13	0.163	0.526	1.000	0.156	0.509	0.999	0.154	0.499	0.999	0.142	0.467	1.000
14	0.177	0.556	1.000	0.170	0.539	1.000	0.168	0.530	0.999	0.155	0.497	1.000
15	0.191	0.584	1.000	0.183	0.567	1.000	0.182	0.557	1.000	0.168	0.525	1.000
16	0.204	0.609	1.000	0.197	0.593	1.000	0.195	0.583	1.000	0.180	0.551	1.000
17	0.217	0.633	1.000	0.209	0.617	1.000	0.207	0.607	1.000	0.192	0.576	1.000
18	0.230	0.655	1.000	0.222	0.639	1.000	0.220	0.630	1.000	0.204	0.598	1.000
19	0.243	0.675	1.000	0.234	0.659	1.000	0.232	0.650	1.000	0.216	0.620	1.000
20	0.255	0.693	1.000	0.246	0.678	1.000	0.244	0.670	1.000	0.228	0.639	1.000
21	0.267	0.711	1.000	0.258	0.696	1.000	0.256	0.687	1.000	0.239	0.658	1.000
22	0.279	0.727	1.000	0.270	0.712	1.000	0.267	0.704	1.000	0.250	0.675	1.000
23	0.290	0.742	1.000	0.281	0.728	1.000	0.279	0.720	1.000	0.261	0.691	1.000
24	0.301	0.756	1.000	0.292	0.742	1.000	0.289	0.734	1.000	0.271	0.707	1.000
25	0.312	0.768	1.000	0.302	0.755	1.000	0.300	0.748	1.000	0.281	0.721	1.000
26	0.323	0.781	1.000	0.313	0.768	1.000	0.310	0.760	1.000	0.292	0.734	1.000
27	0.333	0.792	1.000	0.323	0.779	1.000	0.321	0.772	1.000	0.301	0.747	1.000
28	0.343	0.802	1.000	0.333	0.790	1.000	0.330	0.783	1.000	0.311	0.758	1.000
29	0.353	0.812	1.000	0.343	0.800	1.000	0.340	0.793	1.000	0.320	0.769	1.000
30	0.362	0.821	1.000	0.352	0.810	1.000	0.350	0.803	1.000	0.330	0.780	1.000
31	0.372	0.830	1.000	0.361	0.819	1.000	0.359	0.812	1.000	0.339	0.790	1.000
32	0.381	0.838	1.000	0.370	0.827	1.000	0.368	0.821	1.000	0.347	0.799	1.000
33	0.389	0.846	1.000	0.379	0.835	1.000	0.376	0.829	1.000	0.356	0.808	1.000
34	0.398	0.853	1.000	0.388	0.843	1.000	0.385	0.837	1.000	0.364	0.816	1.000
35	0.407	0.859	1.000	0.396	0.850	1.000	0.393	0.844	1.000	0.373	0.824	1.000
36	0.415	0.866	1.000	0.404	0.856	1.000	0.402	0.851	1.000	0.381	0.831	1.000
37	0.423	0.872	1.000	0.412	0.863	1.000	0.410	0.857	1.000	0.389	0.838	1.000
38	0.431	0.877	1.000	0.420	0.868	1.000	0.417	0.863	1.000	0.396	0.844	1.000
39	0.439	0.883	1.000	0.428	0.874	1.000	0.425	0.869	1.000	0.404	0.851	1.000
40	0.446	0.888	1.000	0.435	0.879	1.000	0.433	0.874	1.000	0.411	0.857	1.000
41	0.453	0.892	1.000	0.443	0.884	1.000	0.440	0.879	1.000	0.419	0.862	1.000
42	0.461	0.897	1.000	0.450	0.889	1.000	0.447	0.884	1.000	0.426	0.868	1.000
43	0.468	0.901	1.000	0.457	0.894	1.000	0.454	0.889	1.000	0.433	0.873	1.000
44	0.475	0.905	1.000	0.464	0.898	1.000	0.461	0.893	1.000	0.440	0.878	1.000
45	0.481	0.909	1.000	0.471	0.902	1.000	0.468	0.898	1.000	0.446	0.882	1.000
46	0.488	0.913	1.000	0.477	0.906	1.000	0.474	0.901	1.000	0.453	0.887	1.000
47	0.494	0.916	1.000	0.484	0.909	1.000	0.481	0.905	1.000	0.459	0.891	1.000
48	0.501	0.919	1.000	0.490	0.913	1.000	0.487	0.909	1.000	0.466	0.895	1.000
49	0.507	0.922	1.000	0.496	0.916	1.000	0.493	0.912	1.000	0.472	0.898	1.000
50	0.513	0.925	1.000	0.502	0.919	1.000	0.499	0.915	1.000	0.478	0.902	1.000

Table 5.5 Variation in Time-Zero Probability of Fatigue-Crack Initiation with Service Life Interval for Milwaukee-Style Mast-Arm Supports in Madison, Wisconsin.

Location: Madison							Latitude: 43.1405°					
							Longitude: -89.3452°					
Number of Years in Service	Orientation of Sign: N-S			Orientation of Sign: NE-SW			Orientation of Sign: E-W			Orientation of Sign: SE-NW		
	Probability of Failure			Probability of Failure			Probability of Failure			Probability of Failure		
	E2	E3	E4	E2	E3	E4	E2	E3	E4	E2	E3	E4
0	0.000	0.000	0.000	0.000	0.000	0.000	0.000	0.000	0.000	0.000	0.000	0.000
1	0.000	0.000	0.289	0.000	0.000	0.427	0.000	0.000	0.473	0.000	0.000	0.414
2	0.001	0.003	0.602	0.001	0.005	0.736	0.001	0.005	0.773	0.001	0.005	0.725
3	0.002	0.008	0.769	0.003	0.015	0.866	0.003	0.015	0.889	0.003	0.015	0.859
4	0.004	0.018	0.858	0.005	0.030	0.926	0.006	0.030	0.941	0.006	0.030	0.921
5	0.006	0.031	0.909	0.008	0.049	0.956	0.009	0.049	0.966	0.010	0.049	0.953
6	0.009	0.047	0.939	0.011	0.071	0.973	0.013	0.071	0.979	0.014	0.071	0.970
7	0.012	0.064	0.958	0.015	0.095	0.982	0.017	0.095	0.987	0.019	0.095	0.981
8	0.015	0.083	0.970	0.020	0.120	0.988	0.022	0.120	0.991	0.024	0.120	0.987
9	0.019	0.103	0.979	0.024	0.146	0.992	0.027	0.146	0.994	0.030	0.146	0.991
10	0.023	0.124	0.984	0.029	0.172	0.994	0.032	0.172	0.996	0.036	0.172	0.994
11	0.027	0.145	0.988	0.035	0.198	0.996	0.038	0.198	0.997	0.042	0.198	0.995
12	0.032	0.166	0.991	0.040	0.224	0.997	0.043	0.223	0.998	0.048	0.224	0.997
13	0.036	0.187	0.993	0.045	0.249	0.998	0.049	0.249	0.998	0.054	0.249	0.997
14	0.041	0.208	0.995	0.051	0.273	0.998	0.055	0.273	0.999	0.061	0.273	0.998
15	0.046	0.229	0.996	0.057	0.297	0.999	0.061	0.297	0.999	0.067	0.297	0.998
16	0.051	0.249	0.997	0.062	0.321	0.999	0.067	0.320	0.999	0.074	0.321	0.999
17	0.056	0.270	0.997	0.068	0.343	0.999	0.073	0.343	0.999	0.080	0.343	0.999
18	0.061	0.289	0.998	0.074	0.365	0.999	0.080	0.364	1.000	0.087	0.365	0.999
19	0.066	0.308	0.998	0.080	0.386	0.999	0.086	0.385	1.000	0.094	0.386	0.999
20	0.071	0.327	0.998	0.086	0.406	1.000	0.092	0.406	1.000	0.100	0.406	1.000
21	0.076	0.345	0.999	0.092	0.425	1.000	0.098	0.425	1.000	0.107	0.425	1.000
22	0.081	0.363	0.999	0.098	0.444	1.000	0.105	0.444	1.000	0.114	0.444	1.000
23	0.086	0.380	0.999	0.104	0.462	1.000	0.111	0.462	1.000	0.120	0.462	1.000
24	0.092	0.397	0.999	0.110	0.479	1.000	0.117	0.479	1.000	0.127	0.480	1.000
25	0.097	0.413	0.999	0.115	0.496	1.000	0.123	0.496	1.000	0.133	0.496	1.000
26	0.102	0.429	0.999	0.121	0.512	1.000	0.129	0.512	1.000	0.140	0.512	1.000
27	0.107	0.444	1.000	0.127	0.527	1.000	0.135	0.527	1.000	0.146	0.528	1.000
28	0.112	0.459	1.000	0.133	0.542	1.000	0.141	0.542	1.000	0.153	0.542	1.000
29	0.117	0.473	1.000	0.139	0.556	1.000	0.147	0.556	1.000	0.159	0.556	1.000
30	0.123	0.487	1.000	0.144	0.570	1.000	0.153	0.570	1.000	0.165	0.570	1.000
31	0.128	0.500	1.000	0.150	0.583	1.000	0.159	0.583	1.000	0.171	0.583	1.000
32	0.133	0.513	1.000	0.156	0.596	1.000	0.165	0.595	1.000	0.178	0.596	1.000
33	0.138	0.525	1.000	0.161	0.608	1.000	0.171	0.608	1.000	0.184	0.608	1.000
34	0.143	0.538	1.000	0.167	0.620	1.000	0.177	0.619	1.000	0.190	0.620	1.000
35	0.148	0.549	1.000	0.172	0.631	1.000	0.182	0.630	1.000	0.196	0.631	1.000
36	0.153	0.561	1.000	0.178	0.642	1.000	0.188	0.641	1.000	0.202	0.642	1.000
37	0.158	0.572	1.000	0.183	0.652	1.000	0.194	0.652	1.000	0.208	0.652	1.000
38	0.163	0.582	1.000	0.189	0.662	1.000	0.199	0.662	1.000	0.213	0.662	1.000
39	0.167	0.593	1.000	0.194	0.672	1.000	0.205	0.671	1.000	0.219	0.672	1.000
40	0.172	0.603	1.000	0.199	0.681	1.000	0.210	0.681	1.000	0.225	0.681	1.000
41	0.177	0.612	1.000	0.205	0.690	1.000	0.216	0.690	1.000	0.230	0.690	1.000
42	0.182	0.622	1.000	0.210	0.699	1.000	0.221	0.698	1.000	0.236	0.699	1.000
43	0.186	0.631	1.000	0.215	0.707	1.000	0.226	0.707	1.000	0.241	0.707	1.000
44	0.191	0.640	1.000	0.220	0.715	1.000	0.232	0.715	1.000	0.247	0.715	1.000
45	0.196	0.648	1.000	0.225	0.723	1.000	0.237	0.722	1.000	0.252	0.723	1.000
46	0.200	0.657	1.000	0.230	0.730	1.000	0.242	0.730	1.000	0.258	0.730	1.000
47	0.205	0.665	1.000	0.235	0.737	1.000	0.247	0.737	1.000	0.263	0.737	1.000
48	0.210	0.672	1.000	0.240	0.744	1.000	0.252	0.744	1.000	0.268	0.744	1.000
49	0.214	0.680	1.000	0.245	0.751	1.000	0.257	0.751	1.000	0.273	0.751	1.000
50	0.219	0.687	1.000	0.250	0.758	1.000	0.262	0.757	1.000	0.278	0.758	1.000

Table 5.6 Variation in Time-Zero Probability of Fatigue-Crack Initiation with Service Life Interval for Milwaukee-Style Mast-Arm Supports in Oshkosh, Wisconsin.

Location: Oshkosh							Latitude: 43.9844°					
							Longitude: -88.5569°					
Number of Years in Service	Orientation of Sign: N-S			Orientation of Sign: NE-SW			Orientation of Sign: E-W			Orientation of Sign: SE-NW		
	Probability of Failure			Probability of Failure			Probability of Failure			Probability of Failure		
	E2	E3	E4	E2	E3	E4	E2	E3	E4	E2	E3	E4
0	0.000	0.000	0.000	0.000	0.000	0.000	0.000	0.000	0.000	0.000	0.000	0.000
1	0.001	0.002	0.572	0.001	0.002	0.543	0.001	0.002	0.530	0.001	0.002	0.601
2	0.004	0.015	0.840	0.004	0.016	0.822	0.004	0.017	0.813	0.004	0.017	0.858
3	0.009	0.040	0.929	0.009	0.042	0.919	0.010	0.044	0.914	0.009	0.044	0.939
4	0.015	0.073	0.965	0.016	0.075	0.959	0.018	0.080	0.956	0.017	0.080	0.970
5	0.023	0.110	0.981	0.024	0.113	0.977	0.026	0.119	0.975	0.025	0.119	0.984
6	0.031	0.149	0.989	0.033	0.153	0.987	0.036	0.160	0.985	0.034	0.160	0.991
7	0.041	0.188	0.993	0.043	0.194	0.992	0.046	0.202	0.991	0.044	0.202	0.994
8	0.050	0.227	0.996	0.052	0.233	0.995	0.057	0.242	0.994	0.054	0.242	0.997
9	0.060	0.265	0.997	0.063	0.272	0.996	0.068	0.282	0.996	0.065	0.281	0.998
10	0.070	0.302	0.998	0.073	0.308	0.998	0.079	0.319	0.997	0.075	0.319	0.998
11	0.080	0.336	0.999	0.084	0.344	0.998	0.090	0.355	0.998	0.086	0.354	0.999
12	0.091	0.369	0.999	0.094	0.377	0.999	0.101	0.388	0.999	0.097	0.388	0.999
13	0.101	0.401	0.999	0.105	0.408	0.999	0.112	0.420	0.999	0.107	0.420	0.999
14	0.111	0.430	0.999	0.115	0.438	0.999	0.123	0.450	0.999	0.118	0.450	1.000
15	0.121	0.458	1.000	0.126	0.466	0.999	0.134	0.478	0.999	0.129	0.478	1.000
16	0.131	0.484	1.000	0.136	0.492	1.000	0.145	0.504	1.000	0.139	0.504	1.000
17	0.141	0.509	1.000	0.146	0.517	1.000	0.155	0.529	1.000	0.150	0.529	1.000
18	0.151	0.532	1.000	0.156	0.540	1.000	0.166	0.552	1.000	0.160	0.552	1.000
19	0.161	0.554	1.000	0.166	0.562	1.000	0.176	0.574	1.000	0.170	0.573	1.000
20	0.171	0.575	1.000	0.176	0.582	1.000	0.186	0.594	1.000	0.180	0.594	1.000
21	0.180	0.594	1.000	0.186	0.602	1.000	0.197	0.613	1.000	0.190	0.613	1.000
22	0.190	0.613	1.000	0.195	0.620	1.000	0.206	0.631	1.000	0.199	0.631	1.000
23	0.199	0.630	1.000	0.205	0.637	1.000	0.216	0.648	1.000	0.209	0.648	1.000
24	0.208	0.646	1.000	0.214	0.653	1.000	0.226	0.664	1.000	0.218	0.664	1.000
25	0.217	0.662	1.000	0.223	0.669	1.000	0.235	0.679	1.000	0.228	0.679	1.000
26	0.226	0.676	1.000	0.232	0.683	1.000	0.244	0.694	1.000	0.237	0.694	1.000
27	0.234	0.690	1.000	0.241	0.697	1.000	0.253	0.707	1.000	0.245	0.707	1.000
28	0.243	0.703	1.000	0.249	0.710	1.000	0.262	0.720	1.000	0.254	0.720	1.000
29	0.251	0.715	1.000	0.258	0.722	1.000	0.271	0.732	1.000	0.263	0.732	1.000
30	0.259	0.727	1.000	0.266	0.733	1.000	0.279	0.743	1.000	0.271	0.743	1.000
31	0.267	0.738	1.000	0.274	0.744	1.000	0.288	0.754	1.000	0.279	0.754	1.000
32	0.275	0.748	1.000	0.283	0.754	1.000	0.296	0.764	1.000	0.287	0.764	1.000
33	0.283	0.758	1.000	0.290	0.764	1.000	0.304	0.773	1.000	0.295	0.773	1.000
34	0.291	0.768	1.000	0.298	0.774	1.000	0.312	0.782	1.000	0.303	0.782	1.000
35	0.298	0.777	1.000	0.306	0.782	1.000	0.320	0.791	1.000	0.311	0.791	1.000
36	0.306	0.785	1.000	0.313	0.791	1.000	0.327	0.799	1.000	0.318	0.799	1.000
37	0.313	0.793	1.000	0.321	0.799	1.000	0.335	0.807	1.000	0.326	0.807	1.000
38	0.320	0.801	1.000	0.328	0.806	1.000	0.342	0.814	1.000	0.333	0.814	1.000
39	0.327	0.808	1.000	0.335	0.813	1.000	0.349	0.821	1.000	0.340	0.821	1.000
40	0.334	0.815	1.000	0.342	0.820	1.000	0.356	0.828	1.000	0.347	0.828	1.000
41	0.341	0.822	1.000	0.349	0.827	1.000	0.363	0.834	1.000	0.354	0.834	1.000
42	0.348	0.828	1.000	0.356	0.833	1.000	0.370	0.841	1.000	0.361	0.840	1.000
43	0.354	0.834	1.000	0.362	0.839	1.000	0.377	0.846	1.000	0.368	0.846	1.000
44	0.361	0.840	1.000	0.369	0.845	1.000	0.384	0.852	1.000	0.374	0.852	1.000
45	0.367	0.846	1.000	0.375	0.850	1.000	0.390	0.857	1.000	0.381	0.857	1.000
46	0.373	0.851	1.000	0.382	0.855	1.000	0.396	0.862	1.000	0.387	0.862	1.000
47	0.379	0.856	1.000	0.388	0.860	1.000	0.403	0.867	1.000	0.393	0.867	1.000
48	0.386	0.861	1.000	0.394	0.865	1.000	0.409	0.871	1.000	0.399	0.871	1.000
49	0.391	0.865	1.000	0.400	0.870	1.000	0.415	0.876	1.000	0.405	0.876	1.000
50	0.397	0.870	1.000	0.406	0.874	1.000	0.421	0.880	1.000	0.411	0.880	1.000

Table 5.7 Variation in Time-Zero Probability of Fatigue-Crack Initiation with Service Life Interval for Milwaukee-Style Mast-Arm Supports in Wisconsin Rapids, Wisconsin.

Location: Wisconsin Rapids							Latitude: 44.3592°					
							Longitude: -89.8369°					
Number of Years in Service	Orientation of Sign: N-S			Orientation of Sign: NE-SW			Orientation of Sign: E-W			Orientation of Sign: SE-NW		
	Probability of Failure			Probability of Failure			Probability of Failure			Probability of Failure		
	E2	E3	E4	E2	E3	E4	E2	E3	E4	E2	E3	E4
0	0.000	0.000	0.000	0.000	0.000	0.000	0.000	0.000	0.000	0.000	0.000	0.000
1	0.000	0.001	0.510	0.000	0.001	0.501	0.000	0.000	0.341	0.000	0.000	0.450
2	0.002	0.008	0.799	0.002	0.008	0.793	0.000	0.002	0.657	0.001	0.004	0.754
3	0.004	0.024	0.906	0.004	0.023	0.902	0.001	0.008	0.811	0.002	0.013	0.878
4	0.008	0.047	0.951	0.007	0.045	0.948	0.003	0.017	0.888	0.004	0.027	0.933
5	0.012	0.073	0.972	0.012	0.071	0.971	0.005	0.029	0.931	0.007	0.044	0.961
6	0.017	0.103	0.983	0.017	0.100	0.982	0.007	0.044	0.955	0.010	0.065	0.976
7	0.023	0.134	0.990	0.022	0.131	0.989	0.009	0.061	0.970	0.014	0.087	0.985
8	0.029	0.166	0.993	0.028	0.162	0.993	0.012	0.079	0.979	0.018	0.111	0.990
9	0.036	0.197	0.995	0.034	0.194	0.995	0.015	0.098	0.985	0.022	0.135	0.993
10	0.042	0.229	0.997	0.041	0.224	0.997	0.019	0.118	0.989	0.027	0.160	0.995
11	0.049	0.259	0.998	0.047	0.255	0.998	0.022	0.138	0.992	0.032	0.185	0.996
12	0.056	0.289	0.998	0.054	0.284	0.998	0.026	0.159	0.994	0.036	0.209	0.997
13	0.063	0.317	0.999	0.061	0.312	0.999	0.030	0.179	0.995	0.042	0.234	0.998
14	0.071	0.345	0.999	0.068	0.340	0.999	0.034	0.200	0.996	0.047	0.258	0.999
15	0.078	0.371	0.999	0.076	0.366	0.999	0.038	0.220	0.997	0.052	0.281	0.999
16	0.085	0.396	0.999	0.083	0.391	0.999	0.042	0.240	0.998	0.058	0.304	0.999
17	0.093	0.420	1.000	0.090	0.415	1.000	0.046	0.260	0.998	0.063	0.326	0.999
18	0.100	0.443	1.000	0.097	0.438	1.000	0.051	0.279	0.999	0.068	0.347	0.999
19	0.107	0.465	1.000	0.104	0.460	1.000	0.055	0.298	0.999	0.074	0.367	1.000
20	0.115	0.486	1.000	0.111	0.481	1.000	0.060	0.317	0.999	0.080	0.387	1.000
21	0.122	0.506	1.000	0.119	0.500	1.000	0.064	0.335	0.999	0.085	0.407	1.000
22	0.129	0.525	1.000	0.126	0.519	1.000	0.069	0.352	0.999	0.091	0.425	1.000
23	0.136	0.543	1.000	0.133	0.537	1.000	0.073	0.369	0.999	0.096	0.443	1.000
24	0.144	0.560	1.000	0.140	0.555	1.000	0.078	0.386	1.000	0.102	0.460	1.000
25	0.151	0.577	1.000	0.147	0.571	1.000	0.082	0.402	1.000	0.108	0.477	1.000
26	0.158	0.592	1.000	0.154	0.587	1.000	0.087	0.417	1.000	0.113	0.493	1.000
27	0.165	0.607	1.000	0.160	0.602	1.000	0.092	0.432	1.000	0.119	0.508	1.000
28	0.172	0.621	1.000	0.167	0.616	1.000	0.096	0.447	1.000	0.124	0.523	1.000
29	0.178	0.635	1.000	0.174	0.630	1.000	0.101	0.461	1.000	0.130	0.537	1.000
30	0.185	0.648	1.000	0.181	0.643	1.000	0.105	0.475	1.000	0.135	0.551	1.000
31	0.192	0.660	1.000	0.187	0.655	1.000	0.110	0.488	1.000	0.141	0.564	1.000
32	0.198	0.672	1.000	0.194	0.667	1.000	0.114	0.501	1.000	0.146	0.577	1.000
33	0.205	0.683	1.000	0.200	0.678	1.000	0.119	0.514	1.000	0.152	0.589	1.000
34	0.211	0.694	1.000	0.207	0.689	1.000	0.124	0.526	1.000	0.157	0.601	1.000
35	0.218	0.704	1.000	0.213	0.700	1.000	0.128	0.538	1.000	0.162	0.612	1.000
36	0.224	0.714	1.000	0.219	0.710	1.000	0.133	0.549	1.000	0.167	0.623	1.000
37	0.230	0.724	1.000	0.225	0.719	1.000	0.137	0.560	1.000	0.173	0.634	1.000
38	0.237	0.733	1.000	0.231	0.728	1.000	0.142	0.571	1.000	0.178	0.644	1.000
39	0.243	0.741	1.000	0.237	0.737	1.000	0.146	0.581	1.000	0.183	0.654	1.000
40	0.249	0.750	1.000	0.243	0.745	1.000	0.150	0.591	1.000	0.188	0.664	1.000
41	0.255	0.758	1.000	0.249	0.753	1.000	0.155	0.601	1.000	0.193	0.673	1.000
42	0.260	0.765	1.000	0.255	0.761	1.000	0.159	0.611	1.000	0.198	0.682	1.000
43	0.266	0.773	1.000	0.261	0.768	1.000	0.163	0.620	1.000	0.203	0.690	1.000
44	0.272	0.780	1.000	0.266	0.776	1.000	0.168	0.629	1.000	0.208	0.698	1.000
45	0.278	0.786	1.000	0.272	0.782	1.000	0.172	0.637	1.000	0.213	0.706	1.000
46	0.283	0.793	1.000	0.277	0.789	1.000	0.176	0.646	1.000	0.218	0.714	1.000
47	0.289	0.799	1.000	0.283	0.795	1.000	0.181	0.654	1.000	0.223	0.721	1.000
48	0.294	0.805	1.000	0.288	0.801	1.000	0.185	0.662	1.000	0.227	0.729	1.000
49	0.300	0.811	1.000	0.294	0.807	1.000	0.189	0.670	1.000	0.232	0.736	1.000
50	0.305	0.816	1.000	0.299	0.813	1.000	0.193	0.677	1.000	0.237	0.742	1.000

Table 5.8 Variation in Time-Zero Probability of Fatigue-Crack Initiation with Service Life Interval for Osseo-Style Mast-Arm Supports in Milwaukee, Wisconsin.

Location: Milwaukee							Latitude: 42.9550°					
							Longitude: -87.9044°					
Number of Years in Service	Orientation of Sign: N-S			Orientation of Sign: NE-SW			Orientation of Sign: E-W			Orientation of Sign: SE-NW		
	Probability of Failure			Probability of Failure			Probability of Failure			Probability of Failure		
	E2	E3	E4	E2	E3	E4	E2	E3	E4	E2	E3	E4
0	0.000	0.000	0.000	0.000	0.000	0.000	0.000	0.000	0.000	0.000	0.000	0.000
1	0.000	0.000	0.358	0.000	0.000	0.307	0.000	0.000	0.257	0.000	0.000	0.326
2	0.000	0.001	0.674	0.000	0.000	0.622	0.000	0.000	0.564	0.000	0.001	0.642
3	0.000	0.003	0.823	0.000	0.002	0.784	0.000	0.001	0.738	0.000	0.003	0.799
4	0.001	0.008	0.897	0.001	0.005	0.870	0.000	0.004	0.836	0.001	0.007	0.880
5	0.002	0.014	0.937	0.001	0.009	0.917	0.001	0.007	0.892	0.001	0.012	0.925
6	0.002	0.023	0.959	0.001	0.015	0.945	0.001	0.012	0.927	0.002	0.020	0.951
7	0.004	0.032	0.973	0.002	0.022	0.963	0.002	0.017	0.949	0.003	0.028	0.967
8	0.005	0.044	0.981	0.003	0.030	0.974	0.002	0.024	0.963	0.004	0.038	0.977
9	0.006	0.056	0.987	0.004	0.040	0.981	0.003	0.032	0.973	0.006	0.050	0.983
10	0.008	0.069	0.990	0.005	0.050	0.986	0.004	0.040	0.980	0.007	0.062	0.988
11	0.009	0.083	0.993	0.006	0.061	0.990	0.005	0.049	0.985	0.009	0.074	0.991
12	0.011	0.098	0.995	0.007	0.072	0.992	0.006	0.059	0.988	0.011	0.088	0.993
13	0.013	0.113	0.996	0.008	0.084	0.994	0.007	0.069	0.991	0.012	0.102	0.995
14	0.015	0.128	0.997	0.010	0.097	0.995	0.008	0.080	0.993	0.014	0.116	0.996
15	0.017	0.143	0.998	0.011	0.109	0.996	0.009	0.091	0.994	0.016	0.130	0.997
16	0.019	0.159	0.998	0.012	0.122	0.997	0.010	0.102	0.995	0.018	0.144	0.997
17	0.021	0.174	0.998	0.014	0.135	0.998	0.012	0.113	0.996	0.020	0.159	0.998
18	0.024	0.189	0.999	0.016	0.148	0.998	0.013	0.125	0.997	0.023	0.174	0.998
19	0.026	0.205	0.999	0.017	0.161	0.998	0.014	0.137	0.997	0.025	0.188	0.999
20	0.028	0.220	0.999	0.019	0.174	0.999	0.016	0.149	0.998	0.027	0.203	0.999
21	0.031	0.235	0.999	0.021	0.187	0.999	0.017	0.161	0.998	0.030	0.217	0.999
22	0.033	0.250	0.999	0.023	0.201	0.999	0.019	0.172	0.999	0.032	0.231	0.999
23	0.036	0.264	1.000	0.024	0.214	0.999	0.021	0.184	0.999	0.035	0.245	0.999
24	0.039	0.279	1.000	0.026	0.226	0.999	0.022	0.196	0.999	0.037	0.259	0.999
25	0.041	0.293	1.000	0.028	0.239	0.999	0.024	0.208	0.999	0.040	0.273	1.000
26	0.044	0.307	1.000	0.030	0.252	1.000	0.026	0.219	0.999	0.042	0.286	1.000
27	0.047	0.321	1.000	0.032	0.264	1.000	0.027	0.231	0.999	0.045	0.300	1.000
28	0.049	0.334	1.000	0.034	0.277	1.000	0.029	0.242	0.999	0.048	0.313	1.000
29	0.052	0.347	1.000	0.036	0.289	1.000	0.031	0.254	1.000	0.050	0.325	1.000
30	0.055	0.360	1.000	0.038	0.301	1.000	0.033	0.265	1.000	0.053	0.338	1.000
31	0.058	0.373	1.000	0.041	0.312	1.000	0.035	0.276	1.000	0.056	0.350	1.000
32	0.061	0.385	1.000	0.043	0.324	1.000	0.037	0.287	1.000	0.059	0.362	1.000
33	0.063	0.397	1.000	0.045	0.335	1.000	0.038	0.298	1.000	0.061	0.374	1.000
34	0.066	0.409	1.000	0.047	0.347	1.000	0.040	0.309	1.000	0.064	0.386	1.000
35	0.069	0.421	1.000	0.049	0.358	1.000	0.042	0.319	1.000	0.067	0.397	1.000
36	0.072	0.432	1.000	0.051	0.368	1.000	0.044	0.329	1.000	0.070	0.408	1.000
37	0.075	0.443	1.000	0.054	0.379	1.000	0.046	0.340	1.000	0.072	0.419	1.000
38	0.078	0.454	1.000	0.056	0.389	1.000	0.048	0.350	1.000	0.075	0.430	1.000
39	0.081	0.464	1.000	0.058	0.400	1.000	0.050	0.360	1.000	0.078	0.440	1.000
40	0.084	0.474	1.000	0.060	0.410	1.000	0.052	0.369	1.000	0.081	0.451	1.000
41	0.086	0.485	1.000	0.063	0.419	1.000	0.054	0.379	1.000	0.084	0.461	1.000
42	0.089	0.494	1.000	0.065	0.429	1.000	0.056	0.388	1.000	0.087	0.470	1.000
43	0.092	0.504	1.000	0.067	0.439	1.000	0.058	0.397	1.000	0.089	0.480	1.000
44	0.095	0.513	1.000	0.069	0.448	1.000	0.060	0.407	1.000	0.092	0.489	1.000
45	0.098	0.522	1.000	0.072	0.457	1.000	0.062	0.416	1.000	0.095	0.499	1.000
46	0.101	0.531	1.000	0.074	0.466	1.000	0.064	0.424	1.000	0.098	0.508	1.000
47	0.104	0.540	1.000	0.076	0.475	1.000	0.067	0.433	1.000	0.101	0.516	1.000
48	0.107	0.549	1.000	0.079	0.483	1.000	0.069	0.441	1.000	0.104	0.525	1.000
49	0.110	0.557	1.000	0.081	0.492	1.000	0.071	0.450	1.000	0.106	0.533	1.000
50	0.113	0.565	1.000	0.083	0.500	1.000	0.073	0.458	1.000	0.109	0.541	1.000

Table 5.9 Variation in Time-Zero Probability of Fatigue-Crack Initiation with Service Life Interval for Osseo-Style Mast-Arm Supports in Eau Claire, Wisconsin.

Location: Eau Claire							Latitude: 44.8664°					
							Longitude: -91.4878°					
Number of Years in Service	Orientation of Sign: N-S			Orientation of Sign: NE-SW			Orientation of Sign: E-W			Orientation of Sign: SE-NW		
	Probability of Failure			Probability of Failure			Probability of Failure			Probability of Failure		
	E2	E3	E4	E2	E3	E4	E2	E3	E4	E2	E3	E4
0	0.000	0.000	0.000	0.000	0.000	0.000	0.000	0.000	0.000	0.000	0.000	0.000
1	0.000	0.000	0.171	0.000	0.000	0.137	0.000	0.000	0.150	0.000	0.000	0.186
2	0.000	0.000	0.445	0.000	0.000	0.390	0.000	0.000	0.412	0.000	0.000	0.469
3	0.000	0.000	0.633	0.000	0.000	0.578	0.000	0.000	0.600	0.000	0.000	0.655
4	0.000	0.001	0.751	0.000	0.000	0.703	0.000	0.000	0.723	0.000	0.001	0.770
5	0.000	0.002	0.826	0.000	0.001	0.787	0.000	0.001	0.803	0.000	0.002	0.841
6	0.000	0.003	0.876	0.000	0.002	0.844	0.000	0.002	0.857	0.000	0.003	0.888
7	0.000	0.005	0.909	0.000	0.003	0.883	0.000	0.003	0.894	0.000	0.005	0.918
8	0.001	0.008	0.932	0.000	0.004	0.911	0.000	0.004	0.920	0.001	0.008	0.940
9	0.001	0.010	0.948	0.001	0.006	0.931	0.000	0.006	0.939	0.001	0.011	0.954
10	0.001	0.014	0.960	0.001	0.008	0.946	0.001	0.007	0.952	0.001	0.014	0.965
11	0.002	0.018	0.969	0.001	0.011	0.957	0.001	0.010	0.962	0.001	0.018	0.973
12	0.002	0.022	0.975	0.001	0.013	0.966	0.001	0.012	0.970	0.002	0.022	0.979
13	0.002	0.027	0.980	0.001	0.016	0.972	0.001	0.015	0.976	0.002	0.027	0.983
14	0.003	0.032	0.984	0.002	0.020	0.978	0.001	0.018	0.980	0.003	0.032	0.986
15	0.003	0.037	0.987	0.002	0.023	0.982	0.001	0.022	0.984	0.003	0.037	0.989
16	0.004	0.043	0.989	0.002	0.027	0.985	0.002	0.025	0.987	0.004	0.043	0.991
17	0.004	0.048	0.991	0.003	0.031	0.987	0.002	0.029	0.989	0.004	0.049	0.993
18	0.005	0.055	0.993	0.003	0.036	0.989	0.002	0.033	0.991	0.005	0.055	0.994
19	0.005	0.061	0.994	0.003	0.040	0.991	0.003	0.038	0.992	0.005	0.062	0.995
20	0.006	0.068	0.995	0.004	0.045	0.992	0.003	0.042	0.993	0.006	0.068	0.996
21	0.007	0.074	0.996	0.004	0.050	0.993	0.003	0.047	0.994	0.006	0.075	0.996
22	0.007	0.081	0.996	0.004	0.055	0.994	0.004	0.052	0.995	0.007	0.082	0.997
23	0.008	0.088	0.997	0.005	0.060	0.995	0.004	0.057	0.996	0.008	0.089	0.997
24	0.009	0.095	0.997	0.005	0.066	0.996	0.004	0.062	0.996	0.008	0.097	0.998
25	0.010	0.103	0.998	0.006	0.071	0.996	0.005	0.067	0.997	0.009	0.104	0.998
26	0.010	0.110	0.998	0.006	0.077	0.997	0.005	0.072	0.997	0.010	0.111	0.998
27	0.011	0.118	0.998	0.007	0.083	0.997	0.006	0.078	0.998	0.011	0.119	0.999
28	0.012	0.125	0.998	0.008	0.089	0.998	0.006	0.084	0.998	0.011	0.126	0.999
29	0.013	0.133	0.999	0.008	0.094	0.998	0.007	0.089	0.998	0.012	0.134	0.999
30	0.014	0.140	0.999	0.009	0.100	0.998	0.007	0.095	0.998	0.013	0.142	0.999
31	0.015	0.148	0.999	0.009	0.106	0.998	0.008	0.101	0.999	0.014	0.149	0.999
32	0.016	0.155	0.999	0.010	0.113	0.999	0.008	0.107	0.999	0.015	0.157	0.999
33	0.017	0.163	0.999	0.011	0.119	0.999	0.009	0.112	0.999	0.016	0.165	0.999
34	0.017	0.171	0.999	0.011	0.125	0.999	0.009	0.118	0.999	0.017	0.172	0.999
35	0.018	0.178	0.999	0.012	0.131	0.999	0.010	0.124	0.999	0.018	0.180	0.999
36	0.019	0.186	0.999	0.013	0.137	0.999	0.010	0.130	0.999	0.019	0.188	1.000
37	0.020	0.193	0.999	0.013	0.144	0.999	0.011	0.136	0.999	0.020	0.195	1.000
38	0.021	0.201	1.000	0.014	0.150	0.999	0.011	0.142	0.999	0.021	0.203	1.000
39	0.022	0.209	1.000	0.015	0.156	0.999	0.012	0.148	0.999	0.021	0.210	1.000
40	0.023	0.216	1.000	0.015	0.162	0.999	0.013	0.155	1.000	0.022	0.218	1.000
41	0.025	0.224	1.000	0.016	0.169	0.999	0.013	0.161	1.000	0.024	0.225	1.000
42	0.026	0.231	1.000	0.017	0.175	1.000	0.014	0.167	1.000	0.025	0.233	1.000
43	0.027	0.238	1.000	0.018	0.181	1.000	0.015	0.173	1.000	0.026	0.240	1.000
44	0.028	0.246	1.000	0.018	0.187	1.000	0.015	0.179	1.000	0.027	0.248	1.000
45	0.029	0.253	1.000	0.019	0.194	1.000	0.016	0.185	1.000	0.028	0.255	1.000
46	0.030	0.260	1.000	0.020	0.200	1.000	0.017	0.191	1.000	0.029	0.262	1.000
47	0.031	0.267	1.000	0.021	0.206	1.000	0.017	0.197	1.000	0.030	0.269	1.000
48	0.032	0.275	1.000	0.021	0.212	1.000	0.018	0.203	1.000	0.031	0.277	1.000
49	0.033	0.282	1.000	0.022	0.218	1.000	0.019	0.209	1.000	0.032	0.284	1.000
50	0.035	0.289	1.000	0.023	0.225	1.000	0.019	0.215	1.000	0.033	0.291	1.000

Table 5.10 Variation in Time-Zero Probability of Fatigue-Crack Initiation with Service Life Interval for Osseo-Style Mast-Arm Supports in La Crosse, Wisconsin.

Location: La Crosse							Latitude: 43.8788°					
							Longitude: -91.2527°					
Number of Years in Service	Orientation of Sign: N-S			Orientation of Sign: NE-SW			Orientation of Sign: E-W			Orientation of Sign: SE-NW		
	Probability of Failure			Probability of Failure			Probability of Failure			Probability of Failure		
	E2	E3	E4	E2	E3	E4	E2	E3	E4	E2	E3	E4
0	0.000	0.000	0.000	0.000	0.000	0.000	0.000	0.000	0.000	0.000	0.000	0.000
1	0.000	0.000	0.173	0.000	0.000	0.251	0.000	0.000	0.221	0.000	0.000	0.185
2	0.000	0.000	0.449	0.000	0.000	0.557	0.000	0.000	0.518	0.000	0.000	0.467
3	0.000	0.001	0.636	0.000	0.001	0.732	0.000	0.000	0.699	0.000	0.000	0.653
4	0.001	0.002	0.754	0.000	0.003	0.831	0.000	0.001	0.805	0.000	0.001	0.768
5	0.001	0.004	0.828	0.001	0.006	0.889	0.000	0.002	0.869	0.000	0.002	0.840
6	0.002	0.006	0.877	0.001	0.010	0.924	0.000	0.003	0.909	0.000	0.004	0.887
7	0.003	0.010	0.910	0.001	0.015	0.947	0.000	0.005	0.935	0.001	0.006	0.918
8	0.004	0.014	0.933	0.002	0.021	0.962	0.001	0.008	0.953	0.001	0.009	0.939
9	0.006	0.019	0.949	0.003	0.028	0.972	0.001	0.011	0.965	0.001	0.013	0.954
10	0.007	0.025	0.961	0.003	0.036	0.979	0.001	0.015	0.974	0.001	0.017	0.965
11	0.009	0.031	0.970	0.004	0.044	0.984	0.002	0.019	0.980	0.002	0.021	0.973
12	0.011	0.038	0.976	0.005	0.053	0.988	0.002	0.023	0.984	0.002	0.026	0.978
13	0.012	0.045	0.981	0.006	0.063	0.990	0.002	0.028	0.988	0.003	0.032	0.983
14	0.014	0.053	0.985	0.007	0.072	0.992	0.003	0.033	0.990	0.003	0.037	0.986
15	0.016	0.061	0.987	0.008	0.083	0.994	0.003	0.039	0.992	0.004	0.043	0.989
16	0.018	0.069	0.990	0.009	0.093	0.995	0.004	0.045	0.994	0.004	0.050	0.991
17	0.020	0.078	0.991	0.011	0.104	0.996	0.004	0.051	0.995	0.005	0.057	0.992
18	0.023	0.086	0.993	0.012	0.115	0.997	0.005	0.057	0.996	0.006	0.064	0.994
19	0.025	0.095	0.994	0.013	0.126	0.997	0.006	0.064	0.996	0.006	0.071	0.995
20	0.027	0.105	0.995	0.015	0.137	0.998	0.006	0.070	0.997	0.007	0.078	0.996
21	0.030	0.114	0.996	0.016	0.148	0.998	0.007	0.077	0.998	0.008	0.086	0.996
22	0.032	0.123	0.996	0.017	0.160	0.998	0.008	0.085	0.998	0.009	0.093	0.997
23	0.035	0.133	0.997	0.019	0.171	0.999	0.008	0.092	0.998	0.009	0.101	0.997
24	0.037	0.142	0.997	0.021	0.182	0.999	0.009	0.099	0.998	0.010	0.109	0.998
25	0.040	0.152	0.998	0.022	0.193	0.999	0.010	0.107	0.999	0.011	0.117	0.998
26	0.042	0.162	0.998	0.024	0.205	0.999	0.011	0.114	0.999	0.012	0.125	0.998
27	0.045	0.171	0.998	0.025	0.216	0.999	0.012	0.122	0.999	0.013	0.133	0.999
28	0.048	0.181	0.999	0.027	0.227	0.999	0.012	0.130	0.999	0.014	0.141	0.999
29	0.050	0.191	0.999	0.029	0.238	0.999	0.013	0.137	0.999	0.015	0.150	0.999
30	0.053	0.200	0.999	0.030	0.249	1.000	0.014	0.145	0.999	0.016	0.158	0.999
31	0.056	0.210	0.999	0.032	0.259	1.000	0.015	0.153	0.999	0.017	0.166	0.999
32	0.059	0.219	0.999	0.034	0.270	1.000	0.016	0.161	1.000	0.018	0.174	0.999
33	0.061	0.229	0.999	0.036	0.280	1.000	0.017	0.168	1.000	0.019	0.182	0.999
34	0.064	0.238	0.999	0.037	0.291	1.000	0.018	0.176	1.000	0.020	0.191	0.999
35	0.067	0.247	0.999	0.039	0.301	1.000	0.019	0.184	1.000	0.021	0.199	0.999
36	0.070	0.256	0.999	0.041	0.311	1.000	0.020	0.192	1.000	0.022	0.207	1.000
37	0.072	0.265	1.000	0.043	0.321	1.000	0.021	0.199	1.000	0.023	0.215	1.000
38	0.075	0.274	1.000	0.045	0.331	1.000	0.022	0.207	1.000	0.024	0.223	1.000
39	0.078	0.283	1.000	0.047	0.341	1.000	0.023	0.215	1.000	0.025	0.231	1.000
40	0.081	0.292	1.000	0.049	0.350	1.000	0.024	0.222	1.000	0.027	0.239	1.000
41	0.084	0.301	1.000	0.051	0.360	1.000	0.025	0.230	1.000	0.028	0.247	1.000
42	0.087	0.309	1.000	0.052	0.369	1.000	0.026	0.238	1.000	0.029	0.255	1.000
43	0.089	0.318	1.000	0.054	0.378	1.000	0.027	0.245	1.000	0.030	0.262	1.000
44	0.092	0.326	1.000	0.056	0.387	1.000	0.028	0.253	1.000	0.031	0.270	1.000
45	0.095	0.335	1.000	0.058	0.396	1.000	0.030	0.260	1.000	0.033	0.278	1.000
46	0.098	0.343	1.000	0.060	0.404	1.000	0.031	0.267	1.000	0.034	0.285	1.000
47	0.101	0.351	1.000	0.062	0.413	1.000	0.032	0.275	1.000	0.035	0.293	1.000
48	0.104	0.359	1.000	0.064	0.421	1.000	0.033	0.282	1.000	0.036	0.300	1.000
49	0.106	0.367	1.000	0.066	0.430	1.000	0.034	0.289	1.000	0.038	0.308	1.000
50	0.109	0.375	1.000	0.068	0.438	1.000	0.035	0.296	1.000	0.039	0.315	1.000

Table 5.11 Variation in Time-Zero Probability of Fatigue-Crack Initiation with Service Life Interval for Osseo-Style Mast-Arm Supports in Green Bay, Wisconsin.

Location: Green Bay							Latitude: 44.4794°					
							Longitude: -88.1366°					
Number of Years in Service	Orientation of Sign: N-S			Orientation of Sign: NE-SW			Orientation of Sign: E-W			Orientation of Sign: SE-NW		
	Probability of Failure			Probability of Failure			Probability of Failure			Probability of Failure		
	E2	E3	E4	E2	E3	E4	E2	E3	E4	E2	E3	E4
0	0.000	0.000	0.000	0.000	0.000	0.000	0.000	0.000	0.000	0.000	0.000	0.000
1	0.000	0.000	0.270	0.000	0.000	0.244	0.000	0.000	0.218	0.000	0.000	0.254
2	0.000	0.000	0.580	0.000	0.000	0.548	0.000	0.000	0.514	0.000	0.000	0.560
3	0.000	0.002	0.751	0.000	0.001	0.725	0.000	0.001	0.695	0.000	0.001	0.735
4	0.001	0.004	0.845	0.000	0.004	0.825	0.000	0.003	0.802	0.000	0.003	0.833
5	0.001	0.008	0.900	0.001	0.007	0.884	0.001	0.007	0.867	0.001	0.005	0.890
6	0.002	0.013	0.932	0.001	0.012	0.921	0.001	0.011	0.907	0.001	0.009	0.925
7	0.002	0.019	0.953	0.002	0.017	0.944	0.002	0.016	0.934	0.002	0.014	0.948
8	0.003	0.026	0.966	0.003	0.024	0.960	0.003	0.023	0.952	0.002	0.019	0.962
9	0.004	0.035	0.976	0.004	0.032	0.970	0.004	0.030	0.964	0.003	0.025	0.972
10	0.005	0.044	0.982	0.005	0.040	0.978	0.005	0.039	0.973	0.004	0.032	0.979
11	0.006	0.054	0.986	0.006	0.049	0.983	0.006	0.047	0.979	0.005	0.040	0.984
12	0.007	0.064	0.989	0.007	0.059	0.987	0.007	0.057	0.984	0.006	0.048	0.988
13	0.009	0.075	0.992	0.008	0.069	0.990	0.008	0.067	0.987	0.007	0.057	0.991
14	0.010	0.086	0.994	0.009	0.080	0.992	0.009	0.077	0.990	0.008	0.066	0.993
15	0.012	0.098	0.995	0.011	0.091	0.994	0.011	0.088	0.992	0.009	0.076	0.994
16	0.013	0.110	0.996	0.012	0.102	0.995	0.012	0.099	0.993	0.011	0.086	0.995
17	0.015	0.122	0.997	0.014	0.114	0.996	0.014	0.110	0.995	0.012	0.096	0.996
18	0.017	0.134	0.997	0.015	0.126	0.997	0.015	0.122	0.996	0.013	0.106	0.997
19	0.018	0.147	0.998	0.017	0.137	0.997	0.017	0.133	0.996	0.015	0.117	0.997
20	0.020	0.159	0.998	0.019	0.149	0.998	0.019	0.145	0.997	0.016	0.127	0.998
21	0.022	0.171	0.998	0.021	0.161	0.998	0.020	0.156	0.997	0.018	0.138	0.998
22	0.024	0.184	0.999	0.022	0.173	0.998	0.022	0.168	0.998	0.020	0.149	0.999
23	0.026	0.196	0.999	0.024	0.185	0.999	0.024	0.180	0.998	0.021	0.160	0.999
24	0.028	0.208	0.999	0.026	0.197	0.999	0.026	0.191	0.998	0.023	0.171	0.999
25	0.030	0.221	0.999	0.028	0.208	0.999	0.028	0.203	0.999	0.025	0.181	0.999
26	0.032	0.233	0.999	0.030	0.220	0.999	0.030	0.214	0.999	0.026	0.192	0.999
27	0.034	0.245	0.999	0.032	0.232	0.999	0.032	0.226	0.999	0.028	0.203	0.999
28	0.036	0.256	1.000	0.034	0.243	0.999	0.034	0.237	0.999	0.030	0.213	0.999
29	0.038	0.268	1.000	0.036	0.255	0.999	0.036	0.248	0.999	0.032	0.224	1.000
30	0.040	0.280	1.000	0.038	0.266	1.000	0.038	0.259	0.999	0.034	0.235	1.000
31	0.043	0.291	1.000	0.040	0.277	1.000	0.040	0.270	0.999	0.036	0.245	1.000
32	0.045	0.302	1.000	0.042	0.288	1.000	0.042	0.281	1.000	0.037	0.255	1.000
33	0.047	0.313	1.000	0.044	0.299	1.000	0.044	0.292	1.000	0.039	0.265	1.000
34	0.049	0.324	1.000	0.047	0.309	1.000	0.046	0.302	1.000	0.041	0.276	1.000
35	0.052	0.335	1.000	0.049	0.320	1.000	0.048	0.313	1.000	0.043	0.286	1.000
36	0.054	0.345	1.000	0.051	0.330	1.000	0.050	0.323	1.000	0.045	0.295	1.000
37	0.056	0.356	1.000	0.053	0.340	1.000	0.053	0.333	1.000	0.047	0.305	1.000
38	0.058	0.366	1.000	0.055	0.350	1.000	0.055	0.343	1.000	0.049	0.315	1.000
39	0.061	0.376	1.000	0.058	0.360	1.000	0.057	0.353	1.000	0.051	0.324	1.000
40	0.063	0.386	1.000	0.060	0.370	1.000	0.059	0.363	1.000	0.053	0.334	1.000
41	0.065	0.396	1.000	0.062	0.380	1.000	0.062	0.372	1.000	0.055	0.343	1.000
42	0.068	0.405	1.000	0.064	0.389	1.000	0.064	0.382	1.000	0.058	0.352	1.000
43	0.070	0.414	1.000	0.067	0.398	1.000	0.066	0.391	1.000	0.060	0.361	1.000
44	0.073	0.424	1.000	0.069	0.407	1.000	0.068	0.400	1.000	0.062	0.370	1.000
45	0.075	0.433	1.000	0.071	0.416	1.000	0.071	0.409	1.000	0.064	0.378	1.000
46	0.077	0.442	1.000	0.073	0.425	1.000	0.073	0.417	1.000	0.066	0.387	1.000
47	0.080	0.450	1.000	0.076	0.434	1.000	0.075	0.426	1.000	0.068	0.395	1.000
48	0.082	0.459	1.000	0.078	0.442	1.000	0.077	0.435	1.000	0.070	0.404	1.000
49	0.084	0.467	1.000	0.080	0.451	1.000	0.080	0.443	1.000	0.072	0.412	1.000
50	0.087	0.475	1.000	0.083	0.459	1.000	0.082	0.451	1.000	0.074	0.420	1.000

Table 5.12 Variation in Time-Zero Probability of Fatigue-Crack Initiation with Service Life Interval for Osseo-Style Mast-Arm Supports in Madison, Wisconsin.

Location: Madison							Latitude: 43.1405°					
							Longitude: -89.3452°					
Number of Years in Service	Orientation of Sign: N-S			Orientation of Sign: NE-SW			Orientation of Sign: E-W			Orientation of Sign: SE-NW		
	Probability of Failure			Probability of Failure			Probability of Failure			Probability of Failure		
	E2	E3	E4	E2	E3	E4	E2	E3	E4	E2	E3	E4
0	0.000	0.000	0.000	0.000	0.000	0.000	0.000	0.000	0.000	0.000	0.000	0.000
1	0.000	0.000	0.064	0.000	0.000	0.124	0.000	0.000	0.149	0.000	0.000	0.116
2	0.000	0.000	0.239	0.000	0.000	0.367	0.000	0.000	0.411	0.000	0.000	0.352
3	0.000	0.000	0.408	0.000	0.000	0.555	0.000	0.000	0.599	0.000	0.000	0.539
4	0.000	0.000	0.542	0.000	0.000	0.683	0.000	0.000	0.722	0.000	0.000	0.668
5	0.000	0.000	0.643	0.000	0.001	0.769	0.000	0.001	0.802	0.000	0.001	0.757
6	0.000	0.001	0.720	0.000	0.001	0.829	0.000	0.001	0.856	0.000	0.001	0.819
7	0.000	0.001	0.777	0.000	0.002	0.871	0.000	0.002	0.894	0.000	0.002	0.863
8	0.000	0.002	0.821	0.000	0.003	0.901	0.000	0.003	0.920	0.000	0.004	0.894
9	0.000	0.003	0.855	0.000	0.005	0.923	0.000	0.005	0.938	0.000	0.005	0.917
10	0.000	0.004	0.881	0.000	0.006	0.940	0.001	0.006	0.952	0.001	0.007	0.935
11	0.000	0.005	0.902	0.001	0.008	0.952	0.001	0.008	0.962	0.001	0.009	0.948
12	0.001	0.006	0.919	0.001	0.011	0.961	0.001	0.011	0.970	0.001	0.011	0.958
13	0.001	0.008	0.932	0.001	0.013	0.969	0.001	0.013	0.976	0.001	0.014	0.966
14	0.001	0.010	0.943	0.001	0.016	0.974	0.001	0.016	0.980	0.002	0.017	0.972
15	0.001	0.012	0.951	0.001	0.019	0.979	0.002	0.019	0.984	0.002	0.020	0.977
16	0.001	0.014	0.959	0.001	0.023	0.982	0.002	0.022	0.987	0.002	0.023	0.980
17	0.001	0.016	0.964	0.002	0.026	0.985	0.002	0.026	0.989	0.002	0.027	0.984
18	0.001	0.019	0.969	0.002	0.030	0.988	0.002	0.029	0.991	0.003	0.031	0.986
19	0.002	0.021	0.974	0.002	0.034	0.989	0.003	0.033	0.992	0.003	0.035	0.988
20	0.002	0.024	0.977	0.003	0.038	0.991	0.003	0.037	0.993	0.004	0.039	0.990
21	0.002	0.027	0.980	0.003	0.042	0.992	0.003	0.041	0.994	0.004	0.044	0.991
22	0.002	0.030	0.982	0.003	0.047	0.993	0.004	0.046	0.995	0.004	0.048	0.993
23	0.003	0.034	0.985	0.004	0.051	0.994	0.004	0.050	0.996	0.005	0.053	0.994
24	0.003	0.037	0.986	0.004	0.056	0.995	0.005	0.055	0.996	0.005	0.058	0.994
25	0.003	0.040	0.988	0.004	0.061	0.996	0.005	0.060	0.997	0.006	0.063	0.995
26	0.004	0.044	0.989	0.005	0.066	0.996	0.005	0.065	0.997	0.006	0.068	0.996
27	0.004	0.048	0.991	0.005	0.071	0.997	0.006	0.070	0.998	0.007	0.073	0.996
28	0.004	0.052	0.992	0.005	0.076	0.997	0.006	0.075	0.998	0.007	0.079	0.997
29	0.005	0.055	0.993	0.006	0.081	0.997	0.007	0.080	0.998	0.008	0.084	0.997
30	0.005	0.059	0.993	0.006	0.087	0.998	0.007	0.085	0.998	0.008	0.089	0.997
31	0.005	0.063	0.994	0.007	0.092	0.998	0.008	0.091	0.999	0.009	0.095	0.998
32	0.006	0.068	0.995	0.007	0.098	0.998	0.008	0.096	0.999	0.010	0.101	0.998
33	0.006	0.072	0.995	0.008	0.103	0.998	0.009	0.102	0.999	0.010	0.106	0.998
34	0.006	0.076	0.996	0.008	0.109	0.999	0.009	0.107	0.999	0.011	0.112	0.998
35	0.007	0.080	0.996	0.009	0.114	0.999	0.010	0.113	0.999	0.012	0.118	0.999
36	0.007	0.085	0.996	0.009	0.120	0.999	0.011	0.118	0.999	0.012	0.123	0.999
37	0.008	0.089	0.997	0.010	0.126	0.999	0.011	0.124	0.999	0.013	0.129	0.999
38	0.008	0.094	0.997	0.010	0.131	0.999	0.012	0.130	0.999	0.014	0.135	0.999
39	0.009	0.098	0.997	0.011	0.137	0.999	0.012	0.135	0.999	0.014	0.141	0.999
40	0.009	0.103	0.998	0.011	0.143	0.999	0.013	0.141	1.000	0.015	0.147	0.999
41	0.009	0.107	0.998	0.012	0.149	0.999	0.014	0.147	1.000	0.016	0.153	0.999
42	0.010	0.112	0.998	0.013	0.154	0.999	0.014	0.152	1.000	0.016	0.159	0.999
43	0.010	0.117	0.998	0.013	0.160	0.999	0.015	0.158	1.000	0.017	0.164	0.999
44	0.011	0.121	0.998	0.014	0.166	1.000	0.016	0.164	1.000	0.018	0.170	0.999
45	0.011	0.126	0.998	0.014	0.172	1.000	0.016	0.170	1.000	0.019	0.176	0.999
46	0.012	0.131	0.999	0.015	0.178	1.000	0.017	0.175	1.000	0.019	0.182	1.000
47	0.012	0.135	0.999	0.016	0.183	1.000	0.018	0.181	1.000	0.020	0.188	1.000
48	0.013	0.140	0.999	0.016	0.189	1.000	0.018	0.187	1.000	0.021	0.194	1.000
49	0.013	0.145	0.999	0.017	0.195	1.000	0.019	0.192	1.000	0.022	0.200	1.000
50	0.014	0.150	0.999	0.017	0.201	1.000	0.020	0.198	1.000	0.023	0.205	1.000

Table 5.13 Variation in Time-Zero Probability of Fatigue-Crack Initiation with Service Life Interval for Osseo-Style Mast-Arm Supports in Oshkosh, Wisconsin.

Location: Oshkosh							Latitude: 43.9844°					
							Longitude: -88.5569°					
Number of Years in Service	Orientation of Sign: N-S			Orientation of Sign: NE-SW			Orientation of Sign: E-W			Orientation of Sign: SE-NW		
	Probability of Failure			Probability of Failure			Probability of Failure			Probability of Failure		
	E2	E3	E4	E2	E3	E4	E2	E3	E4	E2	E3	E4
0	0.000	0.000	0.000	0.000	0.000	0.000	0.000	0.000	0.000	0.000	0.000	0.000
1	0.000	0.000	0.216	0.000	0.000	0.196	0.000	0.000	0.186	0.000	0.000	0.238
2	0.000	0.000	0.511	0.000	0.000	0.483	0.000	0.000	0.469	0.000	0.000	0.540
3	0.000	0.001	0.693	0.000	0.001	0.668	0.000	0.001	0.655	0.000	0.001	0.718
4	0.000	0.001	0.800	0.000	0.002	0.780	0.000	0.002	0.769	0.000	0.002	0.820
5	0.000	0.003	0.865	0.000	0.003	0.850	0.000	0.004	0.841	0.000	0.003	0.880
6	0.001	0.005	0.906	0.001	0.006	0.894	0.001	0.006	0.887	0.001	0.006	0.918
7	0.001	0.008	0.933	0.001	0.009	0.924	0.001	0.010	0.918	0.001	0.009	0.942
8	0.001	0.012	0.951	0.001	0.012	0.944	0.001	0.014	0.940	0.001	0.013	0.958
9	0.002	0.016	0.964	0.002	0.017	0.958	0.002	0.018	0.954	0.002	0.018	0.969
10	0.002	0.021	0.972	0.002	0.022	0.968	0.002	0.024	0.965	0.002	0.023	0.977
11	0.002	0.026	0.979	0.003	0.028	0.975	0.003	0.030	0.973	0.003	0.029	0.982
12	0.003	0.032	0.983	0.003	0.034	0.980	0.004	0.036	0.979	0.003	0.035	0.986
13	0.004	0.038	0.987	0.004	0.040	0.984	0.004	0.043	0.983	0.004	0.042	0.989
14	0.004	0.045	0.990	0.005	0.047	0.988	0.005	0.051	0.986	0.005	0.050	0.992
15	0.005	0.052	0.992	0.005	0.055	0.990	0.006	0.059	0.989	0.006	0.057	0.993
16	0.006	0.059	0.993	0.006	0.062	0.992	0.007	0.067	0.991	0.006	0.065	0.995
17	0.007	0.067	0.994	0.007	0.070	0.993	0.008	0.075	0.993	0.007	0.073	0.996
18	0.007	0.075	0.995	0.008	0.079	0.994	0.009	0.084	0.994	0.008	0.082	0.996
19	0.008	0.083	0.996	0.009	0.087	0.995	0.010	0.093	0.995	0.009	0.091	0.997
20	0.009	0.091	0.997	0.010	0.096	0.996	0.011	0.102	0.996	0.010	0.099	0.997
21	0.010	0.100	0.997	0.011	0.104	0.997	0.012	0.111	0.996	0.011	0.108	0.998
22	0.011	0.108	0.998	0.012	0.113	0.997	0.013	0.120	0.997	0.012	0.118	0.998
23	0.012	0.117	0.998	0.013	0.122	0.998	0.014	0.129	0.997	0.013	0.127	0.999
24	0.013	0.126	0.998	0.014	0.131	0.998	0.015	0.139	0.998	0.014	0.136	0.999
25	0.014	0.135	0.999	0.015	0.140	0.998	0.017	0.148	0.998	0.016	0.145	0.999
26	0.015	0.144	0.999	0.016	0.149	0.999	0.018	0.158	0.998	0.017	0.155	0.999
27	0.016	0.153	0.999	0.017	0.159	0.999	0.019	0.167	0.999	0.018	0.164	0.999
28	0.018	0.161	0.999	0.019	0.168	0.999	0.021	0.177	0.999	0.019	0.173	0.999
29	0.019	0.170	0.999	0.020	0.177	0.999	0.022	0.186	0.999	0.020	0.183	0.999
30	0.020	0.179	0.999	0.021	0.186	0.999	0.023	0.195	0.999	0.022	0.192	0.999
31	0.021	0.188	0.999	0.022	0.195	0.999	0.025	0.205	0.999	0.023	0.201	1.000
32	0.022	0.197	0.999	0.024	0.204	0.999	0.026	0.214	0.999	0.024	0.211	1.000
33	0.024	0.206	1.000	0.025	0.213	0.999	0.028	0.223	0.999	0.026	0.220	1.000
34	0.025	0.215	1.000	0.026	0.222	0.999	0.029	0.233	0.999	0.027	0.229	1.000
35	0.026	0.224	1.000	0.028	0.231	1.000	0.031	0.242	0.999	0.029	0.238	1.000
36	0.028	0.232	1.000	0.029	0.240	1.000	0.032	0.251	1.000	0.030	0.247	1.000
37	0.029	0.241	1.000	0.031	0.249	1.000	0.034	0.260	1.000	0.031	0.256	1.000
38	0.030	0.249	1.000	0.032	0.258	1.000	0.035	0.269	1.000	0.033	0.265	1.000
39	0.032	0.258	1.000	0.033	0.266	1.000	0.037	0.278	1.000	0.034	0.274	1.000
40	0.033	0.266	1.000	0.035	0.275	1.000	0.038	0.286	1.000	0.036	0.282	1.000
41	0.034	0.275	1.000	0.036	0.283	1.000	0.040	0.295	1.000	0.037	0.291	1.000
42	0.036	0.283	1.000	0.038	0.292	1.000	0.041	0.304	1.000	0.039	0.299	1.000
43	0.037	0.291	1.000	0.039	0.300	1.000	0.043	0.312	1.000	0.040	0.308	1.000
44	0.039	0.299	1.000	0.041	0.308	1.000	0.044	0.320	1.000	0.042	0.316	1.000
45	0.040	0.307	1.000	0.042	0.316	1.000	0.046	0.329	1.000	0.043	0.324	1.000
46	0.042	0.315	1.000	0.044	0.324	1.000	0.048	0.337	1.000	0.045	0.332	1.000
47	0.043	0.323	1.000	0.045	0.332	1.000	0.049	0.345	1.000	0.047	0.341	1.000
48	0.045	0.331	1.000	0.047	0.340	1.000	0.051	0.353	1.000	0.048	0.348	1.000
49	0.046	0.339	1.000	0.048	0.348	1.000	0.053	0.361	1.000	0.050	0.356	1.000
50	0.047	0.346	1.000	0.050	0.355	1.000	0.054	0.369	1.000	0.051	0.364	1.000

Table 5.14 Variation in Time-Zero Probability of Fatigue-Crack Initiation with Service Life Interval for Osseo-Style Mast-Arm Supports in Wisconsin Rapids, Wisconsin.

Location: Wisconsin Rapids							Latitude: 44.3592°					
							Longitude: -89.8369°					
Number of Years in Service	Orientation of Sign: N-S			Orientation of Sign: NE-SW			Orientation of Sign: E-W			Orientation of Sign: SE-NW		
	Probability of Failure			Probability of Failure			Probability of Failure			Probability of Failure		
	E2	E3	E4	E2	E3	E4	E2	E3	E4	E2	E3	E4
0	0.000	0.000	0.000	0.000	0.000	0.000	0.000	0.000	0.000	0.000	0.000	0.000
1	0.000	0.000	0.172	0.000	0.000	0.166	0.000	0.000	0.083	0.000	0.000	0.135
2	0.000	0.000	0.448	0.000	0.000	0.439	0.000	0.000	0.285	0.000	0.000	0.387
3	0.000	0.000	0.635	0.000	0.000	0.626	0.000	0.000	0.463	0.000	0.000	0.575
4	0.000	0.001	0.753	0.000	0.001	0.745	0.000	0.000	0.597	0.000	0.000	0.701
5	0.000	0.001	0.828	0.000	0.001	0.822	0.000	0.000	0.694	0.000	0.001	0.785
6	0.000	0.003	0.877	0.000	0.002	0.872	0.000	0.001	0.765	0.000	0.001	0.842
7	0.000	0.004	0.910	0.000	0.004	0.906	0.000	0.001	0.817	0.000	0.002	0.882
8	0.000	0.006	0.933	0.000	0.006	0.930	0.000	0.002	0.855	0.000	0.003	0.910
9	0.001	0.009	0.949	0.001	0.008	0.947	0.000	0.002	0.885	0.000	0.004	0.931
10	0.001	0.011	0.961	0.001	0.011	0.959	0.000	0.003	0.907	0.000	0.006	0.946
11	0.001	0.015	0.969	0.001	0.014	0.968	0.000	0.004	0.924	0.001	0.007	0.957
12	0.001	0.018	0.976	0.001	0.018	0.974	0.000	0.006	0.938	0.001	0.009	0.965
13	0.002	0.022	0.981	0.001	0.021	0.980	0.000	0.007	0.948	0.001	0.012	0.972
14	0.002	0.026	0.984	0.002	0.026	0.983	0.001	0.009	0.957	0.001	0.014	0.977
15	0.002	0.031	0.987	0.002	0.030	0.987	0.001	0.010	0.964	0.001	0.017	0.981
16	0.003	0.036	0.990	0.002	0.035	0.989	0.001	0.012	0.970	0.001	0.020	0.984
17	0.003	0.041	0.991	0.003	0.040	0.991	0.001	0.014	0.974	0.002	0.023	0.987
18	0.003	0.047	0.993	0.003	0.045	0.992	0.001	0.017	0.978	0.002	0.027	0.989
19	0.004	0.052	0.994	0.004	0.051	0.994	0.001	0.019	0.981	0.002	0.030	0.991
20	0.004	0.058	0.995	0.004	0.056	0.995	0.001	0.022	0.984	0.002	0.034	0.992
21	0.005	0.064	0.996	0.004	0.062	0.995	0.002	0.024	0.986	0.003	0.038	0.993
22	0.005	0.070	0.996	0.005	0.068	0.996	0.002	0.027	0.988	0.003	0.042	0.994
23	0.006	0.077	0.997	0.005	0.075	0.997	0.002	0.030	0.989	0.003	0.046	0.995
24	0.006	0.083	0.997	0.006	0.081	0.997	0.002	0.033	0.991	0.003	0.051	0.996
25	0.007	0.090	0.998	0.006	0.087	0.998	0.002	0.037	0.992	0.004	0.055	0.996
26	0.007	0.096	0.998	0.007	0.094	0.998	0.003	0.040	0.993	0.004	0.060	0.997
27	0.008	0.103	0.998	0.008	0.100	0.998	0.003	0.043	0.994	0.004	0.064	0.997
28	0.009	0.110	0.999	0.008	0.107	0.998	0.003	0.047	0.994	0.005	0.069	0.998
29	0.009	0.117	0.999	0.009	0.114	0.999	0.003	0.051	0.995	0.005	0.074	0.998
30	0.010	0.124	0.999	0.009	0.121	0.999	0.004	0.054	0.996	0.006	0.079	0.998
31	0.011	0.131	0.999	0.010	0.128	0.999	0.004	0.058	0.996	0.006	0.084	0.998
32	0.011	0.138	0.999	0.011	0.134	0.999	0.004	0.062	0.996	0.006	0.089	0.999
33	0.012	0.145	0.999	0.011	0.141	0.999	0.004	0.066	0.997	0.007	0.094	0.999
34	0.013	0.152	0.999	0.012	0.148	0.999	0.005	0.070	0.997	0.007	0.100	0.999
35	0.014	0.159	0.999	0.013	0.155	0.999	0.005	0.074	0.997	0.008	0.105	0.999
36	0.014	0.166	0.999	0.014	0.162	0.999	0.005	0.078	0.998	0.008	0.110	0.999
37	0.015	0.173	1.000	0.014	0.169	0.999	0.006	0.082	0.998	0.009	0.116	0.999
38	0.016	0.180	1.000	0.015	0.176	1.000	0.006	0.086	0.998	0.009	0.121	0.999
39	0.017	0.187	1.000	0.016	0.183	1.000	0.006	0.091	0.998	0.010	0.126	0.999
40	0.017	0.194	1.000	0.017	0.190	1.000	0.007	0.095	0.998	0.010	0.132	0.999
41	0.018	0.201	1.000	0.017	0.197	1.000	0.007	0.099	0.999	0.011	0.137	0.999
42	0.019	0.208	1.000	0.018	0.204	1.000	0.007	0.104	0.999	0.011	0.143	0.999
43	0.020	0.215	1.000	0.019	0.211	1.000	0.008	0.108	0.999	0.012	0.148	1.000
44	0.021	0.222	1.000	0.020	0.218	1.000	0.008	0.113	0.999	0.012	0.154	1.000
45	0.022	0.229	1.000	0.021	0.225	1.000	0.009	0.117	0.999	0.013	0.159	1.000
46	0.022	0.236	1.000	0.021	0.231	1.000	0.009	0.121	0.999	0.014	0.165	1.000
47	0.023	0.243	1.000	0.022	0.238	1.000	0.009	0.126	0.999	0.014	0.170	1.000
48	0.024	0.250	1.000	0.023	0.245	1.000	0.010	0.130	0.999	0.015	0.176	1.000
49	0.025	0.256	1.000	0.024	0.251	1.000	0.010	0.135	0.999	0.015	0.181	1.000
50	0.026	0.263	1.000	0.025	0.258	1.000	0.011	0.140	0.999	0.016	0.187	1.000

Table 5.15 Inspection Thresholds for Mast-Arm Sign Support Structures in Wisconsin as a Function of Mast-Arm Type, and Detail Configuration.

Location	Service-Life or Elapsed Time from Time-Zero (years)	Mast-Arm Configuration and Detail Type					
		E2 Detail		E3 Detail		E4 Detail	
		Milwaukee Type	Osseo Type	Milwaukee Type	Osseo Type	Milwaukee Type	Osseo Type
Milwaukee	First Inspection	13	> 50	5	19	1	1
	Four-Year Inspection Interval	40	> 50	10	43	NA	2
Eau Claire	First Inspection	28	> 50	9	38	1	2
	Four-Year Inspection Interval	> 50	> 50	20	> 50	NA	3
La Crosse	First Inspection	19	> 50	6	26	1	2
	Four-Year Inspection Interval	> 50	> 50	14	> 50	NA	3
Green Bay	First Inspection	16	> 50	6	24	1	1
	Four-Year Inspection Interval	48	> 50	13	> 50	NA	2
Madison	First Inspection	36	> 50	12	50	1	2
	Four-Year Inspection Interval	> 50	> 50	26	> 50	2	3
Oshkosh	First Inspection	22	> 50	7	31	1	1
	Four-Year Inspection Interval	> 50	> 50	16	> 50	NA	2
Wisconsin Rapids	First Inspection	33	> 50	10	41	1	2
	Four-Year Inspection Interval	> 50	> 50	21	> 50	NA	3

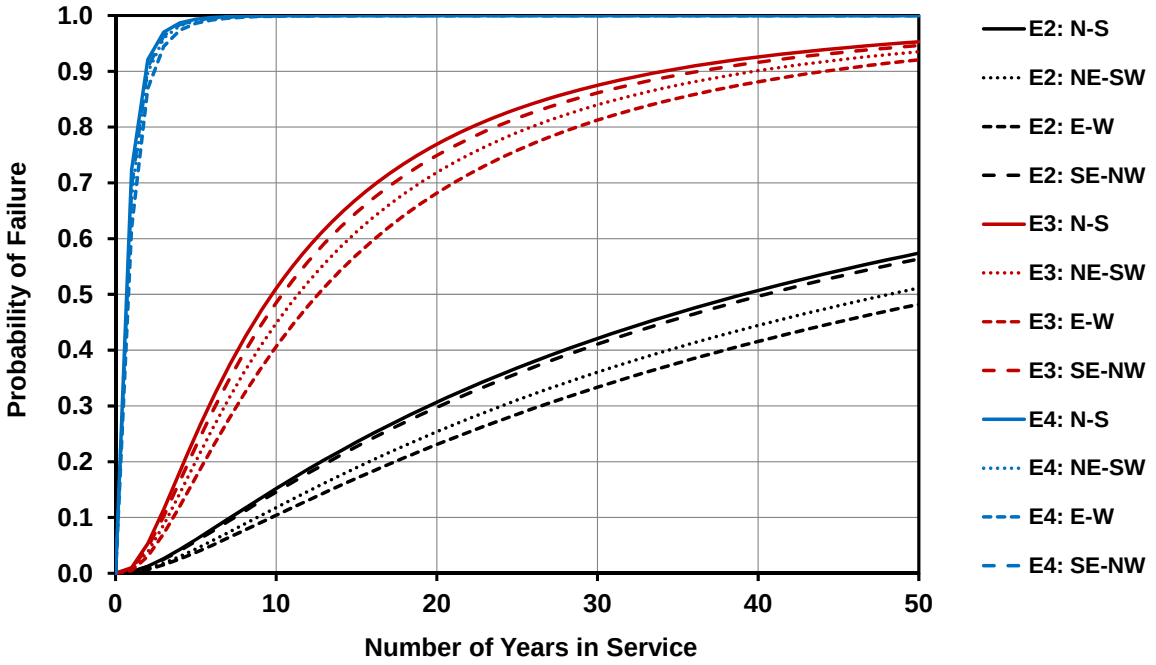

Figure 5.1 Cumulative Distribution Function for Failure Probability (fatigue crack initiation) as a Function of Service Life for Milwaukee-Style Mast-Arms in Milwaukee, Wisconsin.

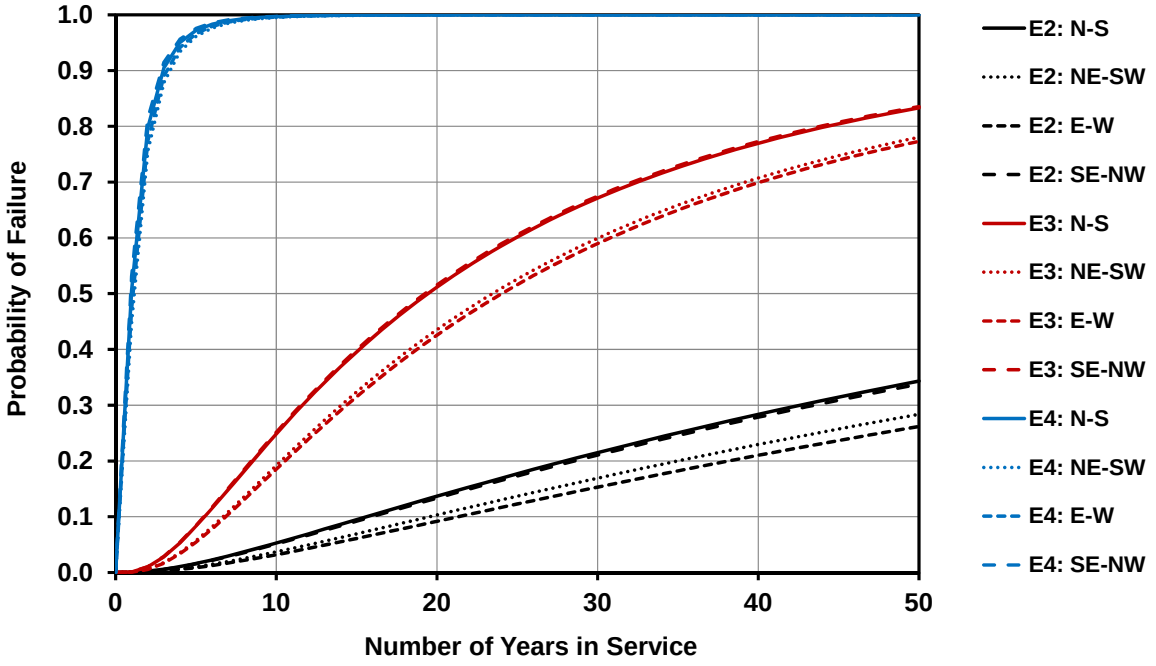

Figure 5.2 Cumulative Distribution Function for Failure Probability (fatigue crack initiation) as a Function of Service Life for Milwaukee-Style Mast-Arms in Eau Claire, Wisconsin.

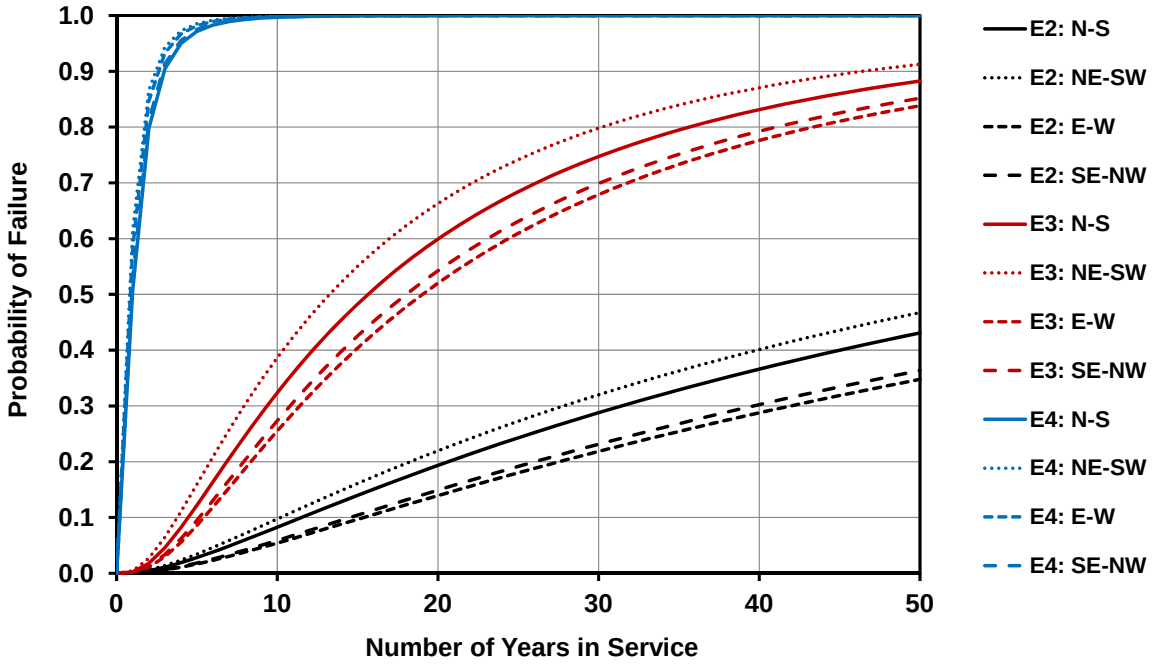

Figure 5.3 Cumulative Distribution Function for Failure Probability (fatigue crack initiation) as a Function of Service Life for Milwaukee-Style Mast-Arms in La Crosse, Wisconsin.

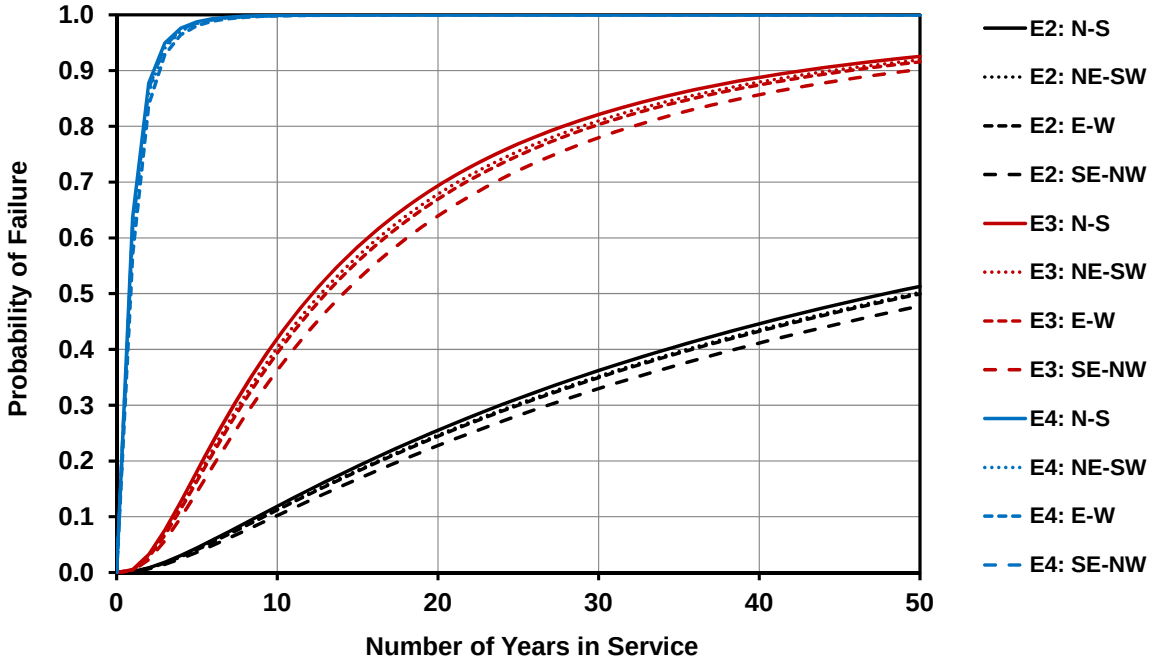

Figure 5.4 Cumulative Distribution Function for Failure Probability (fatigue crack initiation) as a Function of Service Life for Milwaukee-Style Mast-Arms in Green Bay, Wisconsin.

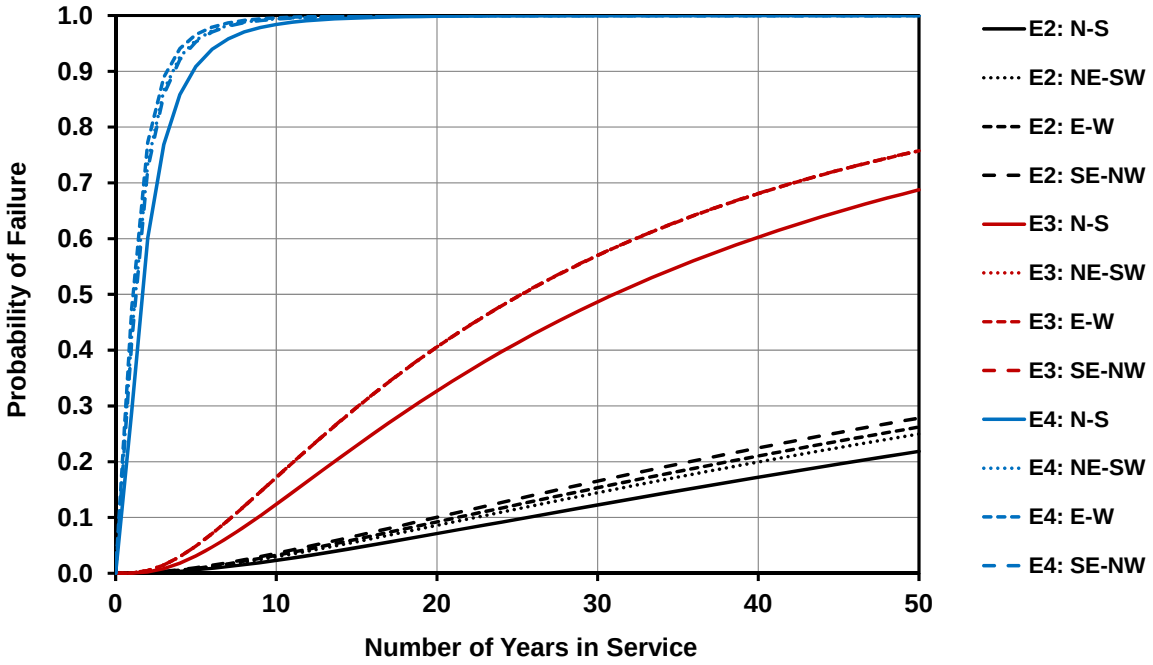

Figure 5.5 Cumulative Distribution Function for Failure Probability (fatigue crack initiation) as a Function of Service Life for Milwaukee-Style Mast-Arms in Madison, Wisconsin.

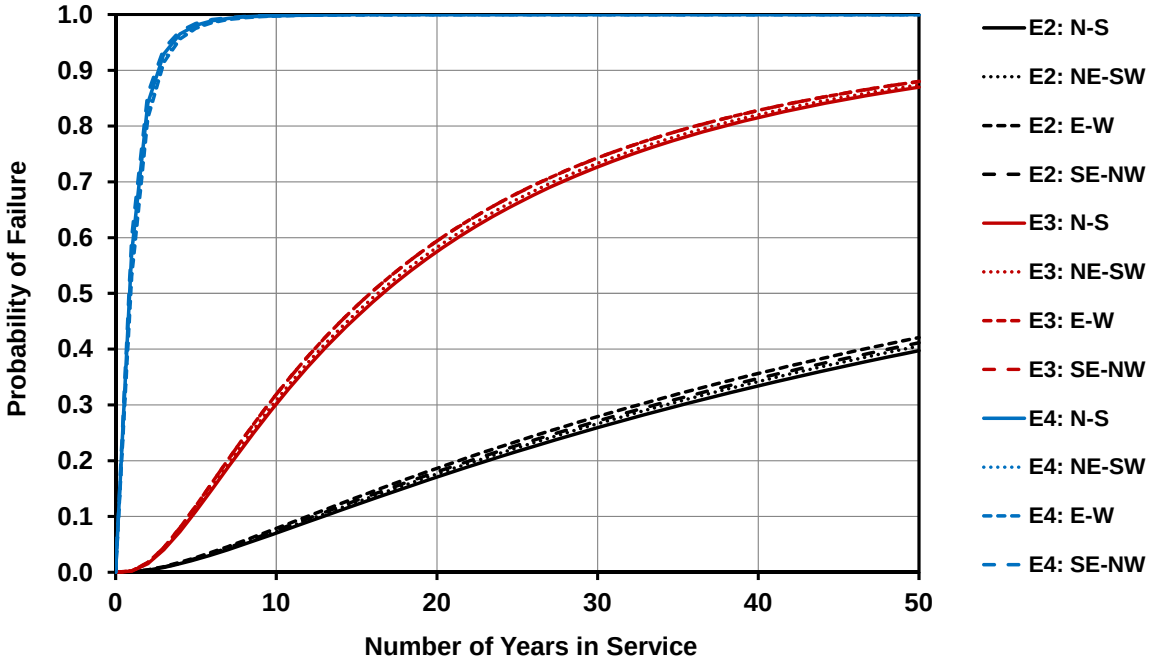

Figure 5.6 Cumulative Distribution Function for Failure Probability (fatigue crack initiation) as a Function of Service Life for Milwaukee-Style Mast-Arms in Oshkosh, Wisconsin.

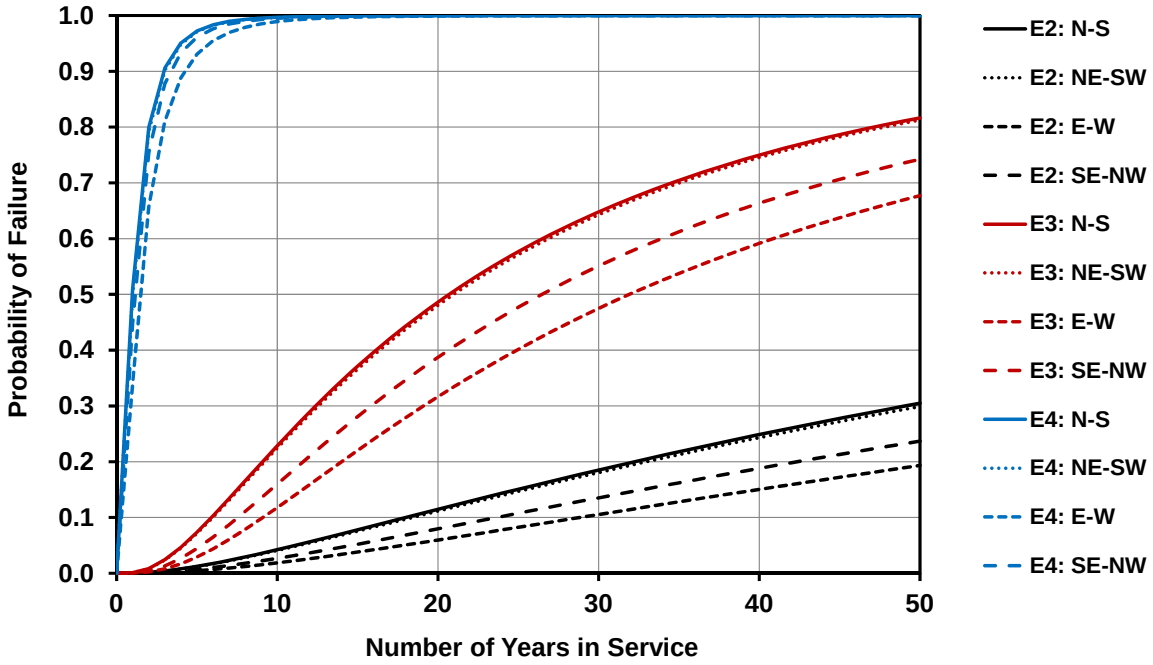

Figure 5.7 Cumulative Distribution Function for Failure Probability (fatigue crack initiation) as a Function of Service Life for Milwaukee-Style Mast-Arms in Wisconsin Rapids, Wisconsin.

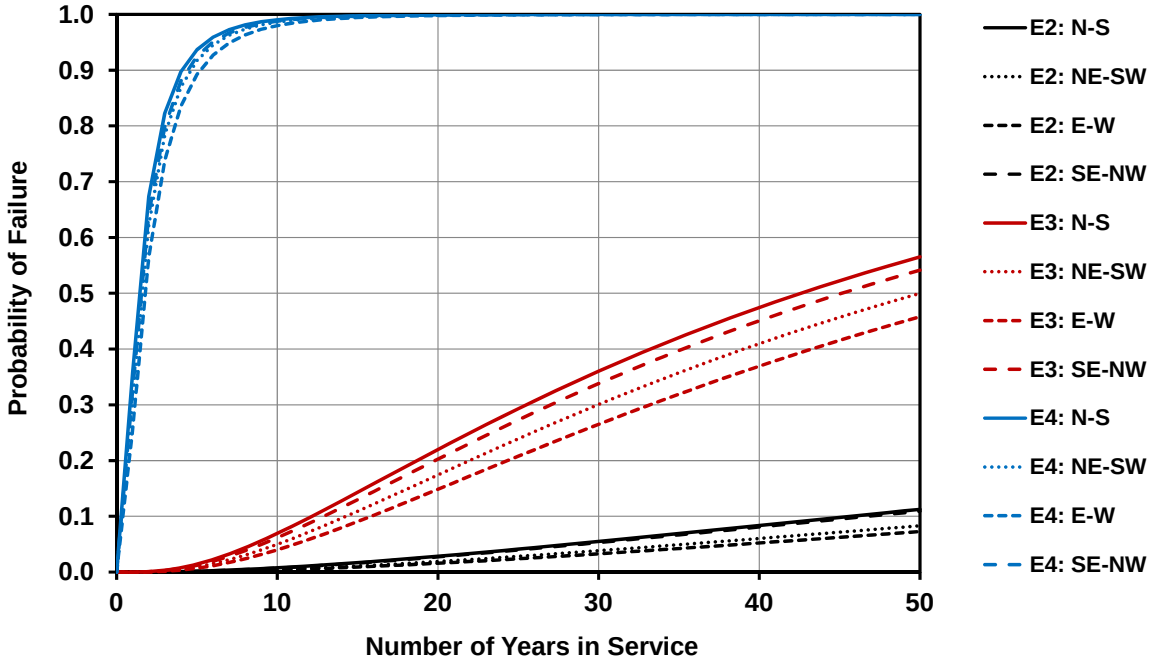

Figure 5.8 Cumulative Distribution Function for Failure Probability (fatigue crack initiation) as a Function of Service Life for Osseo-Style Mast-Arms in Milwaukee, Wisconsin.

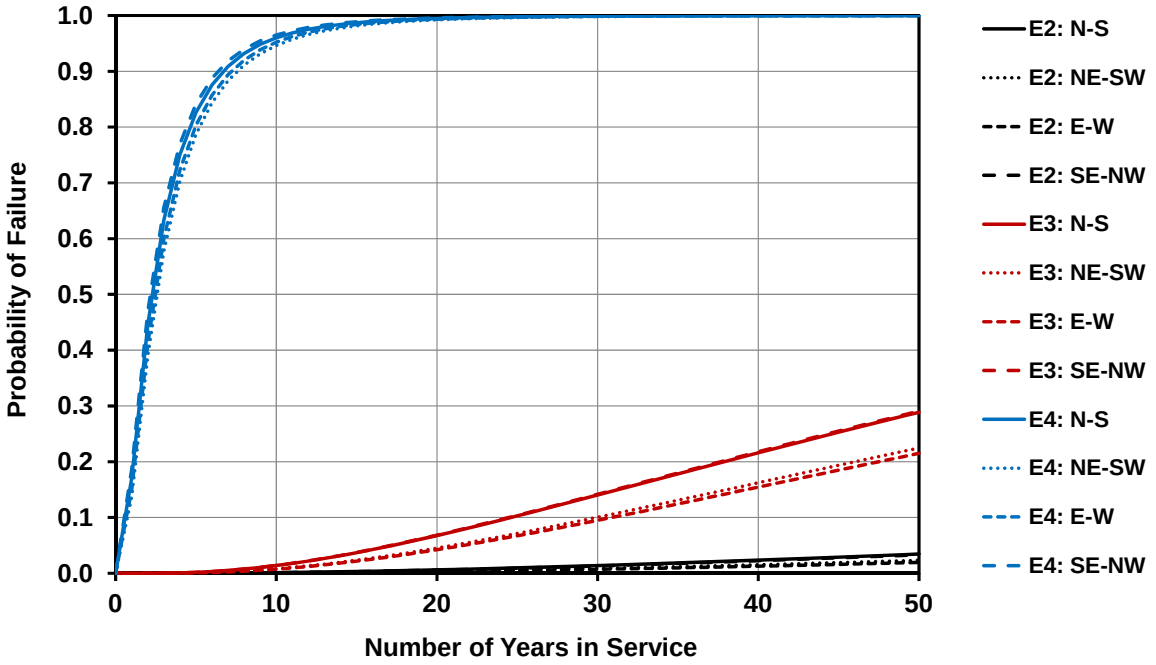

Figure 5.9 Cumulative Distribution Function for Failure Probability (fatigue crack initiation) as a Function of Service Life for Osseo-Style Mast-Arms in Eau Claire, Wisconsin.

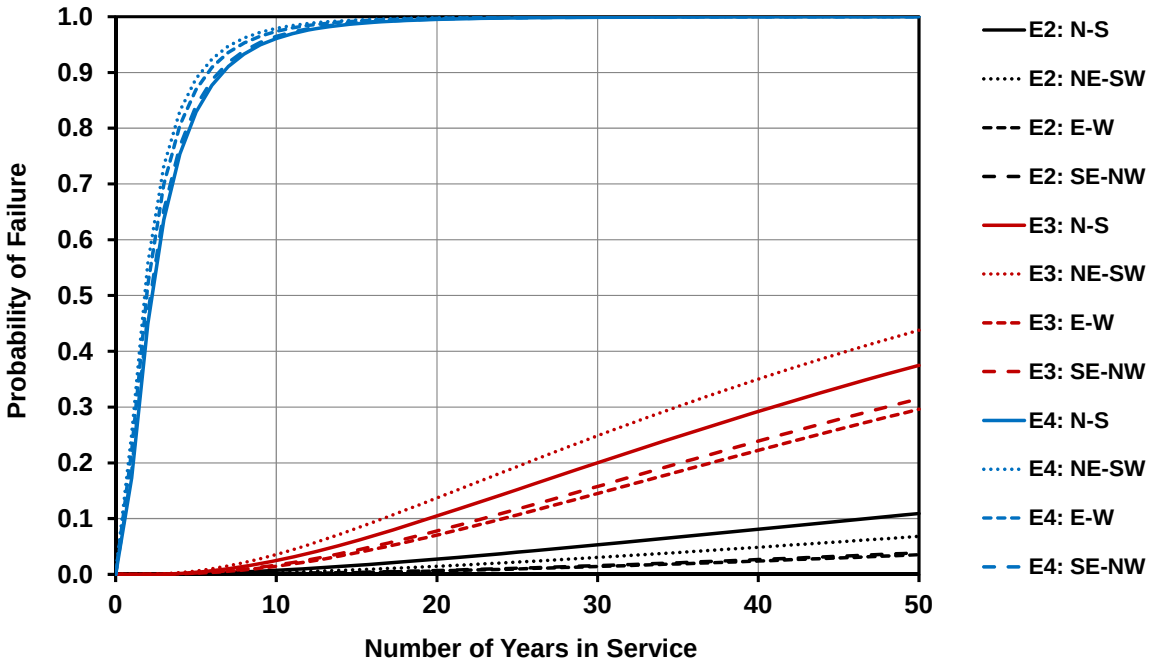

Figure 5.10 Cumulative Distribution Function for Failure Probability (fatigue crack initiation) as a Function of Service Life for Osseo-Style Mast-Arms in La Crosse, Wisconsin.

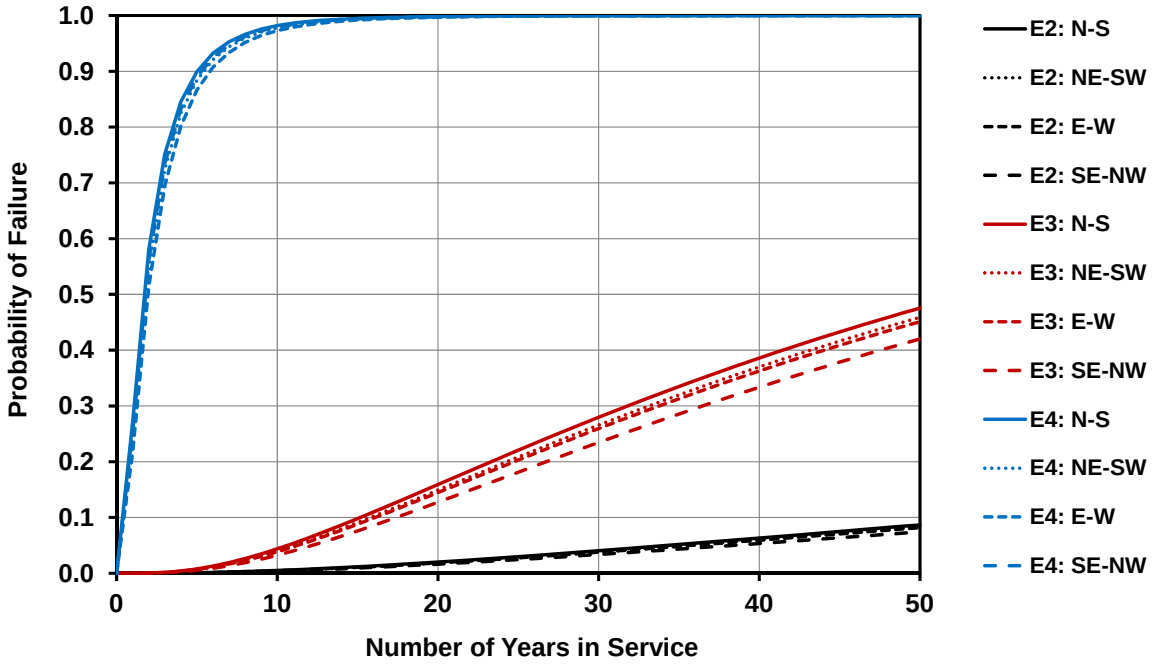

Figure 5.11 Cumulative Distribution Function for Failure Probability (fatigue crack initiation) as a Function of Service Life for Osseo-Style Mast-Arms in Green Bay, Wisconsin.

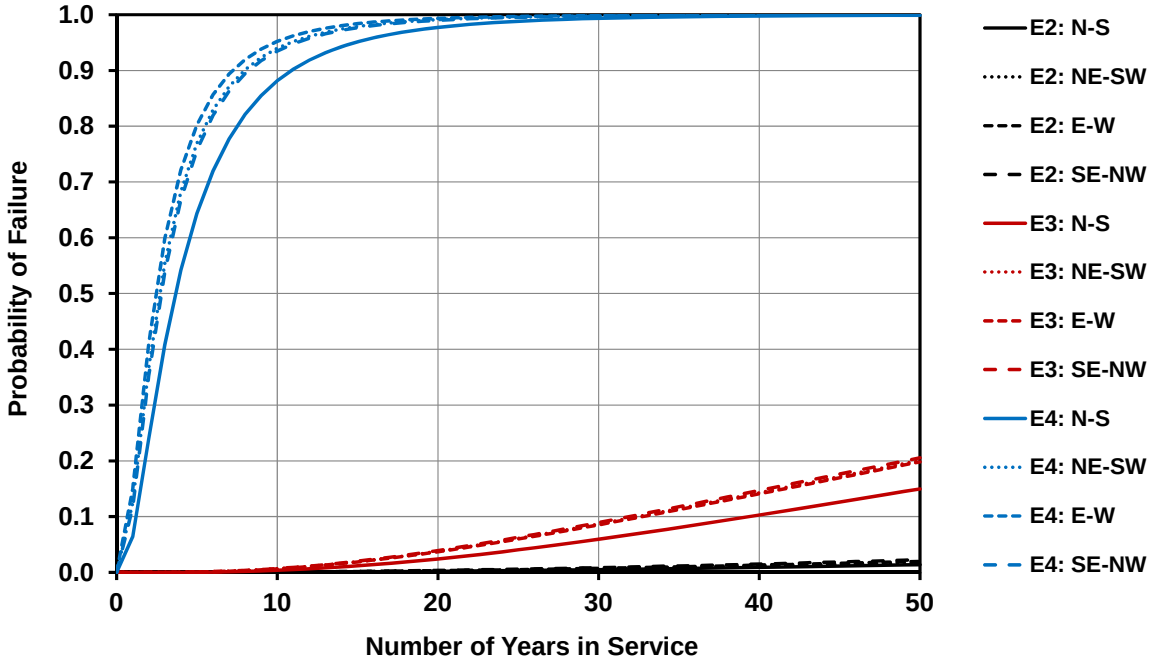

Figure 5.12 Cumulative Distribution Function for Failure Probability (fatigue crack initiation) as a Function of Service Life for Osseo-Style Mast-Arms in Madison, Wisconsin.

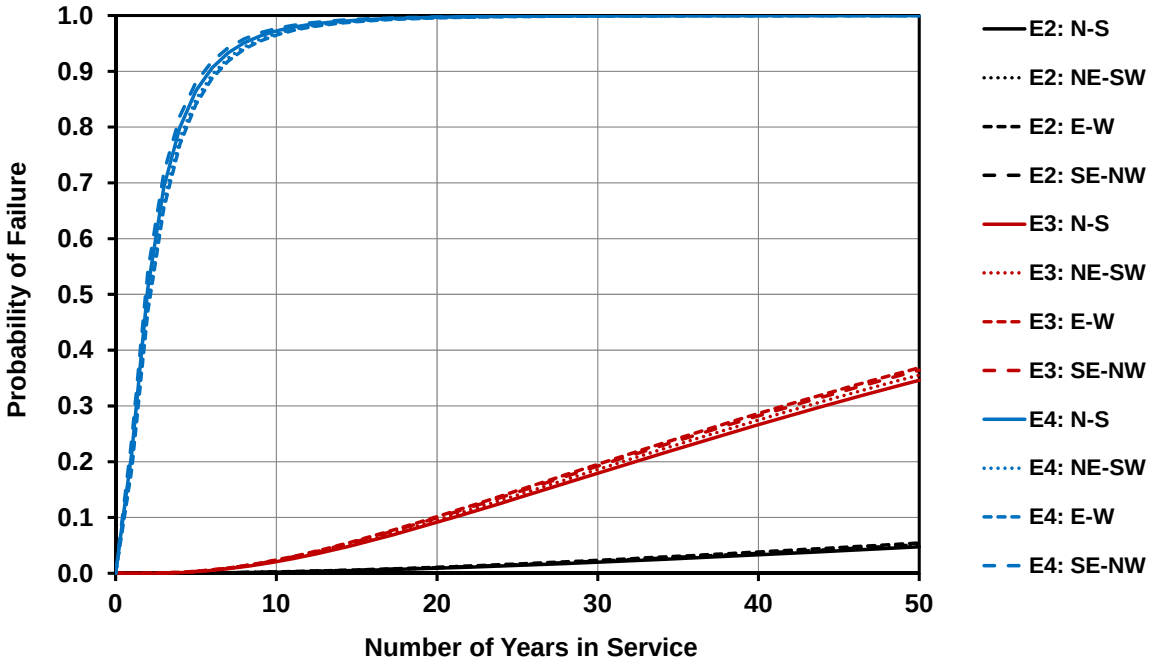

Figure 5.13 Cumulative Distribution Function for Failure Probability (fatigue crack initiation) as a Function of Service Life for Osseo-Style Mast-Arms in Oshkosh, Wisconsin.

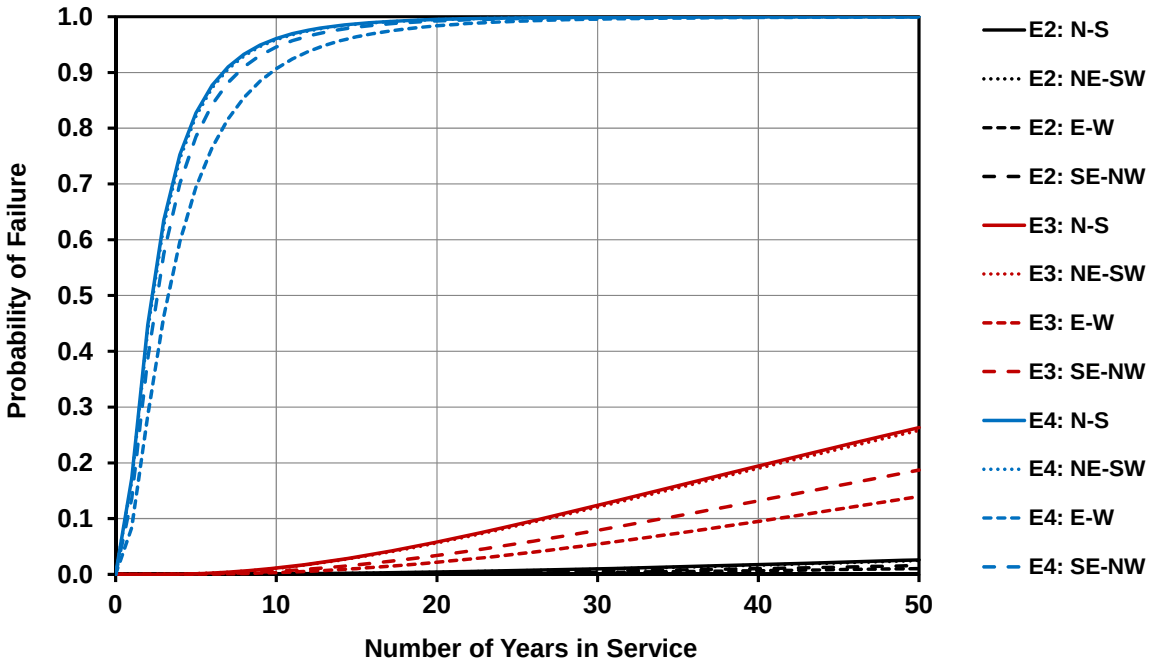

Figure 5.14 Cumulative Distribution Function for Failure Probability (fatigue crack initiation) as a Function of Service Life for Osseo-Style Mast-Arms in Wisconsin Rapids, Wisconsin.

Chapter 6 – Conclusions and Recommendations

6.1 Summary

The present research study set out to formulate, apply, and discuss a reliability-based procedure for quantifying the risk of fatigue-induced fracture in mast-arm sign support structures and to generate inspection protocols for these structural systems using this procedure. This procedure was intended to be used to identify mast-arm support structural system configurations that are likely to result in enhanced susceptibility to premature fatigue-induced cracking and poor in-service performance. It was also used to identify regions within the state of Wisconsin that may be more susceptible to having structures with fatigue problems.

The second chapter of the report (Wind Demand Uncertainty) formalized development of the information needed to determine the stress parameter that was integral to characterizing demand in the reliability-based formulation. A process through which wind speed and direction data was collected, synthesized and statistically analyzed was described. Individual, conditional, and combined probabilities of one-hour averaged wind speed and one-hour averaged wind direction have been computed for discrete locations throughout the state of Wisconsin and at a field monitoring station designed, constructed and deployed as part of the present research effort. An interpolation procedure which allows for the computation of combined probabilities at any location throughout the state of Wisconsin has been presented. Data tables defining the probability of 1-hour averaged wind speed intersected with cardinal direction, $P\left(U = u_i \cap D = d_j\right)$, were developed. These data tables in conjunction with the expected stress-range cycle magnitude and the number of cycles at this magnitude for a one-hour simulated wind record, $n_{cycles/hr,i} \cdot \left(S_{RE}^{m}\right)_i$, and the wind direction relative to the mast-arm axis, θ_j, were addressed in this chapter and completed the characterization of wind demand and its uncertainty.

The third chapter of the research report (Fatigue Life Uncertainty) outlined development of the random variable parameters necessary for defining uncertainty related to fatigue life. A comprehensive synthesis of fatigue testing data, including tests completed as part of the present research effort is included in the discussion within this chapter. Random variable fatigue life modeling parameters, μ_A, CV_A, and a best-fit fatigue life exponent, m, were formulated in this chapter for three proposed detail categories: E2, E3, and E4. These new detail categories were synthesized from the myriad of fatigue tests conducted since 1970 on connections that are typical of those seen in mast-arm sign support structures in Wisconsin. These new detail

categories are based upon stress concentration factors developed using high-fidelity finite element analysis and are shown in later chapters to successfully predict early fatigue-induced cracking failure of a sign support in Osseo, Wisconsin.

The fourth chapter of the report (Modeling Error Uncertainty) outlined formulation of the modeling error uncertainty as a lognormal random variable characterized by two parameters: μ_B and CV_B. This random variable model was formulated using data from a field monitoring station located in Milwaukee, Wisconsin and comparison of acquired data with low-fidelity finite element modeling that included simulated wind loading and response histories.

It should be noted that the random variable model for fatigue damage accumulation has not been addressed in the present research effort. Revision to the widely accepted Miner's Rule for fatigue damage accumulation was simply outside the scope of this effort. The present research report utilizes a lognormal random variable for accumulated fatigue damage with parameters given by $\mu_\Delta = 1.00$ and $CV_\Delta = 0.30$ used by previous researchers (Wirsching 1983, 1984, 1988).

The fifth chapter of the research report (Reliability-Based Risk Assessment and Inspection Protocols) applied the reliability-based assessment procedure for sign support structures and presented cumulative distribution functions illustrating the variation in probabilities of finding fatigue-induced cracks with service life for two sign support structure types, three fatigue detail categories, four fundamental orientations of mast-arm relative to North, and seven different cities within Wisconsin. These cumulative distribution functions were displayed in a tabular format that allowed inspection protocols to be defined and evaluated for these structural systems.

6.2 Conclusions and Recommendations

The research effort facilitates a significant number of conclusions very useful to WisDOT and their management of mast-arm sign support structures and recommendations that can be used to better understand behavior of mast-arm sign support structures, understanding and characterizing wind loading demands, and the susceptibility of these relatively simple structural systems to premature fatigue-induced cracking and poor in-service performance.

A comparison between NCDC-ASOS site data for Milwaukee, Wisconsin and the data acquired at the FMS site indicates that local topography has a significant impact on mean one-hour average wind speed and one-hour wind speed standard deviation and a minor effect on wind direction. A lower mean and standard deviation in the wind speed appears to occur when the sign support structure site is in urban and suburban terrain compared to flat, open terrain like that found at airport ASOS sites. Therefore, use of ASOS sites will

result in higher mean wind speeds, greater wind speed variability and likely greater wind loading demand (from a fatigue point of view) than what will likely occur at a sign structure site in the middle of an urban or suburban terrain.

An interpolation procedure for wind speed probability distributions for each of eight cardinal directions was evaluated using NCDC-ASOS site data and the FMS site data. This evaluation indicated that when interpolating combined probability distributions computed from wind speed and direction statistics gathered from NCDC-ASOS sites, the combined probability distributions in each of the eight cardinal directions appear to be conservative. Greater density of higher wind speed magnitudes result when the interpolation procedure is implemented. The wind speed variability is also likely to be slightly larger than the variability that can be expected at the sign structure location.

Three new detail categories founded on the stress concentration factor approach were proposed; E2, E3, and E4. High-fidelity finite element modeling, comparisons with parametric expressions for computing stress concentration factors (SCFs) proposed by others (Roy et al 2011), and synthesis of hundreds of fatigue tests support these new detail categories. It is recommended that mast-arm sign support structures use these alternate detail categories when fatigue-life is being assessed. Furthermore, it is recommended that the E2, E3, and E4 detail categories be used in reliability assessment procedures and be used to formulate design procedures for infinite life-based assessment.

The high- and low-fidelity finite element modal analysis used to evaluate sensitivity of the model in predicting modal frequencies of vibration and mode shapes indicates that low-fidelity finite element models are acceptable for dynamic analysis of the structural systems.

The one-hour duration transient wind speed histories generated using the Kaimal turbulence spectrum exhibited expected variability about the mean at all one-hour average wind speeds considered and therefore, the simulation procedure developed is deemed accurate for use with the finite element modeling. Comparisons to measured wind speed histories and wind speed variation about the mean indicate that wind speed simulation is a viable procedure for fatigue life estimation (Diekfuss 2013).

The lognormal modeling parameters used to characterize modeling error uncertainty in mast-arm sign support systems were found to be consistent with values that have been assumed in past research when conducting reliability analysis of structures in the offshore industry (Wirsching 1984). The present study provides measured data to formalize these types of assumptions upon a foundation that is more realistic and systematic.

The high-fidelity and low-fidelity finite element models for these sign supports used to identify locations

around the mast-arm perimeter where fatigue-induced cracks were likely to form first indicate that while the Milwaukee-type sign support structure is expected to experience larger magnitude expected stress-range, the location where these stress-ranges occur are significantly different when compared to the Osseo-type sign support structure. The maximum expected stress-ranges in the Milwaukee sign support tend to form near the 80-90 degree location relative to vertical. This location is a significant difference away from the location where peak gravity load tensile stress exists for the Milwaukee sign. In the case of the Osseo sign support structure, the peak expected stress-range magnitudes migrate to locations in the 60-80 degree range from vertical and the stress-range actually reduces at 80-90 degrees from the vertical axis.

The analysis conducted in the present effort indicates that extremely wide spacing of the bolts in the mast-arm-to-pole connection found in the Osseo sign support suggests that there will be a significant tendency for the gravity (dead) load tensile stress-ranges to act in concert with the tensile stress-ranges resulting from the lateral wind loads acting on the sign support. Thus, it is expected that crack initiation is likely to occur in locations lying along a line extending from the centroidal axis of the mast-arm to the top bolt in the connection (on either side of the mast-arm). This is consistent with the crack locations found in the Osseo sign support (Diekfuss 2013).

The reliability-based assessment process developed and implemented in this study suggests that E3 and E4 detail types be avoided in mast-arm sign support structures. The orientation of the bolt holes relative to the centroidal axis of the mast-arm as seen in the Osseo-type mast-arm-to-pole connection, results in significant stress concentration factors that approach the E4 detail category (Diekfuss 2013). As a result, mast-arm-to-pole connection details that are like the Osseo sign support structure studied in this research effort should be avoided as well. Milwaukee-type connection details are preferable and approach E2 type behavior.

The reliability-based assessment conducted suggests that E2 detail types used in Osseo type mast-arm configurations are ideal and may never need inspections during their service life. In other words, the Milwaukee-type connection detail is preferable with larger second moments of area used in the mast-arm as seen in the Osseo sign support. The assessment also suggests that Milwaukee-type mast-arm support structures with E2 detail types can have a significantly reduced number of inspections during their service lives when compared to the assumed four-year inspection cycle currently utilized by WisDOT.

It is recommended that the first inspection interval for Milwaukee-type mast-arm supports with E2 type detail category connections can be assigned in the range from 13 years to 36 years depending upon location. Sign supports located in Milwaukee should have their first inspection interval set at shorter duration than elsewhere within the State. The time to four-year inspection intervals for these sign types and details can then be after 40 years of service life in Milwaukee and longer elsewhere within the State. In fact, the study

conducted suggests that if service lives for these structures is defined as 30 years, there are locations within the State where these structures need never be inspected.

The procedures developed and employed in the present research effort indicate that implementation of state-of-the-art reliability-based assessment procedures can contribute very valuable procedures for assigning inspection protocols (*i.e.* inspection intervals) that are based upon probabilities of finding fatigue-induced cracking in these structures. WisDOT can use the results of the research effort to design inspection intervals based upon risk and thereby better align inspection needs with fiscal and human resources.

6.3 Future Research Recommendations

No comprehensive research effort is complete without recommending additional research efforts to extend the work just completed. This section of the research report outlines several recommendations that can be used by WisDOT to improve their mast-arm sign support structure performance, formulate more reliable inspection intervals and perhaps even formulate designs that need never be inspected once put into service. It also provides recommendations for additional research efforts to achieve these goals.

The synthesis of wind speed data conducted indicates that because sign support structures typically exist at locations that are remote from where wind data is measured (*i.e*. NCDC-ASOS sites), there is a need to develop an accurate methodology for including topographical effects. It is recommended that additional field monitoring systems be deployed throughout the state. This would allow further evaluation, confirmation and modification of the interpolation procedure proposed in this research effort so that combined probabilities of wind speed and wind direction can be accurately computed throughout the State. This would allow much greater understanding of the impact of topography and would facilitate modifications to the interpolation procedure that allow topography to be better incorporated in the procedure.

A brief estimate of the cost for a single field monitoring station at a sign-specific location within the state of Wisconsin is described in the following. The field monitoring station would consist of an anemometer, accelerometers and strain gaging suitable for determining the dynamic properties of the sign support structure, strain histories and wind data including direction and speed. The cost for one station is estimated to be between $15,000 and $20,000. It is recommended that four to five stations throughout the State be deployed in various locations with the goal being to include topographic variety to further evaluate the differences between local sites and ASOS sites. It is recommended that wind measuring devices be deployed on stand-alone towers in the near vicinity of a sign structure and not be attached directly to the sign structure. It is felt that the vibratory nature of the sign support structure will impact the accuracy of the wind instruments. Furthermore, it is recommended that data be collected for a minimum of one year. Modern data acquisition systems serve to minimize the cost of additional years of monitoring through automated acquisition and

storage of data. As a result, the cost estimate for a single station given previously will not be increased significantly if additional years of monitoring are undertaken at a site.

It is suggested that acceptable levels of risk for finding fatigue-induced cracks be discussed and assigned for these structures. Furthermore, it is recommended that these risk levels (*i.e.* probabilities of finding a fatigue-induced crack) be defined in light of service years after installation. In other words, what is the acceptable probability of finding a crack initiating in a mast-arm after 30 years of service? Is it 50%? Is it 25%? If these probabilities could be established, the reliability assessment procedure could be tailored very easily to directly assign inspection intervals. The results of the present study indicate that these inspection intervals would likely be very long in duration. Inspections in some locations may not even be necessary.

The procedures developed in the present study were unable to consider the impact of crack initiation and propagation on remaining service life. If WisDOT would like to determine how crack initiation and crack growth are expected to impact remaining service life after crack initiation has been identified, then a detailed analysis of crack propagation rates and material toughness for WisDOT standard materials for sign supports would need to be undertaken. This would be a very interesting study because it would give WisDOT (and the rest of the engineering community) a better understanding of how long a typical mast-arm can remain in place with a crack prior to full cross-section fracture. This would allow scheduling for re-design, fabrication, and installation of new sign supports when cracks are found. In other words, the sense of emergency repair/replacement may be able to be avoided.

It is recommended that a study similar to the present be undertaken for high-mast luminaire supports and full-span and cantilever sign support structures. The reliability-based procedure developed and implemented in the present study would add to the work previously conducted (Foley et al 2004) for these structural systems. WisDOT would then have the ability to establish inspection protocols for all auxiliary structures in the highway network using the methodology developed in this study.

Finally, it would be interesting to adapt the methodology formulated and implemented in this study to highway bridges in the Wisconsin infrastructure network. A field monitoring program for a typical steel bridge could be developed in a manner analogous to the field monitoring station designed and deployed in this effort. This monitoring system could be used to generate modeling error uncertainty parameters that then could be used directly in a reliability-based assessment of the bridge. Inspection protocols could then be developed for tolerable levels of risk in finding fatigue-induced cracks at critical details in the superstructure. In this way, the procedures developed in this study could be extended to bridges. It should be noted that there is the potential to combine long term sign structure behavior monitoring with long term bridge structure monitoring within a cohesive infrastructure corridor monitoring system.

Wisconsin Highway Research Program
University of Wisconsin-Madison
1415 Engineering Drive
2204 Engineering Hall
Madison, WI 53706
608.890.4966
http://wisdotresearch.wi.gov/whrp